AD-A052 750 MAXWELL LABS INC WOBURN MA UTILITY PRODUCTS DIV F/G 10/2
INDUCTOR NETWORK DEVELOPMENT FOR AIRCRAFT HIGH POWER SUPPLIES.(U)
APR 77 J TENO, R L BRYAN, S GHOSHROY F33615-74-C-2018
UNCLASSIFIED AFAPL-TR-77-15 NL

1 OF 3
AD A052750

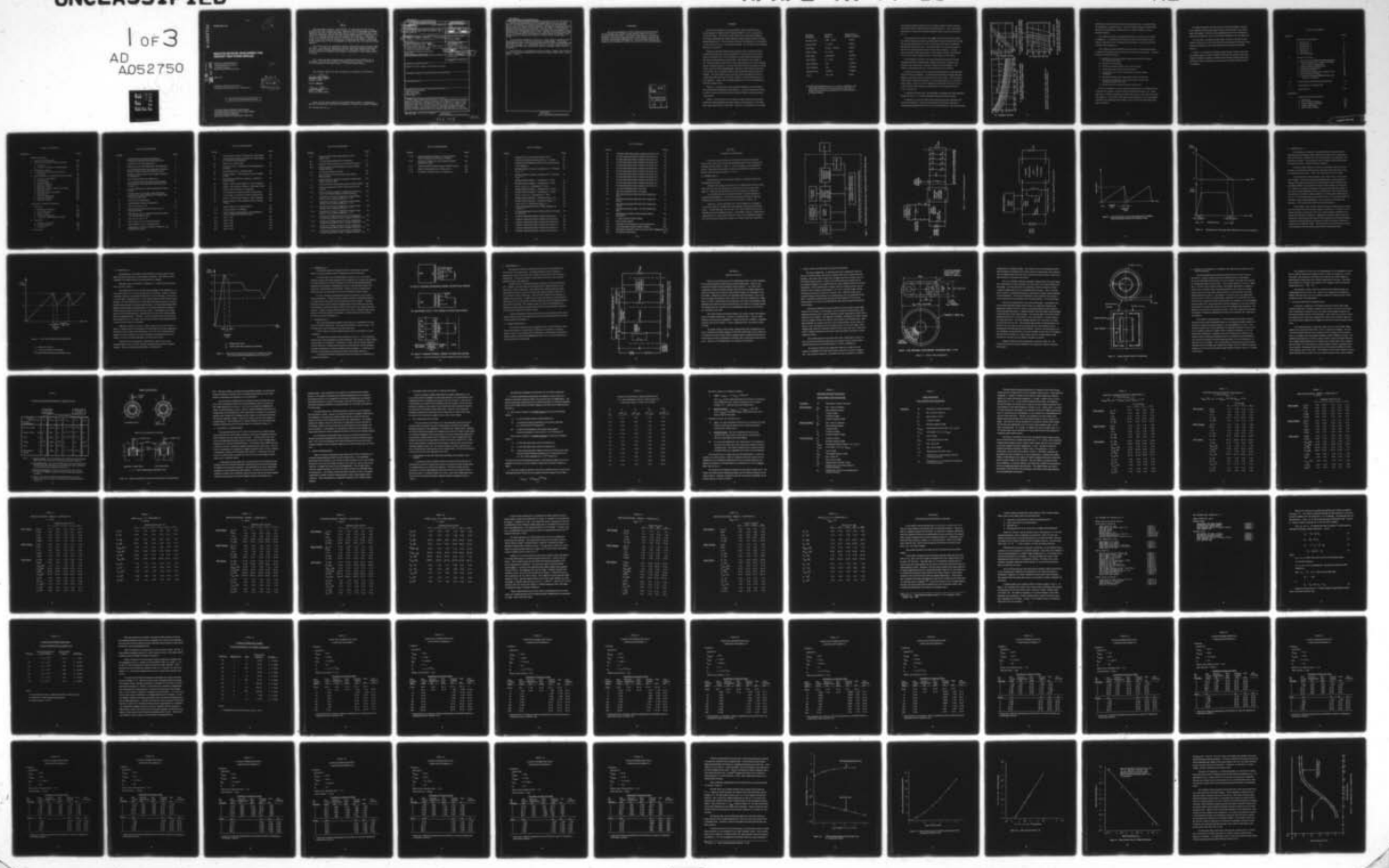

AFAPL-TR-77-15

INDUCTOR NETWORK DEVELOPMENT FOR AIRCRAFT HIGH POWER SUPPLIES

MAXWELL LABORATORIES, INC.
UTILITY PRODUCTS DIVISION
52 CUMMINGS PARK
WOBURN, MASSACHUSETTS 01801

APRIL 1977

TECHNICAL REPORT AFAPL-TR-77-15
Final Report for Period January 1974 – February 1977

Approved for public release; distribution unlimited.

AIR FORCE AERO PROPULSION LABORATORY
AIR FORCE WRIGHT AERONAUTICAL LABORATORIES
AIR FORCE SYSTEMS COMMAND
WRIGHT-PATTERSON AIR FORCE BASE, OHIO 45433

NOTICE

When Government drawings, specifications, or other data are used for any purpose other than in connection with a definitely related Government procurement operation, the United States Government thereby incurs no responsibility nor any obligation whatsoever; and the fact that the government may have formulated, furnished, or in any way supplied the said drawings, specification, or other data, is not to be regarded by implication or otherwise as in any manner licensing the holder or any other person or corporation, or conveying any rights or permission to manufacture, use, or sell any patented invention that may in any way be related thereto.

This final report was submitted by Maxwell Laboratories under Contract F33615-74-C-2018. The effort was sponsored by the Air Force Aero Propulsion Laboratory, Air Force Systems Command, Wright-Patterson AFB, Ohio under Project 3145, Task 314532, and Work Unit 31453215 with Richard L. Verga/POD-1 as the Project Engineer In Charge.

This report has been reviewed by the Information Office (ASD/OIP) and is releasable to the National Technical Information Service (NTIS). At NTIS, it will be available to the general public, including foreign nations.

This technical report has been reviewed and is approved for publication.

Richard L. Verga

RICHARD L. VERGA GS-13
Project Engineer

FOR THE COMMANDER

Philip E. Stover

PHILIP E. STOVER
Chief, High Power Branch

Copies of this report should not be returned unless return is required by security considerations, contractual obligations, or notice on a specific document.

AIR FORCE/56780/7 March 1978 — 100

UNCLASSIFIED

SECURITY CLASSIFICATION OF THIS PAGE (When Data Entered)

REPORT DOCUMENTATION PAGE

READ INSTRUCTIONS BEFORE COMPLETING FORM

1. REPORT NUMBER: AFAPL-TR-77-15	2. GOVT ACCESSION NO.
3. RECIPIENT'S CATALOG NUMBER	
4. TITLE (and Subtitle): INDUCTOR NETWORK DEVELOPMENT FOR AIRCRAFT HIGH POWER SUPPLIES.	5. TYPE OF REPORT & PERIOD COVERED: Final report, Jan [redacted]74 - Feb [redacted]77
	6. PERFORMING ORG. REPORT NUMBER
7. AUTHOR(s): J. Teno, R. L. Bryan, S. Ghoshroy, L. M. Lontai, O. K. Sonju	8. CONTRACT OR GRANT NUMBER(s): F33615-74-C-2018
9. PERFORMING ORGANIZATION NAME AND ADDRESS: Maxwell Laboratories, Inc. Utility Products Division 52 Cummings Park, Woburn MA 01801	10. PROGRAM ELEMENT, PROJECT, TASK AREA & WORK UNIT NUMBERS: 62203F; 3145/32 15
11. CONTROLLING OFFICE NAME AND ADDRESS: Air Force Aero-Propulsion Laboratory AFAPL/POD-1 Wright-Patterson AFB OH 45433	12. REPORT DATE: Apr[redacted]77
	13. NUMBER OF PAGES: 231
14. MONITORING AGENCY NAME & ADDRESS (if different from Controlling Office)	15. SECURITY CLASS. (of this report): Unclassified
	15a. DECLASSIFICATION/DOWNGRADING SCHEDULE

16. DISTRIBUTION STATEMENT (of this Report)

Approved for public release; distribution unlimited.

17. DISTRIBUTION STATEMENT (of the abstract entered in Block 20, if different from Report)

18. SUPPLEMENTARY NOTES

19. KEY WORDS (Continue on reverse side if necessary and identify by block number)

Inductive Energy Storage
Superconductivity
Power Conditioning
Pulsed Power

20. ABSTRACT (Continue on reverse side if necessary and identify by block number)

This report presents the results of a study program undertaken to perform a comparative analysis of several approaches to the generation of high electrical power by storing tens to hundreds of kilojoules of energy in a compact, superconducting inductive system with efficient extraction in short bursts at high repetition rates. The critical factors for the comparison were the weight, volume, dissipation and reliability of the system and components for various operating regimes characterized by pulse power, repetition rate and pulse shape.

DD FORM 1 JAN 73 1473 EDITION OF 1 NOV 65 IS OBSOLETE

UNCLASSIFIED

SECURITY CLASSIFICATION OF THIS PAGE (When Data Entered)

410 640

Research and development work hitherto undertaken in the U.S. and abroad indicate the engineering feasibility of operating inductive storage systems storing ten to perhaps one hundred kilojoules of energy with extraction rates of tens of pulses per second at pulse durations of the order of a few hundred microseconds with state-of-the-art technology. The major effort of this study was directed towards developing analytical tools to predict the performance of superconducting coils at repetition rates of 100 - 1000 pps with pulse discharge times of 20 - 40 microseconds and to evaluate the relative merits of different circuit configurations for storage and extraction of energy at high average power (3 - 10 MW).

As is generally recognized, switching is a major technical problem and must be evaluated in terms of the overall electrical system design. The analyses presented here serve to identify interrelated specific switching requirements and auxilliary equipment; e.g., counterpulse circuits, for three of the most attractive approaches which were selected from about ten candidate schemes initially identified.

At frequencies of a few hundred pulses per second, it appears that inductive storage has a distinct advantage over capacitive storage at power levels of the order 1 - 10 MW.

FOREWORD

The work accomplished in a study of inductor network development for aircraft high power supplies, under Contract F33615-74-C-2018, is presented in this final report. The purpose of this study was to assess the feasibility of developing a lightweight and compact inductive energy storage system by utilizing superconducting coils. Various methods of storage and extraction were considered in order to arrive at one or more optimal systems.

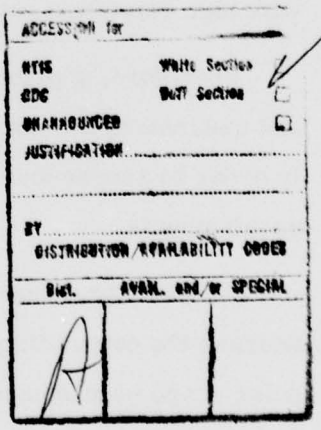

SUMMARY

The work accomplished in a study of inductor network development for aircraft high power supplies under Contract F33615-74-C-2018, is presented in this final report. The purpose of this study was to assess the feasibility of developing a lightweight and compact inductive energy storage system by utilizing superconducting coils. Various methods of storage and extraction were considered in order to arrive at one or more optimal systems. (See the table for the operating parameters of interest.)

Operation of inductive energy storage systems using cryogenic and superconductor technology has been proved feasible at energy levels of tens of kilojoules at extraction rates of tens of pulses per second with pulse durations of the order of several hundred microseconds. But operation in the regime of 100 - 1000 pps repetition rates and 20 - 40 μs discharge times is, to our knowledge, hitherto untreaded territory. It must be understood whereas the matter of storing energy in coils is fairly straightforward, extraction of this energy at these fast rates leads to severe problems related to superconducting losses and thermal stability. The superconductor may go normal, thus increasing the losses and coolant (liquid He) boil-off and at worst, leading to a catastrophic thermal runaway situation. Further, the switching problem is by no means straightforward with high repetition rates.

Therefore, a principal task of the present investigation was to investigate and understand the magnitude of these problems. A systems approach was taken in order to assess and clarify the overall technical situation and developmental requirements.

Further, previous work done on inductive energy storage did not carefully address the output discharge pulse shape which is critical because of the output pulse shape requirements of this study. Therefore, considerable time was spent

Operating Parameter	Operating Range	Significance of Range of Variation
Average Power	3 MW - 10 MW	Critical
Energy/Pulse	3 - 100 kJ	Critical
Pulse Rate	100 pps - 1000 pps	Critical
Output Voltage	40 - 60 kV	Small
Pulse Shape	Trapezoidal	Constant
Pulse Width	20 - 40 μs	Small *
Pulse Risetime	2 μs	Constant
Pulse Falltime	4 μs	Constant
Operating Time	1 minute	Constant
Loads	3 Ω - 5 Ω	Small

* Small range but the absolute size is of major significance, the short pulse width leads to the requirement for high rates of change of flux and current and requires very fast switching for an efficient system.

in developing synthesis techniques for the design/evaluation of pulse-forming networks and finally identifying actual circuit parameters. This work has been summarized in Appendix B, including additional details extracted from Report No. 3.

Of the parameters in the table, the range of variation of the energy stored per pulse and the pulse rate has a profound effect on this particular system study. The average operating power is also a critical parameter but it is defined by the pulse energy and pulse rate. The limited range of the other parameters in the list has a relatively small impact on the system evaluation. As noted below in the table, although the range of pulse length is limited, the relatively low value of the pulse length does have a critical impact on the system.

An investigation was made of the interrelationships between the various operating parameters including pulse length, pulse energy, repetition rate, average power, pulse power, discharge voltage and load resistance. The results are presented in the three related graphs shown in the figure.

Examination of these curves reveals the related boundaries of the parameter space which was investigated. To illustrate how parameters strongly affect one another, consider the case of operation at 60 KV, and 10 MW. From the figure, 10 MW requires about 330 pps which is in the desired range as is $\sim 4.8\Omega$ and a 40 μsec pulse. However, if 60 KV operation is desired with a 20 μ sec pulse at 10 MW, then the load resistance is somewhat below the required 3Ω and at 40 KV is nearly 1Ω.

To extend the present study, the possibility of operating loads with impedances outside the narrow $3 - 5\Omega$ range specified should be carefully evaluated.

A computer code was developed which incorporated system algorithms and energy loss equations. The code can design the energy storage coil and its accompanying supporting structure; the cryogenic subsystem; determine switching

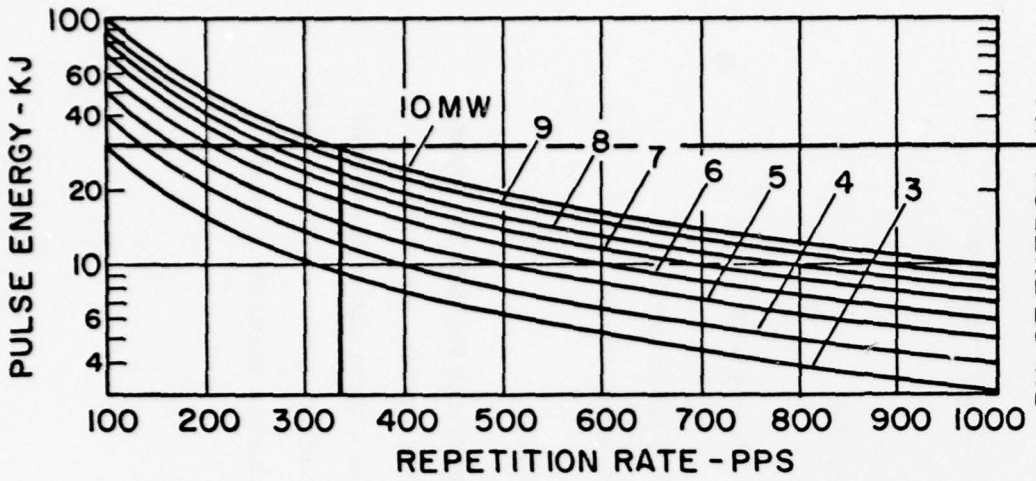

I. PULSE ENERGY VS. REPETITION RATE
CONSTANT AVERAGE POWER CURVES

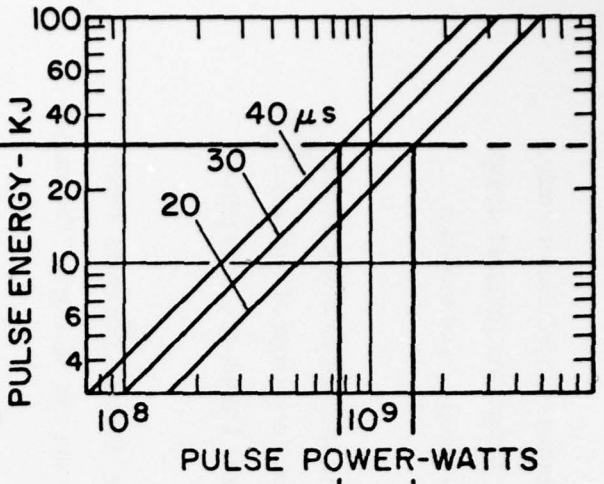

II. PULSE ENERGY VS. PULSE POWER
CONSTANT PULSE LENGTH CURVES

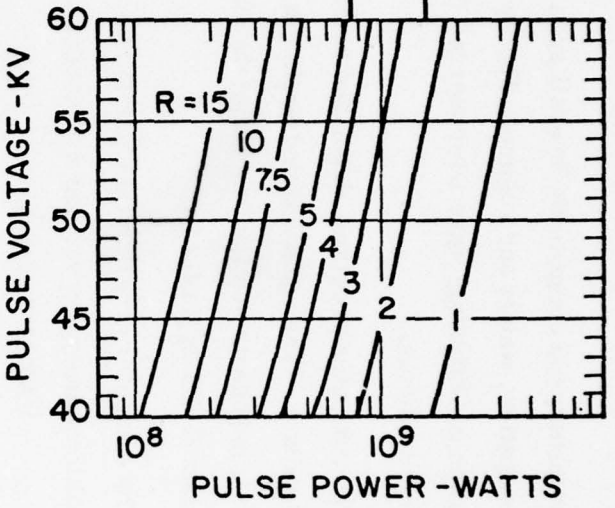

III. PULSE VOLTAGE VS. PULSE POWER
CONSTANT RESISTANCE CURVES

Relationships Between Pulse Energy, Repetition Rate, Pulse Power, Pulse Voltage and Load Impedance.

requirements; and compute the overall system performance - most importantly, the dissipation, weight and volume. The two computer programs (magnet design and power conditioning) were later merged for complete analysis of various candidate systems.

The computer program, described briefly below, is treated in more detail in Appendix A. The equations and scaling laws used for the design of various system components and for computing the superconductor losses are described in Section II and Appendix B.

The computer program (MAXOPT) is a fairly large Fortran program which is capable of analyzing various approaches to inductive energy storage. The major functions of MAXOPT include:

1) Synthesize a current-fed pulse forming network (PFN) to produce the required pulse shape.
2) Specify PFN components.
3) Perform a transient analysis of the PFN discharge.
4) Design the energy storage coil and the dewar.
5) Compute the losses in the superconductor and other system components.
6) Determine switching and counter-pulse circuit requirements.
7) Evaluate the performance of the total system in terms of the dissipation, weight and volume.
8) Report numerical results and produce printer plots.

Numerous computer runs were made using this program to validate the superconductor loss equations, perform conductor optimization studies, etc. Three approaches, selected on the basis of preliminary analysis, were analyzed in detail and compared. A description of the nature of the approaches, power conditioning schematics and operating modes together with our conclusions about their feasibility will follow.

As might be expected, the study does not conclusively identify a uniquely "best" inductive energy storage system which covers the entire range of parameters investigated. The three most promising (about ten were considered) approaches analyzed are more or less feasible depending on the operating point.

It is also clear, and should be stated again, that basic technical developments are required to validate the projections presented here; particularly those related to the behavior of the superconductors and switching/commutation schemes.

However, as compared to capacitive energy storage systems, the results give further support to earlier contentions that inductive energy storage offers distinct advantages in regard to minimizing size/weight of high average power generators; this is especially true as the power and energy storage increase in magnitude.

TABLE OF CONTENTS

TABLE OF CONTENTS

LIST OF ILLUSTRATIONS

LIST OF ILLUSTRATIONS

LIST OF ILLUSTRATIONS

LIST OF ILLUSTRATIONS

LIST OF TABLES

LIST OF TABLES

SECTION I

TECHNICAL APPROACHES

To provide a general frame work for detailed discussion of inductive energy storage systems, some specific approaches that have been actually been evaluated are first outlined. Figure 1 is a block diagram of the generalized system. Schematics which relate to the three most attractive approaches are shown on the accompanying Figures 2 and 3.

1. APPROACH NO. 1

In this scheme, the energy storage inductor is completely charged and discharged on each pulse.

Therefore, the energy stored in the coil is slightly higher than the energy delivered to the load; the differential accounts for the losses in the system. Figure 4 shows the coil current waveform under Approach 1 conditions.

As is evident from the coil current waveform, it is both charged and discharged almost linearly. The pulse-forming network (PFN) converts this discharge into a trapezoidal waveform at the load (shown in Figure 5).

Approach 1, the full discharge case, has the highest rate of change of coil current and hence magnetic field during both the charging and discharging ramps. During discharge, $\dot{B}$ can reach $\sim 10^5$ Tesla/sec which places severe demands on the superconducting magnet. An advantage, however, is that only the energy needed for a single pulse is stored so there can be substantial savings in the coil and cryogenic subsystem weights, as compared with other approaches.

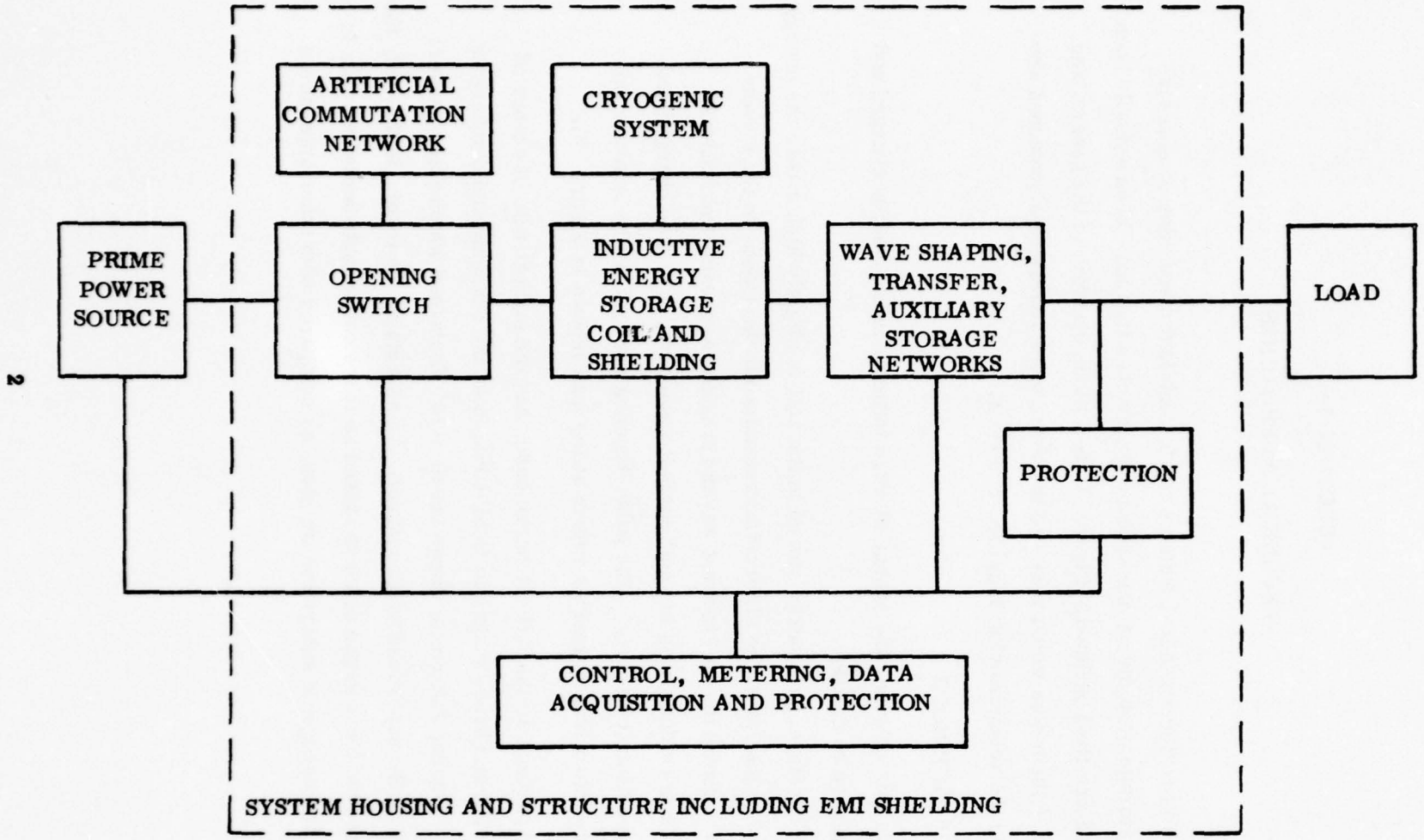

Figure 1. Generalized Block Diagram Showing Major Components of Inductive Energy Storage System.

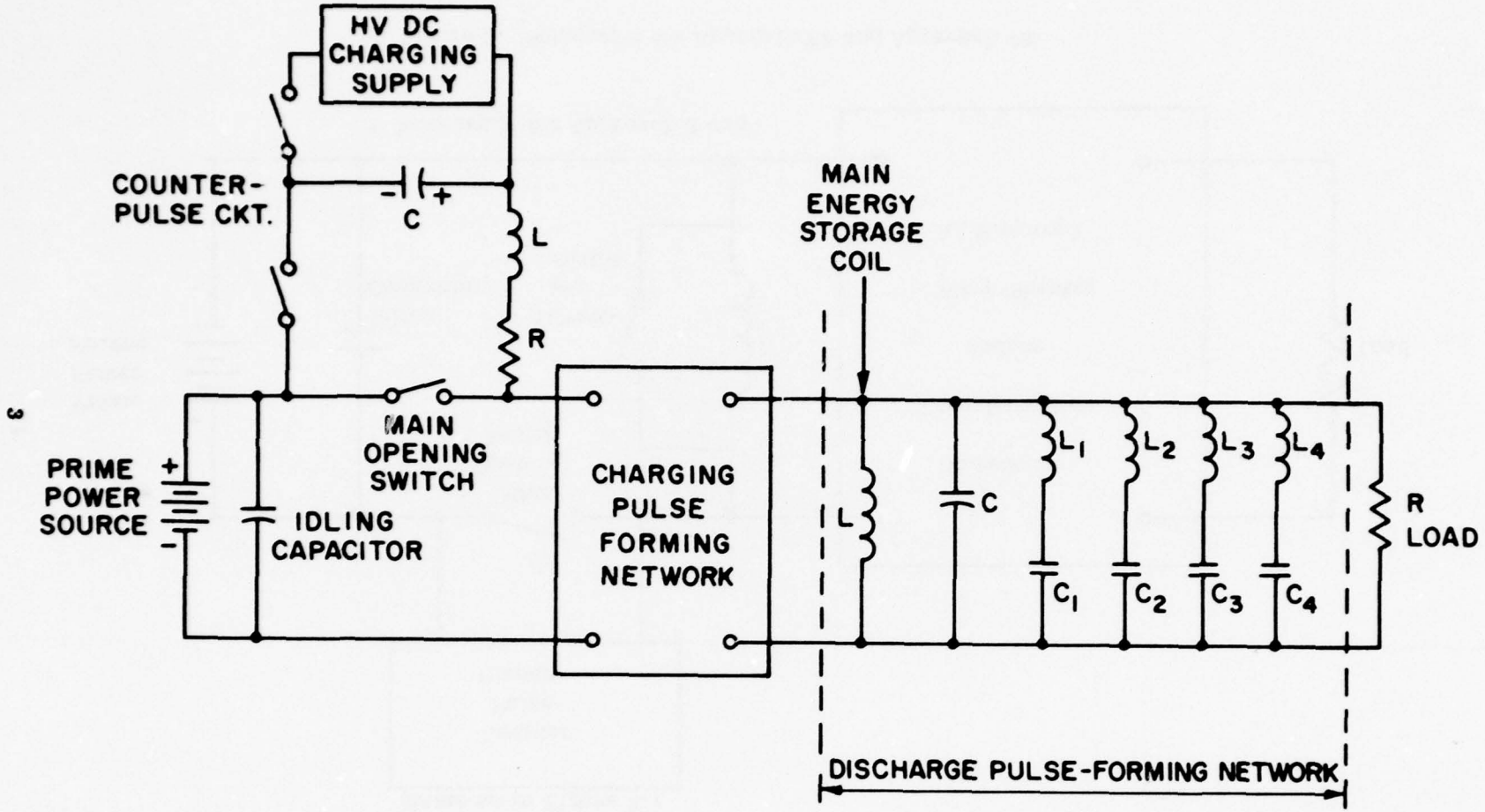

Figure 2. Schematic for Use With Approach #1.

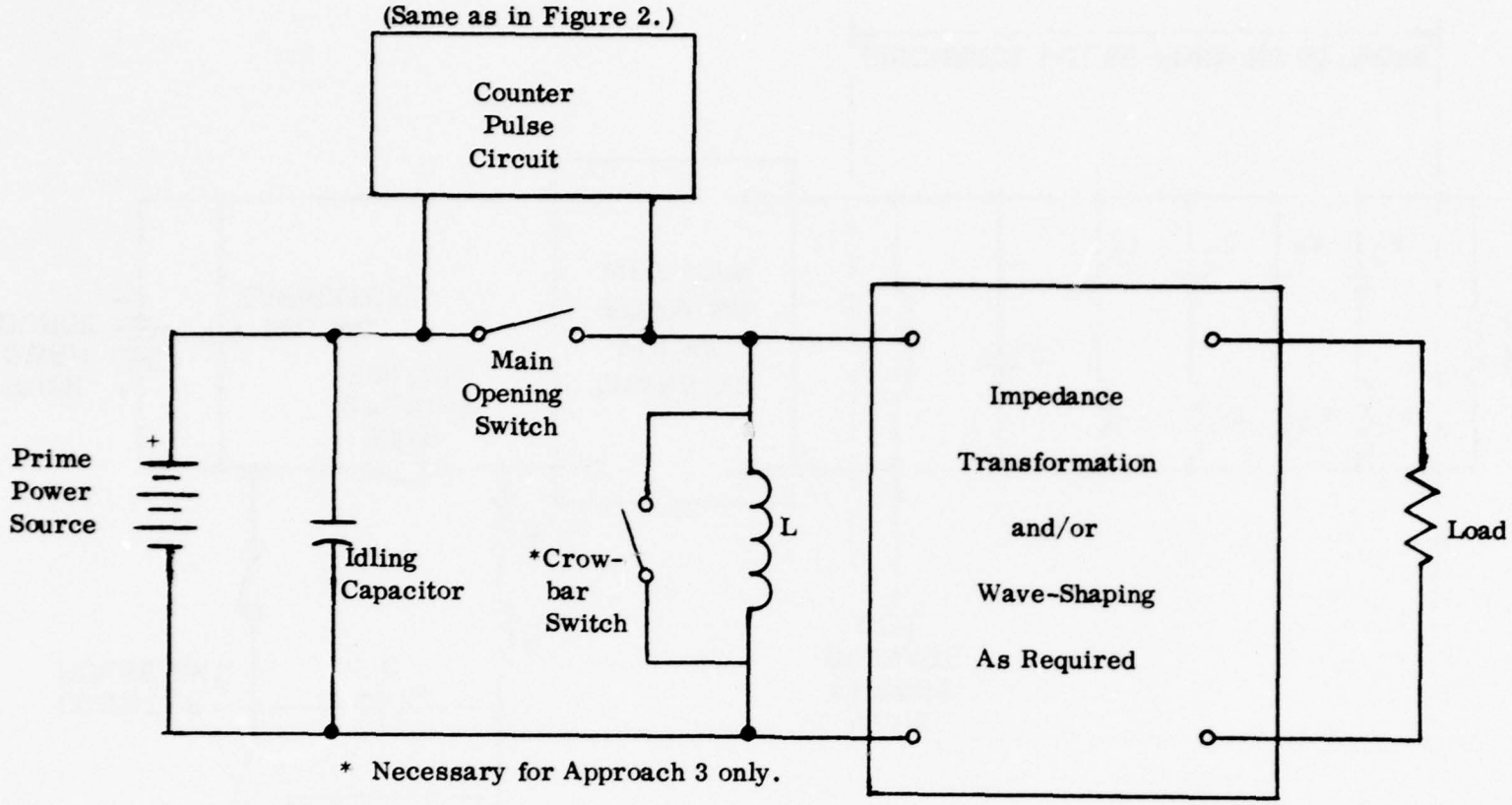

Figure 3. Schematic for Approach #2 and Approach #3.

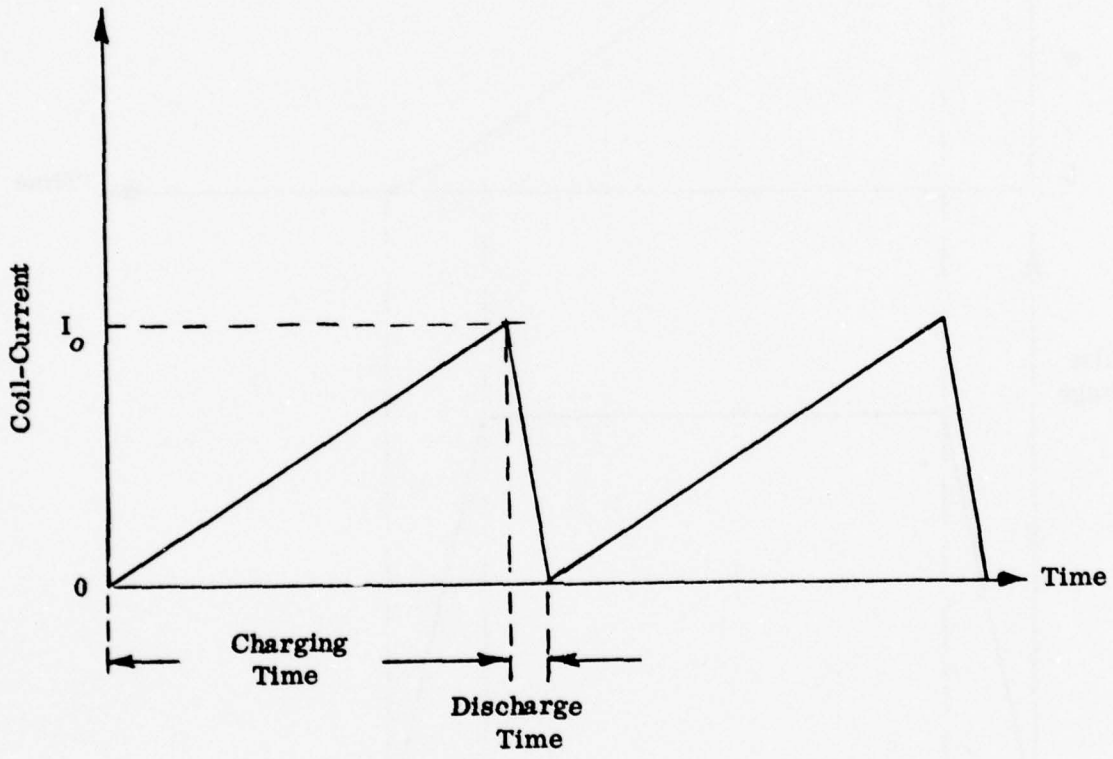

Figure 4. Coil-Current Wave Form Under Approach #1 Condition, Showing Complete Charge and Discharge Cycles.

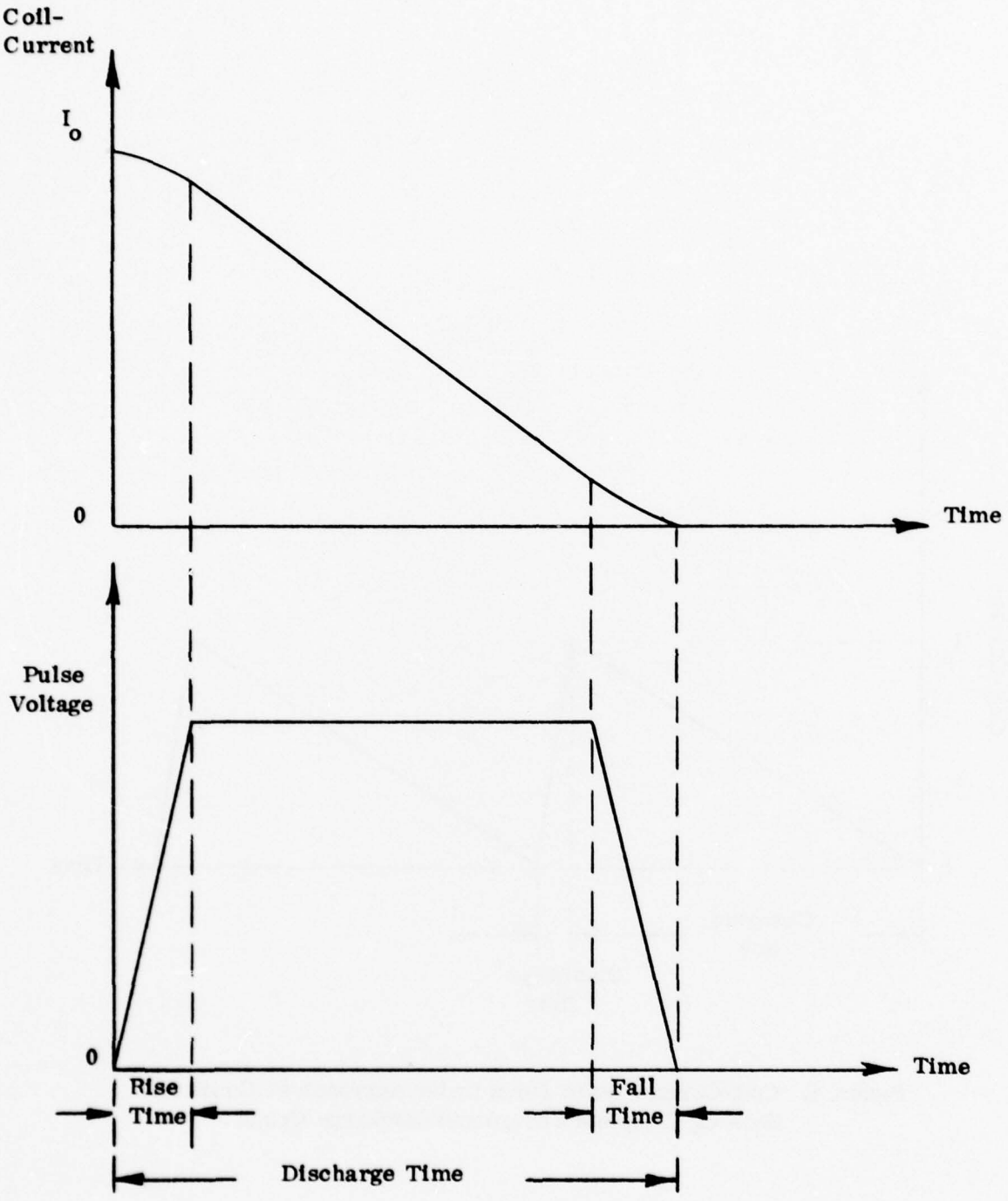

Figure 5. Discharge Coil Current and Load Voltage Wave Forms for Approach 1.

2. APPROACH NO. 2

In this method, the inductor is charged initially to an energy which is significantly greater than the energy required to be delivered by a single pulse. After one discharge is effected, the coil is charged again to its initial state and the process repeated. The schematic is shown in Figure 3 and the coil current waveform under these conditions is shown in Figure 6.

During the initial startup, the coil can be charged up slowly to the peak current I_o and subsequent charging cycles will demand only single pulse energy from the prime power source. Thus, low voltage prime power is needed.

The main features of this approach, on the positive side, are the small rate of change of coil current during the discharge phase, reduced restriking voltage on the main opening switch, low superconductor losses resulting in not only higher stability in its operation but also sizeable reduction in coolant boil-off. Another very important advantage of this approach is that if the change in coil current is kept sufficiently small, say within about 5%, the coil current can be assumed to be virtually constant resulting in a nearly square voltage pulse at the load. This means the pulse-forming network may not be necessary which will reduce the system weight significantly. In our evaluation of the approaches, therefore, a PFN has not been utilized in the second approach.

On the negative side, however, since the amount of energy stored is larger, the coil and dewar sizes will increase relative to Approach #1. Further, in some designs with high current levels in the coil, careful impedance matching may be necessary to interface with the load. Although the restriking voltage on the main switch will be approximately the same for all the approaches, the possible addition of impedance matching hardware would tend to reduce the restrike voltage at the expense of some additional weight. This tradeoff has not been carried out because of uncertainities in the operating characteristics of the opening switch.

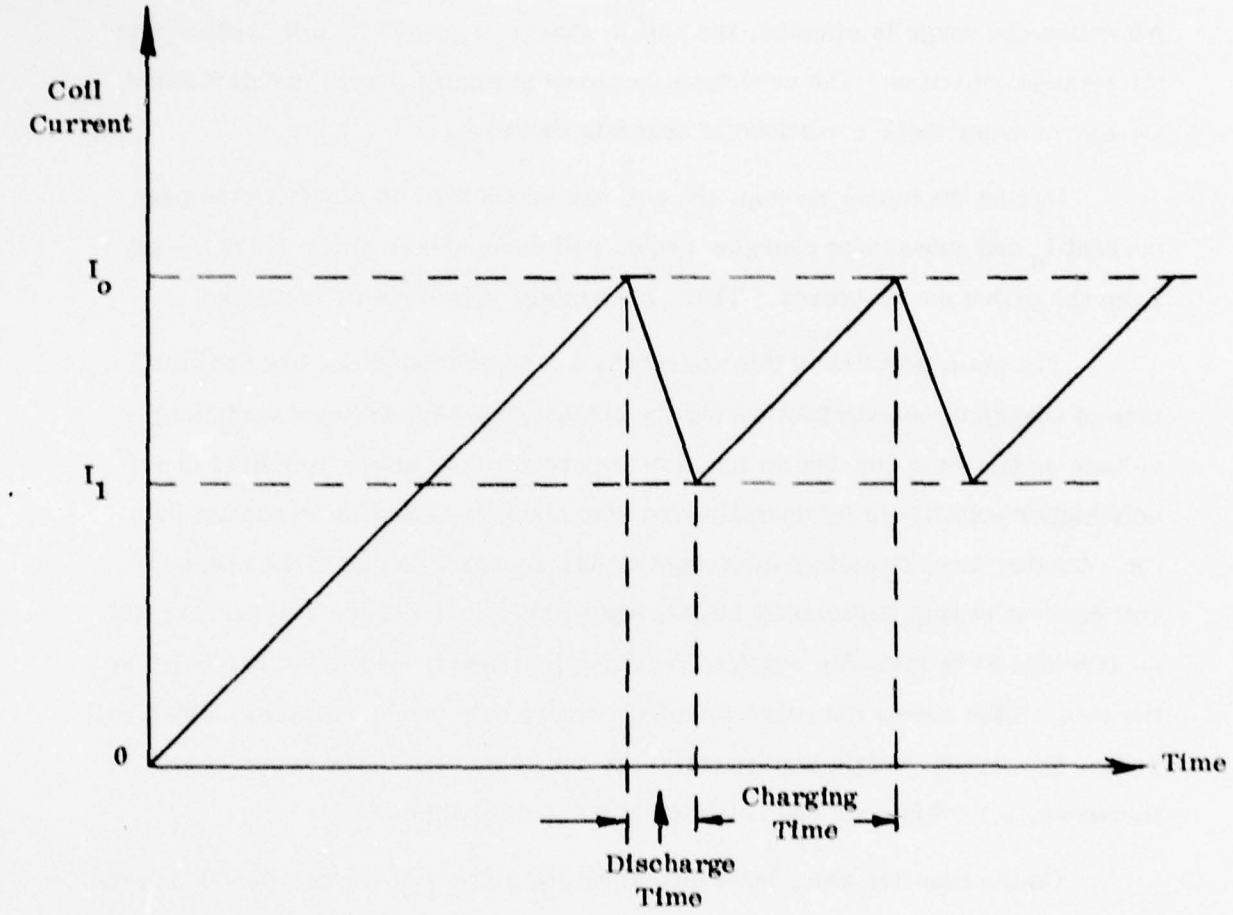

Figure 6. Coil Current Waveform for Approach #2.

I_o = Initial Coil Current

I_1 = Coil Current After One Discharge

Involving Partial Discharge and Recharge Cycles

3. APPROACH NO. 3

In this approach, the inductor is also charged to an energy which is much larger than pulse energy and a train of pulses is extracted. The inductor is then recharged to the initial energy level and the process is repeated.

Therefore, this is an extension of Approach 2. A typical coil current waveform is shown in Figure 7.

This approach has more or less the same advantages of the Approach 2, i.e., it has lower losses, etc., but here the coil size is the largest. In order to achieve a practical coil size, the operating B-field level has to be quite high, of the order of 6 or more tesla, requiring in turn, a more massive support structure and the dewar housing. The main switch will have to open under even larger currents, requiring greater energy storage in the counter pulse network. An added disadvantage of this approach is the problem of effecting some sort of variable impedance matching to extract the same amount of energy with every pulse. Concerning the wave shape, since the coil will discharge into a resistive load, the coil current will essentially follow an exponential curve. Therefore, even if the change in coil current is kept fairly small by use of a very large coil, the energy delivered will gradually fall off as more and more pulses are extracted.

Approach 3 requires a low loss crowbar switch to carry current between pulses. Consideration of the advantages and disadvantages for all three approaches discussed so far, it appears that Approaches 1 and 2 are most favorable and that Approach 3 clearly requires the most development and extension of current technology. It is also, with high probability, the largest and heaviest.

While the first three approaches outlined above appear to be of most practical interest, other schemes have been considered but rejected for detailed analysis. There are discussed briefly below for completeness.

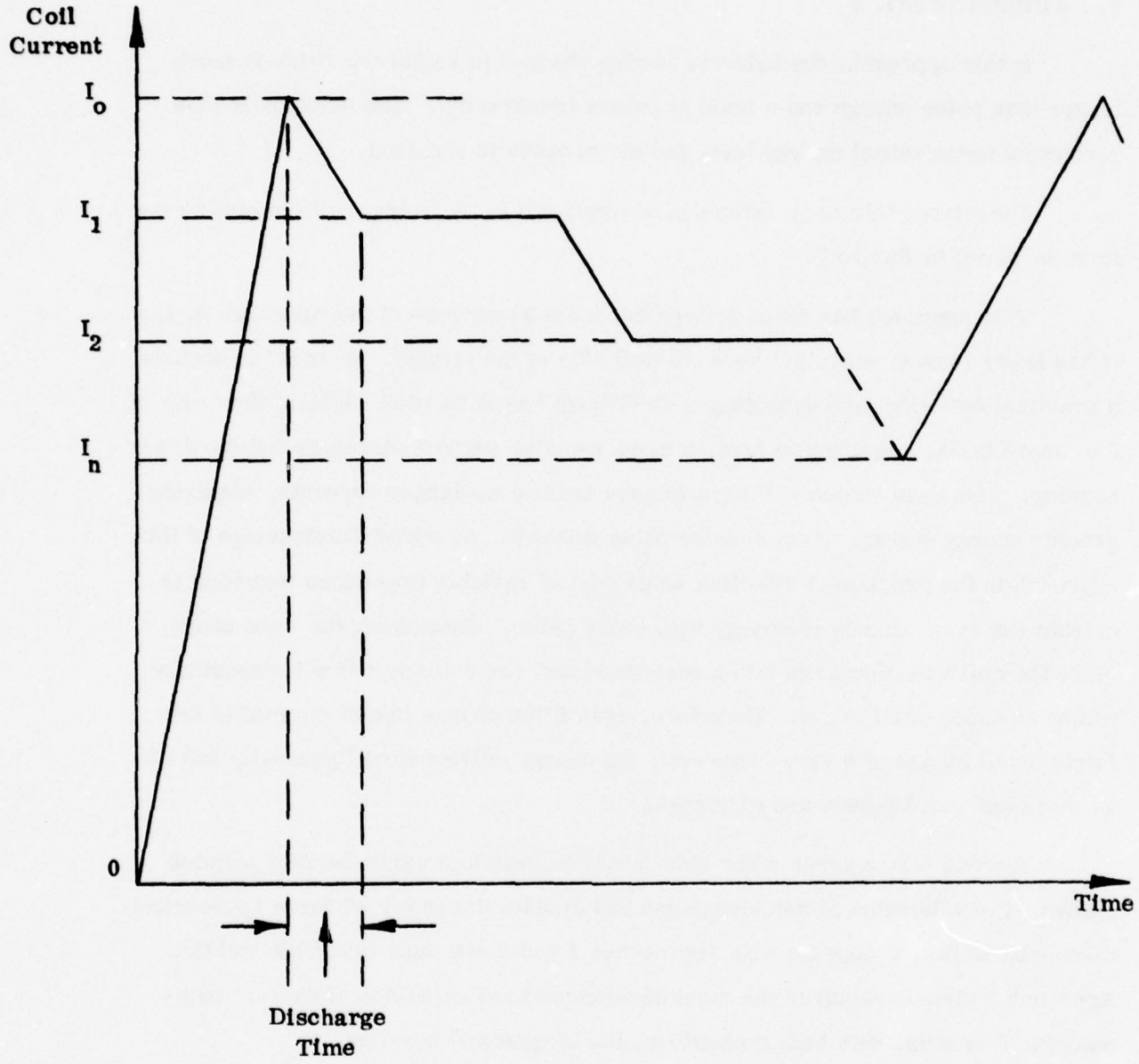

I_o = Initial Coil Current

I_n = Coil Current After n pulses are extracted.

Figure 7. Coil Current Waveform for Approach 3 Conditions Involving Pulse Trains Extracted Sequentially from a Large Coil.

4. APPROACH NO. 4

This method consists of charging a number of independent or parallel inductors (each providing one pulse of energy) to provide a pulse train.

From the point of view of superconductor operation, there is not much difference between the present approach and the Approach #1, because each individual coil will undergo the same rates of change of current and field during discharge. Depending on the number of independent coils used, each individual inductor will operate at a reduced pulsed repetition rate, which may reduce charging losses and allow longer recovery times in the event an individual coil goes normal.

It is our considered opinion that the inherent complexities of this method make it unattractive. Firstly, housing a number of parallel, independent inductors in a single dewar will create serious problems with mutual coupling. Secondly, the large number of leads required will greatly increase heat leaks into the dewar. The switching, crowbar and control circuitry will be much more complex than other schemes. Finally, it appears that the system will require a relatively large volume because of the large number of components. Further discussion of the circuits involved is provided in Appendix C.

5. APPROACH NO. 5

Here, the energy storage inductor is the primary of a transformer in which there are multiple secondaries. Each secondary transfers a pulse of energy. The secondaries are used in sequence to provide a pulse train.

Several schemes of multi-winding energy storage and extraction are shown in Figure 8.

This approach has much the same problems as for No. 4. The complexities with the dewar and the switching are again substantial. The process of energy transfer is guaranteed to be inefficient. As Appendix C shows, greatest transfer efficiency requires both close coupling between primary and secondaries, and the absolutely conflicting requirement of minimal coupling among secondaries. A compromise to partially meet both these requirements results in unacceptable efficiency.

An analytical treatment of this approach and the reasons for rejecting it are provided in Appendix C.

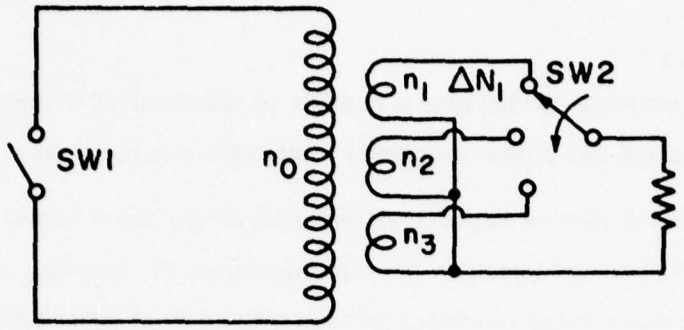

(a) MULTI-WINDING SECONDARY ENERGY EXTRACTION SYSTEM

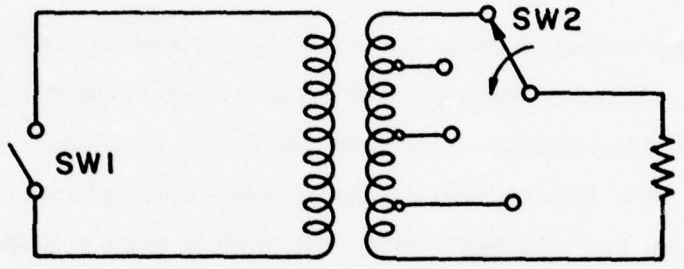

(b) SECONDARY MULTI-TAP ENERGY EXTRACTION SYSTEM

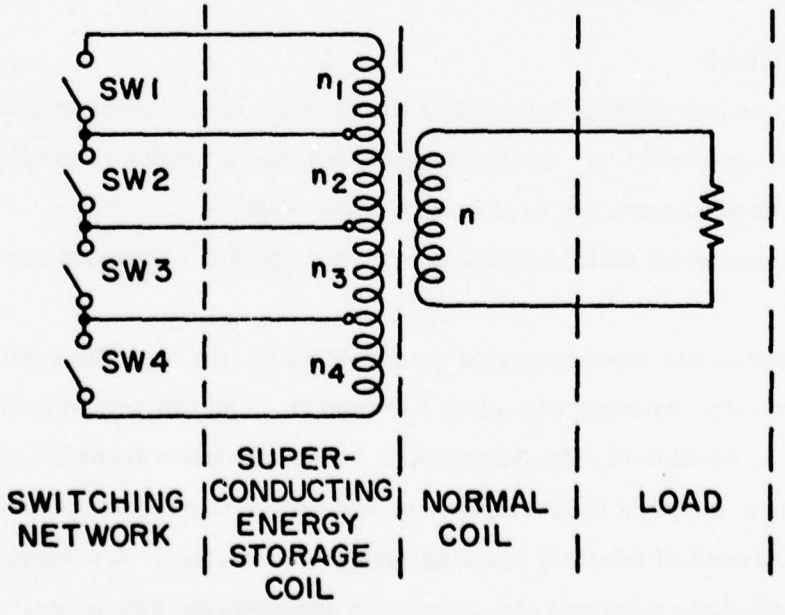

(c) MULTI-WINDING PRIMARY ENERGY EXTRACTION SYSTEM

Figure 8. Various Arrangements of Multi-Winding Pulse Power Systems.

6. APPROACH NO. 6

This approach effects the energy transfer from the superconducting coil to the load in a two-step process. The superconducting energy storage coil discharges at a much slower rate into a transfer coil which is a part of the wave-shaping PFN. The normal transfer coil then delivers the pulse at the specified discharge length. (See Figure 9.)

The idea here is to relax the operating conditions for the superconducting coil. Further, any losses which are encountered due to high frequencies in the network are outside of the dewar. The main problem with this approach is that the transfer of energy from one coil to the other requires storing of about 30% or more of pulse energy in capacitors. This will tend to defeat the very purpose of inductive energy storage. In addition, the volume and weight of a normal inductor, which has to work at a much lower current density than its superconducting counterpart, will be quite high. The resistive losses in a normal coil handling tens of kilojoules of energy must be reckoned with and will necessarily require additional cooling and thus additional weight and volume.

Careful consideration of these factors did not point favorably towards undertaking a detailed study of this approach beyond the preliminary analytical one which is also presented in Appendix C.

7. OTHER APPROACHES

Several other approaches were originally conceived which basically employ the same principles of energy storage as discussed in Approaches 1 through 3. However, these involve complex power conditioning, including pulse compression, hybrid (voltage and current fed combination) PFN's, etc., and were considered to be beyond the scope of this study.

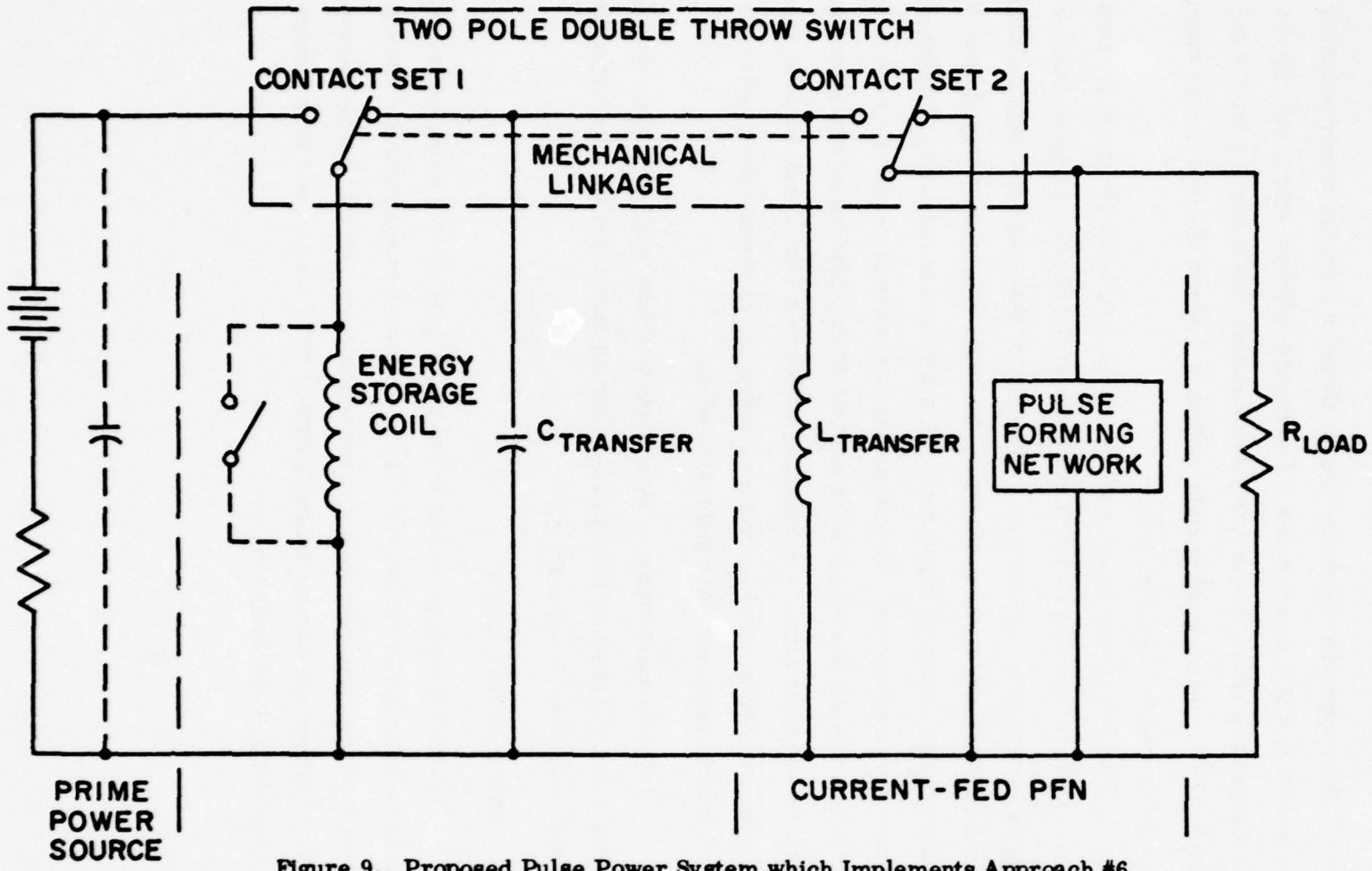

Figure 9. Proposed Pulse Power System which Implements Approach #6, a Superconducting Coil Combined with a Normal Transfer Coil.

SECTION II

MAGNET TOPOLOGY

There are two major types of coil configurations which are viable candidates for the present inductive energy storage system requirements. These are the toroidal coil geometry and the shielded solenoid geometry. The results of the comparative analysis of specific shielded solenoid and torus designs indicate that within the accuracy of the analysis, these inductor designs are comparable in size and weight. Although over parts of the operating range investigated, some variations in scaling characteristics seem to give one or the other configuration a slight edge, it is safe to conclude that for the purposes of the present investigation of high repetition rate inductive energy storage networks, the choice of one energy storage coil configuration over the other does not significantly impact the overall results and conclusions of the study.

The actual selection and detailed design of the energy storage coil configuration for a specific requirement, of course, is another matter. Here the subtle difference in performance capabilities ---especially inherent reliability, scalability, minimum risk and development -- become significant factors and must be studied in detail.

The unique feature of both of these configurations which distinguishes them from a multitude of possible candidates is that their fringe fields may be reduced to an arbitrarily low level without unduly compromising the simplicity and integrity of their design and without substantially sacrificing other critical performance parameters. These two coil configurations are compared in detail below.

1. BASIC TORUS AND SHIELDED SOLENOID GEOMETRIES

The torus configuration is characterized by the arrangement of the coil turns on a toroidal surface such that the magnetic field closes on itself inside the windings. The minor cross section of the windings need not be circular; however, the toroidal surface must be a surface of revolution (about the toroidal axis) if the individual windings are to operate under the same conditions of field and current distribution. If this consideration is relaxed, then the toroidal geometry may be altered to some advantage by flattening it to an oval or racetrack shape, thereby reducing the total system volume and "frontal" area. While the details of non-circular windings and noncircular torus configurations were not considered in this study, it should be mentioned here that both of these departures from the true torus geometry are worthy of consideration for high energy storage and physically large systems.

Noncircular windings of the type considered for large fusion reactor applications, the so-called "D" coil designs, can be essentially constant tension, self-supported structures with a central cylindrical member supporting the radial centering loads of the windings. This approach is definitely advantageous for large systems where the support structure for circular coils would be unnecessarily large. Similarly, distorting the circular torus into a race track geometry can also reduce the system volume; if combined with the constant tension "D" type coil design, where winding shape would vary along the perimeter of the "rack track torus", this could result in optimum utilization of the dewar volume and further reduction of system weight and volume.

The toroidal geometry dealt with in this study is illustrated in Figure 10. The overall torus parameters employed in the inductive energy storage system analysis discussed in the following sections are listed in Appendix B.

The shielded solenoid coil configuration achieves by design the same objective of negligibly low fringe fields which is inherent in the torus configuration. The geometry consists of a solenoidal main coil surrounded by a suitable

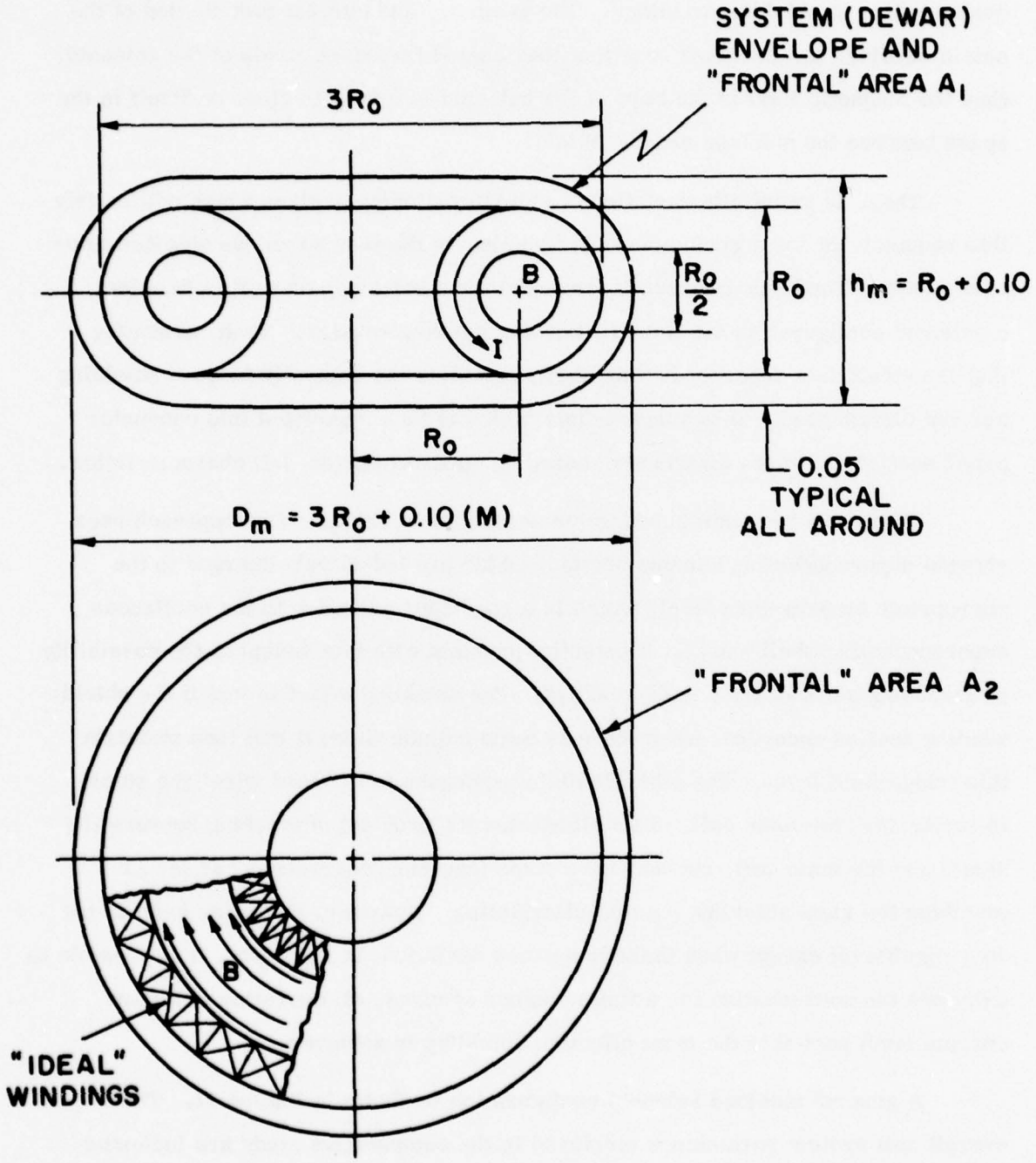

NOTE: THIS ASSUMES 0.05m DEWAR THICKNESS AND $\gamma = 0.5$

Figure 10. Typical Torus Configuration.

configuration of shielding windings. The geometry and current distribution of the shield windings are designed such that they cancel the fringe fields of the solenoid; thus the magnetic field in the bore of the solenoid is forced to close on itself in the space between the solenoid and the shield.

There is an infinite variation of shielding winding designs which will satisfy this requirement for a given solenoid, and clearly there is no unique shielded solenoid design. The basic procedure for designing a shielded solenoid is to select a solenoid configuration and a corresponding shield geometry. Then, assuming that the shield is a superconducting shell, calculate the naturally induced shielding current distribution. This current distribution is then translated into conductor cross section and turns distribution based on superconductor I-H characteristics.

There are two approaches to the actual shield design. One approach uses shorted superconducting winding sections which are inductively charged to the appropriate ampere-turn level, which is a good approximation to the continuous superconducting shell shield. A potential problem with this design is the possibility of quenching some of the shield windings. The shielding effect is lost if the shield winding section recovers when there is some outside field; it will then maintain this fringe field level. The other shielding approach is to "hard wire" the shield in series with the main coil. This eliminates the problem of tracking between the shield and the main coil, but may have some inherent "coarseness" as far as matching the ideal shielding current distribution. However, the latter point is not very significant except when there is a gross deviation; in any event, it is possible to calculate the best location for a finite number of turns, all operating at a fixed current level such that the most effective shielding is achieved.

A general shielded solenoid configuration is shown in Figure 11. The overall coil system parameters employed in the comparative study are indicated in this figure.

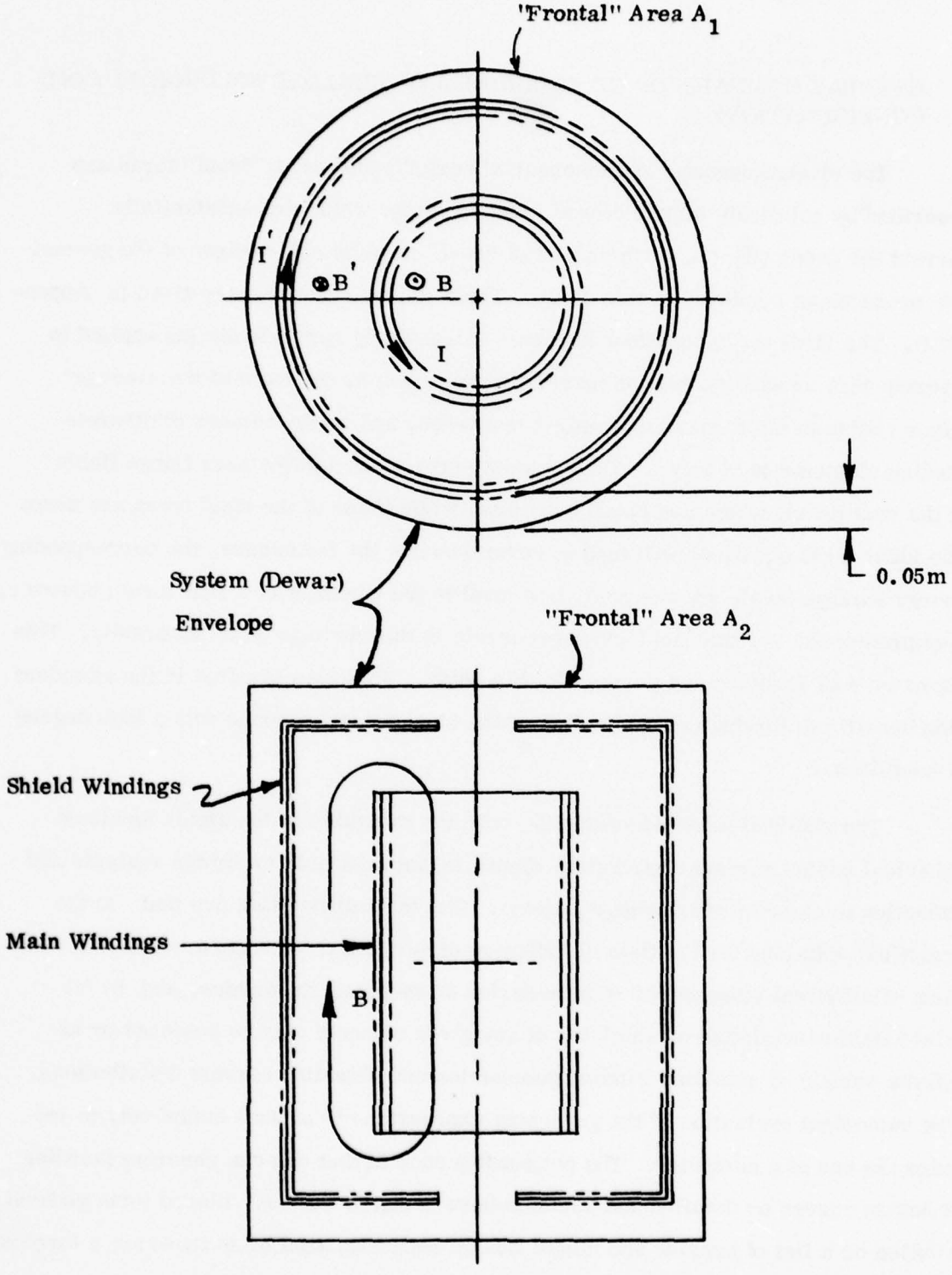

Figure 11. Typical Shielded Solenoid Configuration

2. GENERAL COMPARISION OF TOROIDAL AND SHIELDED SOLENOIDAL COIL CONFIGURATIONS

The electromagnetic and mechanical performance of an "ideal" torus are described by relatively simple closed form equations which are substantially correct for predicting the performance of "real" toroidal coil designs of the geometric proportions employed in this study. These design equations are given in Appendix B. The ideal torus equations become increasingly approximate (as applied to discrete turn or winding section toroidal geometries) as the ratio of the average minor radius to the torus major radius increases, and as the number of discrete winding elements is reduced. The greatest error occurs in the near fringe fields of the real torus, which are small but finite, while those of the ideal torus are zero. The ideal torus equations will tend to underestimate the inductance, the corresponding energy storage level, and the peak field level in the windings of a real torus; however, they predict the average field and force levels in the windings quite accurately. This approach was assumed and pursued in this study. This also resulted in the attendant side benefit of allowing the application of the ideal torus equations with a high degree of confidence.

The shielded solenoid geometry, with the exception of the highly idealized spherical cosine current distribution dipole, is not amenable to simple analysis and reduction to closed form design equations. The main difficulties are that a) the analytical solutions for the field distribution of solenoidal windings are either of the form of elliptical integrals or infinite series of spherical harmonics, and b) the fringe field cancellation or shielding of any given solenoid may be achieved by an infinite variety of shielding winding geometries and shielding current distributions. The numerical evaluation of the governing expressions is of such complexity to require the use of a computer. The net consequence is that one can generate families of design curves or detailed and scalable base designs, but not a closed form general solution or a list of concise and unique design equations similar to those for a toroidal coil geometry.

The scalability of all air core coil configurations is well established, and the laws for uniform geometrical scaling are given in Table 1 for reference. A set of "thin build" coil scaling laws is included in the table because of their utility for approximately scaling single-layer winding configurations of interest. This latter set of equations is valid where the thickness of the windings is much less than the winding radius (i.e., $\frac{\Delta r}{r} < 0.1$).

The geometric scaling of both the toroidal and the shielded solenoid coil configurations follow the same laws. However, the complexity of the analysis of shielded solenoids makes the use of scaling a particularly expedient design tool for evaluating various coil configurations.

3. VOLTAGE WITHSTAND CONSIDERATIONS

In general, a single layer coil winding lends itself to better high voltage withstand design than a multilayer winding. In the former, the turn to turn voltage can be maintained at moderate levels, and voltage related design constraints are generally associated with the coil terminations. In the latter case, however, successive winding layers overlap and an appreciable fraction of the terminal voltage (up to the full terminal voltage level) is imposed on coil turns in close proximity to each other.

The toroidal geometry, closing upon itself, creates an undesirable voltage problem of the nature described above --even for single layer windings. The electric field associated with the torus, particularly in the vicinity of the coil terminations, is a complex three-dimensional distribution which is difficult to analyze. The sensible design approach is to allow a generous safety margin in insulator thickness. Some voltage design problems can be reduced by the "double ended" torus configuration (see Figure 12) which utilizes two matched winding sections, operating electrically in parallel with opposed winding sense and with common terminals on diametrically opposite "ends" of the torus. The windings must be closely matched to achieve uniform division of the current in the two sections assuring a truly toroidal magnetic

TABLE 1

SCALING LAWS FOR GEOMETRICALLY SIMILAR COILS

	UNIFORM SCALING		THIN BUILD SCALING			
SCALING PARAMETERS / SCALED PARAMETER	J & r	(NI) & r	B & r	E & r	F & r	K & r
Current Density J	J	$(NI)/r^2$	B/r	$E^{1/2}/r^{5/2}$	$F^{1/2}/r^2$	-
Ampere Turns (NI)	Jr^2	(NI)	B_r	$E^{1/2}/r^{1/2}$	$F^{1/2}$	Kr
Field B	J_r	(NI)/r	B	$E^{1/2}/r^{3/2}$	$F^{1/2}/r$	K
Energy E	J^2r^5	$(NI)^2r$	B^2r^3	E	Fr	K^2r^3
Force F	J^2r^4	$(NI)^2$	B^2r^2	$E/_r$	F	K^2r^2
Sheet Current Density K	J_r	$(NI)/r$	B	$E^{1/2}/r^{3/2}$	$F^{1/2}/r$	K

NOTE:

a) Uniform Scaling - All coil dimensions are scaled by the same scaling factor and r represents any characteristic dimension of the coil.

b) Thin Build Scaling - The mean coil dimensions are scaled by the same scaling factor, but the build is not (see note below) and r represents any characteristic mean dimension of the coil.

c) Sheet Current Density - Product of current density and coil build ($K = J\Delta r$). For thin build scaling, this relationship determines the coil build.

d) Force - Any net force value such as hoop force per turn, axial compression loan in solenoid, circumferential compression load in Torus, etc.

SINGLE LAYER TORUS

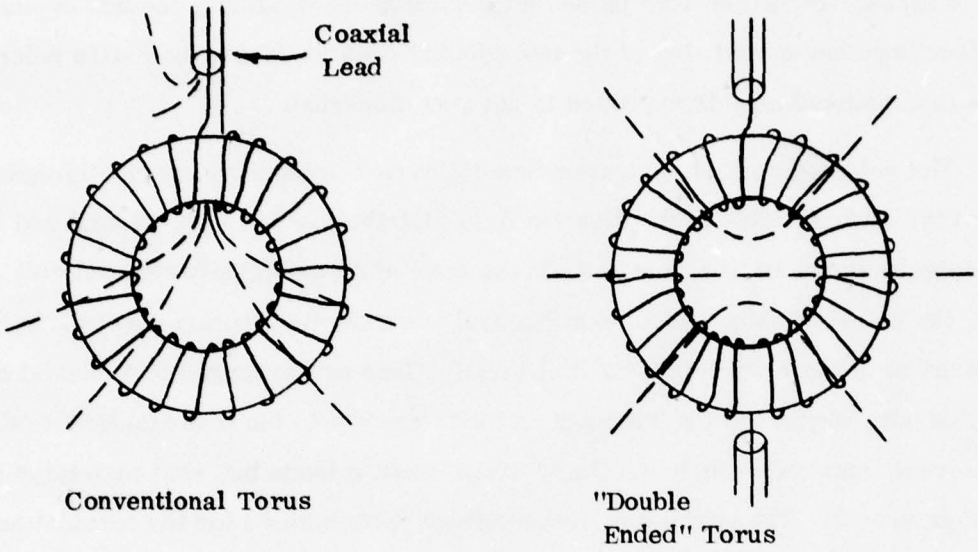

SINGLE LAYER SHIELDED SOLENOID

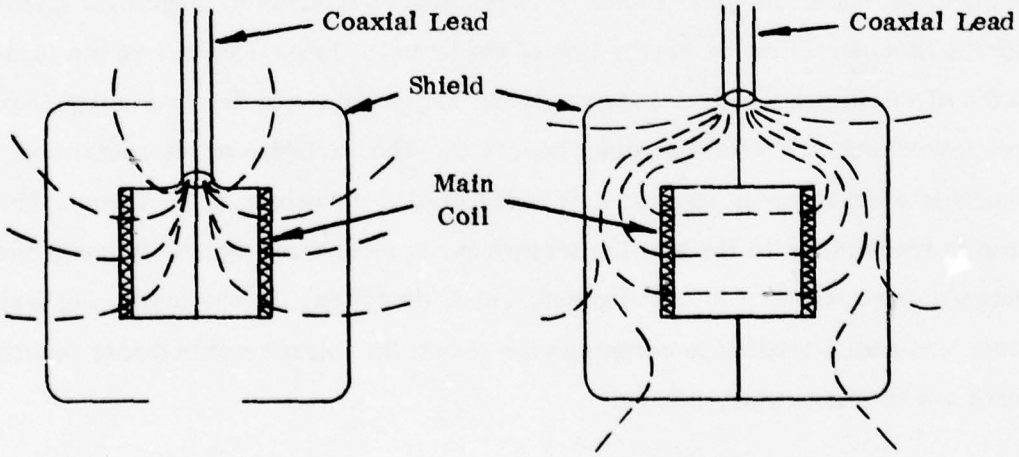

— — — — Denote Approximate Equipotential Lines

Figure 12. Voltage Distribution for Various Energy Storage Coil Configurations

field. With high repetition rate pulsed superconducting windings, the achievement of perfect impedance matching of the two winding regions during the entire pulse profile is questionable; this approach is not recommended.

The solenoid coil configuration has cylindrical symmetry which eliminates some of the uncertainties of the electric field distribution; but very careful and safe design practice is still required. In the case of an inductively charged coil shield, the shield windings assume a "natural" voltage distribution governed by the configuration of main windings; the coil terminations are arranged in a coaxial configuration with respect to the windings and with respect to the external lead design. The alternate approach employes "hard wired" return leads but still maintains a coaxial geometry. The variations in the voltage distributions for the toroidal and shielded solenoidal geometries discussed above are illustrated in Figure 12.

4. MECHANICAL CONSIDERATIONS

The magnetic body force on the turns of an ideal torus is radially outward (in the direction of the local radius of curvature) and varies in magnitude inversely with the distance from the center line of the torus. Lateral forces on the turns (in the circumferential direction around the major axis) are due to winding imperfections and not to inherent toroidal behavior. The variation of the radial body force results in a net force on each turn directed toward the center of the torus. This net force is transmitted to the winding form/support structure, which, in turn, develops a compressive reaction in the circumferential direction. In summary, the main forces are radial tending to compress the torus; the lateral turn support requirements are of a secondary nature.

A solenoidal coil necessarily has a two dimensional force distribution in the conductor due to the sizeable radial field components near the ends of the windings in addition to the axial field component. The radial field level can be substantially increased by closely spacing the shield windings. Furthermore, there may be a condition of unstable force equilibrium between the main coil and the shield wingings which must be taken up by the external support structure connecting the two

winding regions. This condition is very sensitive to the specific coil and shield geometry, and unstable translational and rotational displacement of the respective coil origins and axes may be triggered by mechanical misalignments and magnetic field perturbations due to coarse turn locations, leads and interconnections. The coil/shield mechanical stability is a potential problem to be carefully considered in the basic design.

The force analysis for a shielded solenoid is certainly a more complicated task than that for a torus. However, once the force levels and support requirements are established, the design of the winding support and the overall coil structure require the same care and comparable effort for both configurations. The detailed design of the support structure is dictated by the allowable strain and distortion of the windings, which is in turn governed by the limits imposed by the conductor and the turn geometry. Consequently, the mechanical environment of the conductor is a design constraint which will be comparable for both the torus and the shielded solenoid.

One mechanical consideration which may favor the shielded solenoid is the possible mechanical integration of the shield winding structure and the helium dewar shell. Due to the close proximity of the shield windings and the inner dewar shell, it appears feasible to derive additional support for the shield windings from the dewar wall.

5. OTHER CONSIDERATIONS

There are numerous important design criteria which must be satisfied in any successful superconducting inductive energy storage device. As the preceding general discussion indicates, some necessary design conditions may be more readily achieved in one or the other inductor geometry and, therefore, may be used as arguments for or against the choice of the coil configuration. Other design requirements are equally important, but are not all equally sensitive to the specific choice of coil geometry. For example, there is the matter of choice of wire, wire bundle configuration, specific conductor cooling methods, helium vapor purging requirements,etc. These considerations are important regardless of the specific magnet topology.

6. COMPOSITE WIRE AND OVERALL CONDUCTOR CHOICE

With the exception of highly anisotropic wire bundle configurations, it is very unlikely that the suitability of a given high frequency (AC) superconductor wire configuration will be contingent on the choice of the coil geometry. The torus has a directionally more uniform field distribution than the solenoid, and this fact may possibly be exploited to the benefit of some highly anisotropic conductor which has low tolerance to radial field or field sweep rates. However, for the presently envisioned conductors for the pulsed service required by the scope of this study, the choice of the coil geometry appears to have only a minor impact.

7. HEAT TRANSFER AND COOLING

The heat transfer requirements for a superconducting energy storage coil depend on both the specific wire and overall conductor selected for the specific operational approach to the application. The design of the cooling system, including the helium circulation throughout the windings to meet the heat transfer requirements, is essentially independent of the coil geometry for forced cooling design approaches. Forced helium cooling systems and the radially inward flow arrangement for the shielded solenoid have been discussed in detail in AF Contract #F33615-71-C-1455. This cooling concept is meritorious from the point of improving the overall voltage withstand capability of the coil. The shielded solenoid, perhaps, lends itself to a more straightforward implementation of this cooling scheme, but there is no inherent reason not to use this same approach for the torus.

8. COMPARISON OF SPECIFIC SHIELDED SOLENOID AND TOROIDAL COIL DESIGNS

A comparison between shielded solenoid and toroidal coil geometries was performed to evaluate the impact of the choice of the primary energy storage inductor configuration on the overall study objectives. The basic shielded solenoid geometries (a total of eight different cases) were derived from computer studies performed under AF Contract #F33615-71-C-1455. These coil configurations were then scaled to the specific operating conditions using the scaling laws given in Table 1.

The following assumptions were made for the coil system comparison:

a. Conductor operating characteristics and weight per ampere-meter as a function of peak field as given in Table 2 were used for the two configurations. The conductor operating characteristic in the shielded solenoids was evaluated separately for the main winding and for the shield windings on the basis of the respective peak field levels.

b. The structure weight for the toroidal systems is based on the following criteria:

i) A 3mm thick glass epoxy toroidal winding form.

ii) A toroidal glass epoxy compressive ring structure operating at a stress level of 10^8 Newtons/m^2.

iii) A hoop stress/winding pre-stress glass epoxy support structure operating at a stress level of 2×10^8 Newtons/m^2.

The structure weight for the shielded solenoids is based on the following criteria:

i) A 3mm thick glass epoxy main coil winding form.

ii) A 2mm thick glass epoxy shield coil winding form.

iii) A glass epoxy hoop stress support structure for both the main winding and the shield windings operating at an average tensile stress (i.e. pre-stress neglected) of 3.5×10^7 Newtons/m^2.

For both the torus and the shielded solenoid, a miscellaneous weight term corresponding to 10% of the sum of the conductor weight and the structure weight was added.

c. The dewar weight for both the torus and the shielded solenoid is based on the following expression (derived for the computer program employed in this study):

$$W_{Dewar} = 90 \, (V_{Dewar})^{0.913} \text{ (kg)}$$

TABLE 2

CONDUCTOR OPERATING CHARACTERISTICS FOR
1.1 Cu: NbTi (ASSUMING OVERALL MASS DENSITY OF
COMPOSITE EQUAL TO THAT OF COPPER)

B (T)	J_c ($10^9 A/m^2$)	$\overline{J_c}$ ($10^9 A/m^2$)	$\overline{J_{cp}}$ ($10^9 A/m^2$)	$\delta/\overline{J_{cp}}$ (kg/MA-m)
0	5.27	2.64	2.11	4.25
0.5	4.57	2.28	1.83	4.90
1.0	3.97	1.98	1.59	5.64
1.5	3.45	1.72	1.38	6.49
2.0	3.00	1.50	1.20	7.46
2.5	2.60	1.30	1.04	8.60
3.0	2.25	1.13	0.90	9.93
3.5	1.94	0.97	0.78	11.53
4.0	1.66	0.83	0.66	13.48
4.5	1.41	0.70	0.56	15.90
5.0	1.18	0.59	0.47	18.99
5.5	0.97	0.48	0.39	23.08
6.0	0.78	0.39	0.31	28.74

The dewar volumes are estimated as follows:

i) Torus: $V_{Dewar} = 1.1\, V_{Coil} + 0.005\ (m^3)$

were V_{Coil} is the volume generated by the surface of revolution of lateral projection of the maximum dimensions of the toroidal windings (i.e. a pill box with semi-toroidal sides).

ii) Shielded Solenoid: $V_{Dewar} = 1.1\, V_{Shield} + 0.005\ (m^3)$

where V_{Shield} is the shield winding volume based on the mean diameter and overall length.

d. Coil System Volume and "Frontal Areas":

i) Torus: the outer dimensions of the dewar are assumed to be 10cm greater overall than the maximum torus "pill box with semi-toroidal sides" defined above.

ii) Shielded Solenoid: The outer dimensions of the dewar are assumed to be 10cm greater overall than the mean diameter and the overall length of the shield winding.

iii) For each coil configuration, two "frontal areas" are computed on the basis of the above outer dewar dimensions projected along two orthogonal axes. This yields a minimum and a maximum system envelope frontal area, depending on the choice of coil orientation.

The attempt here is to compare the two coil configurations, as nearly as possible, on a common basis. While the respective data bases used for the two configurations are significantly different and are not internally optimized, the approach is adequate to ascertain whether one configuration is or is not clearly better than the other.

The results of the comparative analysis are presented in tabular form. The format of the tables and the specific parameters for the shielded solenoids are defined in Table 3. Similarly, the table format and the parameter definitions for the toroidal systems are given in Table 4.

TABLE 3

SHIELDED SOLENOID DEFINITION

TABLE FORMAT AND PARAMETER

VARIABLE	"X"	Appropriate Variable Parameter
MAIN WINDING	B_m	Max. Field at Conductor
	$\bar{D}$	Mean Winding Diameter
	ℓ	Winding Length
	W_c	Conductor Weight
	W_s	Structure/Support Weight
SHIELD WINDING	B_m	Max. Field at Conductor
	$\bar{D}$	Mean Winding Diameter
	ℓ	Winding Length
	W_c	Conductor Weight
	W_s	Structure/Support Weight
TOTAL SYSTEM	W_c	Conductor Weight
	W_s	Structure/Support Weight
	W_{Misc}	Miscellaneous Items Weights = $(W_c + W_s)/10$
	W_{Coil}	Coil Weight = $(W_c + W_s + W_{Misc})$
	W_d	Dewar Weight
	W_{tot}	Total Magnet System Weight
	D_m	Max. Dewar OD
	ℓ_m	Max. Dewar Length
	V_{tot}	Magnet System Envelope Volume
	A_1	Frontal Area w/Coil Axis Parallel to Forward Direction
	A_2	Frontal Area w/Coil Axis Perpendicular to Forward Direction

TABLE 4

TORUS DEFINITION

TABLE FORMAT AND PARAMETER

VARIABLE	"X"	Appropriate Variable Parameter
	B_m	Max. Field at Conductor
	R_o	Major Radius of Torus
	W_c	Conductor Weight
	W_s	Structure/Support Weight
	W_{Misc}	Miscellaneous Items Weight = $(W_c + W_s)/10$
	W_{Coil}	Coil Weight = $(W_c + W_s + W_{Misc})$
	W_d	Dewar Weight
	W_{tot}	Total Magnet System Weight
	D_m	Max. Dewar OD
	h_m	Max. Dewar Height
	V_{tot}	Magnet System Envelope Volume
	A_1	Frontal Area w/Torus Midplane Parallel to Forward Direction
	A_2	Frontal Area w/Torus Midplane Perpendicular to Forward Direction

The eight shielded solenoid geometries are compared at the 100 kJ energy storage level at 3T peak field in the main windings (Tables 5 and 6). The geometries designated A through D (Table 5) have a shield to main winding mean diameter ratio of 2/1; and the geometries designated E through H (Table 6) have a corresponding ratio of 1.6/1. For all of these shielded solenoid cases, the difference between the length of the shield and the length of the main winding normalized to the mean diameter of the shield windings is constant at 0.38. Systems with a 1.6 shield to main coil diameter ratio appear to be typically 10% lower in weight and about 40% lower in volume than the corresponding 2/1 ratio designs; the corresponding frontal areas are about 30% lower. However, one drawback to the lower aspect ratio designs is that the peak field level in the shield windings is nearly a factor of two higher. This may be a serious drawback for an inductively charged shield design, and may also add significantly to the AC losses at high repetition rates. On the whole, the geometries "E" through "H" appear to be more favorable than "A" to "D"; but the latter may be considered to be more conservative for the purposes of comparison with toroidal systems.

Two shielded solenoids (A and D) were investigated at fixed energy storage levels of 20 and 200 kJ at variable peak fields from 1 to 5 Tesla, and a comparable toroidal system (maximum minor radius to major radius ratio of 0.5) was evaluated at the same energies and fields ranging up to 6 Tesla. The data for the 20 kJ shielded solenoids is presented in Tables 7 and 8 for geometries A and D respectively, and the Torus data is given in Table 9. The 200 kJ results for the geometries are given in Tables 10, 11 and 12 respectively. All these coil configurations, at both energy levels, appear to exhibit an optimum field level at which the total coil system weight is at a minimum. The coil weight as a function of field level is different, as would be expected, and reflects the variation in the geometries and the corresponding scaling characteristics. The weight minima are a direct consequence of the decrease of the operating current density in the superconductor as the operating field is increased.

TABLE 5

SHIELDED SOLENOID GEOMETRY COMPARISON AT
$E = 100$ kJ and $B_{max} = 3$ T
$D_{Shield}/\overline{D}_{M.Coil} = 2\,(\ell_{Shield}-\ell_{M.Coil})/\overline{D}_{Shield} = 0.375$

		Coil Geometry			
		A	B	C	D
Main Winding	B_m (T)	3.00	3.00	3.00	3.00
	$\overline{D}$ (m)	0.20	0.22	0.25	0.32
	ℓ (m)	0.78	0.65	0.50	0.32
	W_c (kg)	15.30	14.00	12.60	10.90
	W_s (kg)	11.30	11.20	11.10	10.80
Shield Winding	B_m (T)	1.00	1.00	1.00	0.80
	$\overline{D}$ (m)	0.39	0.43	0.50	0.64
	ℓ (m)	0.93	0.81	0.69	0.56
	W_c (kg)	4.60	4.20	3.80	3.30
	W_s (kg)	9.20	9.20	9.20	9.30
Total System	W_c (kg)	19.80	18.30	16.40	14.30
	W_s (kg)	20.50	20.30	20.30	20.10
	W_{Misc} (kg)	4.00	3.80	3.70	3.40
	W_{Coil} (kg)	44.30	42.50	40.40	37.80
	W_d (kg)	13.80	14.70	16.40	21.00
	W_{Tot} (kg)	58.10	57.10	56.70	58.70
	D_m (m)	0.49	0.53	0.60	0.74
	ℓ_m (m)	1.03	0.91	0.79	0.66
	V_{Tot} (m^3)	0.19	0.20	0.22	0.28
	A_1 (m^2)	0.19	0.22	0.28	0.43
	A_2 (m^2)	0.51	0.49	0.47	0.49

TABLE 6

SHIELDED SOLENOID GEOMETRY COMPARISON AT
E = 100 kJ and B_{max} = 3 T

$D_{Shield}/\bar{D}_{M.\,Coil} = 1.6\ (\ell_{Shield} - \ell\ M.\,Coil)/\bar{D}_{Shield} = 0.375$

		Coil Geometry			
		E	F	G	H
Main Winding	B_m (T)	3.00	3.00	3.00	3.00
	$\bar{D}$ (m)	0.20	0.22	0.25	0.33
	ℓ (m)	0.63	0.52	0.40	0.26
	W_c (kg)	15.30	14.10	12.60	11.00
	W_s (kg)	6.50	6.40	6.30	6.60
Shield Winding	B_m (T)	2.00	1.90	1.90	1.60
	$\bar{D}$ (m)	0.31	0.35	0.40	0.53
	ℓ (m)	0.75	0.65	0.56	0.46
	W_c (kg)	7.30	6.80	6.10	5.10
	W_s (kg)	11.80	11.90	12.20	12.50
Total System	W_c (kg)	22.60	20.90	18.70	16.10
	W_s (kg)	18.20	18.30	18.50	19.10
	W_{Misc} (kg)	4.10	3.90	3.70	3.50
	W_{Coil} (kg)	44.90	43.10	40.80	38.60
	W_d (kg)	7.80	8.30	9.30	12.50
	W_{Tot} (kg)	52.70	51.40	50.20	51.20
	D_m (m)	0.41	0.45	0.50	0.63
	ℓ_m (m)	0.85	0.75	0.66	0.56
	V_{Tot} (m^3)	0.11	0.12	0.13	0.18
	A_1 (m^2)	0.14	0.16	0.20	0.30
	A_2 (m^2)	0.35	0.34	0.33	0.35

TABLE 7

SHIELDED SOLENOID - DESIGN A - OPERATING AT
E = 20 kJ

		Maximum Field Level (T)				
		1	2	3	4	5
Main Winding	B_m(T)	1.00	2.00	3.00	4.00	5.00
	$\bar{D}$ (m)	0.24	0.15	0.11	0.09	0.08
	ℓ (m)	0.95	0.60	0.46	0.38	0.33
	W_c(kg)	4.30	4.50	5.20	6.40	8.40
	W_s(kg)	6.00	3.40	2.70	2.40	2.20
Shield Winding	B_m(T)	0.30	0.70	1.00	1.30	1.70
	$\bar{D}$ (m)	0.48	0.30	0.23	0.19	0.16
	ℓ (m)	1.13	0.71	0.54	0.45	0.39
	W_c(kg)	1.90	1.60	1.60	1.60	1.60
	W_s(kg)	8.50	3.60	2.50	2.00	1.70
Total System	W_c(kg)	6.10	6.10	6.80	8.00	10.00
	W_s(kg)	14.50	7.00	5.10	4.30	3.90
	W_{Misc}(kg)	2.10	1.30	1.20	1.20	1.40
	W_{Coil}(kg)	22.60	14.40	13.10	13.50	15.20
	W_d (kg)	23.20	6.90	3.60	2.40	1.80
	W_{Tot}(kg)	45.80	21.30	16.70	15.90	17.10
	D_m(M)	0.58	0.40	0.33	0.29	0.26
	ℓ_m(m)	1.23	0.81	0.64	0.55	0.49
	V_{Tot} (m^3)	0.33	0.10	0.06	0.04	0.03
	A_1(m^2)	0.26	0.13	0.09	0.07	0.05
	A_2(m^2)	0.71	0.32	0.21	0.16	0.13

TABLE 8

SHIELDED SOLENOID - DESIGN D - OPERATING AT

E = 20 kJ

		Maximum Field Level (T)				
		1	2	3	4	5
Main Winding	$\bar{B}_m$ (T)	1.00	2.00	3.00	4.00	5.00
	$\bar{D}$ (m)	0.39	0.25	0.19	0.15	0.13
	ℓ (m)	0.39	0.25	0.19	0.15	0.13
	W_c (kg)	3.10	3.20	3.70	4.60	5.90
	W_s (kg)	4.60	2.90	2.40	2.20	2.10
Shield Winding	$\bar{B}_m$ (T)	0.30	0.60	0.80	1.10	1.40
	$\bar{D}$ (m)	0.78	0.49	0.37	0.31	0.27
	ℓ (m)	0.68	0.43	0.33	0.27	0.23
	W_c (kg)	1.40	1.20	1.10	1.10	1.10
	W_s (kg)	7.50	3.60	2.50	2.00	1.70
Total System	W_c (kg)	4.50	4.40	4.90	5.70	7.00
	W_s (kg)	12.20	6.50	4.90	4.20	3.80
	W_{Misc} (kg)	1.70	1.10	1.00	1.00	1.10
	W_{Coil} (kg)	18.40	12.00	10.80	10.90	11.90
	W_d (kg)	35.30	10.40	5.30	3.40	2.40
	W_{Tot} (kg)	53.70	22.40	16.00	14.30	14.30
	D_m (m)	0.88	0.59	0.47	0.41	0.37
	ℓ_m (m)	0.78	0.53	0.43	0.37	0.33
	V_{Tot} (m^3)	0.47	0.15	0.08	0.05	0.04
	A_1 (m^2)	0.60	0.27	0.18	0.13	0.11
	A_2 (m^2)	0.68	0.31	0.20	0.15	0.12

TABLE 9

TORUS -r_2/R_o = 0.5 - OPERATING AT
E = 20 kJ

	Maximum Field Level (T)					
	1	2	3	4	5	6
B_m (T)	1.00	2.00	3.00	4.00	5.00	6.00
R_o (m)	0.33	0.21	0.16	0.13	0.11	0.10
W_c (kg)	3.50	3.70	4.30	5.30	6.90	9.80
W_s (kg)	12.10	7.00	5.40	4.60	4.20	4.00
W_{Misc} (kg)	1.60	1.10	1.00	1.00	1.10	1.40
W_{Coil} (kg)	17.10	11.80	10.60	10.80	12.20	15.20
W_d (kg)	20.30	6.10	3.20	2.20	1.70	1.40
W_{Tot} (kg)	37.40	17.90	13.90	13.00	13.80	16.60
D_m (m)	1.08	0.72	0.57	0.49	0.44	0.40
h_m (m)	0.43	0.31	0.26	0.23	0.21	0.20
V_{Tot} (m^3)	0.33	0.10	0.06	0.04	0.03	0.02
A_1 (m^2)	0.42	0.20	0.13	0.10	0.08	0.07
A_2 (m^2)	0.92	0.41	0.26	0.19	0.15	0.12

TABLE 10

SHIELDED SOLENOID - DESIGN A - OPERATING AT

E = 200 kJ

		Maximim Field Level (T)				
		1	2	3	4	5
Main Winding	B_m (T)	1.0	2.0	3.0	4.0	5.0
	$\bar{D}$ (m)	0.51	0.32	0.25	0.20	0.18
	ℓ (m)	2.05	1.29	0.99	0.81	0.70
	W_c (kg)	19.90	20.80	24.20	29.90	39.10
	W_s (kg)	36.70	24.70	21.40	20.00	19.20
Shield Winding	B_m (T)	0.30	0.70	1.00	1.30	1.70
	$\bar{D}$ (m)	1.02	0.65	0.49	0.41	0.35
	ℓ (m)	2.43	1.53	1.17	0.97	0.83
	W_c (kg)	8.70	7.60	7.20	7.30	7.40
	W_s (kg)	40.50	21.70	16.50	14.20	12.90
Total System	W_c (kg)	28.50	28.40	31.50	37.20	46.50
	W_s (kg)	77.20	46.40	37.90	34.20	32.00
	W_{Misc} (kg)	10.60	7.50	7.00	7.10	7.90
	W_{Coil} (kg)	116.30	82.20	76.30	78.50	86.40
	W_d (kg)	185.30	52.70	25.40	15.30	10.30
	W_{Tot} (kg)	301.50	134.90	101.70	93.80	96.70
	D_m (m)	1.12	0.75	0.59	0.51	0.45
	ℓ_m (m)	2.53	1.63	1.27	1.07	0.93
	V_{Tot} (m^3)	2.49	0.72	0.35	0.22	0.15
	A_1 (m^2)	0.99	0.44	0.28	0.20	0.16
	A_2 (m^2)	2.85	1.22	0.75	0.54	0.42

TABLE 11

SHIELDED SOLENOID - DESIGN D - OPERATING AT

E = 200 kJ

		Maximum Field Level (T)				
		1	2	3	4	5
Main Winding	B_m (T)	1.00	2.00	3.00	4.00	5.00
	$\bar{D}$ (m)	0.84	0.53	0.40	0.33	0.29
	ℓ (m)	0.84	0.53	0.40	0.33	0.29
	W_c (kg)	14.20	15.00	17.40	21.40	28.00
	W_s (kg)	30.90	23.00	20.80	19.80	19.30
Shield Winding	B_m (T)	0.30	0.60	0.80	1.10	1.40
	$\bar{D}$ (m)	1.68	1.06	0.81	0.67	0.57
	ℓ (m)	1.47	0.92	0.71	0.58	0.50
	W_c (kg)	6.50	5.60	5.30	5.20	5.20
	W_s (kg)	40.40	21.70	16.60	14.40	13.10
Total System	W_c (kg)	20.70	20.50	22.60	26.60	33.20
	W_s (kg)	71.30	44.70	37.40	34.20	32.40
	W_{Misc} (kg)	9.20	6.50	6.00	6.10	6.60
	W_{Coil} (kg)	101.30	71.80	66.10	66.80	72.10
	W_d (kg)	286.70	81.10	39.00	23.30	15.60
	W_{Tot} (kg)	388.00	152.90	105.10	90.10	87.70
	D_m (m)	1.78	1.16	0.91	0.77	0.67
	ℓ_m (m)	1.57	1.02	0.81	0.68	0.60
	V_{Tot} (m^3)	3.01	1.08	0.53	0.32	0.21
	A_1 (m^2)	2.47	1.05	0.64	0.46	0.36
	A_2 (m^2)	2.78	1.18	0.73	0.52	0.40

TABLE 12

TORUS -r_2/R_o = 0.5 - OPERATING AT

E = 20 kJ

	Maximum Field Level (T)					
	1	2	3	4	5	6
B_m (T)	1.00	2.00	3.00	4.00	5.00	6.00
R_o (m)	0.73	0.46	0.35	0.29	0.25	0.22
W_c (kg)	28.20	29.60	34.50	42.50	55.60	79.30
W_s (kg)	76.20	48.10	41.20	38.30	36.90	34.80
W_{Misc} (kg)	10.40	7.80	7.60	8.10	9.30	11.40
W_{Coil} (kg)	114.80	85.50	83.30	88.90	101.80	125.50
W_d (kg)	175.40	49.80	24.00	14.40	9.80	7.20
W_{Tot} (kg)	290.20	135.30	107.30	103.30	111.60	132.70
D_m (m)	2.28	1.47	1.15	0.96	0.84	0.76
h_m (m)	0.83	0.56	0.45	0.39	0.35	0.32
V_{Tot} (m^3)	2.87	0.81	0.39	0.24	0.16	0.12
A_1 (m^2)	1.73	0.75	0.47	0.34	0.27	0.22
A_2 (m^2)	4.07	1.70	1.03	0.73	0.56	0.45

At 20 kJ energy storage level, the toroidal coil design reaches the lowest system weight of about 13 kg, followed by the design D solenoid at 14.3 kg and then the design A solenoid at 15.9 kg. The overall coil system volume (about 0.036 m^3) corresponding to these minimum weight design points is essentially the same for the three coil configurations. The minimum frontal area of the design A solenoid, however, is significantly lower than that of the other two configurations (about 0.07 m^2 compared with about 0.1m^2).

For 200 kJ operation, the results indicate that the torus is significantly heavier than the solenoids. The lowest weight reached by the toroidal system is 103 kg, while the design D solenoid attains a weight of 88 kg and the design A solenoid is between these extremes at 94 kg. The total system volumes are nearly equal; the solenoid system volumes are about 0.22 m^2 (each) and the torus system volume is slightly higher at about 0.24 m^3.

Tables 13, 14 and 15 present the results of the inductor system calculations for scaling with energy at a constant maximum field level of 3 Tesla at the conductor. These results clearly show the different scaling characteristics of the three coil geometries considered. The torus starts out as the lowest weight system (approx. 13.9 kg) at 20 kJ and ends up the highest weight system (approx. 107 kg) at 200 kJ. The opposite is true for the design A shielded solenoid which weighs 16.7 kg at 20 kJ and 102 kg at 200 kJ; the design D solenoid is between these extremes at 20 and 200 kJ, but for 50 kJ appears to be the minimum weight system at 33 kg. The total system volume for the torus is only slightly more than the design A solenoid (about the same at 20 kJ - 0.055 m^3 - and 0.39 vs 0.35 m^3 at 200 kJ) while the volume of the design D shielded solenoid is about 50% higher throughout the range of energies considered.

These results indicate that over the range of operating parameters investigated, the toroidal geometry and the shielded solenoid configurations are comparable in weight, volume and frontal area.

TABLE 13

SHIELDED SOLENOID - DESIGN A - OPERATING AT

$B_{Max} = 3$ T

		Energy Level (kJ)			
		20	50	100	200
Main Winding	B_m (T)	3.0	3.0	3.0	3.0
	$\bar{D}$ (m)	0.11	0.16	0.20	0.25
	ℓ (m)	0.46	0.62	0.78	0.99
	W_c (kg)	5.20	9.60	15.30	24.20
	W_s (kg)	2.70	6.00	11.30	21.40
Shield Winding	B_m (T)	1.00	1.00	1.00	1.00
	$\bar{D}$ (m)	0.23	0.31	0.39	0.49
	ℓ (m)	0.54	0.74	0.93	1.17
	W_c (kg)	1.60	2.90	4.60	7.20
	W_s (kg)	2.50	5.20	9.20	16.50
Total System	W_c (kg)	6.80	12.50	19.80	31.50
	W_s (kg)	5.10	11.20	20.50	37.90
	W_{Misc} (kg)	1.20	2.40	4.00	6.90
	W_{Coil} (kg)	13.10	26.10	44.30	76.30
	W_d (kg)	3.60	7.60	13.80	25.40
	W_{Tot} (kg)	16.70	33.70	58.10	101.70
	D_m (m)	0.33	0.41	0.49	0.59
	ℓ_m (m)	0.64	0.84	1.03	1.27
	V_{Tot} (m^3)	0.06	0.11	0.19	0.35
	A_1 (m^2)	0.09	0.13	0.19	0.28
	A_2 (m^2)	0.21	0.34	0.51	0.75

TABLE 14

SHIELDED SOLENOID - DESIGN D - OPERATING AT

$B_{Max} = 3\ T$

		Energy Level (kJ)			
		20	50	100	200
Main Winding	B_m (T)	3.00	3.00	3.00	3.00
	$\bar{D}$ (m)	0.19	0.25	0.32	0.40
	ℓ (m)	0.19	0.25	0.32	0.40
	W_c (kg)	3.70	6.90	10.90	17.40
	W_s (kg)	2.40	5.70	10.80	20.80
Shield Winding	B_m (T)	0.80	0.80	0.80	0.80
	$\bar{D}$ (m)	0.37	0.51	0.64	0.81
	ℓ (m)	0.33	0.44	0.56	0.71
	W_c (kg)	1.10	2.10	3.30	5.30
	W_s (kg)	2.50	5.20	9.30	16.60
Total System	W_c (kg)	4.90	9.00	14.30	22.60
	W_s (kg)	4.90	10.90	20.10	37.40
	W_{Misc} (kg)	1.00	2.00	3.40	6.00
	W_{Coil} (kg)	10.80	21.80	37.80	66.10
	W_d (kg)	5.30	11.40	21.00	39.00
	W_{Tot} (kg)	16.00	33.20	58.70	105.10
	D_m (m)	0.47	0.61	0.74	0.91
	ℓ_m (m)	0.43	0.54	0.66	0.81
	V_{Tot} (m^3)	0.08	0.16	0.28	0.53
	A_1 (m^2)	0.18	0.29	0.44	0.64
	A_2 (m^2)	0.20	0.33	0.49	0.73

TABLE 15

TORUS r_2/R_o = 0.5 - OPERATING AT

B_{Max} = 3 T

	Energy Level (kJ)				
	20	40	50	100	200
B_m (T)	3.00	3.00	3.00	3.00	3.00
R_o (m)	0.16	0.20	0.22	0.27	0.35
W_c (kg)	4.30	9.50	11.70	20.50	34.50
W_s (kg)	5.40	11.10	13.00	23.50	41.20
W_{Misc} (kg)	1.00	2.10	2.50	4.40	7.60
W_{Coil} (kg)	10.60	22.60	27.10	48.40	83.30
W_d (kg)	3.20	6.00	7.10	13.00	24.00
W_{Tot} (kg)	13.90	28.60	34.30	61.50	107.30
D_m (m)	0.57	0.71	0.75	0.91	1.15
h_m (m)	0.26	0.30	0.32	0.38	0.45
V_{Tot} (m^3)	0.06	0.10	0.12	0.20	0.39
A_1 (m^2)	0.13	0.20	0.21	0.31	0.47
A_2 (m^2)	0.26	0.40	0.44	0.65	1.03

SECTION III

SUPERCONDUCTOR MATERIAL SELECTION

It was stated in the introduction that a principal task in this project was to study the superconductor performance under the operating conditions. Therefore, after the computer program was developed, we performed a conductor optimization study and verified the trends of the superconductor losses projected by the program under varying conditions of the critical operating parameters. Sensitivities of the losses and of the conductor weight, etc. to the parameters - such as the B-field, pulse repetition rate, matrix metal resisitivity and thickness of normal matrix layer, etc., were also evaluated.

This section discusses the results and the conclusions drawn from these studies.

It was briefly mentioned in the introduction that under discharge time of the order of 20 - 40μs the rate of change of magnetic field in the superconductor will be about 10^5 Tesla/sec. This high value of $\dot{B}$ is expected to produce large AC losses in both the superconductor and the normal matrix which will tend to drive the superconductor normal. Therefore, the major task in using Type II superconductors for pulsed applications will be to develop intrinsically stable low AC loss conductors in which the flux jumping is either absent or the energy relased by a flux jump is reduced to such a low level that it does not degrade performance. Theory shows that a conductor with these properties will reach full DC critical current values without requiring means to stabilize it.[1] Apart from the point of view of superconductor stability, the losses should also be minimized in order to keep the volume of the cryogen boil-off and hence of the dewar to reasonable values.

---

[1] Brechna, H. - Superconducting Magnet Systems, P. 231, Springer-Verlag, Munich, FRG, 1973.

Losses in superconducting coils, when exposed to time-varying magnetic fields, have several origins which are described below:

1) Hysteretic or superconductor filament magnetization loss
2) Eddy current loss in the normal matrix
3) Self-field loss
4) Magnetization loss in the matrix due to coupling between filaments.

These are, however, only the inherent losses, determined by s.c. wire and material parameters, that are expected in a pulsed coil. There are other non-inherent losses present as well including losses due to conductor motion, mechanical design of coil, conductor bundle and the coil support structure, and electromagnetic losses ($\vec{J} \times \vec{B} \cdot \vec{v}$ type) arising out of cable and braid geometries.

While inherent losses can be expressed analytically, the non-inherent losses certainly are not so amenable to any analytic approach. Since these losses depend so much on the peculiarities of a specific magnet configuration, we do not expect their theoretical predictions to be realistic. Accurate prediction will require sound experimental results which are unfortunately lacking. We believe that our loss equations reasonably predict the inherent losses; we do not claim that absolute figures of total loss are exact.

Now we will present some data reduced from computer output to describe the nature of dependency of different loss mechanisms on the critical parameters - specifically: magnitude of B-field, repetition rate and matrix metal resistivity. The equations which determine these losses are described in detail in Appendix B of this report.

A typical sample of the computer printout is shown on pages 47 and 48. On page 48, are reproduced the results of the energy storage coil design which includes such parameters as the peak energy stored, maximum B-field, winding weight and volume, etc. The output corresponds to a run which designed a coil for full discharge case operating at a 3 Tesla maximum field, energy level of 20 kJ and a pulse repetition rate of 200 pps. On page 48, the computed values of the different losses from this run are printed.

FULL DISCHARGE CASE (APPROACH NO. -1)

ENERGY STORAGE COIL DESIGN VARIABLES

ELECTROMAGNETIC PARAMETERS

ENERGY STORED PER PULSE	1.842E+04	J
INDUCTANCE OF THE ENERGY STORAGE COIL	5.526E-05	H
PEAK COIL CURRENT	2.582E+04	A
PEAK COIL VOLTAGE	5.640E+04	V
VOLTS PER TURN	1.457E+03	V
MAXIMUM MAGNETIC FIELD	3.000E+00	TESLA
CRITICAL CURRENT DENSITY AT ZERO FIELD	5.270E+09	A/M2
S.C. DESIGN CURRENT DENSITY	1.000E+09	A/M2
CRITICAL CURRENT DENSITY AT OPERATING FIELD	2.694E+09	A/M2

PHYSICAL PARAMETERS OF TORUS

MAJOR RADIUS OF THE TORUS	1.575E-01	M
MINOR RADIUS OF THE TORUS	3.937E-02	M
MEAN RADIUS OF THE WINDING	7.875E-02	M
TOROID MEAN MINOR RADIUS / MAJOR RADIUS	2.500E-01	--
TOROID MEAN WINDING RADIUS / MAJOR RADIUS	5.000E-01	--
FRONTAL AREA OF THE COIL	1.860E-02	M2

WINDING PARAMETERS

AREA OF S.C. / AREA OF COMPOSITE CORE	5.000E-01	--
AREA OF COMPOSITE CORE / AREA OF WIRE	9.800E-01	--
AREA OF WIRES / AREA OF BRAID	3.300E-01	--
AREA OF BRAIDS / AREA OF CABLE	3.300E-01	--
NO. OF TURNS IN THE WINDING	3.872E+01	--
MEAN LENGTH PER TURN	3.720E-01	M
DIAMETER OF EACH SUPERCONDUCTING FILAMENT	6.000E-06	M
DIAMETER OF THE COMPOSITE CORE	1.697E-04	M
DIAMETER OF EACH WIRE	1.714E-04	M
DIAMETER OF EACH CIRCULAR BRAID	2.984E-03	M
MEAN DIAMETER OF PURE MATRIX LAYER	1.706E-04	M
AREA OF EACH BRAID	6.994E-06	M2
AREA OF CABLE CONSISTING OF ONE OR MORE BRAIDS	2.755E-04	M2
AREA OF COMPOSITE CORE PER WIRE	2.262E-08	M2
TOTAL AREA OF SUPERCONDUCTOR IN THE CABLE	1.491E-05	M2
AREA OF SUPERCONDUCTOR PER WIRE	1.131E-08	M2
NO. OF BRAIDS IN THE CABLE	1.300E+01	--
TOTAL NO. OF WIRES REQUIRED	1.318E+03	--

WINDING WEIGHTS AND VOLUMES

TOTAL VOLUME OF MATRIX MATERIAL IN THE COIL	2.234E-04	M3
VOLUME OF CU IN THE MATRIX LAYER	8.762E-06	M3
TOTAL VOLUME OF S.C. MATERIAL	2.147E-04	M3
WEIGHT OF WINDING MATERIAL	3.855E+00	KG
WEIGHT OF S.C. MATERIAL	1.889E+00	KG

FULL DISCHARGE CASE (APPROACH NO. -1)

ENERGY STORAGE COIL LOSSES

CHARGING LOSSES

EDDY CURRENT LOSS DURING CHARGING	2.250E-02 J
FILAMENT MAG LOSS DURING CHARGING	1.316E+00 J
SELF FIELD LOSS DURING CHARGING	3.854E-02 J
MATRIX CHARGING LOSS DUE TO FILAMENT COUPLING	1.096E+01 J
TOTAL CHARGING LOSS	1.234E+01 J

DISCHARGE LOSSES

EDDY CURRENT LOSS DURING DISCHARGE	4.996E+00 J
FILAMENT MAG LOSS DURING DISCHARGE	1.316E+00 J
SELF FIELD LOSS DURING DISCHARGE	3.854E-02 J
MATRIX DISCHARGE LOSS DUE TO FILAMENT COUPLING	2.586E+01 J
TOTAL DISCHARGE LOSS	3.221E+01 J
TOTAL LOSS PER PULSE	4.455E+01 J

Table 16 is a summary of computer runs performed to study the sensitivity of losses to $\dot{B}$. The maximum design flux density was kept constant at 3 Tesla and the pulse repetition rate was varied from 5 to 10,000 pps. The discharge time was kept constant at $30\mu s$, so $\dot{B}$ did not charge during the discharge ramp. However, $\dot{B}$ changes during the charging cycle as the rep rate is changed.

Using $\dot{B}_d$ and $\dot{B}_c$ to represent the rates of change of B-field during the discharge and charging ramps respectively, we have:

$$\dot{B}_d = -(B_2 - B_1)/T_d \tag{1}$$

$$\dot{B}_c = (B_2 - B_1)/T_c \tag{2}$$

$$T_c = T - T_d = (\frac{1}{f} - T_d) \tag{3}$$

$$\therefore \dot{B}_c = \Delta B/(\frac{1}{f} - T_d) \tag{4}$$

Where

B_2 & B_1 are fields at the start and end of each discharge pulse

f is the pulse frequency

T_c, T_d and T are the charging time, discharge time and pulse width respectively.

Since $T_d << \frac{1}{f}$ for f within our operating range,

$$\dot{B}_c \approx \Delta B\, f$$

or

$$\dot{B}_c \sim B_2\, f \text{ for } B_1 << B_2 \tag{5}$$

Equation (5) shows that the $\dot{B}$ during charging is approximately proportional to the pulse repetition rate.

TABLE 16

CONDUCTOR OPTIMIZATION SERIES

TO STUDY SENSITIVITY OF LOSSES TO $\hat{B}$

Series No.	Operating Resistivity at Zero-Field ρ_o	Matrix Surface Layer λ	PPS Range
A	1.78×10^{-10}	0.90	5 - 1,000
B1	1.0×10^{-9}	0.90	5 - 10,000
B2	1.0×10^{-9}	0.98	5 - 10,000
C1	1.0×10^{-8}	0.90	5 - 10,000
C2	1.0×10^{-8}	0.98	5 - 10,000
D1	1.0×10^{-7}	0.90	5 - 10,000
D2	1.0×10^{-7}	0.98	5 - 10,000

NOTE:

1) For all the above runs, a maximum B-field of 3 Tesla was used.
2) Approach No. 1 (full discharge) was assumed.
3) Energy per pulse = 20 KJ.

While each series in the computer run summary table provides us with the data regarding dependency of the losses on repetition rate, inter-series comparison in its turn will reveal the effects of matrix resistivity and the thickness of the normal matrix layer in the superconducting wire.

Table 17 outlines the runs performed to study the effects of both ΔB and $\dot{B}$. Three different repetition rates (5, 50, and 500 pps) were used. The results of these computer runs are tabulated on Tables 25 through 33.

Tables 18 through 24 are summarized results obtained from computer runs corresponding to Series A through D2 as described in Table 16. Series A, B1, C1 and D1 will be compared to evaluate the effect of matrix resistivity. All of these have the same matrix layer thickness ratio of 0.9. Runs B2, C2, and D2 are similar to A - D1 with the exception that these have a higher layer thickness ratio of 0.98.

It is seen from the table that filament magnetization loss and the self-field loss do not depend on $\dot{B}$. These two losses remain unchanged during the charging and discharge ramps, although the discharge $\dot{B}$ is higher by a few orders of magnitude than the charging $\dot{B}$. Further, the self-field loss constitutes an insignificant part of the total loss, being less than 1% of even the lowest value of the charging loss. This is, however, expected in composite cores of diameter $\sim$ 0.1 cm or less. Given a large number of filaments, the coupling effect becomes dominant. In fact, the coupling constitutes the largest percentage of the total losses during both charging and discharging modes. The total losses increase with increasing B-field level. The data in Tables 25 to 35 indicate that the filament magnetization loss, self-field loss and filament coupling loss each go through a maximum and then decrease at higher fields. This is due to the decrease of the total conductor volume of the coils based on a fixed energy level and constant operating current density. The loss per unit conductor volume, however, increases with increasing field level.

TABLE 17

B-FIELD OPTIMIZATION SERIES

TO STUDY SENSITIVITY OF LOSSES TO ΔB and $\mathring{B}$

Series No.	Approach No.	Reps	Initial Energy Stored	B-Field
E1	1	5	20 KJ	1 - 6 Tesla
E2	1	50	20 KJ	1 - 6 Tesla
E3	1	500	20 KJ	1 - 6 Tesla
F1	2	5	40 KJ	1 - 6 Tesla
F2	2	50	40 KJ	1 - 6 Tesla
F3	2	500	40 KJ	1 - 6 Tesla
F4	2	5	200 KJ	1 - 6 Tesla
F5	2	50	200 KJ	1 - 6 Tesla
F6	2	500	200 KJ	1 - 6 Tesla
G1	3	5	8 MJ	1 - 6 Tesla
G2	3	50	80 MJ	1 - 6 Tesla

NOTE:

1) Energy per pulse in all of the above cases = 20 KJ

TABLE 18

CONDUCTOR OPTIMIZATION STUDY

COMPUTER RUN SERIES A

Conditions:

Approach #1

W_{pulse} = 20 kJ

B_{max} = 3 Tesla

ρ_{300} = 17.8 nΩ-m

ρ_r = 100

ρ_o = 1.78×10^{-10} Ω-m

Matrix Layer Surface $\lambda = 0.90$

Breakdown of Losses per Pulse

Pulse Rep Rate (pps)	Eddy Current (J)	Filament * Magnetization (J)	Self * Field (mJ)	Filament Coupling (J)	Total (J)	Total (ch+disch) (J)
Disch*	26.96	1.316	38.54	28.86	54.14	-
5	.6175	1.316	38.54	3.328	5.29	59.43
10	.6166			6.229	8.195	62.34
20	.6198			10.96	12.93	67.08
40	.6364			17.28	19.27	73.41
100	.6861			24.23	26.26	80.41
200	.7694			25.76	27.89	82.02
400	.9374			25.86	28.15	82.28
1000	1.453			25.86	28.67	82.78

* Characteristics for discharge, filament magnetization and self-field losses are independent of pulse repetition rate.

TABLE 19

CONDUCTOR OPTIMIZATION STUDY

COMPUTER RUN SERIES B-1

Conditions:

Approach #1

W_{pulse} = 20 kJ

B_{max} = 3 Tesla

ρ_{300} = 17.8 mΩ-m

ρ_r = 17.8

ρ_o = 1.0×10^{-9} Ω-m

Matrix Layer Surface λ = 0.90

Breakdown of Losses per Pulse

Pulse Rep Rate (pps)	Eddy Current (mJ)	Filament * Magnetization (J)	Self * Field (mJ)	Filament Coupling (J)	Total (J)	Total (ch+disch) (J)
Disch*	8313	1.316	38.54	25.86	35.53	---
5	25.09	1.316	38.54	.6876	2.076	37.60
10	26.29			1.357	2.738	38.27
20	26.29			2.644	2.738	38.27
40	33.81			5.020	6.408	41.94
100	44.80			10.80	12.20	47.73
200	74.12			17.12	18.55	54.08
400	125.00			22.94	24.42	59.95
1000	281.60			25.76	27.40	62.93

* Characteristics for discharge, filament magnetization and self-field lossess are independent of pulse repetition rate.

TABLE 20

CONDUCTOR OPTIMIZATION STUDY

COMPUTER RUN SERIES B-2

Conditions:

Approach #1

W_{pulse} = 20 kJ

B_{max} = 3 Tesla

ρ_{300} = 17.8 nΩ-m

ρ_r = 17.8

ρ_o = 1.0×10^{-9} Ω-m

Matrix Layer Surface λ = 0.98

	Breakdown of Losses per Pulse					
Pulse Rep Rate (pps)	Eddy Current (mJ)	Filament * Magnetization (J)	Self * Field (mJ)	Filament Coupling (J)	Total (J)	Total (ch+disch) (J)
Disch*	1473	1.316	38.54	25.86	28.69	---
5	.9911	1.316	38.54	.6876	2.043	30.73
10	1.211			1.357	2.713	31.40
20	1.653			2.644	4.000	32.69
40	2.539			5.020	6.372	35.07
100	5.202			10.80	12.16	40.85
200	9.662			17.12	18.48	47.17
400	18.66			22.94	24.32	53.01
1000	46.34			25.76	27.16	55.85

* Characteristics for discharge, filament magnetization and self-field losses are independent of pulse repetition rate.

TABLE 21

CONDUCTOR OPTIMIZATION STUDY

COMPUTER RUN SERIES C-1

Conditions:

Approach #1

W_{pulse} = 20 kJ

B_{max} = 3 Tesla

ρ_{300} = 10 nΩ-m

ρ_r = 1.0

ρ_o = 1.0×10^{-8} Ω-m

Matrix Layer Surface λ = 0.90

Breakdown of Losses per Pulse

Pulse Rep Rate (pps)	Eddy Current (mJ)	Filament * Magnetization (J)	Self * Field (mJ)	Filament Coupling (J)	Total (J)	Total (ch+disch) (J)
Disch*	843.0	1.316	38.54	25.86	28.06	---
5	6.515	1.316	38.54	.07101	1.432	29.49
10	6.598			.1418	1.503	29.56
20	6.853			.2830	1.644	29.71
40	7.364			.5632	1.925	29.99
100	8.899			1.388	2.751	30.81
200	11.470			2.708	4.074	32.14
400	16.660			5.161	6.532	34.59
1000	32.60			11.19	12.58	40.64

* Characteristics for discharge, filament magnetization and self-field losses are independent of pulse repetition rate.

TABLE 22

CONDUCTOR OPTIMIZATION STUDY

COMPUTER RUN SERIES C-2

Conditions:

Approach #1

W_{pulse} = 20 kJ

B_{max} = 3 Tesla

ρ_{300} = 10 nΩ-m

ρ_r = 1.0

ρ_o = 1.0×10^{-8} Ω-m

Matrix Layer Surface $\lambda = 0.98$

Breakdown of Losses per Pulse

Pulse Rep Rate (pps)	Eddy Current (mJ)	Filament * Magnetization (J)	Self * Field (mJ)	Filament Coupling (J)	Total (J)	Total (ch+disch) (J)
Disch*	151.0	1.316	38.54	25.86	27.37	---
5	.2291	1.316	38.54	.07101	1.426	28.79
10	.2503			.1418	1.497	28.87
20	.2957			.2830	1.638	29.01
40	.3866			.5632	1.918	29.29
100	.6600			1.388	2.743	30.11
200	1.1180			2.708	4.064	31.43
400	2.0420			5.161	6.518	33.89
1000	4.8820			11.190	12.55	39.92

* Characteristics for discharge, filament magnetization and self-field losses are independent of pulse repetition rate.

TABLE 23

CONDUCTOR OPTIMIZATION STUDY

COMPUTER RUN SERIES D-1

Conditions:

Approach #1

W_{pulse} = 20 kJ

B_{max} = 3 Tesla

ρ_{300} = 100 nΩ-m

ρ_r = 1.0

ρ_o = 1.0×10^{-7} Ω-m

Matrix Layer Surface λ = 0.90

Breakdown of Losses per Pulse

Pulse Rep Rate (pps)	Eddy Current (mJ)	Filament * Magnetization (J)	Self * Field (mJ)	Filament Coupling (J)	Total (J)	Total (ch+disch) (J)
Disch*	86.46	1.316	38.54	12.38	13.82	---
5	.01297	1.316	38.54	.002526	1.357	15.17
10	.02595			.005057	1.360	15.18
20	.05191			.01012	1.365	15.19
40	.1039			.02024	1.375	15.20
100	.2602			.05066	1.406	15.23
200	.5219			.1015	1.457	15.28
400	1.050			.2039	1.560	15.38
1000	2.674			.5160	1.873	15.70

* Characteristics for discharge, filament magnetization and self-field losses are independent of pulse repetition rate.

TABLE 24

CONDUCTOR OPTIMIZATION STUDY

COMPUTER RUN SERIES D-2

Conditions:

Approach #1

W_{pulse} = 20 kJ

B_{max} = 3 Tesla

ρ_{300} = 100 nΩ-m

ρ_r = 1.0

ρ_o = 1.0×10^{-7} Ω-m

Matrix Layer Surface λ = 0.98

Breakdown of Losses per Pulse

Pulse Rep Rate (pps)	Eddy Current (mJ)	Filament * Magnetization (J)	Self * Field (mJ)	Filament Coupling (J)	Total (J)	Total (ch+disch) (J)
Disch*	5.470	1.316	38.54	12.38	13.74	---
5	3.236	1.316	38.54	.002526	1.360	15.10
10	3.236			.005057	1.363	15.11
20	3.238			.01012	1.368	15.11
40	3.243			.02024	1.378	15.12
100	3.259			.05066	1.409	15.15
200	3.285			.1015	1.459	15.20
400	3.338			.2039	1.562	15.31
1000	3.494			.5160	1.874	15.62

* Characteristics for discharge, filament magnetization and self-field losses are independent of pulse repetition rate.

TABLE 25

B-FIELD OPTIMIZATION STUDY

COMPUTER RUN SERIES E-1

Conditions

Approach #1

W_{pulse} = 20 kJ

$W_{initial}$ = 20 kJ

ρ_{300} = 17.8 nΩ-m

ρ_r = 100

Matrix Layer thickness Ratio = 0.98

Pulse Rep Rate = 5 pps

Breakdown of Losses per Pulse

B_m (T) Charging	Eddy Current (mJ)	Filament * Magnetization (J)	Self * Field (mJ)	Filament Coupling (J)	Total (J)	Total (ch+disch)
1	.1946	.7322	63.31	.5953	1.391	
2	.5857	1.088	47.42	1.785	2.921	
3	1.097	1.316	38.54	3.328	4.684	
4	1.694	1.446	31.85	5.117	6.596	
5	2.356	1.480	25.92	7.088	8.576	
6	3.070	1.405	20.03	9.188	10.62	
Disch.	**(J)**			**(J)**	**(J)**	**(J)**
1	1.297			14.44	16.53	17.92
2	3.904			21.39	26.43	29.35
3	7.309			25.86	34.53	39.21
4	11.29			28.41	41.18	47.77
5	15.70			29.09	46.30	54.89
6	20.46			27.64	49.53	60.14

* Losses due to filament magnetization and self-field are equal for charging and discharging conditions.

TABLE 26

B-FIELD OPTIMIZATION STUDY

COMPUTER RUN SERIES E-2

Conditions:

Approach #1

W_{pulse} = 20 kJ

$W_{initial}$ = 20 kJ

ρ_{300} = 17.8 nΩ-m

ρ_r = 100

Matrix Layer Thickness Ratio = 0.98

Pulse Rep Rate = 50 pps

Breakdown of Losses per Pulse

B_m (T) Charging	Eddy Current (mJ)	Filament * Magnetization (J)	Self * Field (mJ)	Filament Coupling (J)	Total (J)	Total (ch+disch)
1	1.949	.7322	63.31	4.967	5.765	
2	5.864	1.088	47.42	12.45	13.59	
3	10.98	1.316	38.54	19.35	20.72	
4	16.96	1.446	31.85	24.52	26.02	
5	23.59	1.480	25.92	27.31	28.84	
6	30.74	1.405	20.03	27.15	28.61	
Disch.	**(J)**			**(J)**	**(J)**	**(J)**
1	1.297			14.44	16.53	22.30
2	3.904			21.39	26.43	40.02
3	7.309			25.86	34.53	55.24
4	11.29			28.41	41.18	67.19
5	15.70			29.09	46.30	75.14
6	20.46			27.64	49.53	78.14

* Losses due to filament magnetization and self-field are equal for charging and discharging conditions.

TABLE 27

B-FIELD OPTIMIZATION STUDY

COMPUTER RUN SERIES E-3

Conditions:

Approach #1

W_{pulse} = 20 kJ

$W_{initial}$ = 20 kJ

ρ_{300} = 17.8 nΩ-m

ρ_r = 100

Matrix Layer Thickness Ratio = 0.98

Pulse Rep Rate = 500 pps

Breakdown of Losses per Pulse

B_m (T) Charging	Eddy Current (mJ)	Filament * Magnetization (J)	Self * Field (mJ)	Filament Coupling (J)	Total (J)	Total (ch+disch)
1	19.76	.7332	63.31	14.24	15.05	
2	59.45	1.088	47.42	21.39	22.58	
3	111.3	1.316	38.54	25.86	27.33	
4	171.9	1.446	31.85	28.41	30.06	
5	239.2	1.480	25.92	29.09	30.83	
6	311.6	1.405	20.03	27.64	29.37	
Disch.	(J)			(J)	(J)	(J)
1	1.297			14.44	16.53	31.59
2	3.904			21.39	26.43	49.01
3	7.309			25.86	34.53	61.86
4	11.29			28.41	41.18	71.24
5	15.70			29.09	46.36	77.13
6	20.46			27.64	49.53	78.90

* Losses due to filament magnetization and self-field are equal for charging and discharging conditions.

TABLE 28

B-FIELD OPTIMIZATION STUDY

COMPUTER RUN SERIES F-1

Conditions:

Approach #2

W_{pulse} = 20 kJ

$W_{initial}$ = 40 kJ

ρ_{300} = 17.8 nΩ-m

ρ_r = 100

Matrix Layer Thickness Ratio = 0.98

Pulse Rep Rate = 5 pps

Breakdown of Losses per Pulse

B_m (T) Charging	Eddy Current (mJ)	Filament * Magnetization (J)	Self * Field (mJ)	Filament Coupling (J)	Total (J)	Total (ch+disch)
1	2.616	.4151	.7852	5.057	5.475	
2	7.589	.5707	.5676	9.711	10.29	
3	13.74	.6475	.4423	12.07	12.73	
4	20.51	.6642	.3479	12.69	13.38	
5	27.79	.6275	.2672	12.06	12.71	
6	35.25	.5385	.1927	10.35	10.93	
Disch.	**(J)**			**(J)**	**(J)**	**(J)**
1	.1718			7.640	8.228	13.70
2	.4984			10.80	11.87	22.16
3	.9020			12.37	13.92	26.65
4	1.350			12.74	14.76	28.13
5	1.826			12.06	14.51	27.22
6	2.315			10.35	13.20	24.13

* Losses due to filament magnetization and self-field are equal for charging and discharging conditions.

TABLE 29

B-FIELD OPTIMIZATION STUDY

COMPUTER RUN SERIES F-2

Conditions:

Approach #2

W_{pulse} = 20 kJ

$W_{initial}$ = 40 kJ

ρ_{300} = 17.8 nΩ-m

ρ_r = 100

Matrix Layer Thickness Ratio = 0.98

Pulse Rep Rate = 50 pps

Breakdown of Losses per Pulse

B_m (T) Charging	Eddy Current (mJ)	Filament * Magnetization (J)	Self * Field (mJ)	Filament Coupling (J)	Total (J)	Total (ch+disch)
1	.2581	.4151	.7852	.7750	1.191	
2	.7487	.5707	.5676	2.187	2.759	
3	1.355	.6475	.4423	3.810	4.459	
4	2.028	.6642	.3479	5.399	6.066	
5	2.741	.6275	.2672	6.712	7.342	
6	3.477	.5385	.1927	7.382	7.924	
Disch.	(J)			(J)	(J)	(J)
1	.1718			7.646	8.288	9.419
2	.4989			10.80	11.87	14.63
3	.9020			12.37	13.92	18.38
4	1.350			12.74	14.76	20.82
5	1.825			12.06	14.51	21.85
6	2.315			10.35	13.20	21.13

* Losses due to filament magnetization and self-field are equal for charging and discharging conditions.

TABLE 30

B-FIELD OPTIMIZATION STUDY

COMPUTER RUN SERIES F-3

Conditions:

Approach #2

W_{pulse} = 20 kJ

$W_{initial}$ = 40 kJ

ρ_{300} = 17.8 nΩ-m

ρ_r = 100

Matrix Layer Thickness Ratio = 0.98

Pulse Rep Rate = 500 pps

Breakdown of Losses per Pulse

B_m (T) Charging	Eddy Current (mJ	Filament * Magnetization (J)	Self * Field (mJ)	Filament Coupling (J)	Total (J)	Total (ch+disch)
1	2.616	.4151	.7852	5.057	5.475	
2	7.589	.5707	.5675	9.711	10.29	
3	13.74	.6475	.4423	12.07	12.73	
4	20.56	.6642	.3479	12.69	13.38	
5	27.79	.6275	.2672	12.06	12.71	
6	35.25	.5385	.1927	10.35	10.93	
Disch.	(J)			(J)	(J)	(J)
1	.1718			7.640	8.228	13.70
2	.4984			10.80	11.87	22.15
3	.9020			12.37	13.92	26.65
4	1.350			12.74	14.76	28.13
5	1.825			12.06	14.51	27.22
6	2.315			10.35	13.20	24.13

* Losses are due to filament magnetization and self-field are equal for charging and discharging conditions.

TABLE 31

B-FIELD OPTIMIZATION STUDY

COMPUTER RUN SERIES F-4

Conditions:

Approach #2

W_{pulse} = 20 kJ

$W_{initial}$ = 200 kJ

ρ_{300} = 17.8 nΩ -m

ρ_r = 100

Matrix Layer Thickness Ratio = 0.98

Pulse Rep Rate = 5 pps

Breakdown of Losses per Pulse

B_m (T) Charging	Eddy Current (μJ)	Filament * Magnetization (J)	Self * Field (μJ)	Filament Coupling (mJ)	Total (J)	Total (ch+disch)
1	3.708	.2964	11.45	11.77	.3082	
2	10.67	.4047	8.201	34.96	.4397	
3	19.16	.4548	6.326	64.73	.5195	
4	28.50	.4616	4.922	99.22	.5609	
5	38.30	.4312	3.734	137.7	.5689	
6	48.35	.3656	2.656	180.0	.5457	
Disch.	**(mJ)**			**(J)**	**(J)**	**(J)**
1	24.72			5.817	5.817	6.125
2	71.09			8.163	8.163	8.603
3	127.7			9.289	9.289	9.809
4	189.9			9.521	9.521	10.08
5	255.3			8.985	8.985	9.554
6	322.3			7.723	7.723	8.269

* Losses due to filament magnetization and self-field are equal for charging and discharging conditions.

TABLE 32

B-FIELD OPTIMIZATION STUDY

COMPUTER RUN SERIES F-5

Conditions:

Approach #2

W_{pulse} = 20 kJ

$W_{initial}$ = 200 kJ

ρ_{300} = 17.8 nΩ-m

ρ_r = 100

Matrix Layer Thickness Ratio = 0.98

Pulse Rep Rate = 50 pps

Breakdown of Losses per Pulse

B_m (T) Charging	Eddy Current (μJ)	Filament * Magnetization (J)	Self * Field (μJ)	Filament Coupling (J)	Total (J)	Total (ch+disch)
1	37.14	.2964	11.45	.1168	.4132	
2	106.8	.4047	8.201	.3430	.7478	
3	191.9	.4548	6.326	.6269	1.082	
4	285.4	.4616	4.922	.9449	1.407	
5	383.5	.4312	3.734	1.280	1.711	
6	484.2	.3656	2.656	1.608	1.975	
Disch.	(mJ)			(J)	(J)	(J)
1	24.72			5.817	5.817	6.230
2	71.09			8.613	8.163	8.911
3	127.7			9.289	9.289	10.37
4	189.9			9.521	9.521	10.93
5	255.3			8.985	8.985	10.70
6	322.3			7.723	7.723	9.698

* Losses due to filament magnetization and self-field are equal for charging and discharging conditions.

TABLE 33

B-FIELD OPTIMIZATION STUDY

COMPUTER RUN SERIES F-6

Conditions:

Approach #2

W_{pulse} = 20 kJ

$W_{initial}$ = 200 kJ

ρ_{300} = 17.8 nΩ-m

ρ_r = 100

Matrix Layer Thickness Ratio = 0.98

Pulse Rep Rate = 500 pps

Breakdown of Losses per Pulse

B_m (T) Charging	Eddy Current (mJ)	Filament * Magnetization (J)	Self * Field (μJ)	Filament Coupling (J)	Total (J)	Total (ch+disch)
1	.3764	.2964	11.45	1.075	1.372	
2	1.083	.4047	8.201	2.847	3.253	
3	1.945	.4548	6.326	4.625	5.081	
4	2.893	.4616	4.922	6.038	6.503	
5	3.888	.4312	3.734	6.780	7.215	
6	4.908	.3656	2.656	6.529	6.900	
Disch.	(mJ)			(J)	(J)	(J)
1	24.72			5.496	5.817	7.189
2	71.09			7.687	8.163	11.42
3	127.7			8.707	9.289	14.37
4	189.9			8.876	9.521	16.02
5	255.3			8.299	8.985	16.20
6	322.3			7.036	7.723	14.62

* Losses due to filament magnetization and self-field are equal for charging and discharging conditions.

TABLE 34

B-FIELD OPTIMIZATION STUDY

COMPUTER RUN SERIES G-1

Conditions:

Approach #3

W_{pulse} = 20 kJ

$W_{initial}$ = 8.0 MJ

ρ_{300} = 17.8 nΩ-m

ρ_r = 100

Matrix Layer Thickness Ratio = 0.98

Pulse Rep Rate = 5 pps

Breakdown of Losses per Pulse

B_m (T) Charging	Eddy Current (nJ)	Filament * Magnetization (J)	Self * Field (nJ)	Filament Coupling (μJ)	Total (J)	Total (ch+disch)
1	28.44	.1077	1.881	90.46	.1437	
2	81.62	.1372	1.344	268.5	.1832	
3	146.4	.1505	1.034	497.4	.2011	
4	217.4	.1511	.8026	763.2	.2024	
5	291.8	.1408	.6072	1061	.1890	
6	368.0	.1200	.4305	1393	.1618	
Disch.	**(mJ)**			**(J)**	**(J)**	**(J)**
1	.1896			.5069	.6148	.7585
2	.5441			1.253	1.391	1.574
3	.9757			1.894	2.045	2.246
4	1.449			2.289	2.442	2.644
5	1.945			2.367	2.509	2.698
6	2.453			2.102	2.225	2.387

* Losses due to filament magnetization and self-field are equal for charging and discharging conditions.

TABLE 35

B-FIELD OPTIMIZATION STUDY

COMPUTER RUN SERIES G-2

Conditions:

Approach #3

W_{pulse} = 20 kJ

$W_{initial}$ = 80 MJ

ρ_{300} = 17.8 nΩ-m

ρ_r = 100

Matrix Layer Thickness Ratio = 0.98

Pulse Rep Rate = 50 pps

Breakdown of Losses per Pulse

B_m (T) Charging	Eddy Current (nJ)	Filament * Magnetization (J)	Self * Field (pJ)	Filament Coupling (μJ)	Total (J)	Total (ch+disch)
1	13.22	.1231	8.696	42.04	.1642	
2	37.93	.1217	6.214	124.8	.1625	
3	68.02	.1205	4.782	231.1	.1610	
4	101.0	.1162	3.711	354.6	.1554	
5	135.6	.1081	2.808	492.9	.1448	
6	171.0	.09596	1.990	647.1	.1288	
Disch.	**(μJ)**			**(J)**	**(J)**	**(J)**
1	8.798			.02749	.1506	.3149
2	25.25			.07994	.2017	.3642
3	45.28			.1447	.2653	.4263
4	67.24			.2152	.3315	.4869
5	90.27			.2862	.3944	.5392
6	11.38			.3493	.4453	.5741

* Losses due to filament magnetization and self-field are equal for charging and discharging conditions.

Filament magnetization loss occurs from a hysteretic phenomenon resulting in energy loss entirely from the magnetic field. At low frequency field sweeps, filament magnetization loss becomes a significant proportion of the total loss. From Table 25, we see that for 1 Tesla peak field, this loss constitutes more than half of the total charging loss per pulse. We have not studied the effects of filament diameter on this hysteretic loss. Brechna[1] suggests that losses can be reduced by using filaments of 5 microns diameter or less; NbTi filaments of such size are commercially available.

Plots of filament magnetization loss and self-field loss vs the peak B-field are shown in Figure 13.

We know that in any metallic conductor eddy currents will be induced if $\dot{B} \neq 0$. Figure 14 shows the nature of variation of the eddy current loss with the change in $\dot{B}$. The data plotted is from series E1 of the computer run shown in Table 25. Eddy current loss exhibits dependence not only on $\dot{B}$, but also on the maximum and minimum values of the B-field because of matrix magnetoresistance effects. Eddy current loss vs B_{max} plotted in Figure 15. The eddy current loss is inversely proportional to the matrix metal resistivity. Figure 16 shows the plot of eddy-current loss per pulse versus the matrix resistivity at zero field on a log-log scale.

The internal eddy current distribution pattern for transposed cables and braids depends on the manufacturing process, and can be expressed only in terms of empirical data. Therefore, this loss mechanism was not included in this computer program.

From the data we have at the present time, it is clear that in order to reduce eddy current loss, it is desirable to have a high resistivity matrix. This is particularly true for Approach 2 conditions where the superconductor must not go normal. In Approach 1, we are assuming that the conductor will not go normal during the

---

[1] Brechna, H. - Superconducting Magnet Systems, P. 249

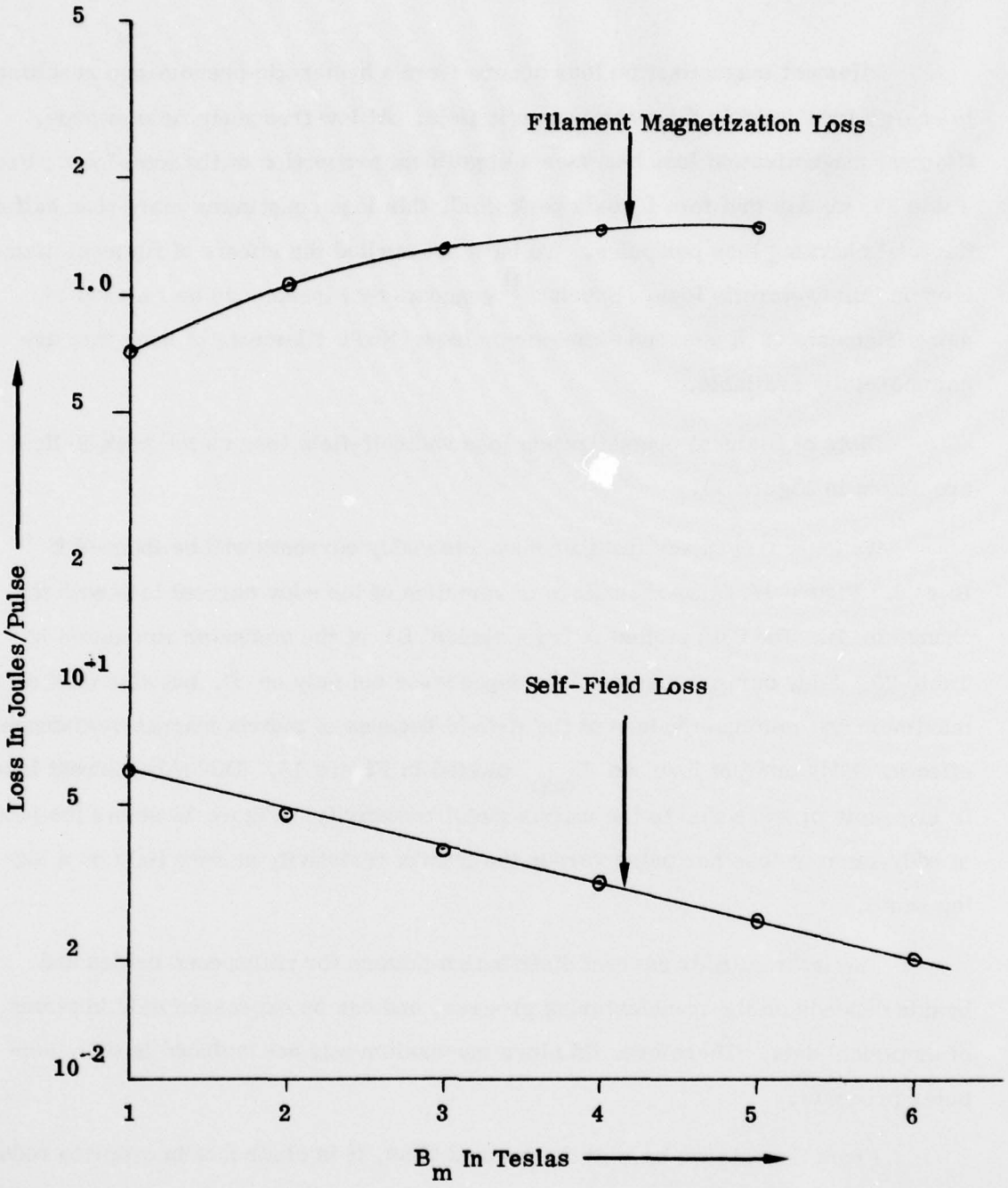

Figure 13. Filament Magnetization and Self-Field Loss Vs. Maximum B-Field.

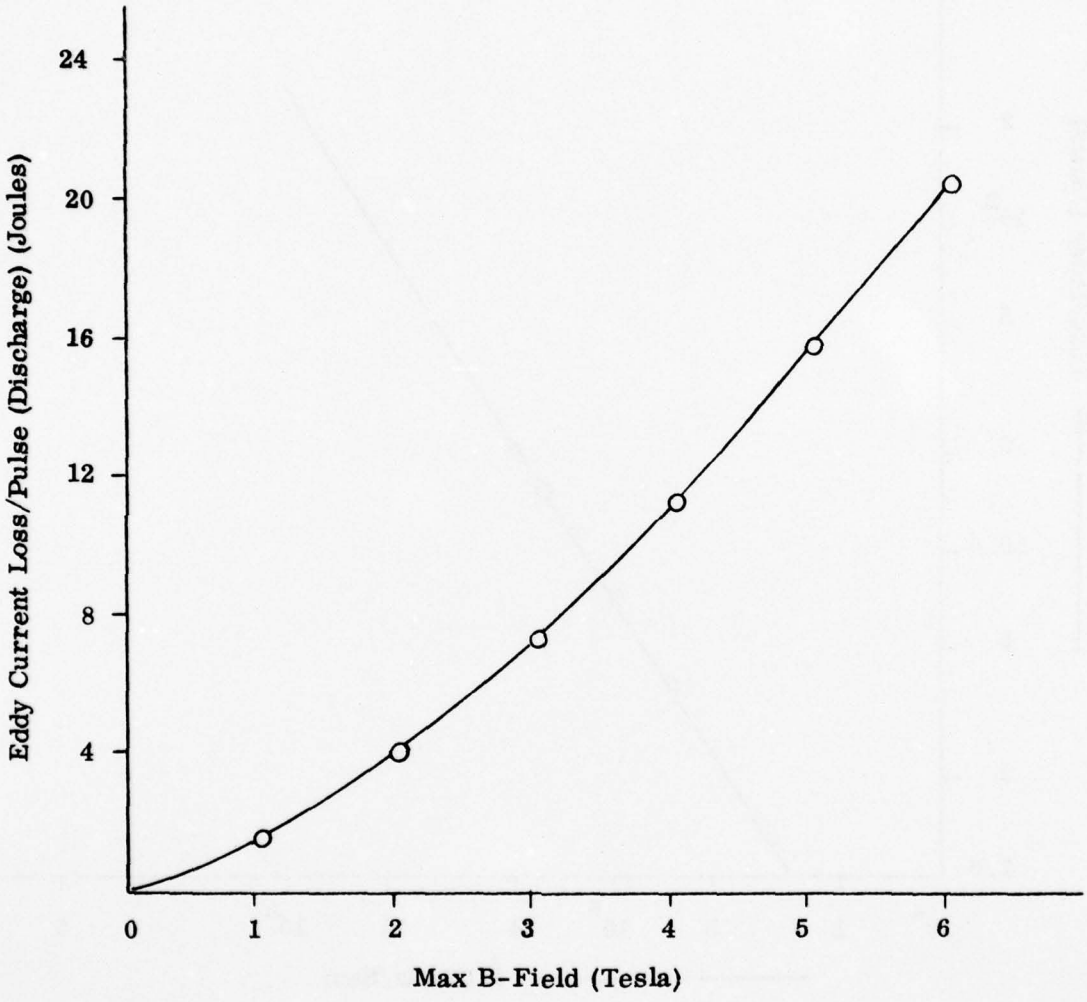

Figure 14. Eddy Current Loss Vs. Maximum Operating B-Field at Constant Discharge Time.

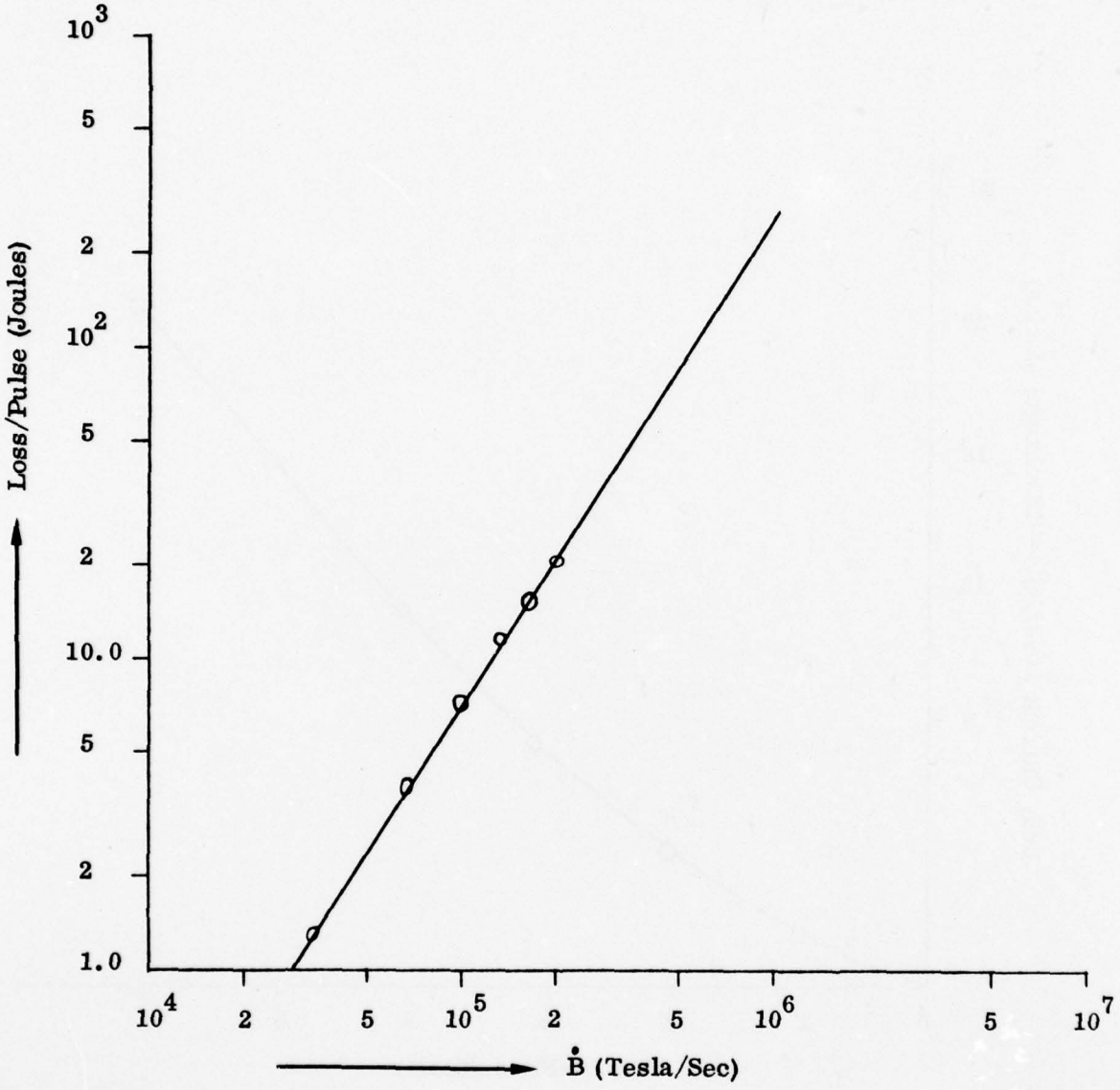

Figure 15. Eddy Current Loss Vs. $\dot{B}$.

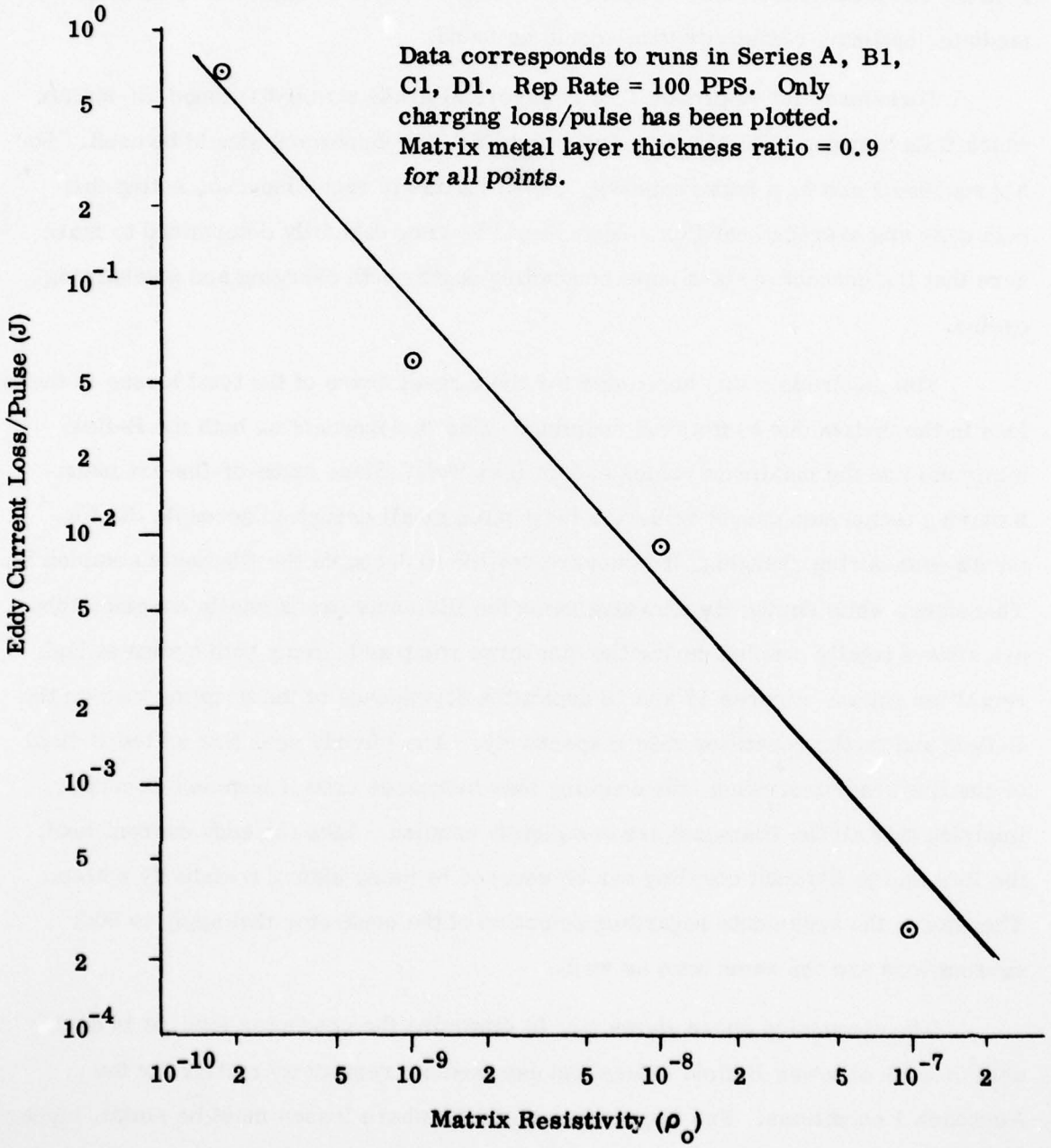

Figure 16. Eddy Current Loss Vs. Matrix Resistivity.

charging cycle. However, it is not so clear as to whether the conductor will remain superconducting during the discharge. If it does go normal in this period, the current will be instantaneously shifted to the normal matrix; if we use a very high resistivity matrix, the joule losses will be excessive. Therefore, for Approach 1, an intermediate, optimum resistivity value could be found.

Therefore, for Approach 1, a commercial grade strain-hardened Cu-matrix which falls between VSF-212 (Supercon) and VSF-232 (Supercon) should be used. For Approaches 2 and 3, a high resistivity Cu-Ni matrix is recommended, noting that both peak and average heat flux values should be very carefully determined to make sure that the conductor stays superconducting during both charging and discharging cycles.

The mechanism that accounted for the largest share of the total losses is the loss in the matrix due to filament coupling. This is dependent on both the B-field minimum and the maximum values and on $\dot{B}$ as well. Since state-of-the-art manufacturing techniques cannot achieve a twist pitch small enough to decouple the filaments even during charging, it is never possible to decouple the filaments completely. Therefore, while during the charging ramp the filaments are partially coupled, they are always totally coupled during the discharge ramp and during both cycles at high repetition rates. Figures 17 and 18 depict the dependence of the coupling loss on the B-field and on the repetition rate respectively. It is clearly seen that as the B-field or the frequency increases, the coupling loss increases until it becomes constant, implying that all the filaments are completely coupled. Like the eddy current loss, the loss due to filament coupling can be reduced by using higher resistivity matrix. Therefore, the arguments regarding selection of the conductor that apply to eddy current loss are the same here as well.

The discussion above shows that to minimize the conductor loss, it is desirable to work at lower B-field values and use medium resistivity matrix for the Approach 1 conditions. For Approaches 2 and 3, where losses must be small, higher B-fields and high resistivity matrix material should be used.

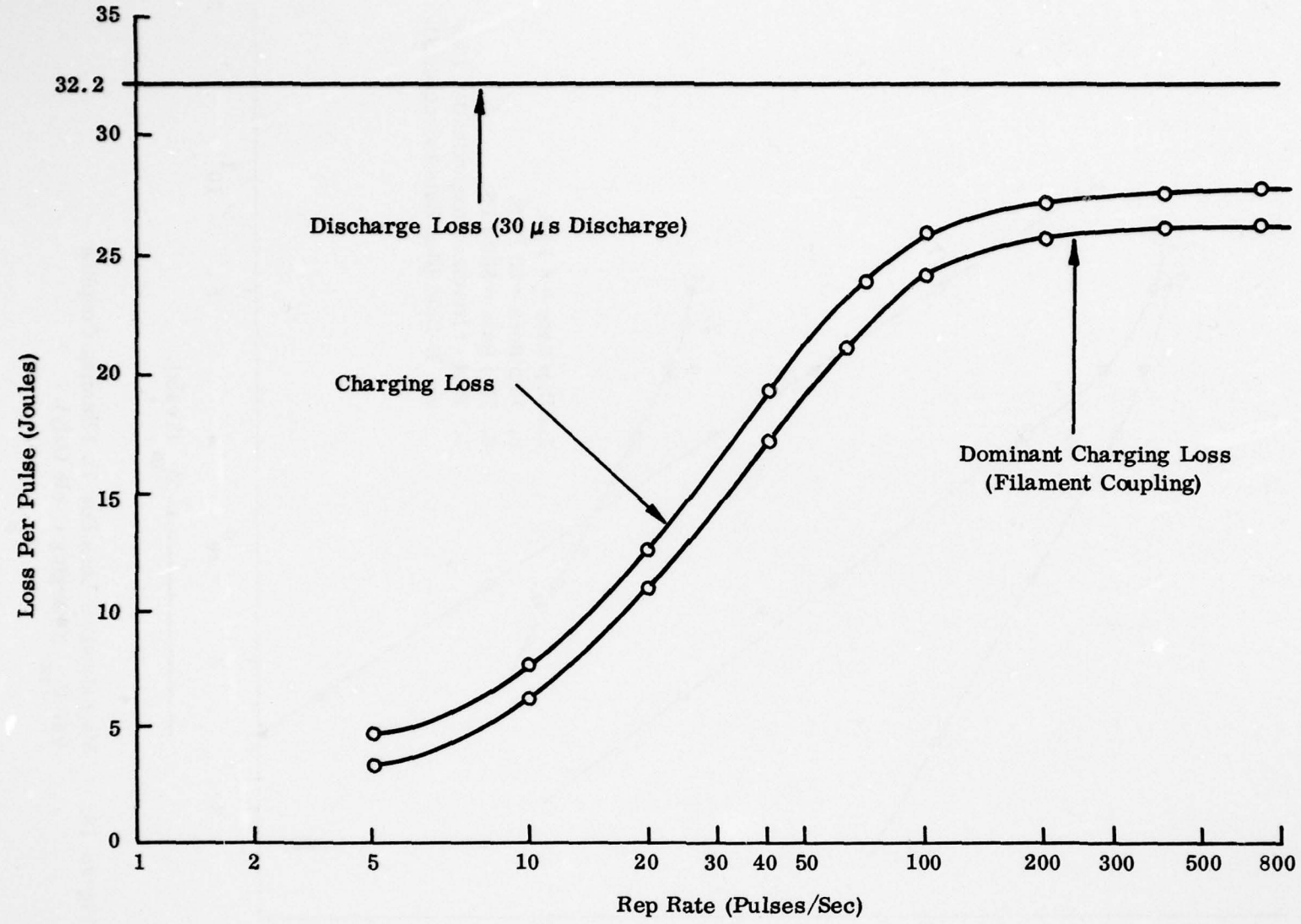

Figure 17. Superconductor Loss Vs. Repetition Rate.

AD-A052 750 MAXWELL LABS INC WOBURN MA UTILITY PRODUCTS DIV F/G 10/2
INDUCTOR NETWORK DEVELOPMENT FOR AIRCRAFT HIGH POWER SUPPLIES.(U)
APR 77 J TENO, R L BRYAN, S GHOSHROY F33615-74-C-2018
UNCLASSIFIED AFAPL-TR-77-15 NL

2 OF 3
AD
AD52750

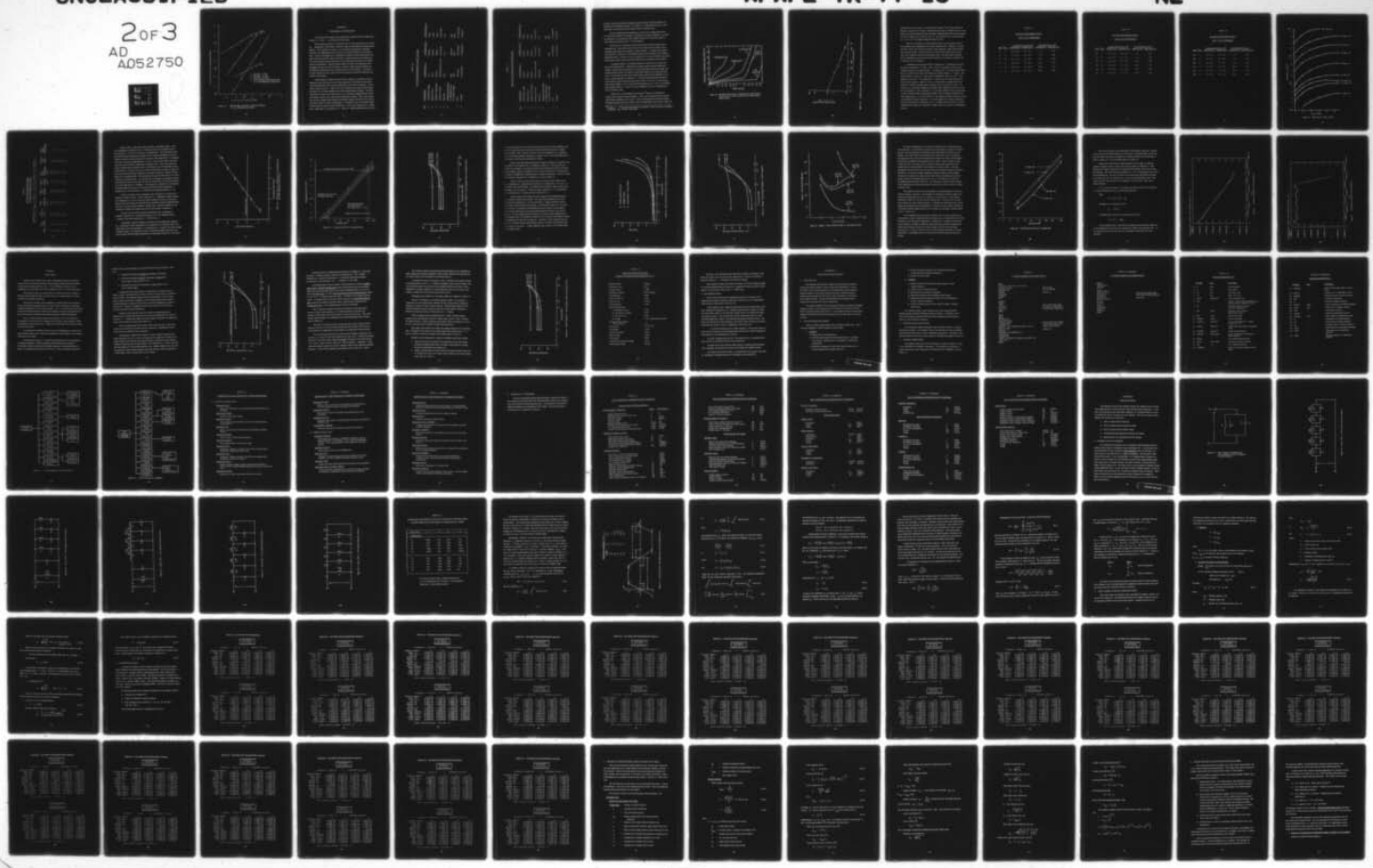

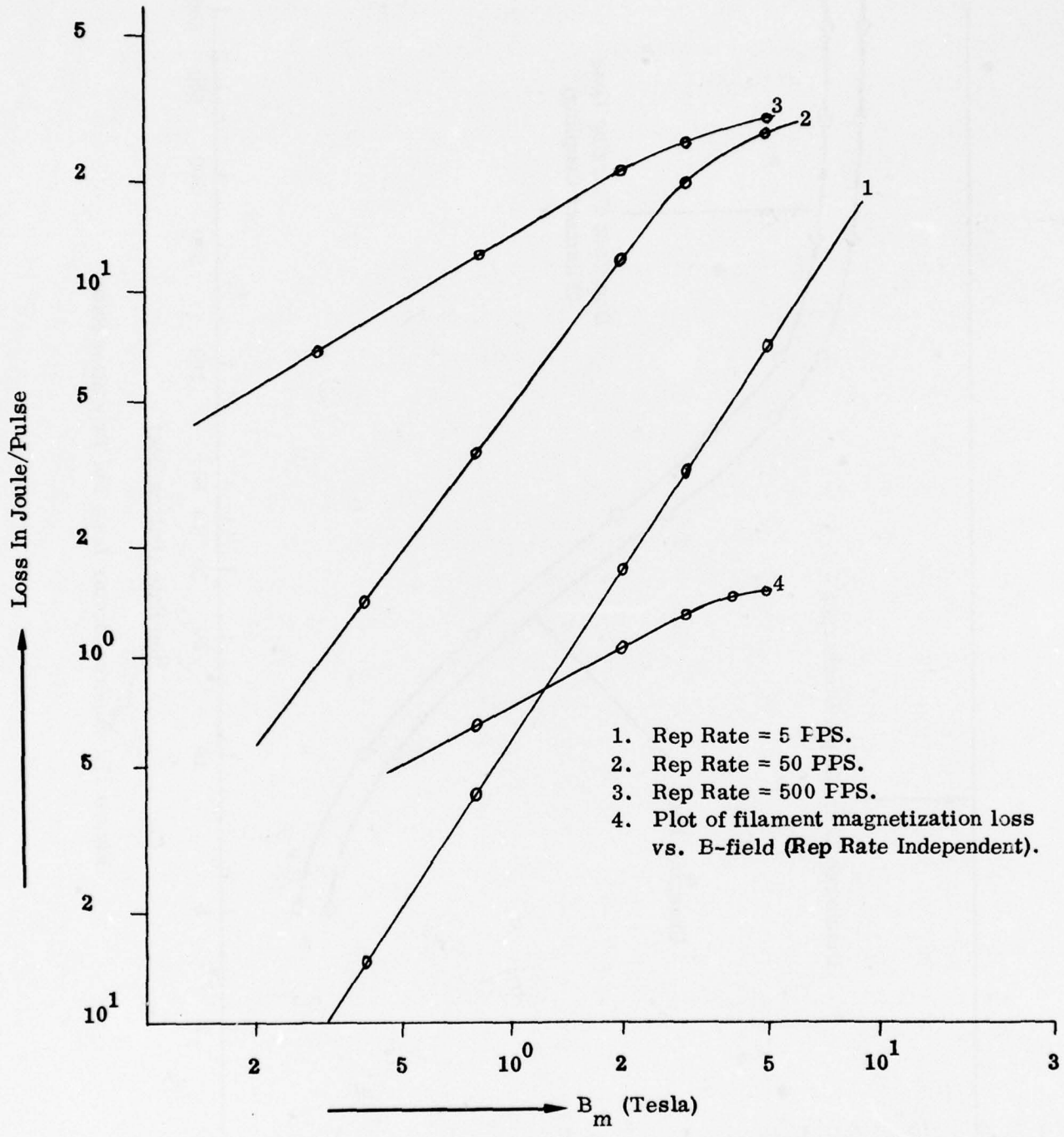

Figure 18. Magnetization Loss Due To Filament Coupling Vs. B_m (Charging Cycle Only).

SECTION IV

COMPARISON OF APPROACHES

The results of the computer runs performed to compare the three Approaches - Numbers 1, 2, and 3 - are presented in this chapter.

In broad general terms the requirements for an airborne pulsed power system are - lightweight, small volume, minimum weight of consumables and minimum dissipation. These objectives, however, are not always simultaneously attainable. Therefore, the optimization process becomes an involved problem in many dimensions. Since the development of a sophisticated automatic system optimization computer code was beyond the scope of this study, comparison between the approaches was done taking into consideration only the most important parameters, the weight, volume and dissipation. Special attention ought to be paid to the magnitude of the dissipation because of its direct influence on both the superconductor stability and the difficulty encountered with the complex process of heat transfer. Two factors, average and peak heat flux, will be taken into account to evaluate the conductor heat transfer requirements.

Before taking a detailed look into the data it might be worthwhile to list the important merits and demerits of the three approaches to provide the reader with a general background of the relative attractiveness of the three approaches. This is done in Tables 36 and 37. Table 36 is for low repetition rates (up to about 400 pps) and Table 37 is for high repetition rates (above approximately 400 pps). The demarcation line of 400 pps is not rigid; in fact, it is a wide band ranging between 300 pps and 500 pps, where we have found that the approaches overlap. Since at low repetition rates the cooling system weight is determined mainly by the size of the coil and not by the volume of coolant requirements, it is possible to work at somewhat higher B-field levels to keep the system weight down. In this regard Approach No. 1 might have a slight edge over Approach No. 2. However, at high repetition rates this is not

TABLE 36

LOW PULSE REPETITION RATES ($\lesssim$ 400 PPS)

NO.	PARAMETER	APPROACH NO. 1	APPROACH NO. 2	APPROACH NO. 3
1.	Total System Weight	Low	Medium	Large
2.	System Volume	Small	Medium	Large
3.	Weight of Consumables	Medium	Medium	Large
4.	Maximum B-Field	Should be Small ($\sim \leq$ 3T)	Can be High	Can be High
5.	Heat Flux	High	Low	Low
6.	Switching Requirements			
	a) Breaking Current	High	Moderate	High
	b) Reverse Voltage	High	High	High
7.	PFN	Necessary	Not Essential	Not Essential
8.	Crowbar	Not Necessary	Not Necessary	Necessary

TABLE 37

HIGH PULSE REPETITION RATES ($\gtrsim$ 400 PPS)

NO.	PARAMETER	APPROACH NO. 1	APPROACH NO. 2	APPROACH NO. 3
1.	Total System Weight	Medium	Medium	Large
2.	System Volume	Medium	Medium	Large
3.	Weight of Consumables	Medium	Medium	Large
4.	Maximum B-Field	Has to be quite small	Can be High	Can be High
5.	Heat Flux	Quite High	Not so High	Low
6.	Switching Requirements			
	a) Breaking Current			High
	b) Reverse Voltage	High	High	High
7.	PFN	Necessary	Not Essential	Not Essential
8.	Crowbar	Not Necessary	Not Necessary	Necessary

possible, since heat transfer limitations mean that weight reduction might not be achieved by using higher B-fields. Nevertheless, we repeat that this is not a firm conclusion, but a broad observation made from our computer data.

For the comparison of the approaches we have used a single B-field level of 3 Tesla and scanned a wide range of frequency from 5pps to 1000 pps. A secondary objective was to study the system weight reduction by varying the B-field at three different repetition rates - 5, 50 and 500 pps.

First of all, we will address the problem of heat transfer from the superconducting coil. As has been stated earlier, the problem of heat transfer from a composite and braided superconductor is quite complex. A complete and satisfactory theoretical evaluation is not possible because so much depends on the manufacturing process,etc. However, we have examined the worst case situations of an adiabatic process, which has provided good insight into the magnitude of the problem.

As mentioned before, two important figures of merit are the average heat flux and the peak heat flux. Although the average heat flux should be kept small enough to ensure that the conductor stays superconducting during the charging, the transient peak heat flux can actually be quite high during the very short discharge cycle. Even if this drives the coil normal during discharge the probability of a recovery is quite high only for Approach 1. Previous experimental and theoretical work shows that a steady state heat flux value of about $0.3\ w/cm^2$ is safe for open pool nucleate boiling: for the very short discharge pulse of 20 - 40μs, the allowable peak transient value of $\sim 10\ w/cm^2$ may be attainable, based on extrapolation of some of Jackson's data.

Figure 19 is a reproduction from Jackson's[1] paper on transient heat transfer from composite superconductors. These curves indicate that the transient heat transfer coefficients have a certain power relationship with the pulse duration. Plotting the break points from Figure 19 and extrapolating the linear fit(see Figure 20)

---

[1] Jackson, J. - "Transient Heat Transfer and Stability of Superconducting Composites," Cryogenics, pp. 103-105, April 1969.

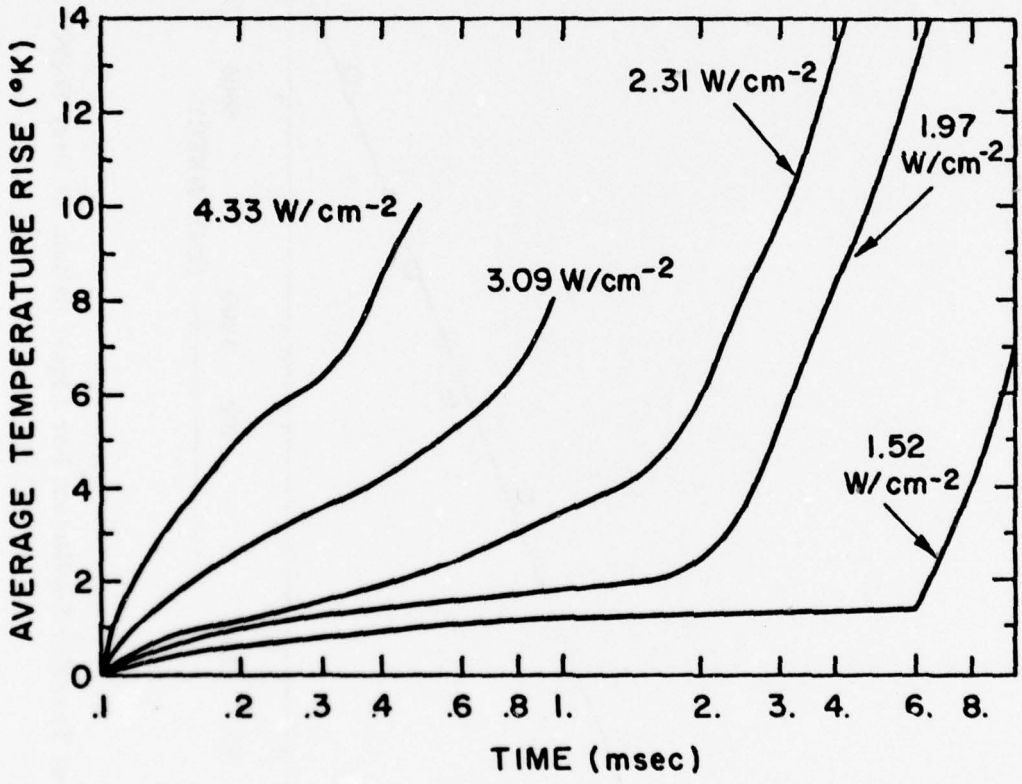

Figure 19. Transient Heat Transfer Coefficient for Liquid Helium. The break in the curve marks the limit of the nucleate boiling region.

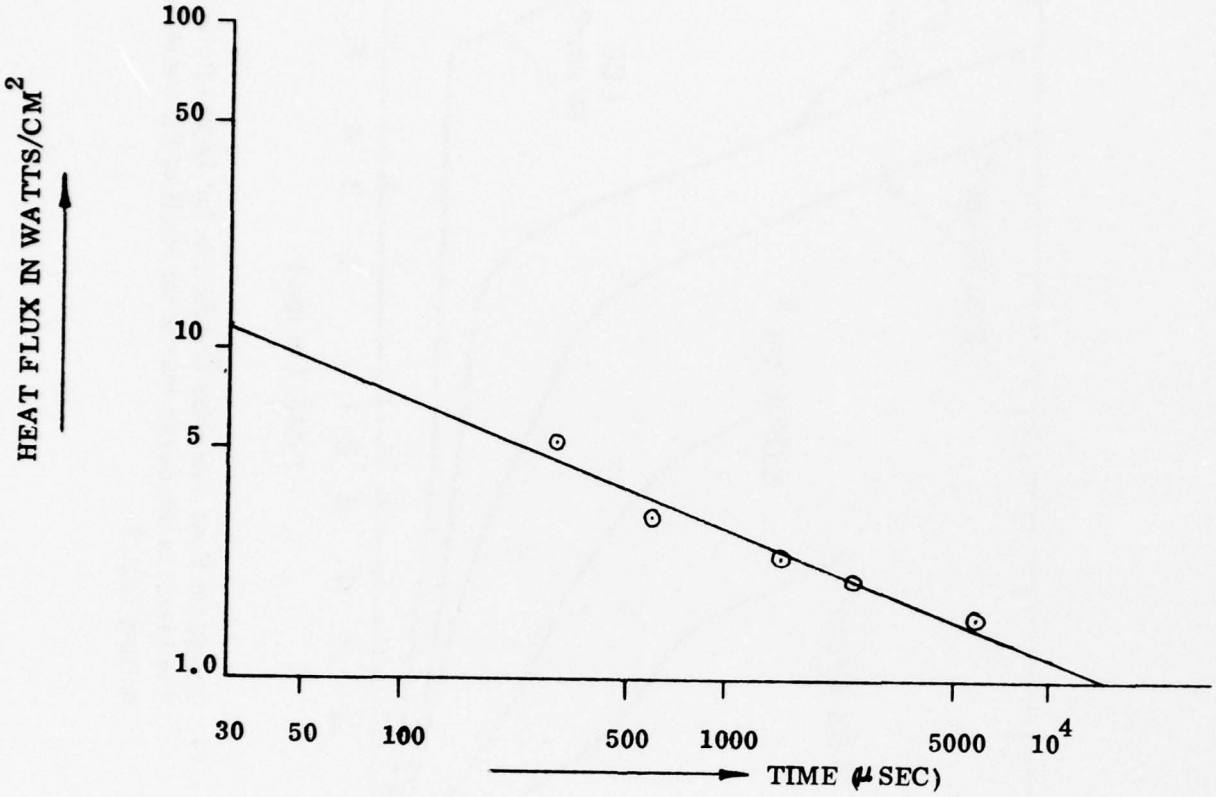

Figure 20. Transient Heat Transfer Coefficient For Liquid Helium At Very Short Pulse Durations.

we find that for a 30μs pulse, a heat flux value of about 12 w/cm^2 can perhaps be attained. Again this is a tentative expectation which must be verified since we do not know of any experimental work that could throw additional light into these projections. For present purposes we will use 0.3 w/cm^2 as the limit for the average heat flux and $\sim$10 w/cm^2 as the highest allowable peak heat flux.

Since in our computer runs the discharge time was kept constant at 30μs, the discharge loss is independent of the pulse repetition rate. Therefore, the peak heat flux, which is the heat flux developed during discharge, will be determined by the maximum B-field. Stated in another way, the allowable peak heat flux value will set the maximum limit of the operating B-field. Once this limit is satisfied the corresponding average heat flux limit determines the maximum repetition rate at which the coil can be pulsed.

Computation of the peak heat flux for Approach No. 1 conditions shows that the limit is reached near 3 Tesla. With 3 Tesla is it possible to work at pulse repetition rates of up to about 500 pps. For Approach No. 2 the peak heat flux limit is never reached for the range of B-field values studied; namely 1 - 6 Tesla. The peak heat flux is reached at 5 Tesla and the magnitude is only 0.5 w/cm^2. (See Tables 38, 39 and 40.) The Approach No. 3 values for the average and peak heat flux are much smaller. Figure 21 shows a semi-log plot of average heat flux vs maximum B-field at constant pulse repetition rate for Approaches 1 and 2. The losses are so small under Approach 3 conditions that cooling does not seem to pose any real problem. In fact, Approach No. 3 can utilize B-field levels of greater than 6 Tesla constrained only by the practical limits of the coil support weight and size under high stresses. As shown in Table 41, the weights of just the coil and the dewar are prohibitively high for Approach 3. The coil weight/size scaling at multimegajoule levels required for Approach 3 are of unverified accuracy; however, the conclusion that the weight of an Approach 3 magnet system is excessive is substantially correct.

TABLE 38

IES ANALYSIS SUMMARY SHEET

HEAT FLUX COMPARISON

Reps	B_{max}	Average Heat-Flux W/cm^2 Approach No. 1	Average Heat-Flux W/cm^2 Approach No. 2	Peak Heat-Flux W/cm^2 Approach No. 1	Peak Heat-Flux W/cm^2 Approach No. 2
5	1	6.7 E-4	2.9 E-5	4.1	0.18
5	2	1.4 E-3	5.1 E-5	8.3	0.32
5	3	2.1 E-3	6.6 E-5	12.7	0.42
5	4	2.9 E-3	7.5 E-5	16.4	0.47
5	5	3.5 E-3	7.6 E-5	19.9	0.47
5	6	4.1 E-3	7.0 E-5	22.6	0.44

TABLE 39

IES ANALYSIS SUMMARY SHEET

HEAT FLUX COMPARISON

Reps	B_{max}	Average Heat-Flux W/cm^2		Peak Heat-Flux W/cm^2	
		Approach No. 1	Approach No. 2	Approach No. 1	Approach No. 2
50	1	8.4 E-3	2.9 E-4	4.1	0.18
50	2	1.9 E-2	5.3 E-4	8.4	0.32
50	3	3.0 E-2	7.0 E-4	12.5	0.42
50	4	4.0 E-2	8.1 E-4	16.4	0.47
50	5	4.9 E-2	8.6 E-4	19.9	0.48
50	6	5.4 E-2	8.2 E-4	22.6	0.44

TABLE 40

IES ANALYSIS SUMMARY SHEET

HEAT FLUX COMPARISON

Reps	B_{max}	Average Heat-Flux W/cm^2 Approach No. 1	Average Heat-Flux W/cm^2 Approach No. 2	Peak Heat-Flux W/cm^2 Approach No. 1	Peak Heat-Flux W/cm^2 Approach No. 2
500	1	1.2 E-1	3.4 E-3	4.1	0.18
500	2	2.3 E-1	6.7 E-3	8.4	0.32
500	3	3.4 E-1	9.7 E-3	12.5	0.42
500	4	4.3 E-1	1.2 E-2	16.4	0.47
500	5	5.0 E-1	1.3 E-2	19.9	0.48
500	6	5.4 E-1	1.2 E-2	22.6	0.44

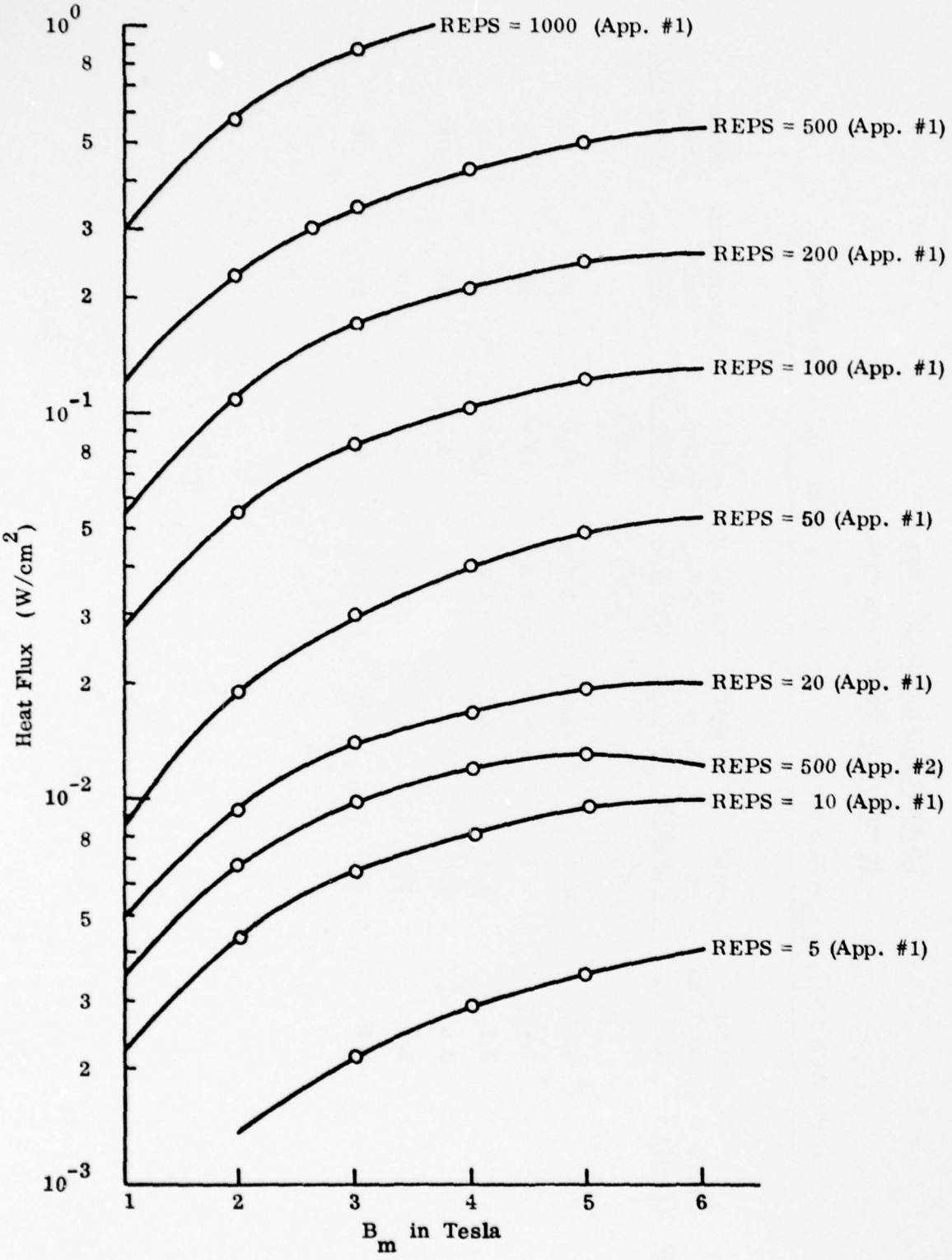

Figure 21. Heat Flux Vs. Max B-Field.

TABLE 41

IES ANALYSIS SUMMARY SHEET

B-FIELD OPTIMIZATION STUDY

APPROACH No. 3, ρ_{300} = 17.8 nΩ -m, ρ_r = 100. λ surface = 0.98 - SERIES G-1

Reps	B_{max} (Tesla)	Total Loss/Pulse (J)	Weight of Dewar (KG) ($x10^3$)	Weight of L-He Boil-Off	Weight of E-S Coil (KG) ($x10^3$)	Total System Weight (KG) ($x10^3$)	Energy per Pulse (KJ)	Initial Energy Stored (MJ)
5	1	0.76	32.0	13.5	1.5	34.0	20	8
5	2	1.6	9.1	5.4	1.3	10.0	20	8
5	3	2.2	4.4	3.2	1.2	5.6	20	8
5	4	2.6	2.6	2.2	1.1	3.7	20	8
5	5	2.7	1.7	1.6	1.0	2.8	20	8
5	6	2.4	1.2	1.3	1.0	2.3	20	8

Figure 22 shows a linear fit of peak heat flux vs operating B-field. From our extrapolation of Jackson's data, as mentioned earlier, the allowable limit of peak heat flux (~ 10 w/cm^2) is drawn as a horizontal line. The intersection of this line with the linear fit provides an estimate of the maximum allowable value of the B-field at which the energy storage coil can operate under Approach No. 1 conditions. This value is found to be approximately 3 Tesla. As discussed earlier, this maximum limit on the B-field is independent of repetition rate. The second constraint (on the maximum pulse repetition rate) is subsequently set by the allowable average heat flux limit. A family of average heat flux characteristics is plotted in Figure 23. Each of these characteristics represents an average heat flux as a function of repetition rate at constant B-field. The permissible average heat flux limit of 0.3 w/cm^2 is shown as a horizontal line. It is evident from the plot that it is possible to achieve about 600 pps at about 2 Tesla and even more for lower fields. These characteristics are all for Approach No. 1 conditions. According to the computed data, the chances of reaching either the peak or the average heat flux limit under Approach No. 2 conditions are very slim indeed, as is manifest from inspecting Tables 38 - 40.

It seems, therefore, that at repetition rates of 500 pps or less where it is possible to operate at about 3 Tesla, Approach No. 1 might gain a slight advantage over Approach No. 2 so far as the total system weight and volume are concerned. This is borne out by Figure 24 which shows the variation of system weight with pulse frequency. The total system weight for Approach No. 1 has been adjusted by subtracting the charging PFN weight since this was not included in Approach 2.

Figure 24 has two system weight characteristics for each Approach. Evidently, Approach No. 1 is indeed preferable to No. 2 for repetition rates of ~ 400 pps or less and for fields below $\sim$ 4 Tesla for No. 2.

It is further evident from Figure 24 that the system weight under Approach No. 2 conditions is rather insensitive to the repetition rate as indicated by the very small slopes of the characteristics. For Approach No. 1, however, the system weight is highly sensitive to the pulsing rate above a certain break point which lies somewhere between 200 and 400 pps depending on the operating B-field level. The reason

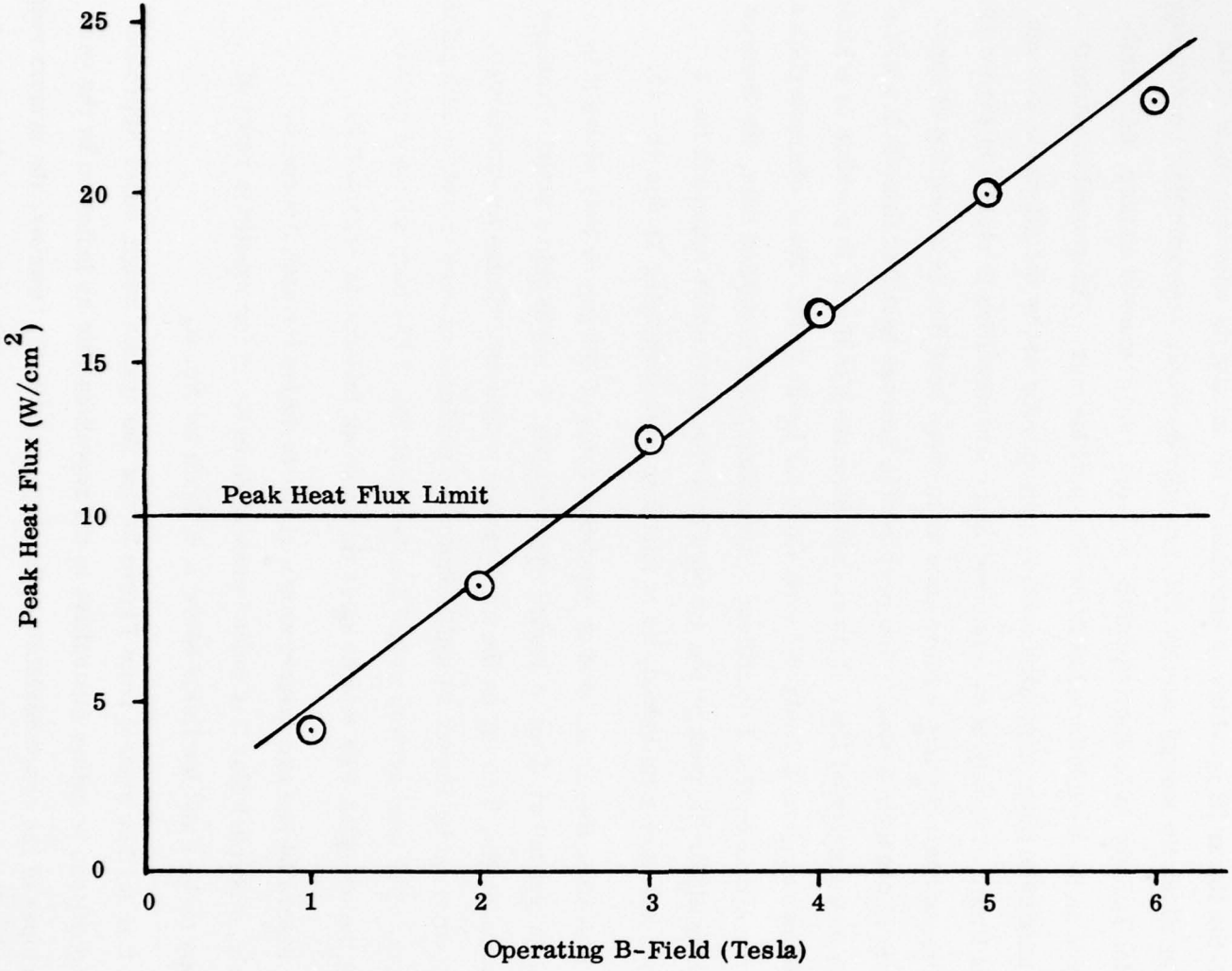

Figure 22. Peak Heat Flux Vs. Operating B-Field (Independent of Rep Rate) Discharge Time = 30 μs.

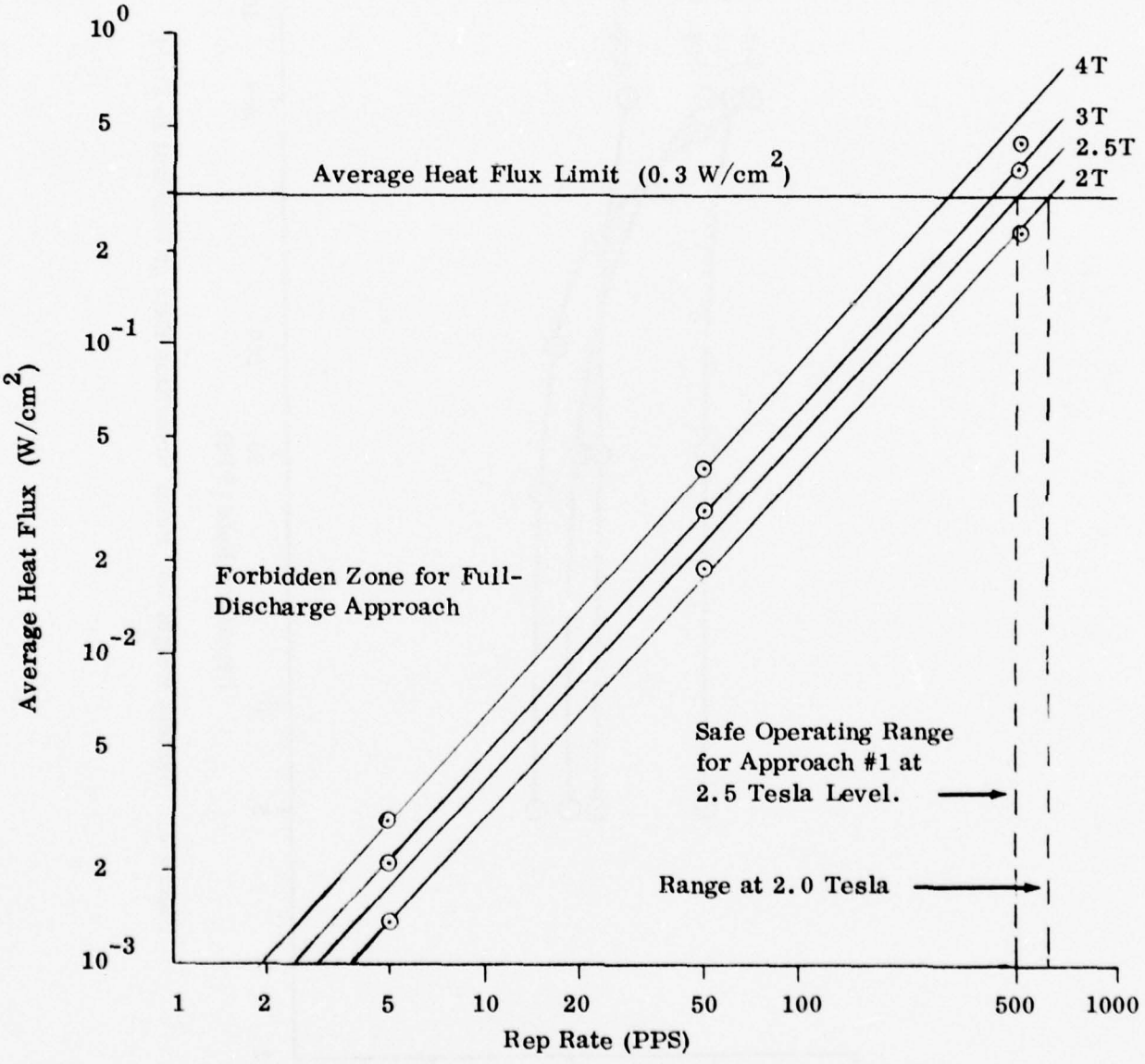

Figure 23. Average Heat Flux Vs. Repetition Rate.

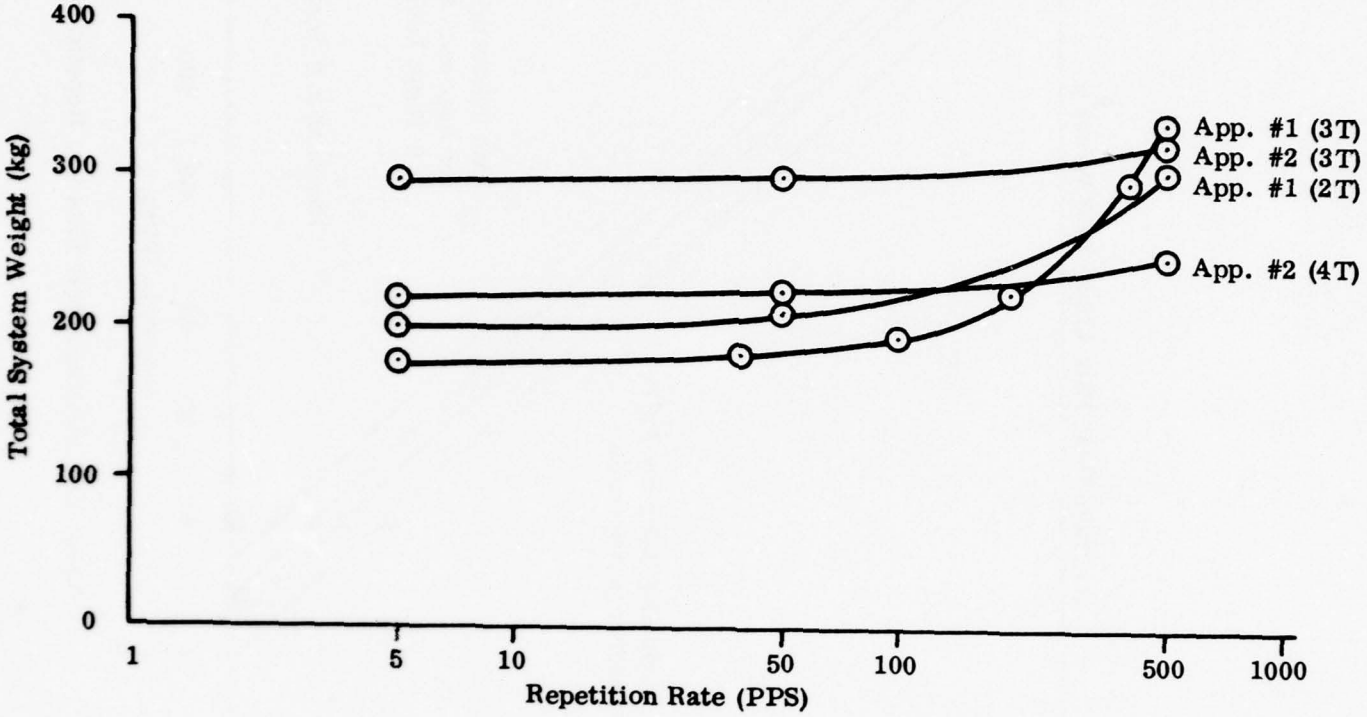

Figure 24. System Weight Vs. Pulse Repetition Rate at Constant B-Field.

for this break point is due to the fact that with the increase in pulse repetition rate, there is a sharp increase in losses and helium boil-off which increases cooling system weight. This, however, does not occur under Approach No. 2 conditions since the amount of helium required for cooling is more or less determined by the coil volume rather than by superconductor losses.

Dewar weight and liquid helium boil-off weight are plotted as a function of the repetition rate for Approach No. 1 conditions in Figure 25. The sum of the two weights is also plotted. It is clearly evident from this figure that the break point in system weight, observed in Figure 24; occurs precisely because of the break point in Figure 25 signifying the sharp increase in cooling requirements. There is no such break point for Approach No. 2 conditions as is seen in Figure 24.

Figure 26 which is a plot of the magnet and dewar system weight versus pulse repetition rate, reinforces the preference for Approach No. 1 over No. 2 at repetition rates below 500 pps. The weight of the coil and the dewar system corresponding to even as high as a 4 Tesla coil under Approach No. 2 is considerably greater than that of a 2 Tesla coil under Approach No. 1.

Another aspect of the magnet and the cooling system weight optimization is the proper selection of the B-field. If the operating repetition rate is below 500 pps where Approach No. 1 is more attractive, a unique B-field level can be found which minimizes the system weight, as illustrated in Figure 27. The minimum occurs at a transition zone following which the reduction in coil weight is progressively offset by the increase in liquid-helium boil-off due to increase in losses. It is also apparent that the minima are sharper at higher pulsing rates. With Approach No. 2 the minima are expected to be reached at much higher B-fields as indicated by the top curve in Figure 26. Therefore, at low repetition rates of (say) 50 - 200 pps, because of the shallow minima, the choice of the B-field value is not of great importance. At high repetition rates, however, the B-field should be carefully chosen.

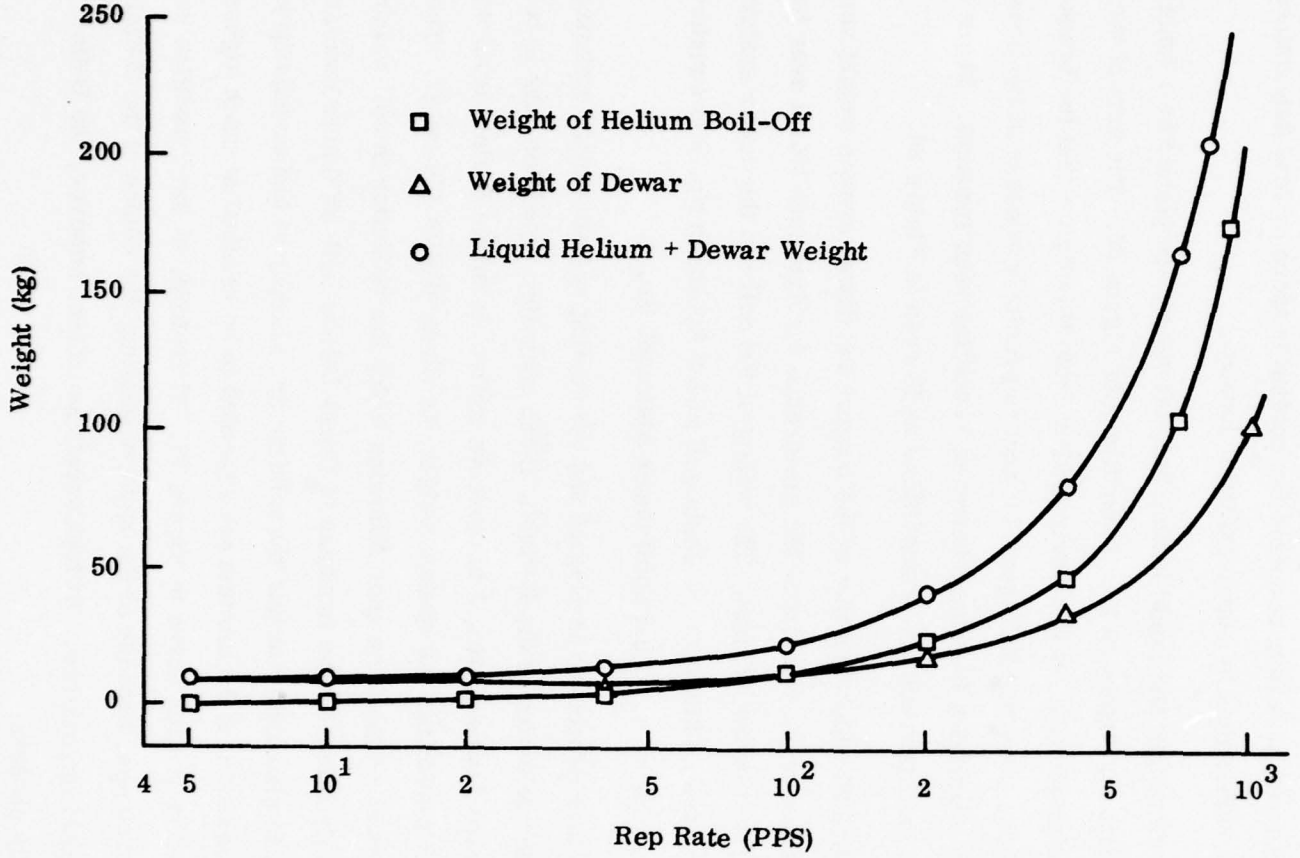

Figure 25. Helium Boil-Off and Dewar Weight as a Function of Pulse Rep Rate.

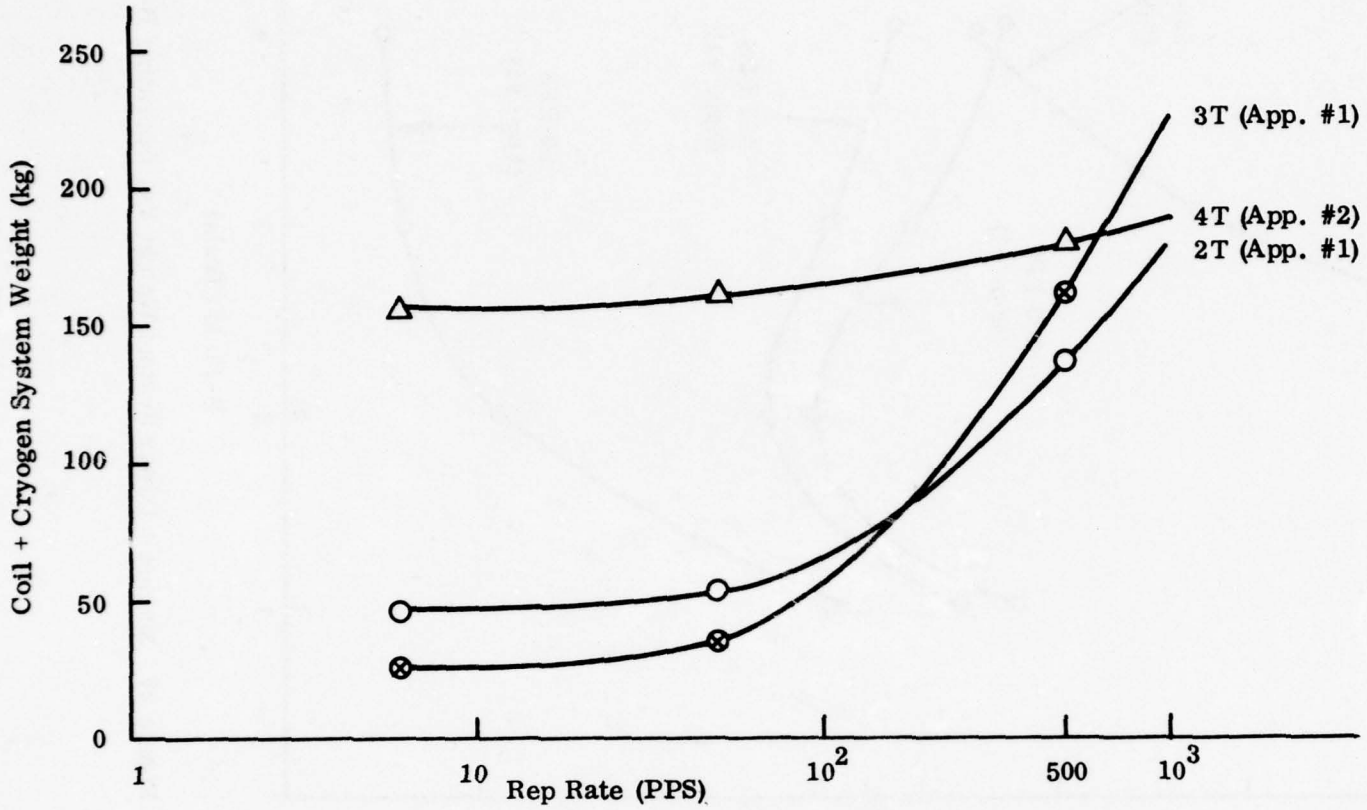

Figure 26. Magnet + Dewar System Weight Vs. Pulse Frequency.

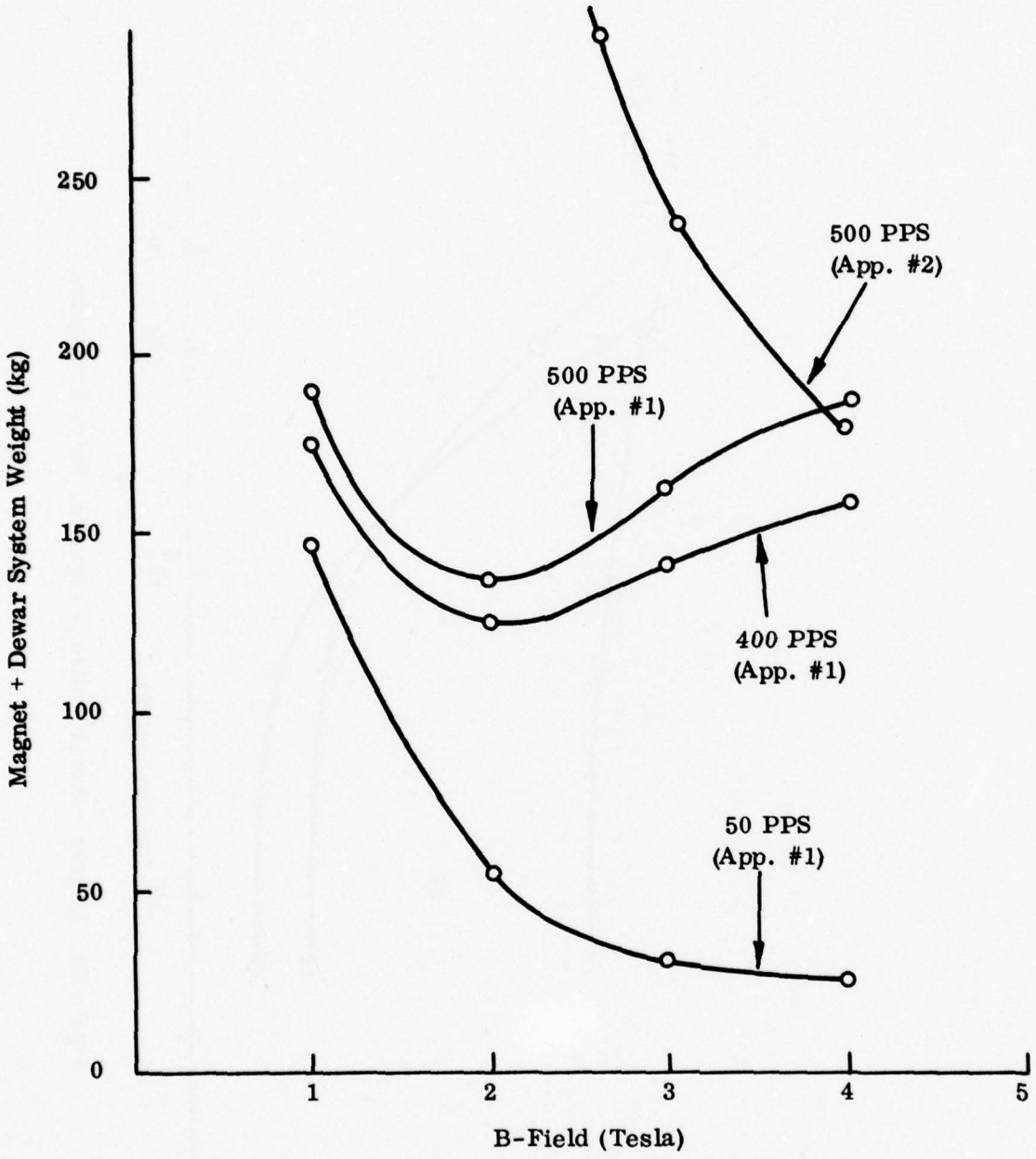

Figure 27. Magnet + Dewar System Weight Vs. Operating B-Field.

For sake of completeness we present the following more detailed discussion of the minimum: as the B-field increases before the minimum is reached, the losses increase, thus increasing the contribution of the liquid-helium boil-off due to coil heating. But as the B-field is increased the coil volume decreases, consequently decreasing the dewar size and thus significantly reducing the weight of liquid-helium boil-off due to radiation losses through the dewar walls. After reaching a certain B-field level the coil weight becomes somewhat constant (with constant current density) since it is determined by stress limits due to high B-fields. Therefore, although the actual coil size decreases the weight of the support structure dominates. Henceforth, as there is no further significant reduction magnet systems weights, the increase in weight due to higher coolant boil-off takes preponderance and total weight reaches the ascending portion of the curve. The minima occur where the two opposing effects balance each other. The minimum is found to be quite shallow at low repetition rates because the losses do not increase as fast as they do at higher repetition rates.

The weight and volume of the consumables are important figures of merit for airborne systems. Moreover, economically it is desirable to keep the weight of the coolant down especially when it is as expensive as liquid helium. In this context, referring to Figure 28, it is observed that Approach No. 2 seems to have an advantage in almost any range of pulse frequency. Although from the point of view of total magnet and cryogenic system optimization, it is better to work at higher B-fields, it is evident that liquid helium boil-off can be minimized by selecting a medium B-field level of 3 Tesla or so.

In our prolonged discussion earlier in this section, we have considered how several factors (losses, helium boil-off, coil weight, etc.) are affected by the B-field. Nonetheless, one last point is appropriate. Approach No. 2 might be favorable because it tends to use higher B-fields for almost any kind of parameter optimization which makes the power density of the system higher and this seems desirable. Approach No. 1, however, because of its heat-flux constraint demands a low operating B-field. This implies that the system will be relatively large with low power density.

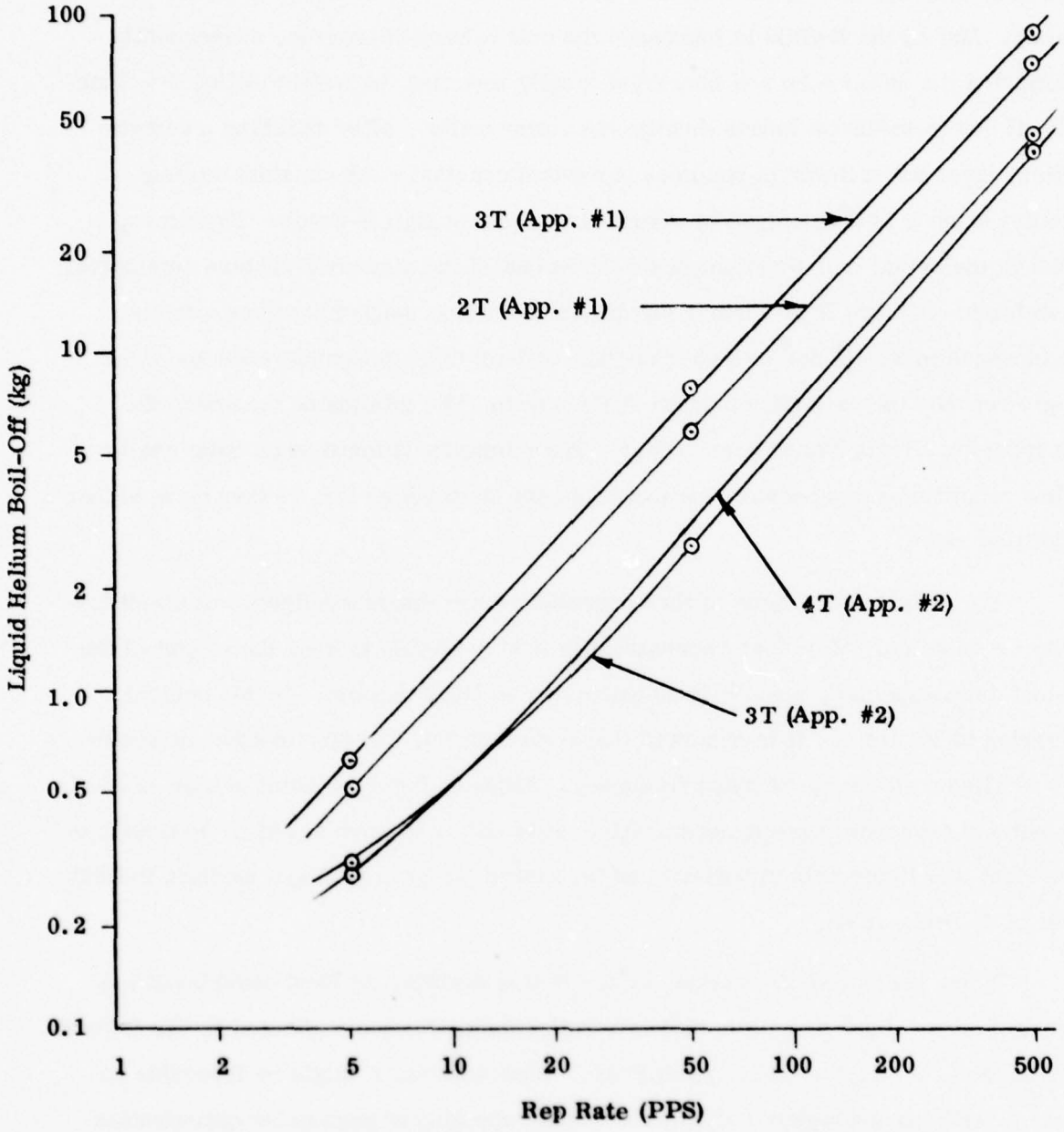

Figure 28. Liquid Helium Boil-Off Vs. Pulsing Rate.

Since the wave-shape of the output pulse is well defined, Approach 1 requires a PFN to convert the linear discharge of the coil into a trapezoidal pulse at the load. The coil current wave-form resulting from a transient analysis of the discharge is shown in Figure 29. The load voltage appears on Figure 30.

Details of the PFN inductor design equations and the output of a separate computer program written to analyze the inductors appear in Appendix B. Both aluminum and copper conductors were analyzed with repetition rates between 5 pps and 1000 pps. The trade-off between Approaches 1 and 2 regarding the PFN occurs in the following way. In order to keep the wave shape fairly trapezoidal the change in current in the coil, for Approach No. 2, has to be kept sufficiently small. This means about 10 times energy has to be initially stored in the coil. This can be shown as follows:

Let I_o be the initial and I_1 the final current in the coil after one discharge. L is the coil inductance and W_p is the energy per pulse.

Then,

$$1/2\ L\ (I_o^2 - I_1^2) = W_p$$

Allowing for a 5% change in current

$$I_1 = 0.95\ I_o$$

Combining these relations, the initial energy stored is

$$1/2\ L\ I_o^2 = 10W_p$$

At low repetition rates, the increase in magnet and dewar system weight due to this additional energy storage far surpasses the weight of the discharge PFN. As the repetition rate is increased, however, the balance slowly tips in the other direction.

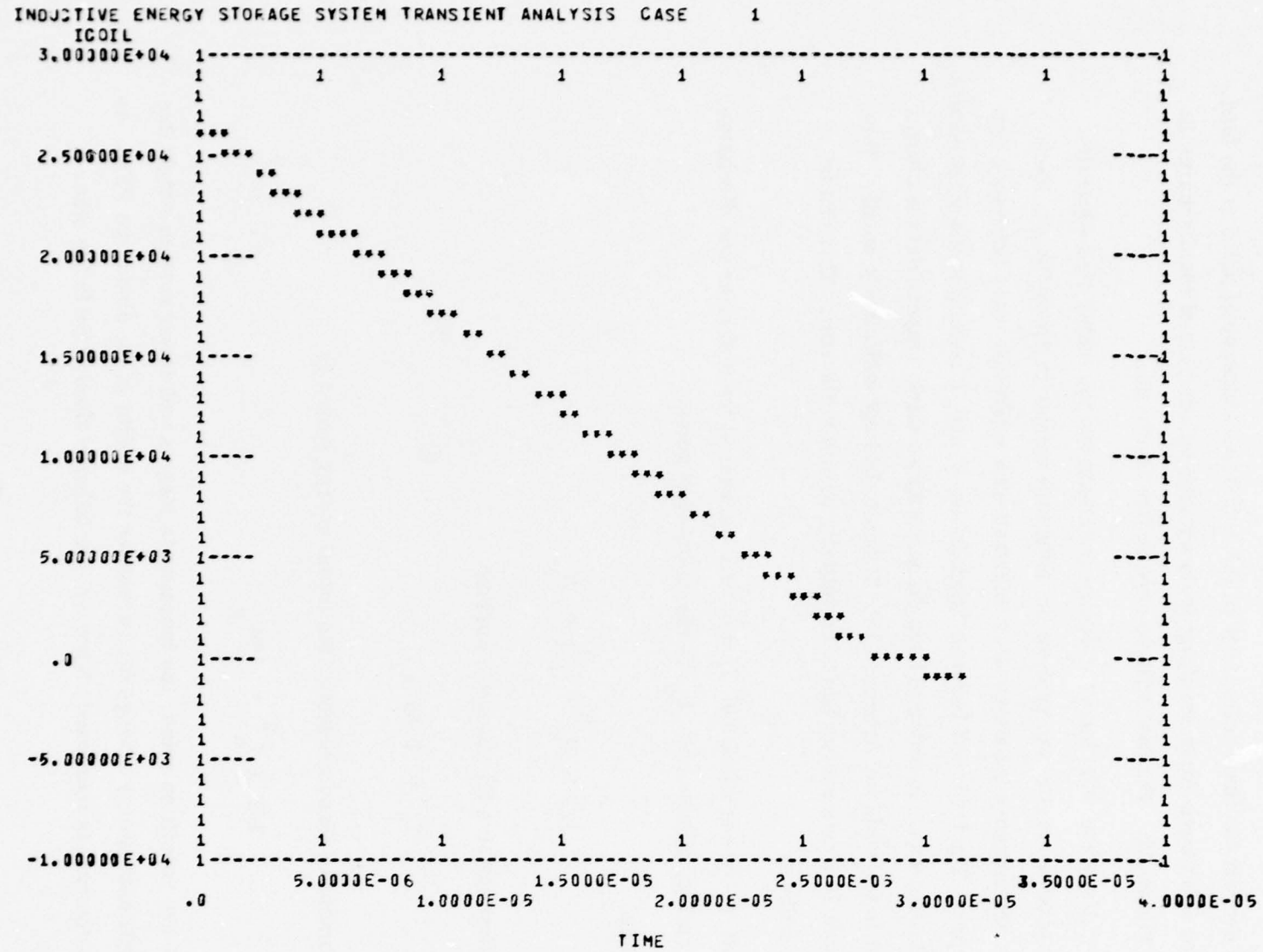

Figure 29. Coil Current as a Function of Time for Approach 1.

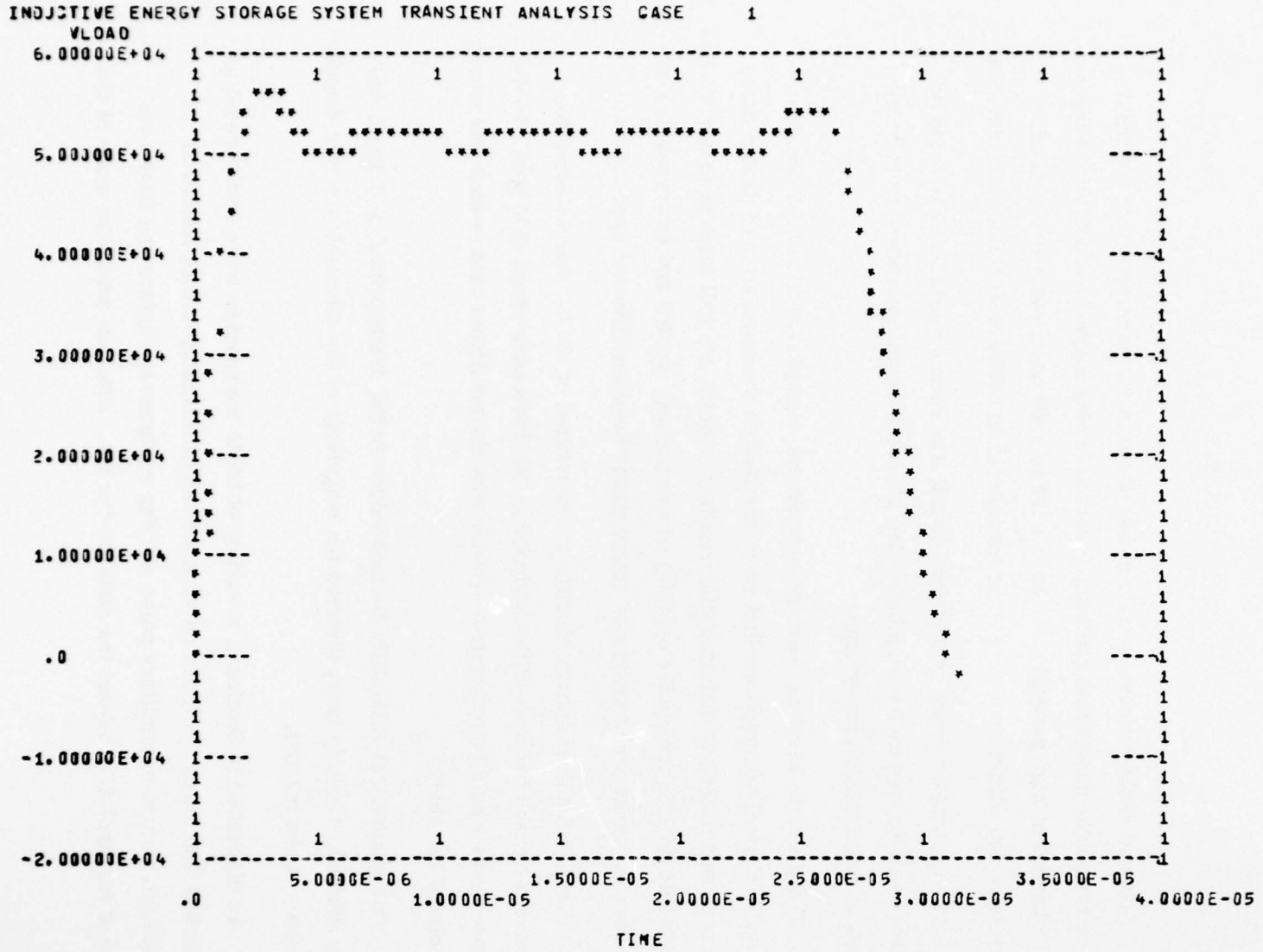

Figure 30. Load Voltage as a function of Time for Approach 1.

SECTION V

CONCLUSIONS

Because of the extremely wide range of operating parameters of potential interest for power generation utilizing superconducting magnets which are charged and discharged at high repetition rates ($\sim$100 to 1000 pps), extensive sets of scaling laws and algorithms were first formulated in order to evaluate performance.

The parameter space is so broad that it was deemed necessary to begin an iterative analytic approach with a base-line subset of certain parameters to bring the task to manageable proportions.

The previous sections, and the appendices, contain details of the considerations and technical assumptions that were involved in the generation of design data, component specifications and operating regimes. Here, we will attempt to summarize how this information (computer outputs) was organized, scaled and interpreted; leading to some general conclusions and comparisons between different approaches.

First, a nominal energy storage in the magnet of 20 kJ was selected for the computer cases because at the midpoint of the frequency range (500 pps) ~10MW of output power would be generated---which was the maximum value which was within the scope of the study.

For mechanical reliability B-field values in the neighborhood of 3 Tesla were mainly studied, which in turn, dictated the magnitude of the allowable current density in the body of the magnet.

As discussed in Section I, a variety of basic approaches were investigated as to technical feasibility, relative advantages and disadvantages with regard to size/weight, nature of auxiliary pulse shaping equipment, engineering limits and degree of extrapolation beyond the state-of-the art. After an extensive study of the

relative merits, three approaches were found which had the most promise. They were:

1) Sequential charging and complete discharging of the magnet

2) Sequential charging and partial discharging of single pulses from a larger magnet (relative to 1))

3) Sequential charging and discharging of a train of pulses, also from a larger magnet.

A parametric study showed that the third approach, involving a train of pulses, required quite high fields (6 Tesla or more) in order to achieve a practical size and weight. The attendant support structure requirements, need for large dewars, high currents which complicate the switching problem and the need for variable impedance matching to the load led to rejection of Approach 3 relative to the first two. Further, this approach would clearly require the most development and extension of present technology.

Having narrowed down the scope of the study by concentration on two approaches, it was then determined that for the base-line discharge value of 20 kJ per pulse at $\approx$500 pps that magnet and dewar weight for Approach 1 (complete discharge of the magnet) was lowest (See Figure 31.).

Here the magnet aspect ratios (major/minor radius and minor radius/bore radius) were held the same to make a direct comparison---modification of these ratios would not change the basic conclusions.

Consequently, emphasis then shifted to a rather detailed evaluation of the single discharge mode (No. 1) and it was found that the magnet-driven system size/weight rapidly decreased with decreasing frequency, leveling off at about 100 pps -- holding the discharge pulse energy constant. The output power, of course, also falls off in proportion to the decreasing repetition rate. Scaling to higher power levels by increasing the magnet energy storage at lower than 500 pps, which corresponds to $\sim$ 10MW output, will be discussed later in this section.

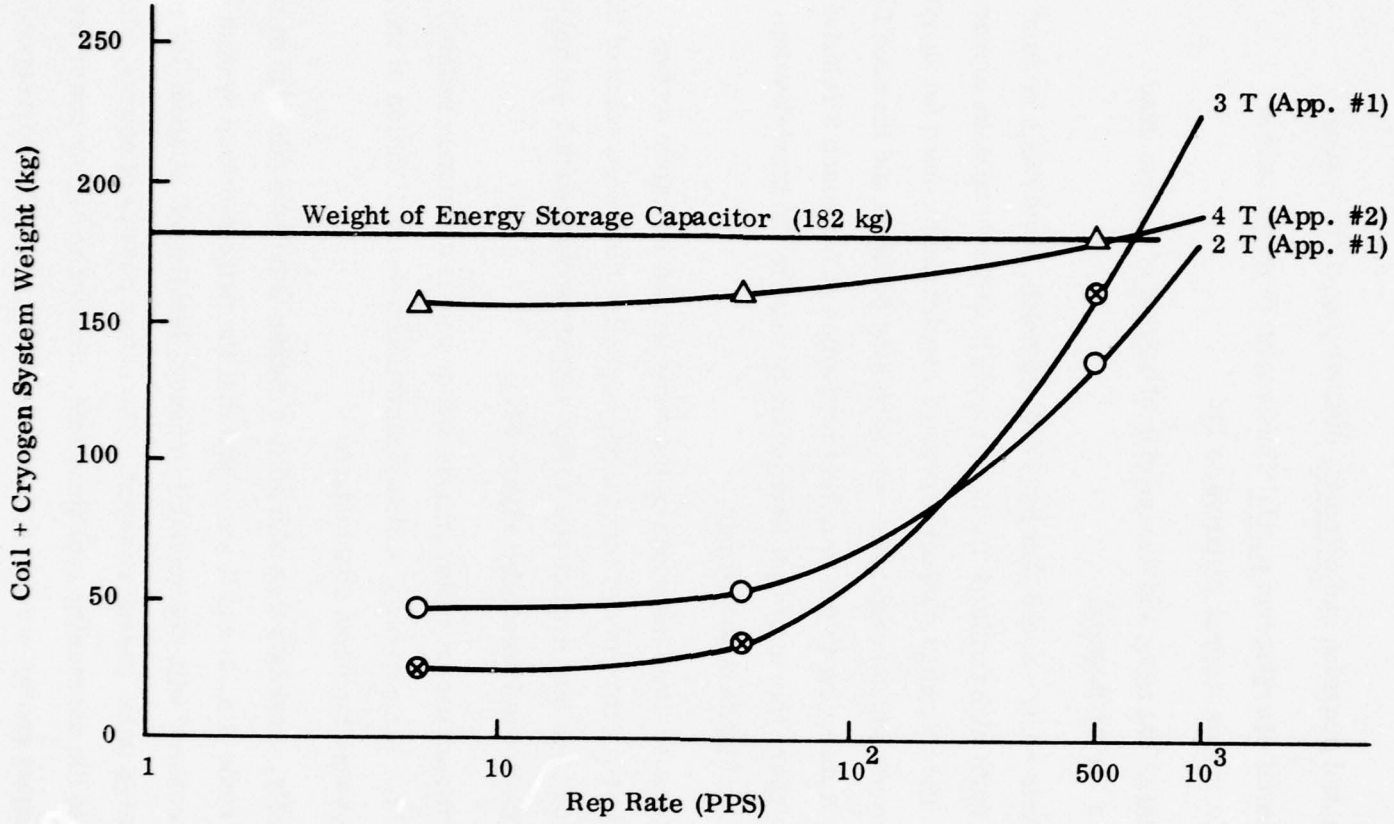

Figure 31. Magnet + Dewar System Weight Vs. Pulse Repetition Rate.

During the process of analyzing the performance of Approach 1, it was found that above a "critical frequency" that lies in a broad band of ~300 - 500 pps -- depending on the detailed requirement, i.e., particular output pulse duration, average power, load impedance, etc. -- Approach 1 is not viable.

The physical basis of this so-called "critical frequency" is that the magnetization losses, filament coupling losses (eddy current losses due to current loops between the superconducting material and normal stabilizing matrix, Cu or Cu-Ni alloys) self field losses and other eddy current losses in the normal material depend on ΔB and B. At higher frequencies (above $\approx$ 500 pps) a 20 kJ magnet cannot be cooled. To explain further, below the critical frequency the energy discharged per pulse controls the cooling and heat flux limits, while at higher frequencies the average power loss is the controlling factor in the heat flux limit.

Thus, to operate at higher frequencies a particular coil storing a given amount of energy (using Approach 1), it would be necessary to decrease the maximum B-field and/or the current density to decrease local losses. This would result in higher weights, as is indicated by the rough extrapolation above 500 pps shown in Figure 31.

This limit in frequency for given energy storage (or power output for given frequency) then led to a more thorough consideration of the effect of the losses on the transition from single pulse heat flux limits to average power heat flux limits.

To reduce the heat flux for given energy storage at higher frequencies, it is necessary to reduce the losses which depend on the ΔB and B during the discharge. This can be done with a larger magnet and partial discharge of the energy (Energy $\sim B^2$ so $\Delta E \sim B \Delta B$ for given value of B). This is basically "Approach 2" which raises the critical frequency to over the 1000 pps which was the maximum specified frequency. It also has the capability of operating at power levels over 10 MW.

The computer analysis also includes weight algorithms for the switching and pulse shaping; and auxiliary equipment, which includes capacitors and inductors for the counter-pulse circuit (needed for the circuit breakers).

A charging PFN may be necessary in order to minimize the transient loading on the prime power source; i.e., to hold the charging currents nearly constant. Because the prime power source has not been specified and the use of such a PFN is independent of whether capacitors or superconducting coils store the energy, this weight is considered to be part of the prime power source.

The <u>total</u> system weights for 20 kJ pulse output are compared in Figure 32.

Taking ~ 50J/pound as a reasonable capacitor weight, it is seen that at frequencies of several hundred pps, inductive storage systems offer a distinct advantage over capacitive energy storage systems. Detailed point designs for well defined operating parameters would be required to decide whether capacitive or inductive storage is preferred at frequencies over ~ 500 pps.

Table 42 contains typical specifications for a 10MW, 500 pps inductive storage system operating near top of the voltage range, namely ~55kV. Because the switch remains a critical component and requires further development, we have set 15% of the total system weight as design/development goal.

The weight of the helium in the table is the weight required for the operating time. Estimates of the coolant losses during standby times indicate that 5 - 10 Kg/hr of helium is required in addition to the weights shown in Table 42.

Consider now the weight-power scaling for repetition rates below 500 pps:

- The local heat losses per pulse do not change for a given coil current density and magnetic field; thus, the helium requirements for cooling increase in proportion to the magnet size.
- Further, point designs for both toroidal and shielded solenoids shown that the weight of the coil is very nearly a linear function of the stored energy in the range 20 - 100 kJ.

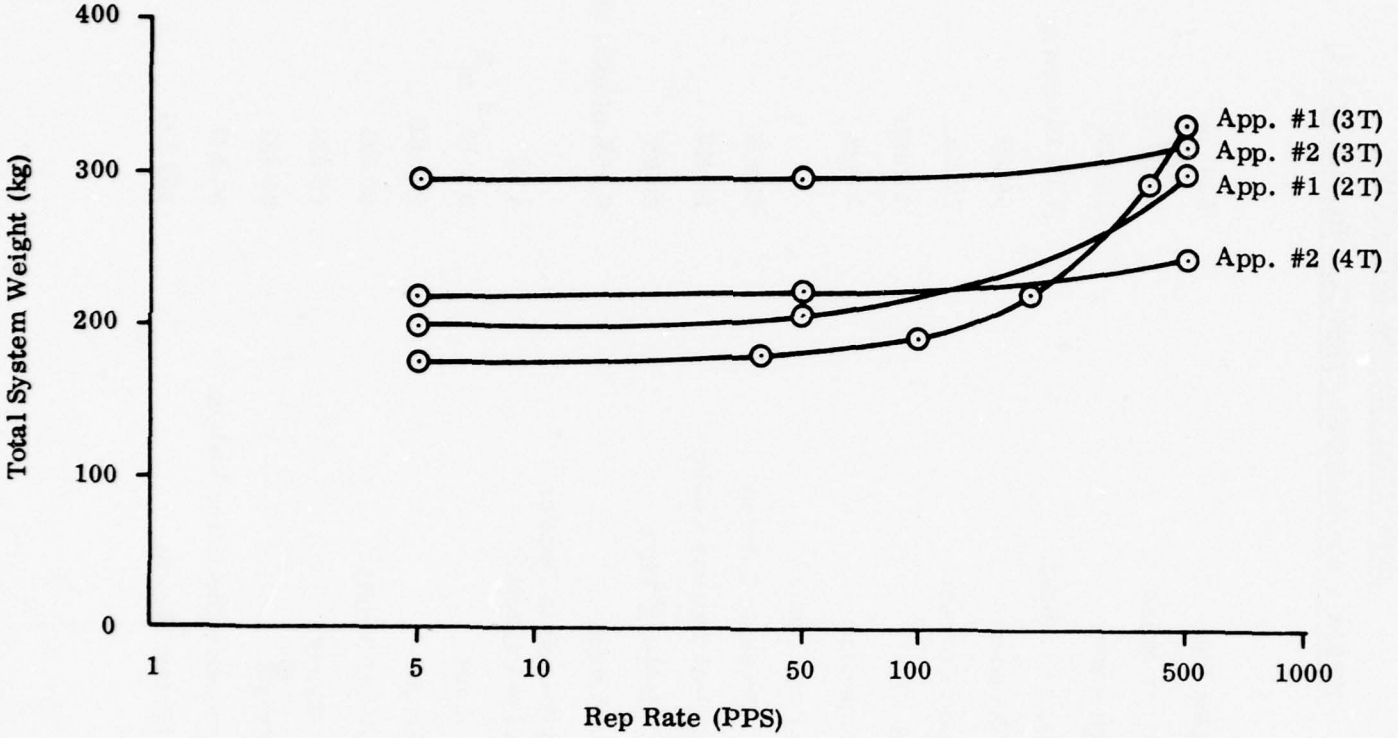

Figure 32. System Weight Vs. Pulse Repetition Rate at Constant B-Field.

TABLE 42

SPECIFICATION OF INDUCTIVE
ENERGY STORAGE SYSTEM (APPROACH NO. 1)

Repetition Rate	500 pps
Energy per Pulse	20 kJ
Average Power	10 MW
Discharge Condition	Full Discharge
Coil Inductance	56 μH
Peak Coil Current	27 KA
Peak B-Field	3 Tesla
Load Impedance	4 ohm
Switch Requirements	
a) Breaking Current	27 KA
b) Peak Inverse Voltage	56 KV
c) Hold-Off Time	30 μS
d) Weight	< 15% of total system weight
Energy Stored in Counter Pulse Capacitor	4 kJ
Coil Volume	2×10^{-2} m^3
Coil Weight	9.2 KG
He Boil-Off Weight	90 KG
Dewar Weight	65 KG
PFN Weight	90 KG
Counter-pulse Capacitor Weight	35 KG
Total System Weight	333 KG

Therefore, referring again to the total system weight as a function of repetition rate (Figure 32), one can scale the output power to values up to 10MW at a particular frequency ($\lesssim$ ~500 pps) by nearly linear relation.

Since capacitor weights also scale with energy, the relative weight advantage of a superconducting discharge system over a capacitive discharge system is maintained, at least for power levels in the 1 - 10MW range.

1. RECOMMENDATIONS

It has become obvious that to significantly improve the accuracy of the weight/power/frequency estimates better data is needed on losses in superconductivity material at high values of ΔB and $\dot{B}$.

On the analytical side, using the existing loss data and empirical fits to this data, operation at frequencies over ~500 pps should be further analyzed to definitively determine whether or not inductive storage systems are superior to capacitive storage systems. This would involve further comparisons of the two most promising approaches; namely, full discharge and partial discharge devices. The large coils needed for partial discharges with small ΔB per discharge need higher fields than the nominal 3 Tesla to significantly reduce their size.

For the full discharge case, smaller magnets ($<$ 20 kJ) must operate at lower values of conductor current density which will raise the critical frequency by lowering the average dissipated power density.

From the component point of view, the design and test of an opening switch that meets the requirements remain to be demonstrated.

It should also be noted that this study is based on existing superconducting wire technology so that advances in this area will impact the detailed results.

It is hoped that the present study, as summarized in this section, will assist in identifying a meaningful program of development and design efforts.

APPENDIX A

COMPUTER PROGRAM MAXOPT

1. INTRODUCTION

This appendix documents the computer codes developed to perform comparisons among inductive energy storage (IES) Approaches 1, 2 and 3. We list the major program functions as a brief discussion of the program's internal operation; list program inputs and options; identify the names, functions and interrelations of the various major subroutines; and list the major output variables. The specific equations and assumptions used to perform the calculations are given in Appendix B.

The program MAXOPT and its separately maintained component LOSSEQS together comprise several thousand lines of Fortran code running at a Control Data Corporation Cybernet data center. A run typically requires a memory field length of 130,000 (octal) words and executes in times on the order of 20 system seconds.

2. MAJOR PROGRAM FUNCTIONS

These are listed in approximate order of execution within a run. Each step uses quantitative results computed in earlier steps.

a. MAXOPT

1) Master control and dispatching
2) Read IES system approach operating parameters - including pulse energy, repetition rate, load impedance, output pulse specification.
3) Synthesize discharge PFN with main energy storage coil, to produce specified pulse shape at the load.

4) Perform transient analysis of PFN during discharge pulse, yielding electrical operating parameters.

5) Design PFN components.

b. LOSSEQS

1) Design toroidal superconducting energy storage coil with support structure.

2) Compute losses in superconductor.

3) Design dewar and cryogenic subsystem.

4) Determine switching and counterpulse requirements.

5) Integrate individual subsystem results into a determination of overall system performance.

6) Produce formatted reports of the computed results, including printer plots.

For transient analysis of the discharge PFN, the program MAXOPT includes portions of MAXAP (Maxwell Analysis Program) - a modified version of the circuit analysis program SCEPTRE which originated under the auspices of the Air Force Weapons Laboratory.

3. PROGRAM INPUTS AND OPTIONS

A set of program inputs with typical values is listed in Table A.1 grouped by particular function. The variables marked with asterisks are used as program control options rather than as system specification parameters. The names, units, and descriptions for the major system inputs are explicitly documented in Table A.2.

4. PROGRAM SUBROUTINES

The program control structure relationships are shown in Figures A.1 and A.2 for MAXOPT and LOSSEQS, respectively. A description of the function of various subroutines, listed separately for MAXOPT and for LOSSEQS, is given in Table A.3.

TABLE A.1

A TYPICAL SAMPLE OF SYSTEM INPUTS

```
$NAM
T=30.0E-6,  TR=2.4E-6,  TF=2.4E-6,
PULSEW=20.0E3,
PFNEPS=0.03,
REPS=5,
*IJTEST=1,
*NPDIS=0,
$END
```

INPUTS FOR PFN SYNTHESIS (GROUP-1)

```
$PDISCH
*XM=1,
*NP=10,
XI0=40.E3,
*DIF=0.5,
$END
```

INPUTS FOR ANALYSIS OF PARTIAL DISCHARGE APPROACHES (GROUP-2)

```
$NAM
BM=3
DELBS=2E-3,
CAPJCO=5.27E9,
CAPJS=2.694E9,
CAPJDS=1E9,
RHO300=1.78E-8,RHOR=100,CMR=3.75E-11
RHOC=8.80E3,
DS=6E-6,
GAMMA1=0.25, GAMMA2=0.5,
ENCAP=400,
ENWBM=100,
XLM1=0.5,XLM2=0.98,XLM3=0.33,XLM4=0.33
XLP=2.E-3,
$END
```

INPUTS FOR COIL DESIGN AND SUPERCONDUCTOR LOSS CALCULATION (GROUP-3)

TABLE A. 1 (Continued)

A TYPICAL SAMPLE OF SYSTEM INPUTS

```
$SWIN
*MCOILOP=1,
*NRUN=1
P=1,
RCONT=2.5E-6,
TARC=1.0E-6
EN1=12000,
ALPHA=1.0,
TPULSE=25.E-6,
U1=0.9,
U2=0.67,
U3=0.8,
U1PP=0.9,
U2PP=0.67
U3PP=0.8,
$END
```

INPUTS FOR COMPUTING
SWITCHING REQUIREMENTS

(GROUP-4)

TABLE A.2

MAJOR PROGRAM INPUTS

	Variable	Unit	Description
1.	Z	Ohm	Load Impedance
2.	T	Sec	Pulse Width
3.	TR	Sec	Pulse Rise Time
4.	TF	Sec	Pulse Fall Time
5.	REPS	Pulses/Sec	Pulse Repetition Rate
6.	XM	-	Number of pulses extracted between two charging cycles (Approach 3 only)
7.	NP	-	Equivalent number of pulses stored for Approach 2.
8.	XI0	Amps	Maximum coil current for Approaches 2 and 3.
9.	BM	Tesla	Maximum B-Field
10.	DELBS	Tesla	Surface-Field Step
11.	CAPJCO	$Amps/m^2$	Zero-Field critical S.C. Current Density at 4.2° K
12.	CAPJS	$Amps/m^2$	Critical Current Density at Operating Field
13.	CAPJDS	$Amps/m^2$	Design Current Density
14.	RHO300	Ohm-meter	Room-Temperature Resistivity of Matrix Material
15.	RHOR	-	Zero-Field Resistivity Ratio
16.	RHOC	Ohm-meter	Resistivity of Matrix Material
17.	DS	m	S.C. Filament Diameter
18.	GAMMA1	-	Ratio of Torus Inner Minor to Major Radii

TABLE A.2 (Continued)

MAJOR PROGRAM INPUTS

	Variable	Unit	Description
19.	GAMMA2	-	Ratio of Torus Outer Minor to Major Radii
20.	ENCAP	-	Number of S.C. Filaments per wire
21.	ENWBM	-	Maximum number of wires per Braid
22.	XLP	-	Conductor Twist Pitch
23.	P	-	Number of isolation switches
24.	RCONT	Ohm	Contact resistance for isolation switches
25.	TARC	Sec	Arcing time of isolation switches
26.	EN1	-	Total number of cycles
27.	ALPHA	-	Number of counterpulse circuits
28.	TPULSE	Sec	Pulse length for counterpulse circuit
29.	U1	-	Weight factor for idling capacitor
30.	U2	-	Volume factor for idling capacitor
31.	U3	-	Dissipation factor for idling capacitor
32.	U1PP	-	Weight factor for counterpulse capacitor
33.	U2PP	-	Volume factor for counterpulse capacitor
34.	U3PP	-	Dissipation factor for counterpulse capacitor

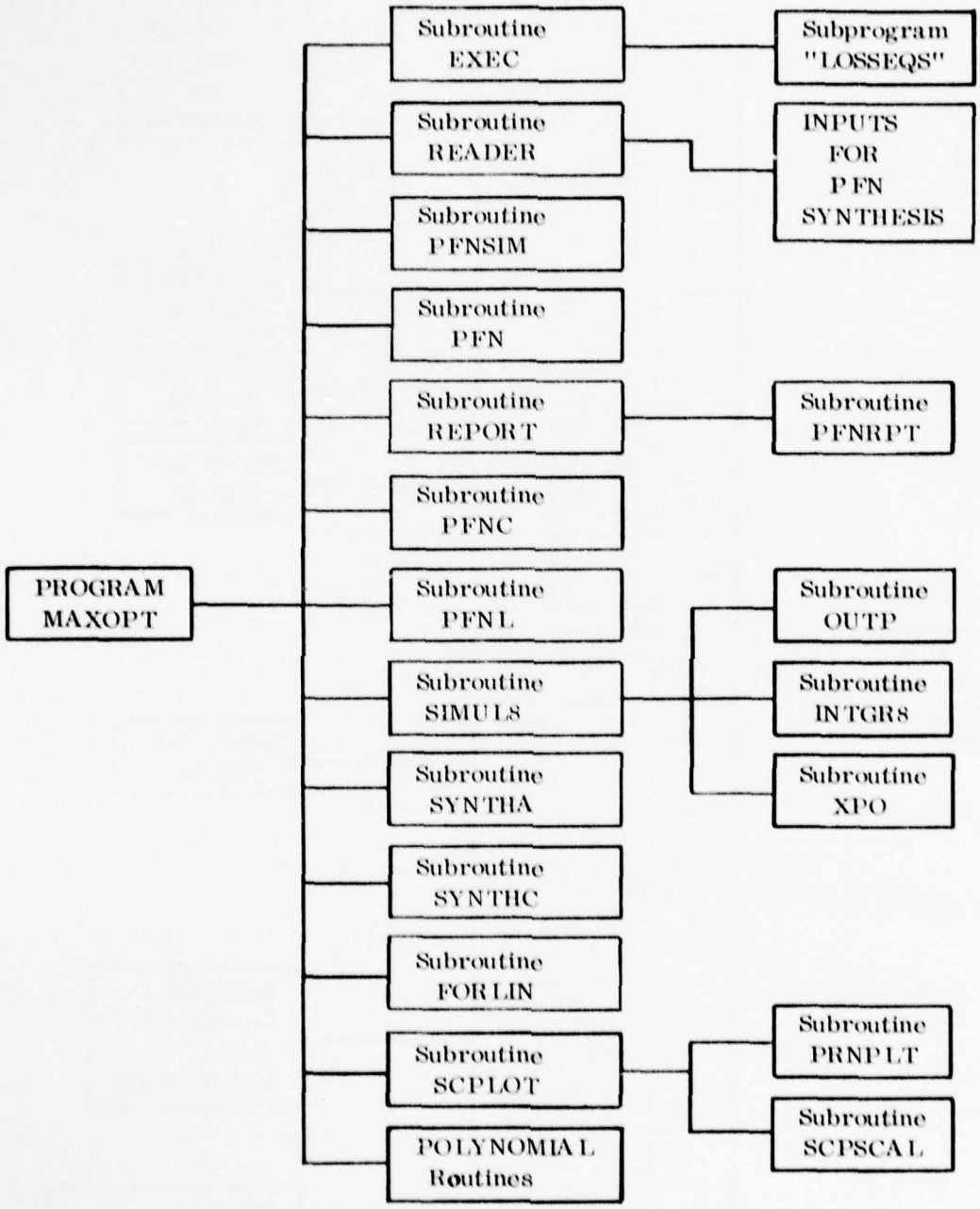

Figure A.1 Control Diagram of Program MAXOPT.

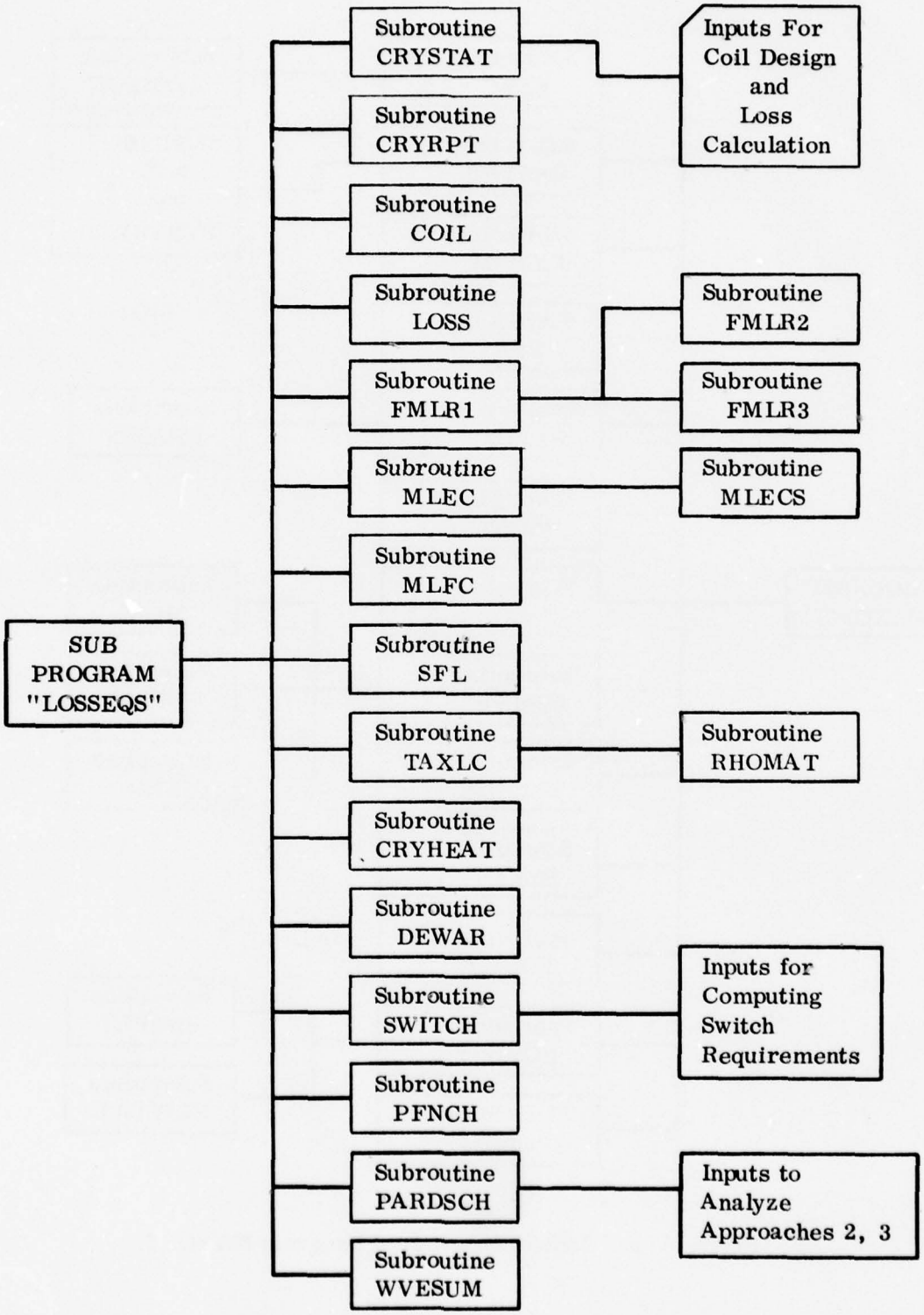

Figure A.2 Control Diagram of "LOSSEQS".

TABLE A.3

DESCRIPTION OF THE FUNCTION OF VARIOUS SUBROUTINES

A. MAXOPT PROGRAM UNITS

Subroutine EXEC

Supervisory subroutine and connecting link between MAXOPT and LOSSEQS.

Subroutine READER

Reads the main system inputs.

Subroutine PFNSIM

Call synthesis routine SYNTHA and also the transient analysis routine SIMUL8.

Subroutine PFN

Mainly a supervisory routine which calls PFNSIM and plotting routines.

Subroutine PFNRPT

Prints results of PFN component design.

Subroutine REPORT

Does printing of the overall system output.

Subroutine PFNC

Designs the capacitive elements of the PFN and computes their dissipation, weights and volumes, etc.

Subroutine PFNL

Designs the inductive elements of the PFN and computes their dissipation, weights and volumes.

Subroutine SIMUL8

Master Transient analysis routine which along with INTGR8, OUTP and XPO does the transient analysis of a Type-A current-fed PFN.

Subroutine SYNTHA

Synthesizes a Type-A current-fed PFN from a Type-C.

TABLE A.3 (Continued)

DESCRIPTION OF THE FUNCTION OF VARIOUS SUBROUTINES

Subroutine SYNTHC

Design a Type-C current-fed PFN identifying real-life network L's and C's with the Fourier components from FORLIN.

Subroutine FORLIN

Does Fourier analysis of the trapezoidal output pulse for use by SYNTHC.

Subroutine SCPLOT

Generates printer plots of transient analysis results using PRNPLT, SCPSCAL, etc.

POLYNOMIAL Routines

Performs arithmetic and evaluation of general polynomials.

B. LOSSEQS Program Units

Subroutine CRYSTAT

Main supervisory routine for "LOSSEQS" subprogram and link between MAXOPT and LOSSEQS. Can be called the counterpart of EXEC. Also reads the inputs for coil design and loss calculations.

Subroutine CRYRPT

Main printing routine for the LOSSEQS part.

Subroutine COIL

Designs the energy storage coil given an inductance value from MAXOPT (or from PARDSCH for partial discharge cases).

Subroutine LOSS

Mainly subroutines which perform superconductor loss calculation.

Subroutine FMLR1, FMLR2, FMLR3

Compute filament magnetization loss in different ranges depending on the degree of penetration of the B-field in the conductors.

TABLE A.3 (Continued)

DESCRIPTION OF THE FUNCTION OF VARIOUS SUBROUTINES

Subroutine MLEC

Calculates eddy-current losses in the matrix. It uses subroutine MLECS to calculate the losses during charging and discharge ramps.

Subroutine MLFC

Computes magnetization loss due to filament coupling.

Subroutine SFL

Computes conductor self-field losses.

Subroutine TAXLC, RHOMAT

Computes time and space averages of various quantities necessary for loss calculation.

Subroutine CRYHEAT

Determines heat flux to be transferred to keep the coil from going normal.

Subroutine DEWAR

Designs the dewar and calculates weight and volume of helium boil-off, etc.

Subroutine SWITCH

Determines the switching requirements, components of counterpulse circuit and idling capacitor.

Subroutine PARDSCH

Activated only for Approaches 2 and 3 (partial discharge). Computes L of the coil and also determines charging power requirements.

Subroutine PFNCH

Designs the components of a charging PFN.

Subroutine WVDSUM

Calculates the overall performance of the system. Adds up weights, volume, and dissipation in different subsystems.

5. MAJOR OUTPUT VARIABLES

The list of important program output variables is included as Table A.4. The variables are grouped under titles describing their relation to the specific areas of the Inductive Energy Storage System. Each quantity is listed with an English description of its significance in the system; the units and internal Fortran names are included for reference.

TABLE A. 4

LIST OF IMPORTANT PROGRAM OUTPUT VARIABLES

Energy Storage Coil Design Variables

Electromagnetic Parameters	Units	Fortran Name
Energy Stored per Pulse	J	E
Inductance of the Energy Storage Coil	H	L
Peak Coil Current	A	PEAKI
Peak Coil Voltage	V	PEAKV
Volts per Turn	V	VT
Maximum Magnetic Field	TESLA	BM
Critical Current Density at Zero Field	A/M2	CAPJCO
S.C. Design Current Density	A/M2	CAPJDS
Critical Current Density at Operating Field	A/M2	CAPJS
Physical Parameters of Torus		
Major Radius of the Torus	M	CAPR
Inner Minor Radius of the Torus	M	R1
Outer Minor Radius of the Winding	M	R2
Toroid Mean Minor Radius/Major Radius	-	GAMMA1
Toroid Mean Winding Radius/Major Radius	-	GAMMA2
Frontal Area of the Coil	M2	AFCOIL
Winding Parameters		
Area of S.C./Area of Composite Core	-	XLM1
Area of Composite Core/Area of Wire	-	XLM2
Area of Wires/Area of Braid	-	XLM3
Area of Braids/Area of Cable	-	XLM4
No. of Turns in the Winding	-	TURNS
Mean Length per Turn	M	XMLT
Diameter of Each Superconducting Filament	M	DS
Diameter of the Composite Core	M	D
Diameter of each Wire	M	DM
Diameter of each Circular Braid	M	DB
Mean Diameter of Pure Matrix Layer	M	DBAR
Area of Each Braid	M2	AB
Area of Cable Consisting of one or more Braids	M2	ACAB

TABLE A.4 (Continued)

LIST OF IMPORTANT PROGRAM OUTPUT VARIABLES

Area of Composite Core per Wire	M2	ACW
Total Area of Superconductor in the Cable	M2	ASCT
Area of Superconductor per Wire	M2	ASCW
No. of Braids in the Cable	-	ENB
Total No. of Wires Required	-	ENW

Winding Weights and Volumes

Total Volume of Matrix Material in the Coil	M3	VM
Volume of Matrix Material in the Matrix Layer	M3	VML
Total Volume of S.C. Material	M3	VSC
Weight of the Winding Material	KG	WC
Weight of the S.C. Material	KG	WSC

Energy Storage Coil Losses

Charging Losses

Eddy Current Loss During Charging	J	TELC1
Filament Magnetization Loss During Charging	J	TFML1
Self Field Loss during Charging	J	TSFL1
Matrix Charging Loss due to Filament Coupling	J	TMLFC1
Total Charging Loss	J	TOTLC

Discharge Losses

Eddy Current Loss During Discharge	J	TELC2
Filament Magnetization Loss During Discharge	J	TFML2
Self Field Loss during Discharge	J	TSFL2
Matrix Discharge Loss due to Filament Coupling	J	TMLFC2
Total Discharge Loss	J	TOTLD
Total Loss per Pulse	J	TOTL

Dewar Variables

Internal Radius of Dewar	M	RD
Height of Dewar	M	HD
Volume of Dewar	M3	VD
Weight of Liquid Helium Boiloff	KG	WHEBO

TABLE A.4 (Continued)

LIST OF IMPORTANT PROGRAM OUTPUT VARIABLES

Thermal Parameters		
Adiabatic Temperature Rise	DEGC	DELTAT
Heat Flux Across Cooling Surface	W/CM2	HFLUX
Switch Requirements		
Isolation Switch		
Dissipation	J	XISOJ
Weight	KG	XISOKG
Volume	M3	XISOV
Idling Capacitor		
Capacitance	FARAD	CIDLE
Energy Stored	J	HIDLE
Dissipation	J	XIDLJ
Weight	KG	XIDLKG
Volume	M3	XIDLV
Counter Pulse Switch		
Dissipation	J	CSWJ
Weight	KG	CSWKG
Volume	M3	CSWV
Resistance and Capacitance		
Capacitance	FARAD	CPULSE
Resistance	OHM	RPULSE
Resistor Parameters		
Dissipation	J	CRESJ
Weight	KG	CRESKG
Volume	M3	CRESV

TABLE A.4 (Continued)

LIST OF IMPORTANT PROGRAM OUTPUT VARIABLES

Capacitor Parameters

Dissipation	J	CCAPJ
Weight	KG	CCAPKG
Volume	M3	CCAPV
Energy Stored	J	WPULSE

The Overall System Components

Inductors

Dissipation per Pulse	J	TTDL
Dissipation (Mission)	J	TTDDL
Ave. Power Dissipation	W	TTPDL
Volume	M3	TTVL
Weight	KG	TTWTL

Capacitors

Dissipation per Pulse	J	TTDC
Dissipation (Mission)	J	TTDDC
Ave. Power Dissipation	W	TTPDC
Volume	M3	TTVC
Weight	KG	TTWTC

Switches

Dissipation per Pulse	J	TDPSW
Dissipation (Mission)	J	TDMSW
Ave. Power Dissipation	W	TPDSW
Volume	M3	TVSW
Weight	KG	THTSW

Energy Storage Coil

Total Loss per Pulse	J	TOTL
Dissipation (Mission)	J	TDCOILM
Average Power Dissipation	W	TPDCOIL
Volume	M3	TVCOIL
Weight	KG	TWTCOIL

TABLE A.4 (Continued)

LIST OF IMPORTANT PROGRAM OUTPUT VARIABLES

Dewar System

Weight of Liquid Helium Boiloff	KG	WHEBO
Volume of Dewar	M3	VD
Weight of Dewar	KG	WDEWAR
Height of Leads	KG	WLEAD
Minimum Volume of Liquid Helium Required	M3	VHEMIN
Minimum Weight of Liquid Helium Required	KG	WHEMIN
Dissipation in the Cryogenic Leads (Mission)	J	XLEADJ
Dissipation in the Cryogenic Leads per Pulse	J	XLEADJP

Overall System Summary

Prime Power Source Voltage	VOLTS	VS
Prime Power Source Average Power	WATTS	PS
Energy at the Load per Pulse	J	WLOADP
Energy at the Load (Mission)	J	WLOADM
Dissipation per Pulse	J	EDSYSP
Dissipation (Mission)	J	TSDYSMM
Average Power Dissipation	W	TPDSYS
Volume	M3	TVSYS
Weight	KG	TWTSYS

APPENDIX B

DESIGN EQUATIONS

This appendix documents the specific equations and relations used for design and computation of the various inductive energy storage system approaches. A computer code subroutine name (referring to Appendix A) is included if there is a clear correspondence between equations and code segments. The several sections of this appendix are listed here for reference.

1) Pulse Forming Network Synthesis

2) Pulse Forming Network Component Design

3) Pulse Forming Network Inductor Tables

4) Toroidal Superconducting Energy Storage Coil Design

5) Superconductor Loss Equations and Dewar Design.

1. CURRENT-FED PFN SYNTHESIS

The mathematical techniques used to synthesize a pulse forming network of arbitrary pulse shape are combined into one description here. The first part of the discussion follows Glasoe & Lebacqz, Pulse Generators, but, for reference, the entire method is presented here as a unified development. The procedure breaks down into three parts. First, using parallel L-C "building blocks" (Figure B.1), a Type C network (Figure B.2) is synthesized to generate the specified pulse shape. Then using Foster's reactance theorem, the Type C network is transformed into a Type A network (Figure B.3). The Type A form is more suitable for inductive energy storage applications since a) only one inductor must be initially charged; b) only two leads need to enter the dewar; and c) spread in component values is minimal. Other types of networks that can be generated are shown in Figures B.4 through B.6. Table B.1 shows typical component values for PFN types C, A, B, F for 8% rise and fall time parameter.

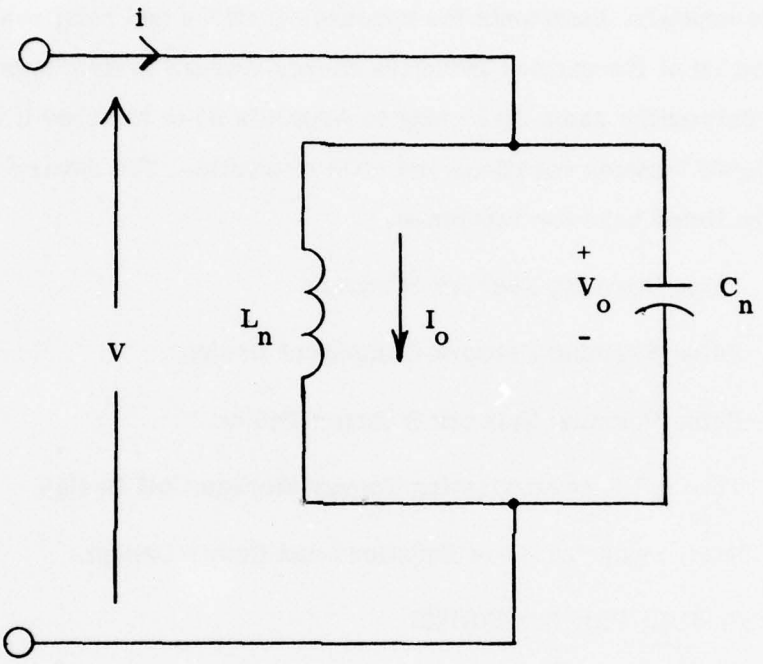

Figure B.1 Type C Network "Building Block" Corresponding to Fourier Coefficient of Pulse Waveform.

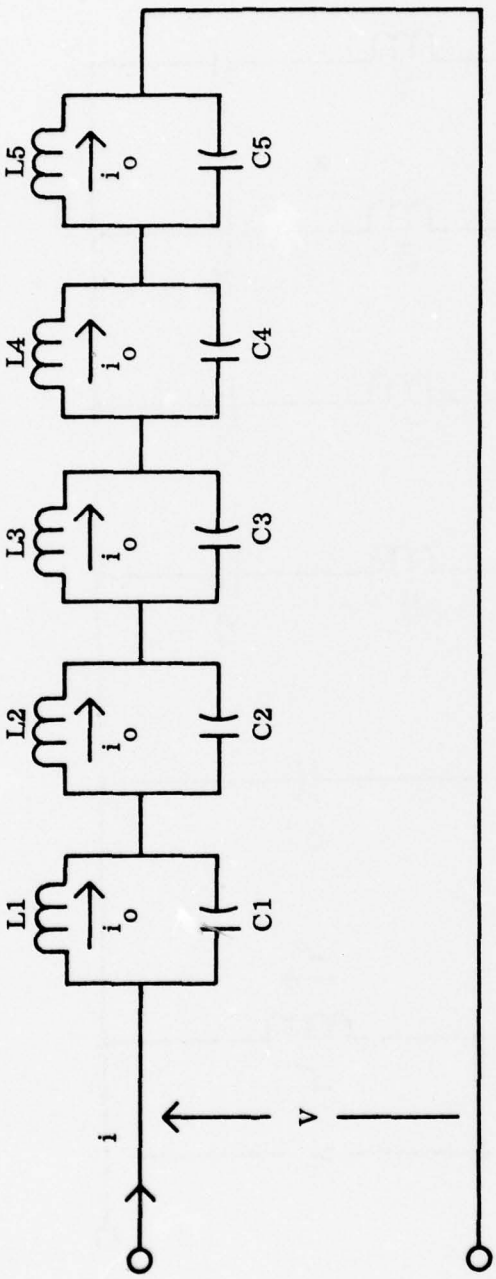

Figure B.2 Type C PFN. A Five-Section Network is Shown.

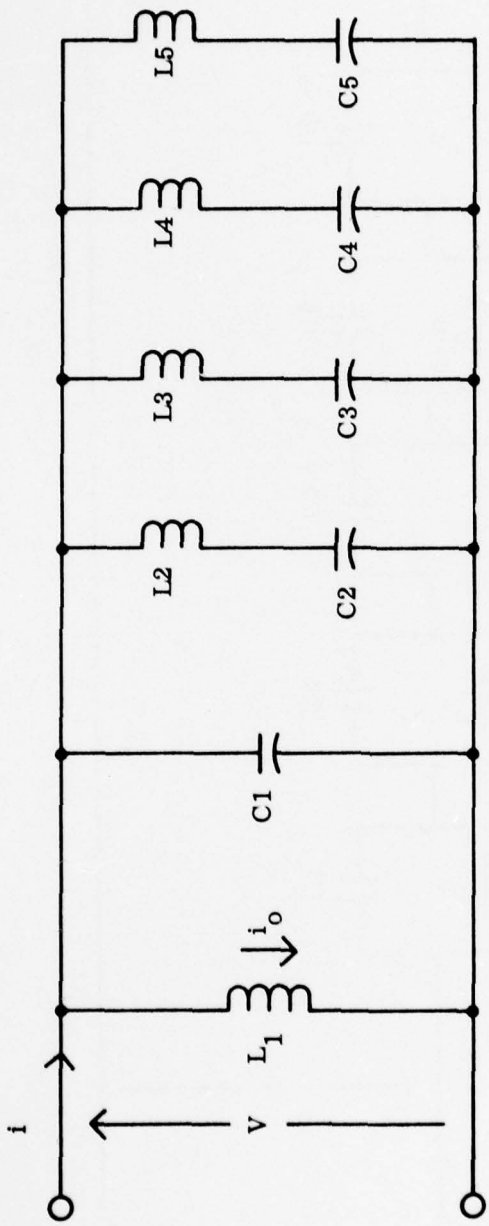

Figure B.3 Type A PFN. A Five-Section Network is shown.

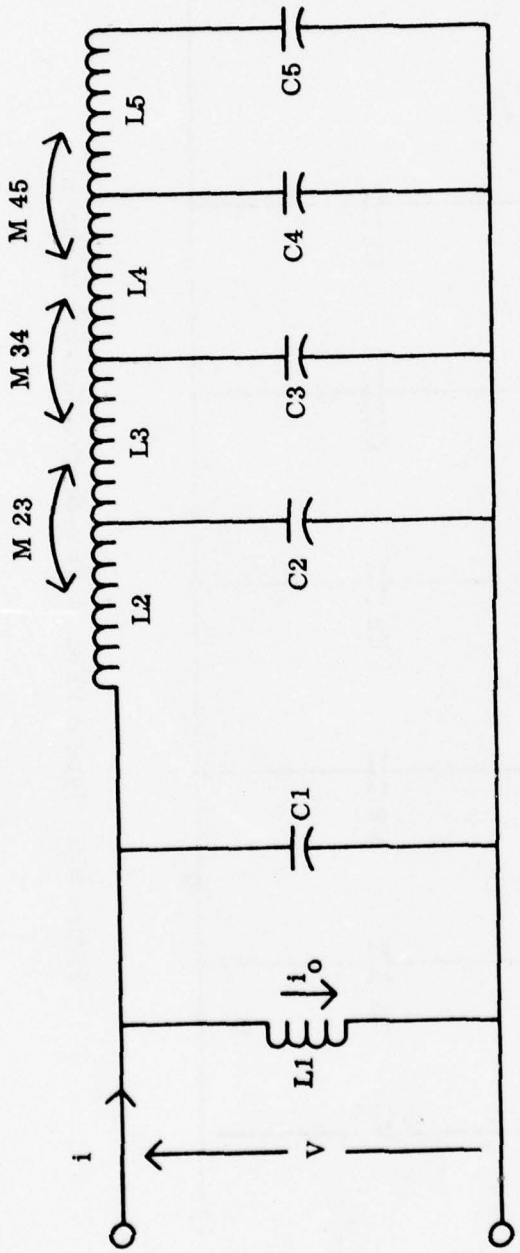

Figure B.4 Type G PFN. A Five-Section Network is shown.

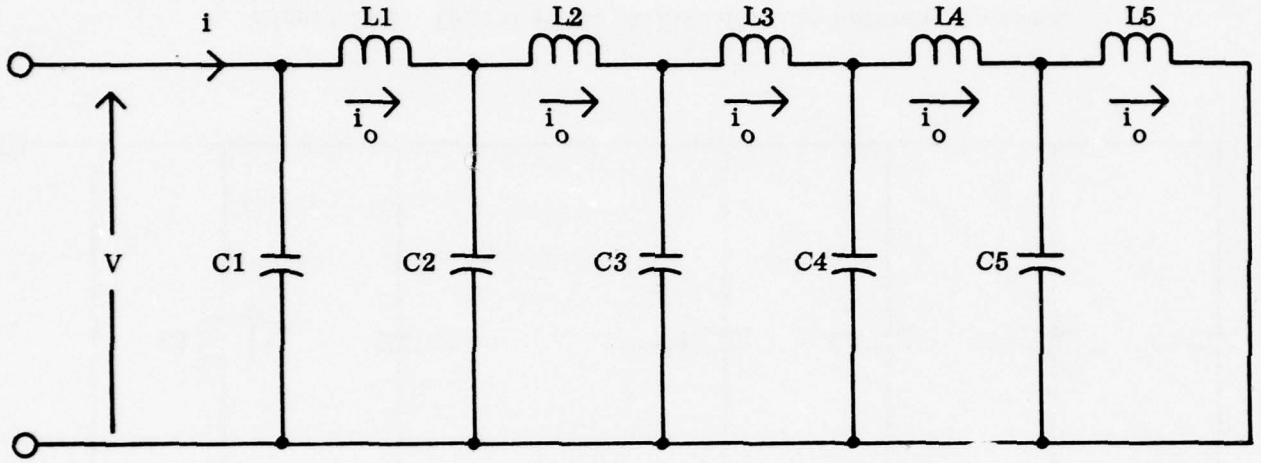

Figure B.5 Type B PFN. A Five-Section Network is shown.

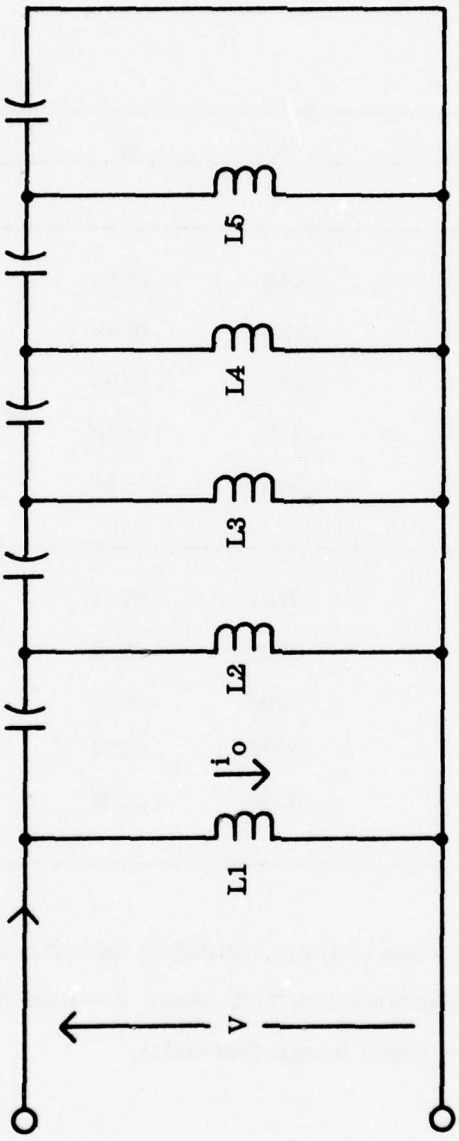

Figure B.6 Type F PFN. A Five-Section Network is shown.

TABLE B.1

NORMALIZED COMPONENT VALUES FOR VARIOUS PFN CONFIGURATIONS - VALUES COMPUTED ON THE BASIS OF 8% RISE AND FALL TIMES

PFN TYPE	C	A	B	F
COMPONENT				
L1	.4003	.456	.0646	.456
L2	.0416	.235	.0642	.054
L3	.0111	.259	.0703	.0090
L4	.00378	.313	.0890	.0012
L5	.00169	.506	.1674	.000076
C1	.253	.0781	.0781	.195
C2	.270	.0893	.0632	.182
C3	.367	.0202	.0658	.423
C4	.547	.0075	.0774	1.83
C5	.740	.0026	.1093	21.2

To convert to actual values, multiply inductances by $Z \times \tau$ and capacitances by τ/Z where Z = load impedance (ohms) and τ = pulse length (seconds).

The synthesis of the Type C PFN can be broken down into several parts. First, the specified voltage pulse is considered to be part of an infinite train of similar pulses. The Fourier series expansion of this voltage wave is then computed, and terms in the series are individually identified with the voltage across the "building block" of Figure B.1. Finally, since the voltage wave is the sum of the Fourier components, the building blocks are connected in series (summing their voltages) resulting in a Type C PFN generating the specified pulse.

Specifically, consider a current-fed transmission line of characteristic impedance Z_o, uniformly charged to a current I_o, with round-trip wave propagation time t. If this is connected to a linear resistive load $R = Z_o$, there will be a voltage pulse of amplitude $I_o Z_o/2$ and length t. If the line is left open, the terminal voltage will be a square wave of period $2t$ and peak amplitude $\pm I_o Z_o$. Each half wave of the resulting infinite train will be identical, except for a factor of ± 2, to the load pulse. This same argument applies, with greater or lesser degree of approximation, to a lumped-constant network generating a pulse with non-zero and not necessarily equal rise and fall times. Hence, as shown in Figure B.7, we may consider the specified load voltage pulse to be part of an infinite train.

An efficient method for computing the Fourier series of a piecewise linear function $F(t)$ was developed. The wave is specified by a series of breakpoint coordinate pairs $(f_0, t_0), (f_1, t_1) \ldots (f_N, t_N)$ where the period of the wave is $(t_N - t_0)$. If the Fourier series to be computed is

$$f(t) = \Sigma (b_n \sin n\omega t + a_n \cos n\omega t) \tag{B.1}$$

then the coefficients are

$$b_n = \frac{1}{(t_N - t_0)} \int_{t_0}^{t_N} f(t) \sin n\omega t \, dt \tag{B.2}$$

Breakpoint Coordinates: N= 5

Point	f	t
P_o	0	0
P1	V_o	T_r
P2	V_o	$T-T_f$
P3	$-V_o$	$T+T_f$
P4	$-V_o$	$2T-T_r$
P5	0	2T

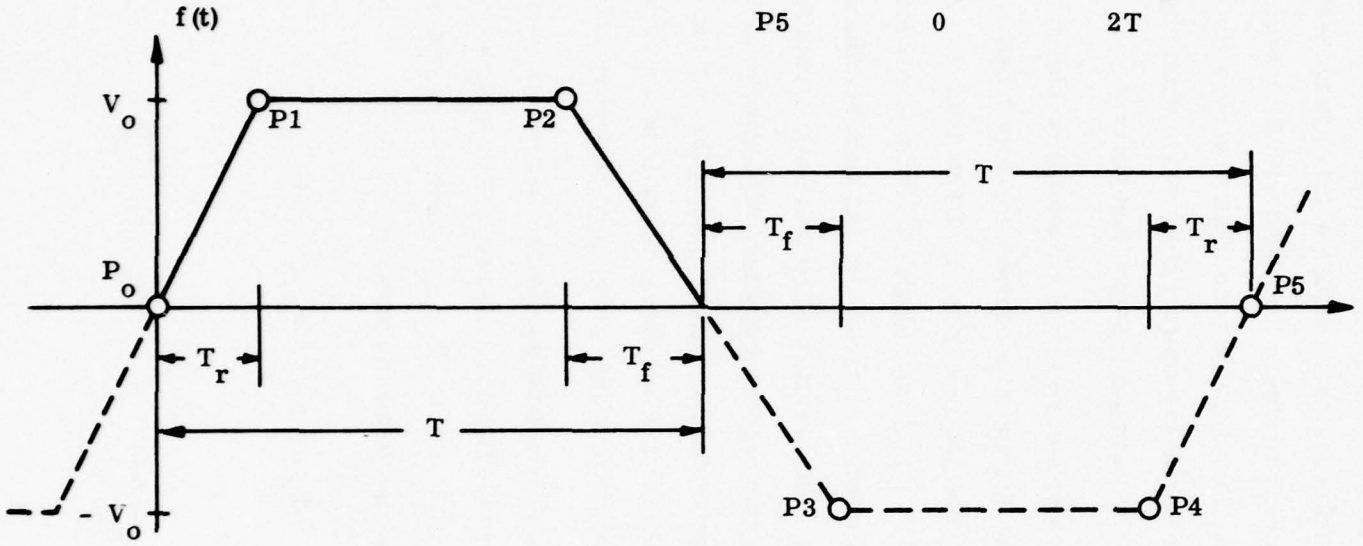

Figure B.7 Piecewise Linear Pulse Shape Shown as Part of Infinite Train.

or

$$b_n = \frac{1}{(t_N - t_0)} \sum_{i=1}^{N} \int_{t_{i-1}}^{t_i} f(t) \sin n\omega t\, dt \qquad \text{(B.3)}$$

where

$$\omega = 1/(2\pi (t_N - t_0))$$

and similarly for the a_n. Since $f(t)$ is piecewise linear, we can find a simple expression for an $f_i^*(t)$ equal to $f(t)$ between the endpoints (f_{i-1}, t_{i-1}), (f_i, t_i):

$$\frac{f_i^* - f_{i-1}}{t - t_{i-1}} = \frac{f_i - f_{i-1}}{t_i - t_{i-1}} \qquad \text{(B.4)}$$

or

$$f_i^* = k_1 t + k_2 \qquad \text{(B.5)}$$

where

$$k_1 = (f_i - f_{i-1})/(t_i - t_{i-1}) \qquad \text{(B.6a)}$$

and

$$k_2 = f_{i-1} + t_{i-1}(f_i - f_{i-1})/t_i - t_{i-1}) \qquad \text{(B.6b)}$$

Using (B.5) in (B.3), which is valid since $f_i^*(t) = f(t)$ between the integration limits, we may evaluate the integral in closed form:

$$\int_{t_i-1}^{t_i} (k_1 t + k_2) \sin n\omega t\, dt = k_1 \int_{t_i-1}^{t_i} t \sin n\omega t\, dt + k_2 \int_{t_{i-1}}^{t_i} \sin n\omega t\, dt$$

$$= \left[-\frac{k_1 t}{n\omega} \cos n\omega t + \frac{k_1}{(n\omega)^2} \sin n\omega t - \frac{k_2}{n\omega} \cos n\omega t \right]_{t - t_{i-1}}^{t = t_i} \qquad \text{(B.7)}$$

and similarly for the a_n and cos terms. The expression (B.7) is evaluated and summed as indicated in (B.6) and (B.3). Considerable computation is avoided by using the recursion formulas

$$\sin nx = \sin x \cos (n-1)x + \cos x \sin (n-1) x$$
$$\cos nx = \cos x \cos (n-1)x - \sin x \sin (n-1) x$$

Having found the Fourier coefficients, we proceed to identify them with the response of the simple circuit of Figure B.1. By inspection, the terminal voltage is

$$v/I_o = \sqrt{(L_n/C_n)} \sin t/\sqrt{(L_nC_n)} + (V_o/I_o) \cos t/\sqrt{(L_nC_n)}$$

Since we have chosen the infinite wave train to be an odd function, we recognize that the cos coefficients a_n must vanish; thus $V_o = 0$. Hence,

$$v/I_o = \sqrt{(L_n/C_n)} \sin t/\sqrt{(L_nC_n)} = b_n \sin n\omega t$$

Thus we can identify

$$b_n = \sqrt{(L_n/C_n)}$$

$$n\omega = \sqrt{(L_nC_n)}$$

Solving these for L_n and C_n we find

$$L_n = b_n n \qquad \text{(B.8a)}$$

$$C_n = n\omega/b_n \qquad \text{(B.8b)}$$

As long as all coefficients b_n are greater than 0, the L_n and C_n will be physically realizable; furthermore, all the L_n have the same initial current (positive) I_o. This is the case for all trapezoidal waveforms of interest.

Several remarks are in order regarding the Fourier series. First, the series converges as $1/n^2$; hence, succeeding PFN sections added in contribute less and less to the waveshape, as expected. Secondly, a process akin to the Gibbs phenomenon occurs as the fractional rise and fall times are decreased. This results in overshoot and ripple distortion of the pulse shape, and the distortion gets worse as more sections are added. There are two factors ameliorating this: a) parasitic capacitances shunting the inductances tend to decrease the high frequency (overshoot) components of the wave; and b) we have powerful transient analysis tools with which we can precisely tailor the component values to yield an optimum pulse shape.

Transforming the Type C network thus found to a Type A network is also largely mathematical. We find the terminal admittance $Y(s)$ of the particular Type C network, expand $Y(s)$ in partial fractions about its roots, and identify the terms thus obtained with physical LC elements. We thus use the fact that the network terminal behavior is completely characterized by its terminal admittance $Y(s)$; in other words, all networks with the same $Y(s)$ have identical terminal behavior.

By inspection, the impedance of the building block of Figure B.1 (with zero initial conditions) is

$$Z_n(s) = \frac{L_n s}{L_n C_n s^2 + 1}$$

where L_n, C_n are given by (B.8) and the symbols n, N now indicate PFN sections, rather than harmonic number or point number. Hence the terminal impedance of the Type C PFN is

$$Z(s) = \sum_{n=1}^{N} Z_n(s) = \sum_{n=1}^{N} \frac{L_n s}{L_n C_n s^2 + 1}$$

Multiplying this out and inverting, we find the terminal admittance

$$Y(s) = \frac{1}{Z(s)} = \frac{\sum_{n=1}^{N} (L_n C_n s^2 + 1)}{\sum_{n=1}^{N} L_n s \prod_{m \neq n}^{N} (L_m C_m s^2 + 1)} \qquad \text{(B.9)}$$

Since the numerator is of degree $2N$ in s and the denominator is of degree $2N-1$, $Y(s)$ has a pole at infinity; since the denominator has a factor of s, there is a pole at zero as well. We then find the remaining $2(N-1)$ imaginary poles of $Y(s)$ and expand in partial fractions giving an expression of the form

$$Y(s) = \frac{A_o}{s} + A_N s + \sum_{n=1}^{N-1} \frac{A_n s}{B_n s^2 + 1} \qquad \text{(B.10)}$$

The computation involved in finding the roots B_n is much reduced by using, where possible, polynomials in s^2 rather than in s. The partial fraction expansion procedure is illustrated for the case $N = 5$. Starting with the multiplied-out form of (B.9) we have

$$Y(s) = \frac{N_5 s^{10} + N_4 s^8 + N_3 s^6 + N_2 s^4 + N_1 s^2 + 1}{D_5 s^9 + D_4 s^7 + D_3 s^5 + D_2 s^3 + D_1 s} = \frac{N(s^2)}{sD(s^2)}$$

Dividing $N(s^2)$ by $D(s^2)$ we get

$$Y(s) = \frac{N_5}{D_5} s + \frac{N'}{sD(s)} \qquad \text{(B.11)}$$

where N' (the remainder) is of degree 4 in s^2. Hence $A_N = N_5/D_5$. We find that $D(s^2)$ has all real, positive coefficients and has all real, negative roots for s^2.

The B_n are the negative reciprocals of these negative roots. Following some uninteresting algebra we find that $A_o = N'_o$ (the constant term of N'). Also,

$$A_n = \left. \frac{N'(s^2)}{(s^2 D(s^2))/(B_n s^2+1)} \right|_{s^2 = -1/B_n} \qquad \text{for } 0 < n < N$$

Having found the A_n, B_n we proceed to identify these with physical admittances. The term A_o/s is the admittance of an inductance $L_1 = 1/A_o$. The term $A_N s$ is a capacitance $C_1 = A_N$. The terms $A_n s/(B_n s^2+1)$ are the admittance of a series combination of $L_{n+1} = B_n/A_n$ and $C_{n+1} = A_n$. Since by (10) the network admittance Y(s) is the sum of these admittances, the network must be the parallel combination of the pieces identified; the network is shown in Figure B.3. A check on the computation is afforded by comparing limiting cases on s. By inspection we find the following must be true:

Type A		Type C	
L_1	=	$\sum_{n=1}^{N} L_n$	(Series combination)
$1/C_1$	=	$\sum_{n=1}^{N} 1/C_n$	(Series combination)

All of the network synthesis procedures discussed above have been implemented in computer code, including polynomial manipulation routines; check cases agree well with results found elsewhere (Glasoe & Lebacqz).

2. PULSE FORMING NETWORK COMPONENT DESIGN

This section shows the relations used in estimating the weights, volumes, etc. for the PFN components. The physical parameters are computed, given the electrical operating conditions from the transient analysis. Capacitor parameters are

determined by standard scaling correlations for existing capacitors. The inductors are designed in considerably more detail, starting with a pre-determined allowable temperature rise assuming worst case (adiabatic) conditions.

a. Capacitors

$$W = \delta_w U_{max}$$

$$V = \delta_v U_{max}$$

$$P = \delta_p U_{max}$$

where

W, V, P are the weight, volume, and dissipation of the capacitor respectively. U_{max} is the maximum (peak) energy stored in the capacitor.

δ_w, δ_v, δ_p are standard scaling coefficients.

b. Toroidal PFN Inductor Design Equations

NOTE: The inductors are sized on the basis of allowable temperature-rise.

Let the allowable adiabatic temperature-rise be $\Delta T(^\circ C)$.

RMS Current through coil = $I_R(A)$

Operating time = $T_M(secs)$

Therefore,

$$T_M \cdot I_R^2 \cdot R_W = W \cdot C_p \cdot \Delta T \qquad (B.12)$$

where,

R_W = Winding resistance (Ω)

W = Winding weight (Kg)

C_p = Specific heat of winding material (J/Kg -°C)

Now,

$$R_W = \rho \frac{\ell}{A_c}$$

or

$$R_W = \rho \cdot \frac{2\pi\bar{\gamma} R_o \cdot N}{A_c} \qquad \text{(B.13)}$$

and

$$W = \delta \cdot 2\pi\bar{\gamma} R_o \cdot N \cdot A_c \qquad \text{(B.14)}$$

Where

$\bar{\gamma}$ = Ratio of mean minor/major radius of the torus.

R_o = Major radius (M)

A_c = Cross-section of the conductor (M^2)

N = Number of turns.

ρ = Resistivity of winding material (Ω - M)

δ = Density of winding material (Kg/M^3)

Substituting for R_W and W from Equations (B. 13) and (B. 14) in (B. 12), we get

$$A_c^2 = \frac{I_R^2 \cdot T_M \cdot \rho}{\delta \cdot C_p \Delta T} \quad (M^4)$$

$$A_c = I_R \sqrt{\frac{T_M \cdot \rho}{\delta C_p \Delta T}} \qquad \text{(B.15)}$$

For charging PFN inductor, skin-depth at even high pps of (say) 1000 is not very small. Therefore, we won't have to use Litz wire. Stranding the conductor will be sufficient.

Hence, for charging PFN, the conductor diameter will be

$$d_c = \sqrt{\frac{4A_c}{\pi\lambda_1}} \quad \text{where } \lambda_1 = \text{area fraction of conductor in wire} \tag{B.16}$$

Since the volts per turn for the charging PFN will be very small, we won't have to worry about corona or breakdown.

$\therefore$ Turn-turn spacing can be just slightly higher than d_c, (say)2mm.

We can write -

$$S = d_c + 0.002 \tag{B.17}$$

For discharge PFN inductor, however, the skin-depth is very small for 30μs discharge which is ~0.4mm. Therefore, we will definitely have to use either Cu or Al tube or Litz wire. The packing factor for Litz wire is around 0.3 or so.

$\therefore$ for discharge PFN.

$$d_c = \sqrt{\frac{4A_c}{\pi\lambda_2}} \qquad \text{where } \lambda_2 = 0.3 \tag{B.18}$$

However, since the volts/turn will be much larger than that in the charging PFN we will have to allow more space for insulation.

Let us use 0.5 cm of solid insulation

$$\therefore \quad s = d_c + 0.005 \tag{B.19}$$

The major radius of the torus is given by,

$$R_o = \left[\frac{LS^2}{4\mu_o \pi^2 (1-\gamma)^2 (1-\sqrt{1-\gamma^2})} \right]^{1/3} \tag{B.20}$$

The number of turns N of the winding is found from the following equation.

$$N = 2\pi R_o(1-\bar{\gamma})/s \qquad (B.21)$$

After determining A_c, R_o and N, these values can be plugged in Equations (B.13) and (B.14) to determine the resistance of the winding and the weight respectively. The dissipation of the inductor can then be calculated from

$$P_w = I_R^2 \cdot R_w \qquad (B.22)$$

3. PFN INDUCTOR TABLES

An auxilliary computer code was written to evaluate just the PFN inductor design equations in the preceding section of this appendix. The electrical parameters used were: inductance INDUC, peak magnetic field BMAX, peak energy stored EMAX, and RMS current IRMS. The physical parameters computed were AREA, diameter DIA, turn spacing SPACED, RADIUS, number of TURNS, WEIGHT, volume VOL, specific weight EN/WT. The electrical parameters computed were resistance RESIS, average power dissipation DISSIP. The sums of inductor weights were also computed.

The design equations were evaluated and printed for the following conditions:

- Discharge and charging PFN
- Copper and aluminum conductor material
- Pulse repetition rates in Hertz of 5, 10, 20, 40, 100, 200, 400, 500, 1000.

The printed output results are reproduced in Table B.2.

TABLE B.2 PFN INDUCTOR PARAMETERS

****
* DISCHARGE *
* PFN Inductor *
****

Frequency = 5.0 Hz ----- COPPER Conductor

Inductor Number		(2)	(3)	(4)	(5)
Induc	(H)	2.828E-05	3.051E-05	3.549E-05	4.805E-05
Area	(m^2)	2.973E-06	1.378E-06	7.895E-07	4.372E-07
Dia	(m)	3.552E-03	2.418E-03	1.830E-03	1.362E-03
Spaced	(m)	8.552E-03	7.418E-03	6.830E-03	6.362E-03
Radius	(m)	1.076E-01	1.003E-01	9.988E-02	1.054E-01
Turns		39.516	42.497	45.940	52.040
Weight	(ks)	3.534E-01	1.643E-01	1.013E-01	6.704E-02
Resis	(m)	7.681E-02	1.663E-01	3.122E-01	6.740E-01
Dissip	(Watts)	3.693E+02	1.717E+02	1.058E+02	7.005E+01
BMax	(Tesla)	1.177E+00	6.286E-01	3.912E-01	2.326E-01
Vol	(m^3)	1.229E-02	9.972E-03	9.835E-03	1.155E-02
EMax	(Joule)	9.067E+02	2.101E+02	8.023E+01	3.331E+01
En/Wt	(J/lb)	1.166E+03	5.812E+02	3.600E+02	2.258E+02
Irms	(Amps)	6.934E+01	3.213E+01	1.841E+01	1.020E+01

Total Inductor Weight = .6860 ks

****
* CHARGING *
* PFN Inductor *
****

Frequency = 5.0 Hz ----- COPPER Conductor

Inductor Number		(2)	(3)	(4)	(5)
Induc	(H)	2.828E-05	3.051E-05	3.549E-05	4.805E-05
Area	(m^2)	2.427E-04	1.125E-04	6.446E-05	3.569E-05
Dia	(m)	2.101E-02	1.430E-02	1.083E-02	8.057E-03
Spaced	(m)	2.301E-02	1.630E-02	1.283E-02	1.006E-02
Radius	(m)	2.081E-01	1.696E-01	1.520E-01	1.430E-01
Turns		28.411	32.686	37.236	44.673
Weight	(ks)	4.013E+01	1.744E+01	1.020E+01	6.376E+00
Resis	(m)	1.309E-03	2.648E-03	4.718E-03	9.616E-03
Dissip	(Watts)	4.193E+04	1.822E+04	1.066E+04	6.662E+03
BMax	(Tesla)	4.373E-01	2.860E-01	2.083E-01	1.471E-01
Vol	(m^3)	8.895E-02	4.817E-02	3.469E-02	2.887E-02
EMax	(Joule)	9.067E+02	2.101E+02	8.023E+01	3.331E+01
En/Wt	(J/lb)	1.027E+01	5.476E+00	3.574E+00	2.375E+00
Irms	(Amps)	5.661E+03	2.623E+03	1.503E+03	8.324E+02

Total Inductor Weight = 74.1435 ks

TABLE B.2 PFN INDUCTOR PARAMETERS (Continued)

****
* DISCHARGE *
* PFN Inductor *
****

Frequency = 10.0 Hz ----- COPPER Conductor

Inductor Number	(2)	(3)	(4)	(5)
Induc (H)	2.828E-05	3.051E-05	3.549E-05	4.805E-05
Area (m^2)	4.205E-06	1.948E-06	1.116E-06	6.182E-07
Dia (m)	4.224E-03	2.876E-03	2.177E-03	1.620E-03
Spaced (m)	9.224E-03	7.876E-03	7.177E-03	6.620E-03
Radius (m)	1.131E-01	1.044E-01	1.032E-01	1.082E-01
Turns	38.532	41.657	45.189	51.356
Weight (kg)	5.125E-01	2.370E-01	1.456E-01	9.607E-02
Resis (m)	5.570E-02	1.199E-01	2.245E-01	4.829E-01
Dissip (Watts)	5.356E+02	2.477E+02	1.522E+02	1.004E+02
BMax (Tesla)	1.091E+00	5.921E-01	3.723E-01	2.235E-01
Vol (m^3)	1.429E-02	1.124E-02	1.086E-02	1.251E-02
EMax (Joule)	9.067E+02	2.101E+02	8.023E+01	3.331E+01
En/Wt (J/lb)	8.042E+02	4.029E+02	2.504E+02	1.576E+02
Irms (Amps)	9.806E+01	4.544E+01	2.604E+01	1.442E+01

Total Inductor Weight = .9912 kg

****
* CHARGING *
* PFN Inductor *
****

Frequency = 10.0 Hz ----- COPPER Conductor

Inductor Number	(2)	(3)	(4)	(5)
Induc (H)	2.828E-05	3.051E-05	3.549E-05	4.805E-05
Area (m^2)	2.427E-04	1.125E-04	6.445E-05	3.569E-05
Dia (m)	2.101E-02	1.430E-02	1.083E-02	8.057E-03
Spaced (m)	2.301E-02	1.630E-02	1.283E-02	1.006E-02
Radius (m)	2.081E-01	1.696E-01	1.520E-01	1.430E-01
Turns	28.411	32.686	37.236	44.673
Weight (kg)	4.012E+01	1.744E+01	1.020E+01	6.375E+00
Resis (m)	1.309E-03	2.648E-03	4.719E-03	9.617E-03
Dissip (Watts)	4.193E+04	1.822E+04	1.066E+04	6.662E+03
BMax (Tesla)	4.373E-01	2.860E-01	2.083E-01	1.471E-01
Vol (m^3)	8.895E-02	4.817E-02	3.469E-02	2.887E-02
EMax (Joule)	9.067E+02	2.101E+02	8.023E+01	3.331E+01
En/Wt (J/lb)	1.027E+01	5.476E+00	3.575E+00	2.375E+00
Irms (Amps)	5.661E+03	2.623E+03	1.503E+03	8.323E+02

Total Inductor Weight = 74.1372 kg

TABLE B.2 PFN INDUCTOR PARAMETERS (Continued)

****
* DISCHARGE *
* PFN Inductor *
****

Frequency = 20.0 Hz ----- COPPER Conductor

Inductor Number	(2)	(3)	(4)	(5)
Induc (H)	2.828E-05	3.051E-05	3.549E-05	4.805E-05
Area (m^2)	5.746E-06	2.756E-06	1.579E-06	8.743E-07
Dia (m)	5.024E-03	3.420E-03	2.589E-03	1.926E-03
Spaced (m)	1.002E-02	8.420E-03	7.589E-03	6.926E-03
Radius (m)	1.196E-01	1.092E-01	1.071E-01	1.115E-01
Turns	37.479	40.740	44.356	50.587
Weight (kg)	7.451E-01	3.427E-01	2.098E-01	1.379E-01
Resis (m)	4.049E-02	8.672E-02	1.617E-01	3.467E-01
Dissip (Watts)	7.787E+02	3.581E+02	2.193E+02	1.441E+02
BMax (Tesla)	1.004E+00	5.538E-01	3.521E-01	2.136E-01
Vol (m^3)	1.688E-02	1.285E-02	1.214E-02	1.369E-02
EMax (Joule)	9.067E+02	2.101E+02	8.023E+01	3.331E+01
En/Wt (J/lb)	5.531E+02	2.786E+02	1.738E+02	1.098E+02
Irms (Amps)	1.387E+02	6.426E+01	3.682E+01	2.039E+01

Total Inductor Weight = 1.4356 kg

****
* CHARGING *
* PFN Inductor *
****

Frequency = 20.0 Hz ----- COPPER Conductor

Inductor Number	(2)	(3)	(4)	(5)
Induc (H)	2.828E-05	3.051E-05	3.549E-05	4.805E-05
Area (m^2)	2.427E-04	1.125E-04	6.444E-05	3.568E-05
Dia (m)	2.101E-02	1.430E-02	1.083E-02	8.056E-03
Spaced (m)	2.301E-02	1.630E-02	1.283E-02	1.006E-02
Radius (m)	2.081E-01	1.696E-01	1.520E-01	1.430E-01
Turns	28.411	32.687	37.237	44.674
Weight (kg)	4.012E+01	1.743E+01	1.020E+01	6.374E+00
Resis (m)	1.309E-03	2.648E-03	4.719E-03	9.618E-03
Dissip (Watts)	4.192E+04	1.822E+04	1.066E+04	6.661E+03
BMax (Tesla)	4.373E-01	2.860E-01	2.083E-01	1.471E-01
Vol (m^3)	8.894E-02	4.816E-02	3.468E-02	2.886E-02
EMax (Joule)	9.067E+02	2.101E+02	8.023E+01	3.331E+01
En/Wt (J/lb)	1.027E+01	5.477E+00	3.575E+00	2.375E+00
Irms (Amps)	5.660E+03	2.623E+03	1.503E+03	8.322E+02

Total Inductor Weight = 74.1244 kg

TABLE B.2 PFN INDUCTOR PARAMETERS (Continued)

```
**********************
*  DISCHARGE         *
* PFN Inductor       *
**********************
```

Frequency = 40.0 Hz ----- COPPER Conductor

Inductor Number	(2)	(3)	(4)	(5)
Induc (H)	2.828E-05	3.051E-05	3.549E-05	4.805E-05
Area (m^2)	8.409E-06	3.897E-06	2.233E-06	1.236E-06
Dia (m)	5.974E-03	4.067E-03	3.078E-03	2.291E-03
Spaced (m)	1.097E-02	9.067E-03	8.078E-03	7.291E-03
Radius (m)	1.270E-01	1.147E-01	1.117E-01	1.154E-01
Turns	36.364	39.747	43.441	49.729
Weight (kg)	1.086E+00	4.968E-01	3.030E-01	1.984E-01
Resis (m)	2.951E-02	6.285E-02	1.167E-01	2.494E-01
Dissip (Watts)	1.135E+03	5.191E+02	3.166E+02	2.073E+02
BMax (Tesla)	9.169E-01	5.143E-01	3.308E-01	2.029E-01
Vol (m^3)	2.023E-02	1.490E-02	1.376E-02	1.517E-02
EMax (Joule)	9.067E+02	2.101E+02	8.023E+01	3.331E+01
En/Wt (J/lb)	3.795E+02	1.922E+02	1.204E+02	7.630E+01
Irms (Amps)	1.961E+02	9.088E+01	5.208E+01	2.884E+01

Total Inductor Weight = 2.0843 kg

```
**********************
*  CHARGING          *
* PFN Inductor       *
**********************
```

Frequency = 40.0 Hz ----- COPPER Conductor

Inductor Number	(2)	(3)	(4)	(5)
Induc (H)	2.828E-05	3.051E-05	3.549E-05	4.805E-05
Area (m^2)	2.426E-04	1.124E-04	6.442E-05	3.567E-05
Dia (m)	2.101E-02	1.430E-02	1.082E-02	8.055E-03
Spaced (m)	2.301E-02	1.630E-02	1.282E-02	1.006E-02
Radius (m)	2.081E-01	1.696E-01	1.520E-01	1.430E-01
Turns	28.413	32.688	37.238	44.676
Weight (kg)	4.010E+01	1.743E+01	1.020E+01	6.372E+00
Resis (m)	1.309E-03	2.649E-03	4.721E-03	9.621E-03
Dissip (Watts)	4.191E+04	1.821E+04	1.066E+04	6.658E+03
BMax (Tesla)	4.374E-01	2.861E-01	2.083E-01	1.471E-01
Vol (m^3)	8.891E-02	4.815E-02	3.467E-02	2.886E-02
EMax (Joule)	9.067E+02	2.101E+02	8.023E+01	3.331E+01
En/Wt (J/lb)	1.028E+01	5.479E+00	3.577E+00	2.376E+00
Irms (Amps)	5.658E+03	2.622E+03	1.502E+03	8.319E+02

Total Inductor Weight = 74.0988 kg

TABLE B.2 PFN INDUCTOR PARAMETERS (Continued)

```
****************
*  DISCHARGE   *
* PFN Inductor *
****************
```

Frequency = 100.0 Hz ----- COPPER Conductor

Inductor Number	(2)	(3)	(4)	(5)
Induc (H)	2.828E-05	3.051E-05	3.549E-05	4.805E-05
Area (m^2)	1.330E-05	6.162E-06	3.531E-06	1.955E-06
Dia (m)	7.512E-03	5.114E-03	3.871E-03	2.881E-03
Spaced (m)	1.251E-02	1.011E-02	8.871E-03	7.881E-03
Radius (m)	1.386E-01	1.234E-01	1.189E-01	1.216E-01
Turns	34.809	38.325	42.107	48.456
Weight (kg)	1.794E+00	8.146E-01	4.942E-01	3.220E-01
Resis (m)	1.950E-02	4.123E-02	7.617E-02	1.618E-01
Dissip (Watts)	1.875E+03	8.513E+02	5.165E+02	3.364E+02
BMax (Tesla)	8.042E-01	4.611E-01	3.012E-01	1.878E-01
Vol (m^3)	2.630E-02	1.854E-02	1.659E-02	1.772E-02
EMax (Joule)	9.067E+02	2.101E+02	8.023E+01	3.331E+01
En/Wt (J/lb)	2.297E+02	1.172E+02	7.379E+01	4.702E+01
Irms (Amps)	3.101E+02	1.437E+02	8.234E+01	4.559E+01

Total Inductor Weight = 3.4248 kg

```
****************
*  CHARGING    *
* PFN Inductor *
****************
```

Frequency = 100.0 Hz ----- COPPER Conductor

Inductor Number	(2)	(3)	(4)	(5)
Induc (H)	2.828E-05	3.051E-05	3.549E-05	4.805E-05
Area (m^2)	2.424E-04	1.123E-04	6.436E-05	3.564E-05
Dia (m)	2.100E-02	1.429E-02	1.082E-02	8.051E-03
Spaced (m)	2.300E-02	1.629E-02	1.282E-02	1.005E-02
Radius (m)	2.080E-01	1.696E-01	1.520E-01	1.430E-01
Turns	28.417	32.692	37.243	44.681
Weight (kg)	4.006E+01	1.741E+01	1.019E+01	6.365E+00
Resis (m)	1.310E-03	2.651E-03	4.724E-03	9.628E-03
Dissip (Watts)	4.186E+04	1.819E+04	1.064E+04	6.652E+03
BMax (Tesla)	4.376E-01	2.862E-01	2.084E-01	1.472E-01
Vol (m^3)	3.884E-02	4.811E-02	3.465E-02	2.884E-02
EMax (Joule)	9.067E+02	2.101E+02	8.023E+01	3.331E+01
En/Wt (J/lb)	1.029E+01	5.485E+00	3.580E+00	2.378E+00
Irms (Amps)	5.653E+03	2.620E+03	1.501E+03	8.312E+02

Total Inductor Weight = 74.0222 kg

TABLE B.2 PFN INDUCTOR PARAMETERS (Continued)

```
****************
*  DISCHARGE   *
* PFN Inductor *
****************
```

Frequency = 200.0 Hz ----- COPPER Conductor

Inductor Number	(2)	(3)	(4)	(5)
Induc (H)	2.828E-05	3.051E-05	3.549E-05	4.805E-05
Area (m^2)	1.880E-05	8.714E-06	4.993E-06	2.765E-06
Dia (m)	8.933E-03	6.081E-03	4.603E-03	3.426E-03
Spaced (m)	1.393E-02	1.108E-02	9.603E-03	8.426E-03
Radius (m)	1.489E-01	1.311E-01	1.254E-01	1.271E-01
Turns	33.583	37.175	41.008	47.388
Weight (kg)	2.630E+00	1.188E+00	7.177E-01	4.656E-01
Resis (m)	1.429E-02	3.005E-02	5.531E-02	1.170E-01
Dissip (Watts)	2.748E+03	1.241E+03	7.500E+02	4.865E+02
BMax (Tesla)	7.222E-01	4.208E-01	2.782E-01	1.756E-01
Vol (m^3)	3.261E-02	2.225E-02	1.944E-02	2.026E-02
EMax (Joule)	9.067E+02	2.101E+02	8.023E+01	3.331E+01
En/Wt (J/lb)	1.567E+02	8.039E+01	5.082E+01	3.252E+01
Irms (Amps)	4.385E+02	2.032E+02	1.164E+02	6.448E+01

Total Inductor Weight = 5.0007 kg

```
****************
*  CHARGING    *
* PFN Inductor *
****************
```

Frequency = 200.0 Hz ----- COPPER Conductor

Inductor Number	(2)	(3)	(4)	(5)
Induc (H)	2.828E-05	3.051E-05	3.549E-05	4.805E-05
Area (m^2)	2.420E-04	1.122E-04	6.427E-05	3.559E-05
Dia (m)	2.098E-02	1.428E-02	1.081E-02	8.045E-03
Spaced (m)	2.298E-02	1.628E-02	1.281E-02	1.005E-02
Radius (m)	2.079E-01	1.695E-01	1.519E-01	1.429E-01
Turns	28.423	32.700	37.251	44.690
Weight (kg)	3.999E+01	1.738E+01	1.017E+01	6.354E+00
Resis (m)	1.312E-03	2.655E-03	4.730E-03	9.641E-03
Dissip (Watts)	4.179E+04	1.816E+04	1.063E+04	6.640E+03
BMax (Tesla)	4.379E-01	2.864E-01	2.086E-01	1.473E-01
Vol (m^3)	8.872E-02	4.805E-02	3.460E-02	2.880E-02
EMax (Joule)	9.067E+02	2.101E+02	8.023E+01	3.331E+01
En/Wt (J/lb)	1.031E+01	5.494E+00	3.586E+00	2.382E+00
Irms (Amps)	5.644E+03	2.616E+03	1.499E+03	8.299E+02

Total Inductor Weight = 73.8943 kg

TABLE B.2 PFN INDUCTOR PARAMETERS (Continued)

****
* DISCHARGE *
* PFN Inductor *
****

Frequency = 400.0 Hz ----- COPPER Conductor

Inductor Number		(2)	(3)	(4)	(5)
Induc	(H)	2.828E-05	3.051E-05	3.549E-05	4.805E-05
Area	(m^2)	2.659E-05	1.232E-05	7.061E-06	3.910E-06
Dia	(m)	1.062E-02	7.232E-03	5.474E-03	4.074E-03
Spaced	(m)	1.562E-02	1.223E-02	1.047E-02	9.074E-03
Radius	(m)	1.608E-01	1.401E-01	1.328E-01	1.335E-01
Turns		32.325	35.971	39.838	46.232
Weight	(kg)	3.864E+00	1.736E+00	1.045E+00	6.749E-01
Resis	(m)	1.050E-02	2.196E-02	4.026E-02	8.482E-02
Dissip	(Watts)	4.038E+03	1.814E+03	1.092E+03	7.053E+02
BMax	(Tesla)	6.441E-01	3.812E-01	2.551E-01	1.631E-01
Vol	(m^3)	4.100E-02	2.711E-02	2.313E-02	2.350E-02
EMax	(Joule)	9.067E+02	2.101E+02	8.023E+01	3.331E+01
En/Wt	(J/lb)	1.067E+02	5.501E+01	3.491E+01	2.243E+01
Irms	(Amps)	6.202E+02	2.874E+02	1.647E+02	9.119E+01

Total Inductor Weight = 7.3192 kg

****
* CHARGING *
* PFN Inductor *
****

Frequency = 400.0 Hz ----- COPPER Conductor

Inductor Number		(2)	(3)	(4)	(5)
Induc	(H)	2.828E-05	3.051E-05	3.549E-05	4.805E-05
Area	(m^2)	2.413E-04	1.118E-04	6.407E-05	3.548E-05
Dia	(m)	2.095E-02	1.426E-02	1.080E-02	8.033E-03
Spaced	(m)	2.295E-02	1.626E-02	1.280E-02	1.003E-02
Radius	(m)	2.077E-01	1.693E-01	1.518E-01	1.428E-01
Turns		28.436	32.714	37.267	44.708
Weight	(kg)	3.985E+01	1.732E+01	1.013E+01	6.333E+00
Resis	(m)	1.315E-03	2.661E-03	4.743E-03	9.666E-03
Dissip	(Watts)	4.165E+04	1.810E+04	1.059E+04	6.618E+03
BMax	(Tesla)	4.385E-01	2.868E-01	2.088E-01	1.475E-01
Vol	(m^3)	8.847E-02	4.792E-02	3.451E-02	2.873E-02
EMax	(Joule)	9.067E+02	2.101E+02	8.023E+01	3.331E+01
En/Wt	(J/lb)	1.034E+01	5.513E+00	3.599E+00	2.391E+00
Irms	(Amps)	5.627E+03	2.608E+03	1.494E+03	8.274E+02

Total Inductor Weight = 73.6380 kg

TABLE B.2 PFN INDUCTOR PARAMETERS (Continued)

```
****************
*  DISCHARGE   *
* PFN Inductor *
****************
```

Frequency = 500.0 Hz ----- COPPER Conductor

Inductor Number	(2)	(3)	(4)	(5)
Induc (H)	2.828E-05	3.051E-05	3.549E-05	4.805E-05
Area (m^2)	2.973E-05	1.378E-05	7.895E-06	4.372E-06
Dia (m)	1.123E-02	7.647E-03	5.788E-03	4.307E-03
Spaced (m)	1.623E-02	1.265E-02	1.079E-02	9.307E-03
Radius (m)	1.649E-01	1.432E-01	1.355E-01	1.358E-01
Turns	31.915	35.573	39.448	45.842
Weight (kg)	4.375E+00	1.962E+00	1.180E+00	7.610E-01
Resis (m)	9.510E-03	1.986E-02	3.636E-02	7.651E-02
Dissip (Watts)	4.572E+03	2.051E+03	1.233E+03	7.952E+02
BMax (Tesla)	6.199E-01	3.687E-01	2.477E-01	1.590E-01
Vol (m^3)	4.426E-02	2.899E-02	2.454E-02	2.472E-02
EMax (Joule)	9.067E+02	2.101E+02	8.023E+01	3.331E+01
En/Wt (J/lb)	9.420E+01	4.865E+01	3.092E+01	1.989E+01
Irms (Amps)	6.934E+02	3.213E+02	1.841E+02	1.020E+02

Total Inductor Weight = 8.2783 kg

```
****************
*  CHARGING    *
* PFN Inductor *
****************
```

Frequency = 500.0 Hz ----- COPPER Conductor

Inductor Number	(2)	(3)	(4)	(5)
Induc (H)	2.828E-05	3.051E-05	3.549E-05	4.805E-05
Area (m^2)	2.409E-04	1.116E-04	6.398E-05	3.543E-05
Dia (m)	2.093E-02	1.425E-02	1.079E-02	8.027E-03
Spaced (m)	2.293E-02	1.625E-02	1.279E-02	1.003E-02
Radius (m)	2.076E-01	1.693E-01	1.517E-01	1.427E-01
Turns	28.443	32.721	37.275	44.718
Weight (kg)	3.978E+01	1.729E+01	1.012E+01	6.322E+00
Resis (m)	1.317E-03	2.665E-03	4.749E-03	9.679E-03
Dissip (Watts)	4.157E+04	1.807E+04	1.057E+04	6.606E+03
BMax (Tesla)	4.388E-01	2.870E-01	2.090E-01	1.476E-01
Vol (m^3)	8.835E-02	4.786E-02	3.447E-02	2.870E-02
EMax (Joule)	9.067E+02	2.101E+02	8.023E+01	3.331E+01
En/Wt (J/lb)	1.036E+01	5.523E+00	3.605E+00	2.395E+00
Irms (Amps)	5.619E+03	2.604E+03	1.492E+03	8.262E+02

Total Inductor Weight = 73.5097 kg

TABLE B.2 PFN INDUCTOR PARAMETERS (Continued)

```
*****************
*  DISCHARGE    *
* PFN Inductor *
*****************
```

Frequency =1000.0 Hz ----- COPPER Conductor

Inductor Number	(2)	(3)	(4)	(5)
Induc (H)	2.828E-05	3.051E-05	3.549E-05	4.805E-05
Area (m^2)	4.205E-05	1.948E-05	1.116E-05	6.182E-06
Dia (m)	1.336E-02	9.094E-03	6.884E-03	5.122E-03
Spaced (m)	1.836E-02	1.409E-02	1.188E-02	1.012E-02
Radius (m)	1.790E-01	1.539E-01	1.445E-01	1.436E-01
Turns	30.633	34.312	38.197	44.577
Weight (kg)	6.447E+00	2.877E+00	1.723E+00	1.107E+00
Resis (m)	7.006E-03	1.456E-02	2.655E-02	5.563E-02
Dissip (Watts)	6.737E+03	3.007E+03	1.800E+03	1.157E+03
BMax (Tesla)	5.481E-01	3.309E-01	2.249E-01	1.462E-01
Vol (m^3)	5.661E-02	3.600E-02	2.977E-02	2.924E-02
EMax (Joule)	9.067E+02	2.101E+02	8.023E+01	3.331E+01
En/Wt (J/lb)	6.393E+01	3.318E+01	2.117E+01	1.368E+01
Irms (Amps)	9.806E+02	4.544E+02	2.604E+02	1.442E+02

Total Inductor Weight = 12.1535 kg

```
*****************
*  CHARGING     *
* PFN Inductor *
*****************
```

Frequency =1000.0 Hz ----- COPPER Conductor

Inductor Number	(2)	(3)	(4)	(5)
Induc (H)	2.828E-05	3.051E-05	3.549E-05	4.805E-05
Area (m^2)	2.391E-04	1.108E-04	6.349E-05	3.515E-05
Dia (m)	2.085E-02	1.420E-02	1.075E-02	7.996E-03
Spaced (m)	2.285E-02	1.620E-02	1.275E-02	9.996E-03
Radius (m)	2.072E-01	1.689E-01	1.514E-01	1.424E-01
Turns	28.476	32.758	37.315	44.763
Weight (kg)	3.943E+01	1.714E+01	1.003E+01	6.267E+00
Resis (m)	1.325E-03	2.682E-03	4.780E-03	9.743E-03
Dissip (Watts)	4.121E+04	1.791E+04	1.048E+04	6.549E+03
BMax (Tesla)	4.403E-01	2.879E-01	2.096E-01	1.480E-01
Vol (m^3)	8.773E-02	4.754E-02	3.425E-02	2.852E-02
EMax (Joule)	9.067E+02	2.101E+02	8.023E+01	3.331E+01
En/Wt (J/lb)	1.045E+01	5.572E+00	3.637E+00	2.416E+00
Irms (Amps)	5.576E+03	2.584E+03	1.481E+03	8.198E+02

Total Inductor Weight = 72.8653 kg

TABLE B.2 PFN INDUCTOR PARAMETERS (Continued)

****
* DISCHARGE *
* PFN Inductor *
****

Frequency = 5.0 Hz ----- ALUMINUM Conductor

Inductor Number	(2)	(3)	(4)	(5)
Induc (H)	2.828E-05	3.051E-05	3.549E-05	4.805E-05
Area (m^2)	4.537E-06	2.102E-06	1.205E-06	6.671E-07
Dia (m)	4.388E-03	2.987E-03	2.261E-03	1.683E-03
Spaced (m)	9.388E-03	7.987E-03	7.261E-03	6.683E-03
Radius (m)	1.145E-01	1.054E-01	1.040E-01	1.089E-01
Turns	38.307	41.463	45.013	51.194
Weight (kg)	1.687E-01	7.794E-02	4.786E-02	3.154E-02
Resis (m)	8.441E-02	1.816E-01	3.395E-01	7.299E-01
Dissip (Watts)	4.058E+02	1.875E+02	1.151E+02	7.587E+01
BMax (Tesla)	1.072E+00	5.838E-01	3.680E-01	2.214E-01
Vol (m^3)	1.480E-02	1.156E-02	1.111E-02	1.275E-02
EMax (Joule)	9.067E+02	2.101E+02	8.023E+01	3.331E+01
En/Wt (J/lb)	2.442E+03	1.225E+03	7.621E+02	4.799E+02
Irms (Amps)	6.934E+01	3.213E+01	1.841E+01	1.020E+01

Total Inductor Weight = .3261 kg

****
* CHARGING *
* PFN Inductor *
****

Frequency = 5.0 Hz ----- ALUMINUM Conductor

Inductor Number	(2)	(3)	(4)	(5)
Induc (H)	2.828E-05	3.051E-05	3.549E-05	4.805E-05
Area (m^2)	3.704E-04	1.716E-04	9.836E-05	5.446E-05
Dia (m)	2.596E-02	1.767E-02	1.338E-02	9.953E-03
Spaced (m)	2.796E-02	1.967E-02	1.538E-02	1.195E-02
Radius (m)	2.369E-01	1.922E-01	1.716E-01	1.605E-01
Turns	26.626	30.704	35.054	42.174
Weight (kg)	1.982E+01	8.593E+00	5.017E+00	3.126E+00
Resis (m)	1.488E-03	3.003E-03	5.340E-03	1.085E-02
Dissip (Watts)	4.767E+04	2.067E+04	1.207E+04	7.519E+03
BMax (Tesla)	3.599E-01	2.371E-01	1.738E-01	1.238E-01
Vol (m^3)	1.313E-01	7.011E-02	4.983E-02	4.078E-02
EMax (Joule)	9.067E+02	2.101E+02	8.023E+01	3.331E+01
En/Wt (J/lb)	2.079E+01	1.111E+01	7.269E+00	4.842E+00
Irms (Amps)	5.661E+03	2.623E+03	1.503E+03	8.324E+02

Total Inductor Weight = 36.5580 kg

TABLE B.2 PFN INDUCTOR PARAMETERS (Continued)

```
****************
*  DISCHARGE   *
* PFN Inductor *
****************
```

Frequency = 10.0 Hz ----- ALUMINUM Conductor

Inductor Number	(2)	(3)	(4)	(5)
Induc (H)	2.828E-05	3.051E-05	3.549E-05	4.805E-05
Area (m^2)	6.416E-06	2.973E-06	1.704E-06	9.434E-07
Dia (m)	5.218E-03	3.552E-03	2.689E-03	2.001E-03
Spaced (m)	1.022E-02	8.552E-03	7.689E-03	7.001E-03
Radius (m)	1.211E-01	1.103E-01	1.081E-01	1.123E-01
Turns	37.240	40.528	44.162	50.406
Weight (kg)	2.455E-01	1.128E-01	6.898E-02	4.531E-02
Resis (m)	6.140E-02	1.313E-01	2.447E-01	5.242E-01
Dissip (Watts)	5.904E+02	2.712E+02	1.659E+02	1.090E+02
BMax (Tesla)	9.848E-01	5.452E-01	3.475E-01	2.113E-01
Vol (m^3)	1.754E-02	1.325E-02	1.246E-02	1.399E-02
EMax (Joule)	9.067E+02	2.101E+02	8.023E+01	3.331E+01
En/Wt (J/lb)	1.679E+03	8.467E+02	5.287E+02	3.341E+02
Irms (Amps)	9.806E+01	4.544E+01	2.604E+01	1.442E+01

Total Inductor Weight = .4725 kg

```
****************
*  CHARGING    *
* PFN Inductor *
****************
```

Frequency = 10.0 Hz ----- ALUMINUM Conductor

Inductor Number	(2)	(3)	(4)	(5)
Induc (H)	2.828E-05	3.051E-05	3.549E-05	4.805E-05
Area (m^2)	3.704E-04	1.716E-04	9.835E-05	5.446E-05
Dia (m)	2.596E-02	1.767E-02	1.337E-02	9.953E-03
Spaced (m)	2.796E-02	1.967E-02	1.537E-02	1.195E-02
Radius (m)	2.369E-01	1.922E-01	1.716E-01	1.605E-01
Turns	26.626	30.704	35.054	42.174
Weight (kg)	1.982E+01	8.593E+00	5.017E+00	3.126E+00
Resis (m)	1.488E-03	3.003E-03	5.340E-03	1.085E-02
Dissip (Watts)	4.767E+04	2.067E+04	1.207E+04	7.518E+03
BMax (Tesla)	3.600E-01	2.371E-01	1.738E-01	1.238E-01
Vol (m^3)	1.313E-01	7.011E-02	4.983E-02	4.077E-02
EMax (Joule)	9.067E+02	2.101E+02	8.023E+01	3.331E+01
En/Wt (J/lb)	2.079E+01	1.111E+01	7.269E+00	4.843E+00
Irms (Amps)	5.661E+03	2.623E+03	1.503E+03	8.323E+02

Total Inductor Weight = 36.5548 kg

TABLE B.2 PFN INDUCTOR PARAMETERS (Continued)

****
* DISCHARGE *
* PFN Inductor *
****

Frequency = 20.0 Hz ----- ALUMINUM Conductor

Inductor Number	(2)	(3)	(4)	(5)
Induc (H)	2.828E-05	3.051E-05	3.549E-05	4.805E-05
Area (m^2)	9.074E-06	4.205E-06	2.409E-06	1.334E-06
Dia (m)	6.206E-03	4.224E-03	3.198E-03	2.380E-03
Spaced (m)	1.121E-02	9.224E-03	8.198E-03	7.380E-03
Radius (m)	1.288E-01	1.160E-01	1.128E-01	1.163E-01
Turns	36.112	39.519	43.229	49.529
Weight (kg)	3.580E-01	1.636E-01	9.966E-02	6.521E-02
Resis (m)	4.477E-02	9.525E-02	1.768E-01	3.772E-01
Dissip (Watts)	8.610E+02	3.933E+02	2.397E+02	1.568E+02
BMax (Tesla)	8.980E-01	5.055E-01	3.259E-01	2.005E-01
Vol (m^3)	2.109E-02	1.542E-02	1.417E-02	1.554E-02
EMax (Joule)	9.067E+02	2.101E+02	8.023E+01	3.331E+01
En/Wt (J/lb)	1.151E+03	5.838E+02	3.659E+02	2.322E+02
Irms (Amps)	1.387E+02	6.426E+01	3.682E+01	2.039E+01

Total Inductor Weight = .6864 kg

****
* CHARGING *
* PFN Inductor *
****

Frequency = 20.0 Hz ----- ALUMINUM Conductor

Inductor Number	(2)	(3)	(4)	(5)
Induc (H)	2.828E-05	3.051E-05	3.549E-05	4.805E-05
Area (m^2)	3.703E-04	1.716E-04	9.833E-05	5.445E-05
Dia (m)	2.595E-02	1.767E-02	1.337E-02	9.952E-03
Spaced (m)	2.795E-02	1.967E-02	1.537E-02	1.195E-02
Radius (m)	2.369E-01	1.922E-01	1.715E-01	1.605E-01
Turns	26.627	30.705	35.055	42.175
Weight (kg)	1.982E+01	8.591E+00	5.016E+00	3.125E+00
Resis (m)	1.488E-03	3.004E-03	5.341E-03	1.085E-02
Dissip (Watts)	4.766E+04	2.066E+04	1.206E+04	7.517E+03
BMax (Tesla)	3.600E-01	2.371E-01	1.738E-01	1.238E-01
Vol (m^3)	1.313E-01	7.010E-02	4.982E-02	4.077E-02
EMax (Joule)	9.067E+02	2.101E+02	8.023E+01	3.331E+01
En/Wt (J/lb)	2.080E+01	1.111E+01	7.271E+00	4.844E+00
Irms (Amps)	5.660E+03	2.623E+03	1.503E+03	8.322E+02

Total Inductor Weight = 36.5485 kg

TABLE B.2 PFN INDUCTOR PARAMETERS (Continued)

****
* DISCHARGE *
* PFN Inductor *
****

Frequency = 40.0 Hz ----- ALUMINUM Conductor

Inductor Number		(2)	(3)	(4)	(5)
Induc	(H)	2.828E-05	3.051E-05	3.549E-05	4.805E-05
Area	(m^2)	1.283E-05	5.946E-06	3.407E-06	1.887E-06
Dia	(m)	7.380E-03	5.024E-03	3.803E-03	2.830E-03
Spaced	(m)	1.238E-02	1.002E-02	8.803E-03	7.830E-03
Radius	(m)	1.377E-01	1.226E-01	1.183E-01	1.210E-01
Turns		34.932	38.439	42.215	48.561
Weisht	(ks)	5.234E-01	2.378E-01	1.443E-01	9.406E-02
Resis	(m)	3.273E-02	6.924E-02	1.280E-01	2.720E-01
Dissip	(Watts)	1.259E+03	5.719E+02	3.471E+02	2.262E+02
BMax	(Tesla)	8.128E-01	4.652E-01	3.035E-01	1.890E-01
Vol	(m^3)	2.574E-02	1.821E-02	1.633E-02	1.750E-02
EMax	(Joule)	9.067E+02	2.101E+02	8.023E+01	3.331E+01
En/Wt	(J/lb)	7.874E+02	4.015E+02	2.527E+02	1.609E+02
Irms	(Amps)	1.961E+02	9.088E+01	5.208E+01	2.884E+01

Total Inductor Weisht = .9996 ks

****
* CHARGING *
* PFN Inductor *
****

Frequency = 40.0 Hz ----- ALUMINUM Conductor

Inductor Number		(2)	(3)	(4)	(5)
Induc	(H)	2.828E-05	3.051E-05	3.549E-05	4.805E-05
Area	(m^2)	3.702E-04	1.716E-04	9.830E-05	5.443E-05
Dia	(m)	2.595E-02	1.766E-02	1.337E-02	9.950E-03
Spaced	(m)	2.795E-02	1.966E-02	1.537E-02	1.195E-02
Radius	(m)	2.369E-01	1.922E-01	1.715E-01	1.604E-01
Turns		26.628	30.706	35.056	42.177
Weisht	(ks)	1.981E+01	8.588E+00	5.014E+00	3.124E+00
Resis	(m)	1.488E-03	3.005E-03	5.342E-03	1.086E-02
Dissip	(Watts)	4.764E+04	2.065E+04	1.206E+04	7.514E+03
BMax	(Tesla)	3.600E-01	2.371E-01	1.738E-01	1.238E-01
Vol	(m^3)	1.312E-01	7.008E-02	4.981E-02	4.076E-02
EMax	(Joule)	9.067E+02	2.101E+02	8.023E+01	3.331E+01
En/Wt	(J/lb)	2.080E+01	1.112E+01	7.273E+00	4.845E+00
Irms	(Amps)	5.658E+03	2.622E+03	1.502E+03	8.319E+02

Total Inductor Weisht = 36.5359 ks

TABLE B.2 PFN INDUCTOR PARAMETERS (Continued)

```
****************
*  DISCHARGE   *
* PFN Inductor *
****************
```

Frequency = 100.0 Hz ----- ALUMINUM Conductor

Inductor Number	(2)	(3)	(4)	(5)
Induc (H)	2.828E-05	3.051E-05	3.549E-05	4.805E-05
Area (m^2)	2.029E-05	9.402E-06	5.388E-06	2.983E-06
Dia (m)	9.280E-03	6.317E-03	4.782E-03	3.558E-03
Spaced (m)	1.428E-02	1.132E-02	9.782E-03	8.558E-03
Radius (m)	1.514E-01	1.330E-01	1.269E-01	1.284E-01
Turns	33.309	36.916	40.757	47.142
Weight (kg)	8.679E-01	3.915E-01	2.364E-01	1.532E-01
Resis (m)	2.171E-02	4.560E-02	8.384E-02	1.772E-01
Dissip (Watts)	2.087E+03	9.416E+02	5.685E+02	3.684E+02
BMax (Tesla)	7.047E-01	4.120E-01	2.732E-01	1.729E-01
Vol (m^3)	3.425E-02	2.321E-02	2.017E-02	2.090E-02
EMax (Joule)	9.067E+02	2.101E+02	8.023E+01	3.331E+01
En/Wt (J/lb)	4.749E+02	2.439E+02	1.543E+02	9.882E+01
Irms (Amps)	3.101E+02	1.437E+02	8.234E+01	4.559E+01

Total Inductor Weight = 1.6490 kg

```
****************
*  CHARGING    *
* PFN Inductor *
****************
```

Frequency = 100.0 Hz ----- ALUMINUM Conductor

Inductor Number	(2)	(3)	(4)	(5)
Induc (H)	2.828E-05	3.051E-05	3.549E-05	4.805E-05
Area (m^2)	3.699E-04	1.714E-04	9.822E-05	5.438E-05
Dia (m)	2.594E-02	1.766E-02	1.337E-02	9.946E-03
Spaced (m)	2.794E-02	1.966E-02	1.537E-02	1.195E-02
Radius (m)	2.368E-01	1.922E-01	1.715E-01	1.604E-01
Turns	26.632	30.710	35.061	42.182
Weight (kg)	1.979E+01	8.579E+00	5.009E+00	3.121E+00
Resis (m)	1.489E-03	3.007E-03	5.346E-03	1.087E-02
Dissip (Watts)	4.759E+04	2.063E+04	1.205E+04	7.507E+03
BMax (Tesla)	3.602E-01	2.372E-01	1.739E-01	1.239E-01
Vol (m^3)	1.311E-01	7.002E-02	4.977E-02	4.073E-02
EMax (Joule)	9.067E+02	2.101E+02	8.023E+01	3.331E+01
En/Wt (J/lb)	2.083E+01	1.113E+01	7.281E+00	4.850E+00
Irms (Amps)	5.653E+03	2.620E+03	1.501E+03	8.312E+02

Total Inductor Weight = 36.4980 kg

TABLE B.2 PFN INDUCTOR PARAMETERS (Continued)

```
****************
*  DISCHARGE   *
* PFN Inductor *
****************
```

Frequency = 200.0 Hz ----- ALUMINUM Conductor

Inductor Number	(2)	(3)	(4)	(5)
Induc (H)	2.828E-05	3.051E-05	3.549E-05	4.805E-05
Area (m^2)	2.869E-05	1.330E-05	7.619E-06	4.219E-06
Dia (m)	1.104E-02	7.512E-03	5.687E-03	4.232E-03
Spaced (m)	1.604E-02	1.251E-02	1.069E-02	9.232E-03
Radius (m)	1.636E-01	1.422E-01	1.346E-01	1.351E-01
Turns	32.046	35.701	39.573	45.967
Weight (ks)	1.276E+00	5.725E-01	3.443E-01	2.222E-01
Resis (m)	1.595E-02	3.334E-02	6.106E-02	1.285E-01
Dissip (Watts)	3.068E+03	1.377E+03	8.280E+02	5.344E+02
BMax (Tesla)	6.275E-01	3.727E-01	2.500E-01	1.603E-01
Vol (m^3)	4.319E-02	2.837E-02	2.407E-02	2.432E-02
EMax (Joule)	9.067E+02	2.101E+02	8.023E+01	3.331E+01
En/Wt (J/lb)	3.230E+02	1.668E+02	1.059E+02	6.813E+01
Irms (Amps)	4.385E+02	2.032E+02	1.164E+02	6.448E+01

Total Inductor Weight = 2.4147 ks

```
****************
*  CHARGING    *
* PFN Inductor *
****************
```

Frequency = 200.0 Hz ----- ALUMINUM Conductor

Inductor Number	(2)	(3)	(4)	(5)
Induc (H)	2.828E-05	3.051E-05	3.549E-05	4.805E-05
Area (m^2)	3.693E-04	1.711E-04	9.807E-05	5.430E-05
Dia (m)	2.592E-02	1.764E-02	1.336E-02	9.938E-03
Spaced (m)	2.792E-02	1.964E-02	1.536E-02	1.194E-02
Radius (m)	2.367E-01	1.921E-01	1.714E-01	1.603E-01
Turns	26.638	30.717	35.068	42.191
Weight (ks)	1.975E+01	8.565E+00	5.000E+00	3.116E+00
Resis (m)	1.491E-03	3.011E-03	5.353E-03	1.088E-02
Dissip (Watts)	4.751E+04	2.060E+04	1.203E+04	7.494E+03
BMax (Tesla)	3.604E-01	2.374E-01	1.740E-01	1.239E-01
Vol (m^3)	1.309E-01	6.993E-02	4.971E-02	4.068E-02
EMax (Joule)	9.067E+02	2.101E+02	8.023E+01	3.331E+01
En/Wt (J/lb)	2.086E+01	1.115E+01	7.293E+00	4.859E+00
Irms (Amps)	5.644E+03	2.616E+03	1.499E+03	8.299E+02

Total Inductor Weight = 36.4347 ks

TABLE B.2 PFN INDUCTOR PARAMETERS (Continued)

****
* DISCHARGE *
* PFN Inductor *
****

Frequency = 400.0 Hz ----- ALUMINUM Conductor

Inductor Number	(2)	(3)	(4)	(5)
Induc (H)	2.828E-05	3.051E-05	3.549E-05	4.805E-05
Area (m^2)	4.058E-05	1.880E-05	1.078E-05	5.967E-06
Dia (m)	1.312E-02	8.934E-03	6.763E-03	5.032E-03
Spaced (m)	1.812E-02	1.393E-02	1.176E-02	1.003E-02
Radius (m)	1.775E-01	1.528E-01	1.435E-01	1.428E-01
Turns	30.765	34.443	38.327	44.710
Weight (kg)	1.879E+00	8.392E-01	5.027E-01	3.231E-01
Resis (m)	1.175E-02	2.444E-02	4.458E-02	9.344E-02
Dissip (Watts)	4.520E+03	2.018E+03	1.209E+03	7.770E+02
BMax (Tesla)	5.552E-01	3.347E-01	2.272E-01	1.475E-01
Vol (m^3)	5.517E-02	3.518E-02	2.917E-02	2.872E-02
EMax (Joule)	9.067E+02	2.101E+02	8.023E+01	3.331E+01
En/Wt (J/lb)	2.193E+02	1.138E+02	7.255E+01	4.686E+01
Irms (Amps)	6.202E+02	2.874E+02	1.647E+02	9.119E+01

Total Inductor Weight = 3.5443 kg

****
* CHARGING *
* PFN Inductor *
****

Frequency = 400.0 Hz ----- ALUMINUM Conductor

Inductor Number	(2)	(3)	(4)	(5)
Induc (H)	2.828E-05	3.051E-05	3.549E-05	4.805E-05
Area (m^2)	3.682E-04	1.706E-04	9.777E-05	5.414E-05
Dia (m)	2.588E-02	1.762E-02	1.334E-02	9.923E-03
Spaced (m)	2.788E-02	1.962E-02	1.534E-02	1.192E-02
Radius (m)	2.365E-01	1.919E-01	1.713E-01	1.602E-01
Turns	26.651	30.731	35.084	42.209
Weight (kg)	1.969E+01	8.535E+00	4.983E+00	3.105E+00
Resis (m)	1.495E-03	3.018E-03	5.367E-03	1.091E-02
Dissip (Watts)	4.734E+04	2.053E+04	1.198E+04	7.468E+03
BMax (Tesla)	3.609E-01	2.377E-01	1.742E-01	1.241E-01
Vol (m^3)	1.306E-01	6.974E-02	4.958E-02	4.058E-02
EMax (Joule)	9.067E+02	2.101E+02	8.023E+01	3.331E+01
En/Wt (J/lb)	2.094E+01	1.119E+01	7.319E+00	4.875E+00
Irms (Amps)	5.627E+03	2.608E+03	1.494E+03	8.274E+02

Total Inductor Weight = 36.3080 kg

TABLE B.2 PFN INDUCTOR PARAMETERS (Continued)

```
**********************
*  DISCHARGE         *
* PFN Inductor       *
**********************
```

Frequency = 500.0 Hz ----- ALUMINUM Conductor

Inductor Number	(2)	(3)	(4)	(5)
Induc (H)	2.828E-05	3.051E-05	3.549E-05	4.805E-05
Area (m^2)	4.537E-05	2.102E-05	1.205E-05	6.671E-06
Dia (m)	1.388E-02	9.446E-03	7.150E-03	5.321E-03
Spaced (m)	1.888E-02	1.445E-02	1.215E-02	1.032E-02
Radius (m)	1.824E-01	1.565E-01	1.466E-01	1.455E-01
Turns	30.350	34.031	37.915	44.289
Weight (kg)	2.130E+00	9.497E-01	5.681E-01	3.646E-01
Resis (m)	1.065E-02	2.212E-02	4.031E-02	8.437E-02
Dissip (Watts)	5.122E+03	2.284E+03	1.366E+03	8.769E+02
BMax (Tesla)	5.331E-01	3.228E-01	2.199E-01	1.434E-01
Vol (m^3)	5.985E-02	3.782E-02	3.112E-02	3.040E-02
EMax (Joule)	9.067E+02	2.101E+02	8.023E+01	3.331E+01
En/Wt (J/lb)	1.935E+02	1.005E+02	6.419E+01	4.152E+01
Irms (Amps)	6.934E+02	3.213E+02	1.841E+02	1.020E+02

Total Inductor Weight = 4.0123 kg

```
**********************
*  CHARGING          *
* PFN Inductor       *
**********************
```

Frequency = 500.0 Hz ----- ALUMINUM Conductor

Inductor Number	(2)	(3)	(4)	(5)
Induc (H)	2.828E-05	3.051E-05	3.549E-05	4.805E-05
Area (m^2)	3.676E-04	1.704E-04	9.762E-05	5.406E-05
Dia (m)	2.586E-02	1.760E-02	1.333E-02	9.916E-03
Spaced (m)	2.786E-02	1.960E-02	1.533E-02	1.192E-02
Radius (m)	2.364E-01	1.918E-01	1.712E-01	1.601E-01
Turns	26.657	30.738	35.092	42.218
Weight (kg)	1.965E+01	8.520E+00	4.974E+00	3.100E+00
Resis (m)	1.497E-03	3.022E-03	5.374E-03	1.092E-02
Dissip (Watts)	4.726E+04	2.049E+04	1.196E+04	7.455E+03
BMax (Tesla)	3.612E-01	2.379E-01	1.744E-01	1.242E-01
Vol (m^3)	1.304E-01	6.964E-02	4.951E-02	4.052E-02
EMax (Joule)	9.067E+02	2.101E+02	8.023E+01	3.331E+01
En/Wt (J/lb)	2.097E+01	1.121E+01	7.331E+00	4.884E+00
Irms (Amps)	5.619E+03	2.604E+03	1.492E+03	8.262E+02

Total Inductor Weight = 36.2445 kg

TABLE B.2 PFN INDUCTOR PARAMETERS (Continued)

```
****************
*  DISCHARGE   *
* PFN Inductor *
****************
```

Frequency =1000.0 Hz ----- ALUMINUM Conductor

Inductor Number	(2)	(3)	(4)	(5)
Induc (H)	2.828E-05	3.051E-05	3.549E-05	4.805E-05
Area (m^2)	6.416E-05	2.973E-05	1.704E-05	9.434E-06
Dia (m)	1.650E-02	1.123E-02	8.503E-03	6.328E-03
Spaced (m)	2.150E-02	1.623E-02	1.350E-02	1.133E-02
Radius (m)	1.989E-01	1.691E-01	1.573E-01	1.548E-01
Turns	29.061	32.733	36.604	42.936
Weight (kg)	3.146E+00	1.396E+00	8.323E-01	5.319E-01
Resis (m)	7.868E-03	1.626E-02	2.952E-02	6.154E-02
Dissip (Watts)	7.565E+03	3.358E+03	2.002E+03	1.279E+03
BMax (Tesla)	4.680E-01	2.873E-01	1.979E-01	1.306E-01
Vol (m^3)	7.766E-02	4.776E-02	3.844E-02	3.662E-02
EMax (Joule)	9.067E+02	2.101E+02	8.023E+01	3.331E+01
En/Wt (J/lb)	1.310E+02	6.838E+01	4.382E+01	2.846E+01
Irms (Amps)	9.806E+02	4.544E+02	2.604E+02	1.442E+02

Total Inductor Weight = 5.9061 kg

```
****************
*  CHARGING    *
* PFN Inductor *
****************
```

Frequency =1000.0 Hz ----- ALUMINUM Conductor

Inductor Number	(2)	(3)	(4)	(5)
Induc (H)	2.828E-05	3.051E-05	3.549E-05	4.805E-05
Area (m^2)	3.648E-04	1.691E-04	9.688E-05	5.364E-05
Dia (m)	2.576E-02	1.754E-02	1.327E-02	9.878E-03
Spaced (m)	2.776E-02	1.954E-02	1.527E-02	1.188E-02
Radius (m)	2.358E-01	1.914E-01	1.708E-01	1.598E-01
Turns	26.689	30.773	35.131	42.263
Weight (kg)	1.948E+01	8.445E+00	4.931E+00	3.073E+00
Resis (m)	1.507E-03	3.042E-03	5.410E-03	1.099E-02
Dissip (Watts)	4.684E+04	2.031E+04	1.186E+04	7.390E+03
BMax (Tesla)	3.625E-01	2.387E-01	1.749E-01	1.246E-01
Vol (m^3)	1.294E-01	6.916E-02	4.918E-02	4.027E-02
EMax (Joule)	9.067E+02	2.101E+02	8.023E+01	3.331E+01
En/Wt (J/lb)	2.116E+01	1.131E+01	7.396E+00	4.927E+00
Irms (Amps)	5.576E+03	2.584E+03	1.481E+03	8.198E+02

Total Inductor Weight = 35.9259 kg

4. TOROIDAL SUPERCONDUCTING ENERGY STORAGE COIL DESIGN

This section presents the design equations for the main energy storage coil. The coil configuration uses a thick toroidal coil with pancake windings of circular cross-section. Several of the expressions used, most notedly that relating coil stored energy to the coil geometry, were based on the AERL Final Report, "Study of Development of an Inductive Energy Storage System", Contract No. F33615-69-C-1934.

The coil geometry is sized based on the coil electrical parameters - energy and inductance - and on the several design parameters listed. Then the winding and conductor physical parameters are determined.

The procedure is given in the following pages under Subroutine COIL.

Subroutine COIL

Inductive Energy Storage Coil Design

Design Inputs: Assume: Toroidal Geometry

L	=	Inductance of the coil (Henry)
I	=	Peak coil current (Amps.)
J_{ds}	=	Design current density of the superconductor (Amp/m^2)
d	=	Diameter of the superconductor filaments (M)
γ_1	=	Ratio of mean minor radius to major radius of the torus
γ_2	=	Ratio of mean winding radius to major radius of the torus
λ_1	=	Packing factor relating superconductor to composite core
λ_2	=	Packing factor relating composite core to wire
λ_3	=	Packing factor relating wires to braid
λ_4	=	Packing factor relating braids to cable

B_m = Maximum design field (tesla)

n = Number of filaments of superconductors per wire

N_{wbm} = Maximum number of wires per braid

V = Coil voltage (volts)

Design Equations:

Thick toroidal coils with pancake winding

$$B_{max} = \frac{B_o}{1-\gamma_1} \tag{B.23}$$

$$E = \frac{2\pi^2 R_o^3 B_o^2}{\mu_o} \left[u + \frac{1}{v}(w_1+w_2)\right] \tag{B.24}$$

$$L = E\frac{\mu_o^2 N^2}{2\pi R_o^2 B_o^2} \tag{B.25}$$

Where

u, v, w_1 w_2 are defined at the end of this section.

B_o = Center field (Tesla)

$\bar{J}_{max}$ = Overall current - density in the winding (A/m^2)

E = Energy stored in the coil per pulse (Joules)

N = No. of turns in the coil

R_o = Major radius of the torus (M)

μ_o = Permeability of free-space (H/M)

From Equation (B.23)

$$B_o = (1-\gamma_1)\, Bm \tag{B.26}$$

From Equation (B.24)

$$R_o = \left[L I_2^2 \mu_o / (u + \frac{w_1+w_2}{v}) 4\pi^2 B_o^2 \right]^{1/3} \tag{B.27}$$

From Equation (B.25)

$$N = \frac{2\pi R_o B_o}{\mu_o} \sqrt{\frac{L}{2E}} \tag{B.28}$$

Now,

$$\bar{J}_{max} = J_{ds} \lambda_1 \lambda_2 \lambda_3 \lambda_4 \tag{B.29}$$

Evaluating B_o from Equation (B.23), we can substitute it in Equation (B.27) and evaluate R_o with the calculated value of $\bar{J}_{max}$ from Equation (B.29)

$$E = \frac{1}{2} LI^2 \tag{B.30}$$

Substituting for B_o, R_o, $\bar{J}_{max}$ and E in Equation (B.28) we can determine N. Now, the following quantities are determined, with units given.

Total area of superconductor per wire (m^2):

$$A_{scw} = \pi d^2 n/4$$

Area of core per wire (m^2):

$$A_{cw} = A_{scw}/\lambda_1$$

Cross-sectional area of each wire (m^2):

$$A_w = A_{cw}/\lambda_2 = A_{scw}/\lambda_1\lambda_2$$

Total superconductor area required to handle the current (m^2):

$$A_{sct} = I/J_{ds}$$

Total number of wires required:

$$n_w = \frac{A_{sct}}{A_{scw}}$$

If $n_w \leq n_{wbm}$, then

Number of braids, $N_b = 1$ and number of wires/braid, $n_{wb} = n_w$.

If $n_w > n_{wbm}$, then

Number of braids, $n_b = \frac{n_w}{n_{wbm}}$ (rounded off to the next higher interger)

and wires/braid, $n_{wb} = n_w/n_b$.

Several braided conductors can be made into a cable. They will have to be twisted.

Area of each braid (m^2)

$$A_b = A_w \cdot n_{wb}/\lambda_3$$

Area of cable (m^2)

$$A_{cab} = N_b A_b/\lambda_4$$

We are assuming a single-layer winding with pancake shaped cable.

Diameter of each braid (m):

$$D_b = \sqrt{\frac{4}{\pi} A_b}$$

Diameter of each wire (m):

$$D_w = \sqrt{\frac{4}{\pi} A_w}$$

Diameter of core in each wire (m):

$$D_c = \sqrt{\frac{4}{\pi} A_{cw}}$$

Mean Minor radius of the torus (m):

$$R_1 = \gamma_1 \cdot R_o$$

Mean radius of the winding (m):

$$R_2 = \gamma_2 \cdot R_o$$

G_t is the gap per turn (m):

$$G_t = \frac{2\pi R_o (1-\gamma_2)}{N}$$

V_t is the volts per turn (V):

$$V_t = V_{peak}/N$$

Mean length of the winding per turn (m):

$$\ell_{mt} = 2\pi \sqrt{\left(\frac{R_1+R_2}{2}\right)^2 + \left(\frac{R_o}{N}\right)^2}$$

Volume of the superconductor in the coil (m^3):

$$V_{sc} = N \cdot n_w \cdot A_{scw} \cdot \ell_{mt}$$

Volume of the matrix material (m^3)

$$V_m = V_{sc}(1-\lambda_1\lambda_2)/\lambda_1\lambda_2$$

Frontal area of the coil (m^2):

$$A_{fc} = 2(R_o+R_2) \cdot R_1$$

Coil material volume (m^3):

$$V_c = A_w \cdot N_w \cdot N \cdot \ell_{mt}$$

Coil material mass (kg):

$$W_c = \rho_c \cdot V_c$$

Mass of the superconducting material (kg):

$$W_{sc} = \lambda_1\lambda_2 W_c$$

The auxiliary variables used in the stored energy equation are defined here.

$$u = (1-(1-\gamma_1^2)^{1/2})$$

$$v = (\gamma_2 - \gamma_1)^2$$

$$w_1 = \frac{1}{3}\left[(2+3\gamma_2(\gamma_2-\gamma_1)+\gamma_1^2)(1-\gamma_1^2)^{1/2} - (2+\gamma_2^2)(1-\gamma_2^2)^{1/2}\right]$$

$$w_2 = \gamma_2(\sin^{-1}\gamma_1 - \sin^{-1}\gamma_2)$$

5. SUPERCONDUCTING LOSS EQUATIONS AND DEWAR DESIGN

This section discusses the evaluation of AC losses in the superconductor due to the various mechanisms mentioned below. The design of the dewar/cryostat subsystem, based in part on the superconductor losses, is also included.

The loss equations evaluate the losses in the superconducting windings resulting from the following mechanisms:

1) Magnetization losses -- the superconductor "field shielding" currents locally exceed the critical current density beyond which the magnetic field can no longer be excluded; local portions of the superconductor thus transfer to the normal state.

2) Matrix losses due to filament coupling-- this loss in the matrix material in the composite core is due to induced transverse currents between superconductor filaments caused by insufficient twisting. The critical twist pitch, which value separates the complete decoupling approximation from the complete coupling approximation, is so small for these applications ($\sim 12\mu$m for 3 Tesla, 30μsec discharge pulse) as to guarantee that filaments are coupled.

3) Matrix losses due to induced axial eddy currents in the pure matrix layer at the wire surface.

4) Self-field losses---these are miniscule compared with the other loss mechanisms.

As discussed in the main text of this report, additional, uncomputable loss mechanisms exist which are not described here. In addition, joule losses resulting from an unrecovered normal transitions are not evaluated.

The loss equations presented here are the result of an extensive study of available literature. The prime objective was a complete, self consistent set of relations based on the best available theoretical and experimental data. In

the numerous conflicts and inconsistencies among the various sources, best technical judgement was used to determine the most reliable expressions.

A prime source was a series of articles appearing in the Journal of Physics (Inst. of Physics) (U.K.) (VIII, No. 11, Nov. 1970) regarding Experimental and Theoretical Studies of Superconducting Composites. The articles used are listed here:

1) N.N. Wilson, et al., "Basic Ideas and Theory".

2) N.N. Wilson and C.R. Walters, "Stability and Flux Penetration in Multi-Filamentary Systems".

3) N. N. Wilson and C. R. Walters, "Magnetization and Stability Experiments".

4) P.F. Smith et al., "D.C. Coil Tests".

5) A. H. Spurway, et al., "A.C. Coil Tests".

An additional reference was H. Brechna, Superconducting Magnet Systems, Springer-Verlag, 1973. Numerous other sources in the literature were used for cross-checking and reference.

The formidable complexity of many of the expressions appearing in this section arises from a simple source. The loss expressions in the literature are presented in differential form, i.e. power per unit volume. Our applications require losses expressed as energy per pulse; hence, the expressions given here have been mathematically integrated in both time and space.

a. Summary of Assumptions and Approximate Range of Validity of Loss Equations

Symbols are defined with the equations.

AD-A052 750 MAXWELL LABS INC WOBURN MA UTILITY PRODUCTS DIV F/G 10/2
INDUCTOR NETWORK DEVELOPMENT FOR AIRCRAFT HIGH POWER SUPPLIES.(U)
APR 77 J TENO, R L BRYAN, S GHOSHROY F33615-74-C-2018
UNCLASSIFIED AFAPL-TR-77-15 NL

3 OF 3
AD
AD52750

END
DATE FILMED
5-78
DDC

(1) Conductor Configuration

- Twisted, multifilament composite superconductor wire of circular cross section (See Figure B.8 for definition of geometric parameters).

- Materials:

  Superconductor - typically NbTi

  Matrix - Copper, cupro-nickel alloys and tertiary matrix systems

- Dimensions:

  D_w - 10^{-4} m to 10^{-3} m

  d - 5×10^{-6} m to 5×10^{-5} m

  ℓ_p - 10^{-3} m to 10^{-2} m

  λ_s - typically 0.5

(2) Coil Pulse Shape

- Steady state cyclic operation with ramp charge and discharge current wave form (See Figure B.9 for definition of pulse parameters).

- Operating parameters:

  B - up to 4 Tesla

  I/I_c - up to 1.0

  t_{pp} - 1 ms to 10 ms

  t_d - 20μs to 40μs

(3) Radial Field Distribution in Windings

- For the purposes of averaging the local coil losses, a linear field variation across the radial winding thickness is assumed. (See Figure B.10 for definition of field distribution dependent parameters.)

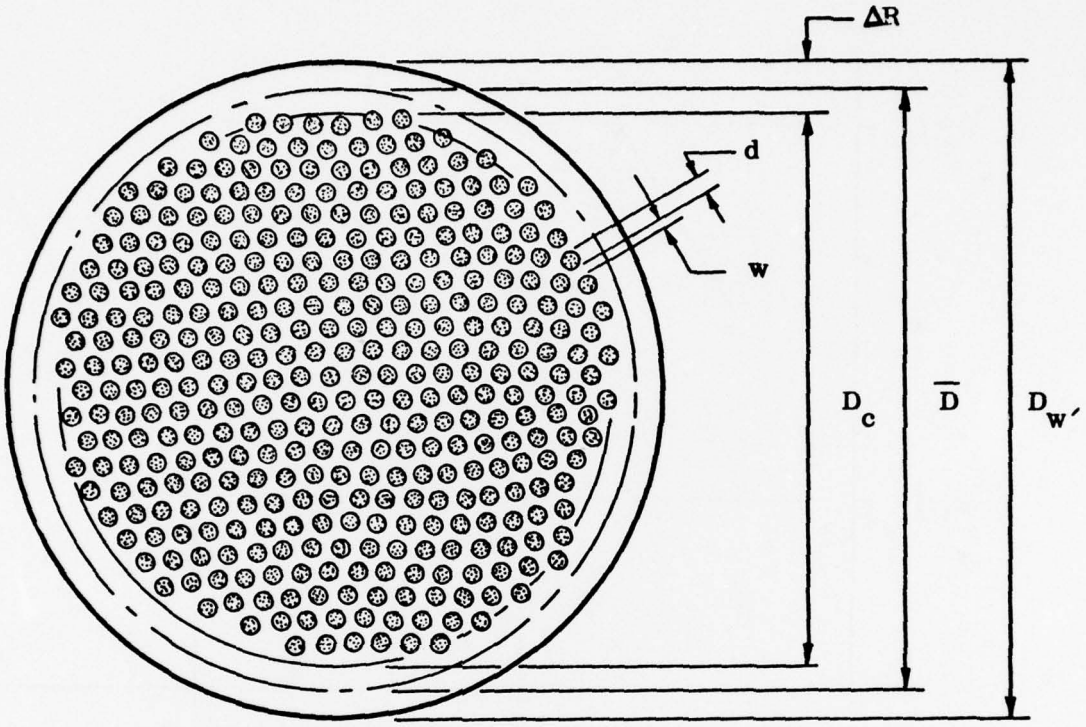

D_w = Wire Diameter

D_c = Composite Core Diameter

$\overline{D}$ = Mean Diameter of Pure Matrix Material Layer at Wire Surface

ΔR = Radial Thickness of Pure Matrix Material Layer

d = Superconductor Filament Diameter

w = Superconductor Filament Spacing

ℓp = 4ℓ = Pitch for 360° Twist

λ = A_{sc}/A_{wire} = Superconductor Volume Fraction

λs = A_{sc}/A_{core}

Figure B.8 Composite Superconductor Wire Dimensions.

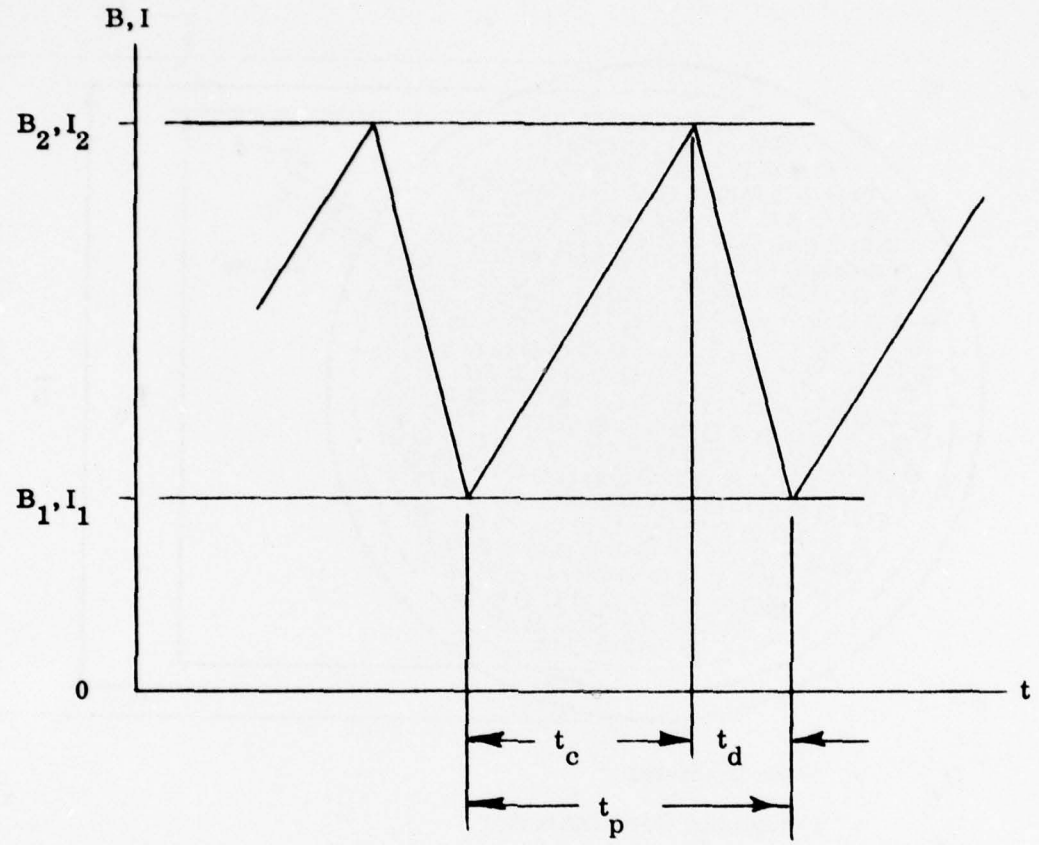

t_c = Charging Time

t_d = Discharge Time

$t_p = t_c + t_d = (\text{Rep Rate})^{-1}$

$|\dot{B}_c| = (B_2 - B_1) t_c^{-1} = \text{Constant}$

$|\dot{B}_d| = (B_2 - B_1) t_d^{-1} = \text{Constant}$

Figure B.9 Assumed Coil Current (I) and Coil Field (B) Wave Form.

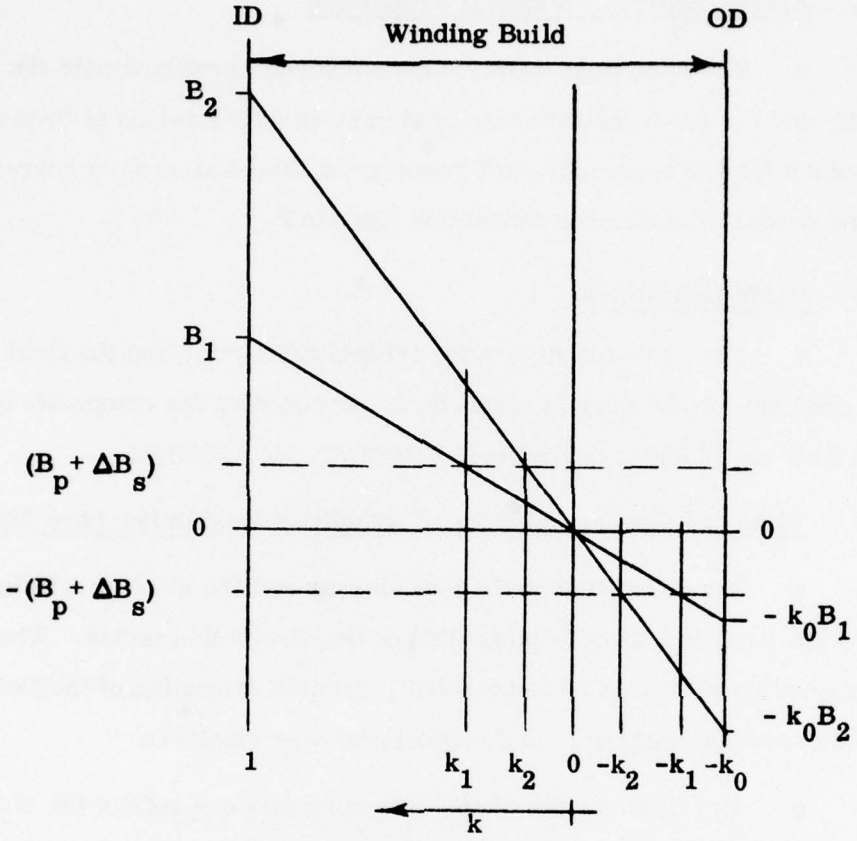

k_0 depends on coil geometry, $k_0 = 0$ for Torus

$$k_1 = \frac{B_p + \Delta B_s}{B_1} \leq 1$$

$$k_2 = \frac{B_p + \Delta B_s}{B_2} \leq 1$$

B_1 and B_2 are the lower and upper operating field limits.

Figure B.10 Assumed Linear Field Distribution Across the Radial Winding Thickness.

(4) Approximation of Material Properties

- The analytical expressions employed to approximate the matrix metal resistivity and the superconductor critical current as a function of field level and the expressions for the superconductor penetration field and surface currents are summarized and described under the subroutine RHOMAT.

(5) Basic Definitions

- The expressions for the critical twist pitch and the field diffusion time constant for the normal metal layer surrounding the composite core (See Figure B.8) are given under subroutines RHOMAT and TAXLC.

(6) Time and Spacial Averages of Quantities used in the Loss Equations

- The derivation of the local losses and the average winding losses requires the time and spacial integration of the dissipation terms. Where closed form integration proved to be impractical, suitable averaging of the field and field sweep rate dependent quantities in the equations was employed

- The final results of the averaging process reflect the analytical forms selected for the field dependent matrix resistivity and superconductor critical current density, the assumption of constant $\dot{B}$ for both the charging and discharging cycles and the linear field distribution across the winding build.

- The time average of a quantity, for the case of $\dot{B}$ = constant, reduces to an average with respect to B over the local range of field variation. The spacial average over the coil build, for the case of a linear B and $\dot{B}$ distribution, reduces to an average with respect to k (the normalized distribution) over the interval of $-k_o$ to 1 (See Figure B.10).

- It is the averaged quantities which are listed.

b. Loss Equations

The superconductor filament magnetization losses are governed by three sets of equations which depend on the local field cycle conditions in the windings. The three distinct operating ranges which may occur in the windings are shown in Figure B.10.

Range 1: $k_1 \leq k \leq 1$ and $-k_o \leq -k \leq -k_1$

- full field penetration of filaments during entire cycle
- Subroutine FMLR1

Range 2: $k_2 \leq k \leq 1$ and $-k_1 \leq -k \leq -k_2$

- full field penetration of filaments only during part of the cycle
- Subroutine FMLR2

Range 3: $-k_2 \leq k \leq k_2$

- partial field penetration of filaments during entire cycle
- Subroutines FMLR3

The equations for matrix loss due to filament coupling are given under Sobroutine MLFC.

The equations for matrix loss due to axial eddy current are given under Subroutine MLEC.

The self field loss in the conductor is given under Subroutine SFL.

c. Subroutine LOSS

Function: Receives average value of losses computed in various subroutines and calculates the total loss. Also computes certain parameters as shown below.

Equations:

$$B_p = \frac{\mu_o J_c d_s}{2}$$

$$B_{zero} = 3.44 - 0.4B_m$$

$$B_1 = \frac{\mu_o N I_1}{2\pi(1-\gamma_1)R_o}$$

$$B_2 = \frac{\mu_o N I_2}{2\pi(1-\gamma_2)R_o}$$

$$B' = B_p + \Delta B_s$$

$$K_1 = B'/B_1 \leq 1$$

$$K_2 = B'/B_2 \leq 1$$

Variables:

B_p = Bulk penetration field

B' = External field level at which full penetration of the filament occurs.

K_1, K_2 = Constants defined by torus geometry (Figure B.10)

ΔB_s = Surface field step (approx. 1 to 3 mT)

d. Subroutine RHOMAT

Function: Computes matrix metal resistivity and time-space average of various quantities used in superconductor loss calculation.

Equations

$$\rho_o = \rho_{300}/\rho_R$$

$$\beta = \left(\frac{\Delta\rho}{\Delta B}\right)\frac{1}{\rho_o}$$

$$B = \left(\frac{J_{co}}{J_C} - 1\right) B_o$$

$$\rho_m = \rho_o (1+\beta)$$

$$\tau_o = \mu_o \frac{\bar{D} \cdot \Lambda R}{4\rho_o}$$

$$\tau = \tau_o/(1+\beta B)$$

$$\langle\langle\tau^{-1}\rangle\rangle = \frac{1}{\tau_o}\left[1 + \frac{1}{4}\beta(B_1+B_2)\frac{(1+K_o^2)}{(1+K_o)}\right] = 1/\tau_*$$

$$\langle K^2(B_2-B_1)^2\langle\rho^{-1}\rangle\rangle = \frac{(B_2-B_1)}{2\rho_o\beta(1+K_o)}\left[-\frac{(1+K_o)}{\beta}\left(\frac{1}{B_1} - \frac{1}{B_2}\right)\right.$$

$$+ \ell n \frac{1+\beta B_2}{1+\beta B_1} + K_o^2 \ell n \frac{1+\beta B_2 K_o}{1+\beta B_1 K_o} - \frac{\ell n\{(1+\beta B_2)(1+\beta B_2 K_o)\}}{(\beta B_2)^2}$$

$$\left. + \frac{\ell n\{(1+\beta B_1)(1+\beta B_1 K_o)\}}{(\beta B_1)^2}\right]$$

Subroutine RHOMAT (Continued)

$$\langle K^2 (B_2 - B_1)^2 \langle \tau \rho^{-1} \rangle \rangle = \frac{\tau_o (B_2 - B_1)}{\rho_o \beta (1 + K_o)} \left[\frac{(1 + K_o)}{\beta} \left(\frac{1}{B_1} - \frac{1}{B_2} \right) + \frac{\ell n \left\{ (1 + \beta B_2)\ (1 + \beta B_2 K_o) \right\}}{(\beta B_2)^2} - \frac{\ell n \left\{ (1 + \beta B_1)\ (1 + \beta B_1 K_o) \right\}}{(\beta B_1)^2} \right].$$

$$\langle\langle B \rangle\rangle = \frac{1}{4} (B_1 + B_2) \frac{(1 + K_o^2)}{(1 + K_o)}$$

$$\langle\langle J_c \rangle\rangle = J_{co} B_o (B_o + \langle\langle B \rangle\rangle)^{-1} .$$

Variables

ρ_o = Zero-field resistivity

ρ_{300} = Room temperature resistivity

ρ_R = Zero-field resistivity ratio

J_c = Critical current density at operating field

$\frac{\Delta \rho}{\Delta B}$ = Coefficient of magneto-resistivity

B = Operating field

ρ_m = Operating resistivity

τ = Field diffusion (eddy current decay) time constant for the normal matrix layer.

J_{co} = Zero-field critical current density (at 4.2° K)

B_1 = Lower limit of the operating field

B_2 = Upper limit of the operating field.

NOTE: Quantities included in << >> indicate the time and spatial average of the same.

e. Subroutine TAXLC

Computes 1) $\dot{B}$ during charge and discharge ramps, and 2) critical twist pitch and time-space average of certain quantities as described below.

Equations

$$K_s = \frac{\pi^2}{4} \sqrt{\lambda_1} \quad \frac{w}{w+d}$$

$$\dot{B}_c = (B_2 - B_1)/\tau_c$$

$$\dot{B}_D = (B_2 - B_1)/\tau_D$$

$$\ell_c^2 = K_s \frac{\rho_m J_c d_s}{|\dot{B}|}$$

Where $\dot{B}$ is $\dot{B}_c$ and $\dot{B}_D$ during charge and discharge respectively.

$$\ell_{co}^{\ 2} = K_s \frac{\rho_o J_{co} d_s}{|\dot{B}|}$$

$$\ell_c^{\ 2} = \ell_{co}^{\ 2} \frac{B_o(1+\beta B)}{(B_o+B)}$$

$$\ll \ell_c^{-2} \gg = \frac{1}{\ell_{co}^{\ 2}} \quad \frac{1}{\beta B_o} \left[\frac{1}{2} + \frac{\beta B_o - 1}{\beta(B_2 - B_1)} \quad \frac{1}{(1+K_o)} \left\{ \ell_n \frac{1+\beta B_2}{1+\beta B_1} \right.\right.$$

$$+ K_o \ell_n \frac{1+\beta B_2 K_o}{1+\beta B_1 K_o} + \frac{\ell_n (1+\beta B_2)(1+\beta B_2 K_o)}{\beta B_2}$$

$$\left.\left. - \frac{\ell_n (1+\beta B_1)(1+\beta B_1 K_o}{\beta B_1} \right\} \right]$$

Subroutine TAXLC (Continued)

Variables

K_s = A numerical factor determined by the conductor configuration.

d_s = Superconductor filament diameter.

w = Spacing between superconductor filaments.

λ_2 = Packing factor.

ℓ_{co} = Critical twist pitch at zero-field.

ℓ_c = Critical twist-pitch at operating field.

f. Subroutines FMLR1, FMLR2 and FMLR3

Function: Compute superconductor filament magnetization loss for different ranges of penetration.

Please refer to Figures B.9 and B.10 for the identification of different quantities used in the design equations below.

Range 1 (FMLR1)

- full field penetration of filaments during entire ramp.

$$K_1 \leq K \leq 1 \text{ and } -K_o \leq -K \leq K_1$$

Average loss within K-range in per unit superconductor volume per charge or discharge cycle (assumed ramp up and down as shown in Figure B.9) is given by:

$$< \frac{\Delta Q_{f1}}{\Delta V_s} > \sim \frac{2d}{\pi^2} \frac{J_{co} B_o}{(K' - K_1)} \left\{ \left(1 + \frac{\Delta d}{d}\right) \left[K' \ell_n \frac{B_o + B_2 K'}{B_o + B_1 K'} \right. \right.$$

$$- K_1 \ell n \frac{B_o + B_2 K_1}{B_o + B_1 K_1} + \frac{B_o}{B_2} \ell n \frac{B_o + B_2 K'}{B_o + B_2 K_1}$$

$$- \frac{B_o}{B_1} \ell n \frac{B_o + B_1 K'}{B_o + B_1 K_1} \Bigg] + \frac{\eta^2}{3 B_{op}^2 (B_o + B_{op})^2} \Bigg[\frac{(K'^5 - K_1^5)(B_2^4 - B_1^4)}{20}$$

$$+ \frac{(K'^4 - K_1^4)}{12} B_o (B_2^3 - B_1^4) \Bigg] \Bigg\} .$$

Where $K' = 1$ or K_o.

Range 2 (FMLR2)

$$K_2 \leq K \leq K_1 \text{ and } -K_1' \leq -K \leq -K_2$$

$$K_1 \leq 1 \text{ and } -K_o \leq -K_1' \leq -K_2$$

- full field penetration of filaments during only part of the ramp.

Average Loss

$$< \frac{\Delta Q_{f2}}{\Delta V_s} > \sim \frac{2d}{\pi^2} \frac{J_{co} B_o}{(K - K_2)} \Bigg\{ \left(1 + \frac{\Delta d}{d}\right)$$

$$\left[\frac{B_o + B_2 K'}{B_2} \ell n \frac{B_o + B_2 K'}{B_o + B_p + \Delta B_s} - (K - K_2) \right]$$

$$+ \frac{\eta^2}{3 B_{op}^2 (B_o + B_{op})^2} \Bigg[\frac{(K'^5 - K_2^5) B_2^4}{20} + \frac{(K'^4 - K_2^4) B_o B_2^3}{12}$$

$$- (K' - K_2)(B_p + \Delta B_s)^3 \left(\frac{B_p + \Delta B_s}{4} + \frac{B_o}{3} \right) \Bigg]$$

$$+ \frac{\pi^2}{96 B_o (B_p + \Delta B_s)^2} \Bigg[4 (K' - K_2) B_p^2 (B_p + 3 \Delta B_s)$$

$$- 6 (K'^2 - K_2^2) B_p B_1 (B_p + 2 \Delta B_s)$$

$$+ 4 (K'^3 - K_2^3) B_1^2 (B_p + \Delta B_s) - (K'^4 - K_2^4) B_1^3 \Big] \Bigg\}$$

Where $K' = K_1$ or K_1'.

Range 3 (FMLR3)

$$0 \leq K \leq K_2 \quad \text{and} \quad -K_2' \leq -K \leq 0$$

$$(K_2 \leq 1 \quad \text{and} \quad -K_o \leq K_2')$$

Average Loss

$$< \frac{\Delta Q_{f3}}{\Delta V_s} > \sim \frac{d}{48} J_{co} \frac{K'^3 (B_2 - B_1)^3 - 6K' (B_2 - B_1) \Delta B_s^2 + 8 \Delta B_s^3}{(B_p + \Delta B_s)^2}$$

Where

$K' = K_2$ or K_2'.

g. Subroutine MLFC

Function: Compute loss in the composite core due to filament coupling.

The average loss in the winding build per unit matrix volume within the wire core per charging or discharge cycle is given by:

$$< \frac{\Delta Q_m}{\Delta V_{mc}} > \sim \frac{2(D_c-d)}{\pi^2} \frac{J_{co}B_o}{(1+K_o)} \left\{ \ell n \frac{B_o+B_2}{B_o+B_1} + \ell n \frac{B_o+B_2K_o}{B_o+B_1K_o} \right.$$

$$+ \frac{B_o}{B_2} \ell n \left[\frac{(B_o+B_2)(B_o+B_2K_o)}{B_o^2} \right]$$

$$\left. - \frac{B_o}{B_1} \ell n \left[\frac{(B_o+B_1)(B_o+B_1K_o)}{B_o^2} \right] \right\}$$

$$\left\{ 1 - \exp -\left(\frac{8}{3\sqrt{\lambda_s}} \frac{d}{(D_c-d)} \ell^2 << \ell_c^{-2} >> \right) \right\}$$

h. Subroutines MLEC and MLECS

Function: Compute eddy-current loss in the pure matrix layer at the wire surface.

The average loss per unit layer volume per charging or discharge cycle is given by:

$$< \frac{\Delta Q_e}{\Delta V_{m\ell}} > \sim \frac{\overline{D}^2}{8} \frac{1}{t_a} \left[< K^2 (B_2 - B_1)^2 < \rho^{-1} >> - \right.$$

$$- \left\{ < K^2 (B_2 - B_1)^2 < \tau\rho^{-1} >> \right\} \left\{ \frac{2t_p}{t_a t_b} \frac{\left(1 - e^{-t_b/\tau_*}\right)\left(1 - e^{-t_a/\tau_*}\right)}{1 - e^{-t_p/\tau_*}} \right.$$

$$\left. \left. - \frac{t_p^2}{2t_a t_b^2} \frac{\left(1 - e^{-t_b/\tau_*}\right)^2 \left(1 - e^{-2t_a/\tau_*}\right)}{1 - e^{-t_p/\tau_*}^2} \right\} \right]$$

For charging:

$$t_a = t_c$$

$$t_b = t_d$$

For discharge:

$$t_a = t_d$$

$$t_b = t_c$$

i. Subroutine SFL

Function: Compute the self field loss per unit volume of the superconductor.

The equation for the average loss has the form as shown below:

$$< \frac{\Delta Q_{sf}}{\Delta V_s} > \sim \frac{B_s^* < < J_c >> D_c}{4} \left\{ g^2 + 2 (1 - g)[\ell n (1 - g) + g] \right\}$$

Where:

$$B_s^* = \lambda_s \frac{\mu_o J_c D_c}{4}$$

$$g = \frac{J_2 - J_1}{2J_c} = \frac{I_2 - I_1}{2I_c}$$

$I_2 - I_1$ = Net change in the wire transport current during the ramp.

j. Dewar/Cryostat Design

The subroutine CRYHEAT computes the thermal effects on the superconducting coil material, for determining the transient and steady-state heat transfer characteristics. Two quantities are computed; an adiabatic ΔT per pulse, making the worst case assumption that each superconducting wire is uncooled, using its heat capacity to absorb the losses computed by the loss equations; and an isothermal heat flux, the value required to carry off the energy dissipated per pulse, and leave the conductor at the same temperature at the beginning of each pulse. These quantities are printed to compare the thermal performance of the system under study with established maximum limits for superconductors.

The DEWAR subroutine computes the size and weight of the dewar and liquid helium it contains. A "first cut" at the dewar size (pill box shape) is chosen so as to be just big enough to contain the toroidal coil, with an appropriate packing factor. The dewar height is then adjusted, if necessary, to provide enough volume to store any additional liquid helium. A dewar wall heat leak figure of 10 watts per square meter of dewar surface area is included to provide for standby losses.

k. Subroutine CRYHEAT

Function: Computes temperature rise of the coil in the absence of any cooling and the resulting heat-flux across the wire surface. The purpose is to check the heat-transfer requirements and know whether the coil is going to go normal.

Equations:

$$W_m = V_m \cdot \rho_c$$

$$\Delta T = \frac{P_{we}}{(W_m \cdot C_{pm} + W_{sc} \cdot C_{pse})}$$

$$A_{sw} = \pi D_w n_w \ell_{mt} \cdot N$$

$$Q = \frac{P_{we} \times 10^{-4}}{(T \cdot A_{sw} \cdot \xi_s)}$$

Variables:

V_m = Volume of the matrix material

ρ_c = Density of matrix material

W_m = Weight of the matrix material

P_{we} = Loss per pulse

C_{pm} = Specific-heat of matrix material

C_{pse} = Specific-heat of super-conductor material

A_{sw} = Area of surface for heat-transfer

ΔT = Temperature rise in °C.

ξ_s = Wire effective surface-area ratio

Variables: (Continued)

Q = Heat-flux across wire surface (W/cm^2)

T = Length of the pulse

ℓ_{mt} = Mean length per turn of the winding

N = Number of turns of the coil

n_w = Number of superconducting wires in cable

1. Subroutine DEWAR

Function: Designs the DEWAR to satisfy the heat-transfer requirements of the energy-storage coil.

Equations:

$$R_D = R_o(1+\gamma_2)(1+\lambda)$$

$$h_d = 2R_o\gamma_2(1+\lambda)$$

$$V_{DC} = \pi R_D^2 \rho_D$$

$$V_B = 2\pi R_o^3(\gamma_2^2 - \gamma_1^2)$$

$$V_{st} = \lambda_s \cdot V_B$$

$$V_{HP} = P_{we} \cdot N_P/(Q_{He}\rho_{He})$$

$$H_{BO} = 1.01 \times 10^{-8} \times I_{RMS}$$

$$V_{HL} = H_{BO} \cdot t_m/\rho_{HE}$$

$$P\ell = V_{H\ell} \cdot \rho_{HE} \cdot Q_{HE}$$

$$V_w = A_w n_w \cdot N \cdot \ell_{mt}$$

Equations: (Continued)

$$V_{HF} = V_B - V_w$$

$$A_{TB} = 2\pi R_D^2$$

$$A_S = 2\pi R_D h_d$$

$$V_{HTB} = 10.0 \cdot A_{TB} \cdot t_m / (Q_{HE} \cdot \rho_{HE})$$

$$V_{HS} = 10.0 \cdot A_s \cdot t_m / (Q_{HE} \cdot \rho_{HE})$$

$$V_{HBO} = V_{HP} + V_{HL} + V_{HTB} + V_{HS}$$

$$W_{HBO} = V_{HBO} \cdot \rho_{He}$$

$$V_{Hmin} = V_{HBO} - V_{HP}$$

$$W_{Hmin} = V_{Hmin} \cdot \rho_{He}$$

$$W_{Lead} = 0.69\, I_{rms} \cdot 10^{-3}$$

$$W_D = 90.0\, (V_D)^{0.913}$$

Variables

R_d = Dewar Internal radius

h_d = Height of Dewar

γ_1, γ_2 = Minor to major radius ratios

R_o = Toroidal - coil major radius

V_{DC} = Volume of dewar which is big enough to hold the coil

V_B = Volume of the winding build.

Variables (Continued)

V_{st} = Volume of the support structure

Q_{He} = Latent heat of vaporization of liquid He

ρ_{He} = Density of liquid helium

V_{HP} = Volume of Helium boil-off due to power loss in superconductor.

H_{BO} = Rate of boil-off due to dissipation in the leads

t_m = Mission-time

V_{HL} = Volume of liquid - Helium boil-off due to dissipation in the leads.

λ = Packing factor relating torus size to dewar size

P_ℓ = Dissipation in the leads

V_W = Volume of the winding

V_{HF} = Volume of Helium required to cover the coil

A_{TB} = Dewar - surface-area (top and bottom)

A_S = Dewar surface-area (sides)

V_{HTB} = Boil-off due to radiation through top and bottom

V_{HS} = Boil-off due to radiation through side

V_{HBO} = Volume of total Helium boil-off

W_{HYBO} = Weight of Helium boil-off

Variables - (Continued)

V_{Hmin} = Minimum volume of Helium required

W_{Hmin} = Minimum weight of the Helium required

W_{Lead} = Weight of boil-off due to lead-losses

W_D = Dewar weight

NOTE: The DEWAR subroutine includes a simple iterative algorithm which solves for the dewar volume. It initially selects a volume of dewar which is just big enough to hold the coil (a pill box type of shape is assumed). After computation of the Helium boil-off, it checks whether the dewar volume is sufficient to store that amount of He. If it is not, the volume is recomputed. Everytime, however, the volume is recomputed, He boil-off has to be recomputed too because radiation losses depend on volume and surface area. In the iteration, dewar top and bottom surface areas are kept constant (i.e., dewar ID is not varied). Only the height is adjusted.

APPENDIX C

ANALYSIS OF OTHER APPROACHES

1. APPROACH 4

a. Statement of Approach

A number of parallel or independent inductors (each providing one pulse of energy) may be used to provide a pulse train.

b. General Discussion

This approach can be implemented. The major factors that influence its attractiveness are weight and the complexity of the switching required to connect, discharge, and disconnect the inductors when they supply their charge to the load.

One factor that will have a substantial impact on the weight of the inductor system is that, as discussed below, it is desirable to minimize the mutual coupling between the individual inductors. The complexity of the charging system control is increased, and the inductance of the individual inductors must be closely controlled if the mutual coupling is significant. This requirement will influence the design of the inductors, which may have to be either toroidal or shielded units. The Dewar for the system will, consequently, be large and the cooling requirement significant.

The stray inductance that must be charged or discharged during switching will inevitably be higher than for a single inductor system. This will increase the switching duty of all the opening switches, and the energy requirement for the counter pulse network for the output switch.

The charging system for the inductors will have a major impact on the design of the charging supply. Two basic options are available -- series and parallel charging. Both of these alternatives will be addressed and a charging arrangement that would permit discharged inductors to be recharged during the discharge cycle will be discussed.

c. Mutual Coupling

A mutually coupled array of inductors forms a transformer. The circuit for such an array has many similarities to the circuit shown in Figure C.5(c), which is discussed in the following section covering Approach 5. The performance of the two cases converge when the transformer circuit of Figure C.15 has a coupling coefficient of unity between the individual primaries and their secondaries, and the coupling between the separate transformers is the same as the coupling between the inductors of the case under discussion. When an inductor is switched into the load, the flux coupling other charged inductors acts to increase the current in the charged inductors and is, consequently, not available to drive the load. The inductor can be sized to supply the required output energy from its uncoupled flux; however, the current in the inductors which have not been discharged will increase with each output pulse. Figure C.1 shows the percentage increase in current for a range of ratio of unswitched and switched inductance for coupling coefficients of 0.1 to 0.5. If the coupling is significant, the initial charge on the individual inductors will have to be adjusted so that the amplitude and energy of the individual pulses in the pulse train do not vary significantly. This control is only possible if parallel charging of the individual inductors is used. Two possible methods for controlling the charge are:

1) To sequentially connect the inductors to the supply so that the currents in the individual inductors are different at the end of the charge period. The current variation must be controlled so that the additional current induced in an inductor by units discharged earlier compensates for the charge deficiency at the end of the charge period.

2) To short circuit inductors as they reach the required charge, and disconnect them from the charging supply.

Thus, if coupling is significant, the inductance of the individual inductors must be adjusted to compensate for the flux which couples other short circuited inductors, and the initial charge on the inductors must be carefully controlled to compensate for the additional charge that the unit absorbs from other, mutually coupled units.

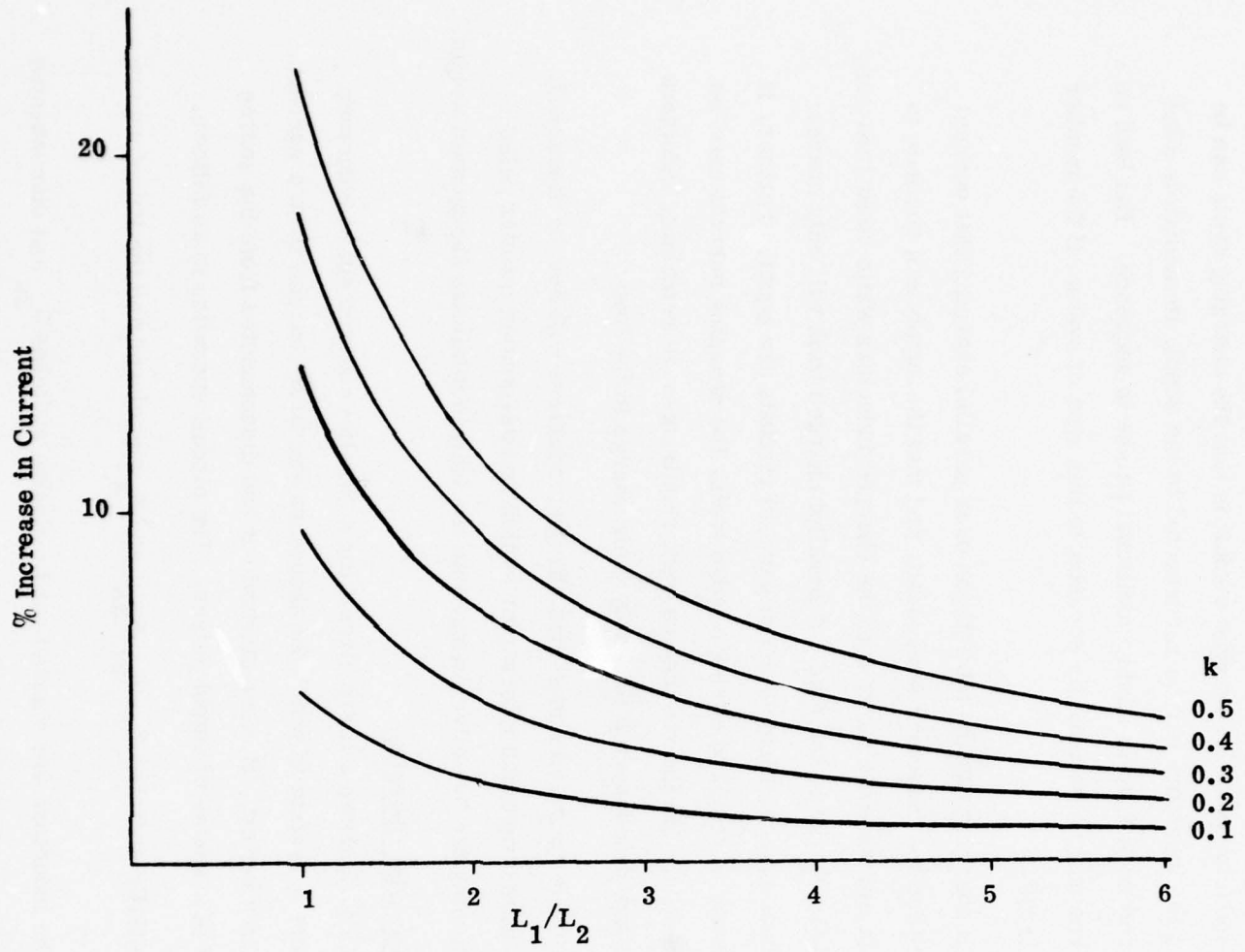

Figure C.1 Percentage Increase in the Current in Remaining Inductors For Coupling Coefficients of 0.1 to 0.5 Over a Range of Inductance Ratios of Remaining Inductance (L_1) to Switched Inductance (L_2).

d. Charging Arrangement

The inductors can either be charged in parallel or in series. One advantage to a multi-inductor parallel charged circuit is that the charging cycle can be arranged so that the inductors can be reconnected to the supply immediately after they discharge and recharged to supply additional pulses in sequence. The load on the current source will be essentially constant in this type of system if the number of inductors is large.

Series charging has the advantages over parallel charging that current equalization between the inductors is assured, and that the supply can continue to supply a constant maintenance current to the charged inductors while other inductors are supplying their charge to the load. A parallel charged bank will only charge evenly if the inductances and losses in the parallel circuits are equal. Further, if charge maintenance is required during a pulse train, the charging current must be adjusted to compensate for the reduced current requirement of remaining inductors as the inductors are disconnected to supply their charge to the load.

Circuits for parallel and series charged inductors will now be discussed. All the circuits have a common interrupter switch and associated counter pulse network for switching the inductive energy into the load to minimize the system weight.

(1) Parallel Charging

Figure C.2 shows a basic circuit for a parallel charged set of inductors. The circuit covers a system in which the inductors are first charged from a current source, shown as a battery, B, then shorted out and disconnected from the source before the start of a series of output pulses. The circuit operation is as follows.

1) Initially switches S_1, S_{31}-S_{3N}, and S_5 are closed and the inductors are charged.

2) The inductors are shorted out by closing switches S_{2n} and disconnected from the source by opening switches S_{3n}

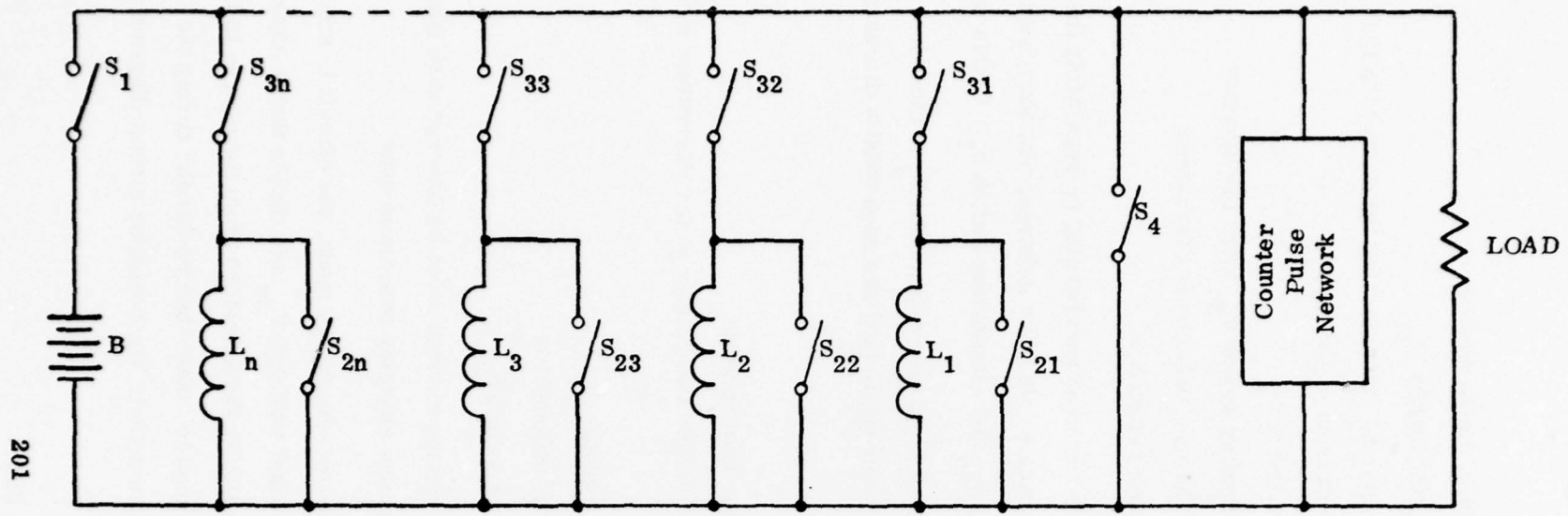

201

Figure C.2 Basic Circuit For Parallel Charged Multi-Inductor Storage System.

3) The inductors are sequentially discharged by

a) Closing the load connecting switch S_{3n}

b) Opening the shorting switch S_{2n} transferring the current in the active inductor to the interrupter switch S_4

c) Opening the interrupter switch S_4

d) Reopening the load connecting switch S_{3n} after the inductor discharges and before the next inductor is discharged

E. Reclosing the interrupter switch S_4.

The circuit can be modified for maintenance charging by separating the charge and load bus; substituting single pole triple throw (charge, off, load) switches for the single pole switches for switches S_{3n} and eliminating switch S_1. In this case,

1) Initially switches S_{3n} are in the charge position and S_4 is closed,

2) When the inductors are fully charged, they are sequentially discharged by

a) Closing switch S_{2n}

b) Placing switch S_{3n} in the load position

c) Opening switch S_{2n} to transfer the current to the interrupter switch, S_4

d) Opening the interrupter switch S_4

e) Placing switch S_{3n} in the off position

f) Reclosing the interrupter switch S_4.

As mentioned previously, the charge current must be lowered each time an inductor is discharged if this maintenance charging scheme is used.

In the continuous sequential charge-discharge mode, the circuit is similar to the maintenance charge circuit except that switches S_{3n} are double throw (charge-load) switches which transfer the connection to the inductors from the charge to the load bus. These switches could be designed to "make-before-break" during the transfer so that switches S_{2n} could be eliminated. The resulting circuit diagram is shown in Figure C.3.

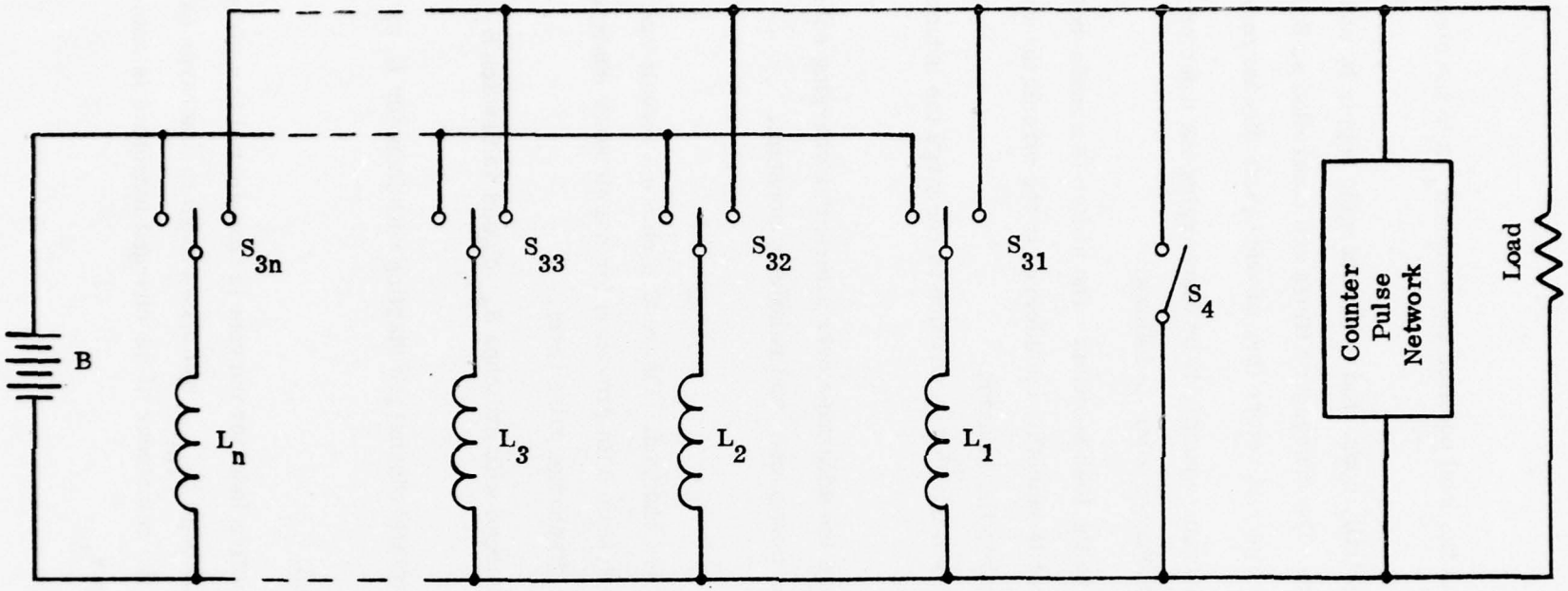

Figure C.3 Basic Circuit For Continuous Sequential Charging Multi-Inductor Storage System

Initially, switch S_{3n} is in the load position and switch S_4 is in the closed position.

The inductors are sequentially connected to the charging supply by changing switches S_{3n} to the charge position. The changeover times are controlled so that all the inductors will reach full charge just before they provide their discharge pulse.

The inductors are discharged sequentially by discharging the inductor with the highest charge for each discharge pulse as follows:

1) Switch S_{3n} is moved to the load position. The switch is a make-before-break design so the inductor current is smoothly transferred to the circuit through S_4.

2) S_4 is opened to discharge the inductor.

3) Switch S_{3n} is returned to the charge position to recharge the inductor.

4) S_4 is reclosed.

This operational mode has the advantage over alternative charging schemes that the load on the power source is continuous, and relatively constant.

(2) Series Charging

The inductors can be series charged. Figure C.4 shows a circuit that could be used for a series charged system with provision for maintenance charging of the charged inductors during the discharge pulse train.

Initially the system is charged with switches S_{2n} closed and switch S_4 closed.

The inductors are sequentially discharged starting with inductor L_1 as follows:

1) S_{1n} and S_{3n} are closed.

2) S_{2n} is opened. The active inductor current is transferred to a circuit through switch S_4, S_{3n}, and S_{11} through $S_{1(n-1)}$ switches closed to discharge earlier inductors. The charge circuit for the remainder of the charged inductors is completed through switches S_{11} through S_{1n}.

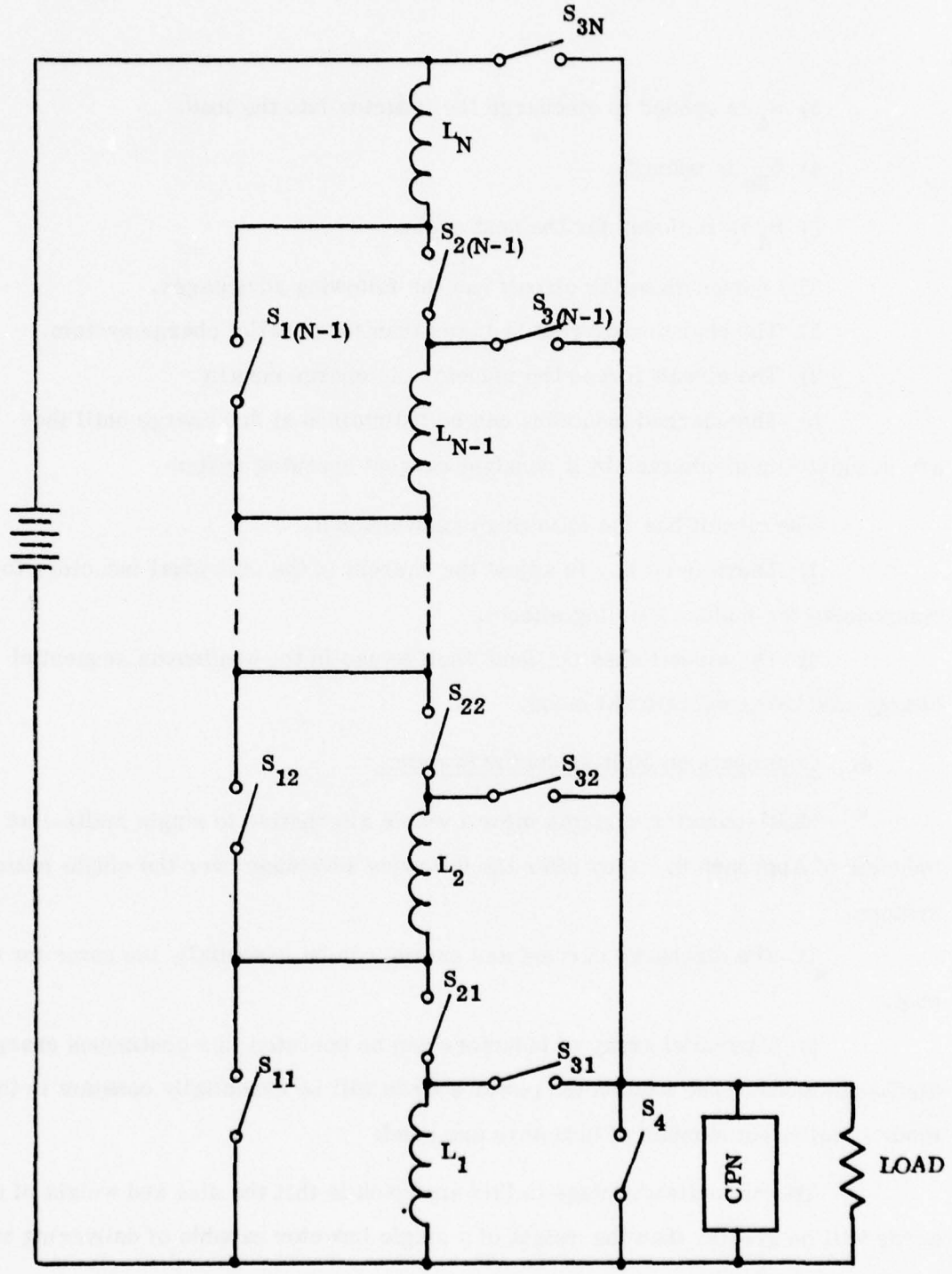

Figure C.4 Circuit For Series Charged Multi-Inductor Storage System.

3) S_4 is opened to discharge the inductor into the load.

4) S_{3n} is opened.

5) S_4 is reclosed for the next cycle.

The series charging circuit has the following advantages.

1) The charging current is lower than the parallel charge system.

2) The circuit forces the inductors to charge equally.

3) The charged inductors can be maintained at full charge until they are sequentially discharged by a constant current charging system.

The circuit has the following disadvantages.

1) There is no way to adjust the current in the individual inductors to compensate for mutual coupling effects.

2) The circuit does not lend itself to use in the continuous sequential charge-discharge operational mode.

e. Comments on Multi-Inductor Systems

Multi-inductor systems offer a viable alternative to single multi-shot inductor of Approach 3. They offer the following advantage over the single inductor system.

1) The discharge current and energy can be essentially the same for each shot.

2) A parallel array of inductors can be operated in a continuous charge-discharge mode. The load on the power source will be essentially constant in this mode if sufficient number of inductors are used.

The main disadvantage to this approach is that the size and weight of the array will be greater than the weight of a single inductor capable of delivering an equal amount of energy.

2. APPROACH 5

a. Statement of Approach

In this approach, the energy storage inductor is the primary of a transformer, and energy is extracted from secondary windings on the transformer.

b. Circuits Considered

The three circuits shown in Figure C.5 were considered as candidates for implementing this approach. The circuits of Figure C.5(a) and (b) have the same transfer circuit during each transformer cycle, so will be treated together.

(1) Transfer Characteristics of Circuits 1(a) and (b)

Figure C.6 is a circuit diagram of the active circuit for supplying a single pulse. The output pulse is initiated by opening switch S. The equation for the current (i_2) in the load resistor when this switch opens is:

$$\frac{d^3 i_2}{dt^3} + \frac{1}{1-k^2}\left\{\frac{1}{\tau_2}\cdot\frac{d^2 i_2}{dt^2} + \frac{1}{\tau_1^2}\cdot\frac{di_2}{dt} + \frac{1}{\tau_1^2\tau_2}\cdot i_2\right\} = 0$$

where

$$k = \frac{M}{\sqrt{L_1 L_2}} \quad \text{(dimensionless)}$$

$$\tau_1 = \sqrt{L_1 C} \quad \text{(sec)}$$

$$\tau_2 = \frac{L_2}{R} \quad \text{(sec)}$$

The choice of time units is arbitrary and can be normalized to units τ_1. The resulting equation for i_2 is:

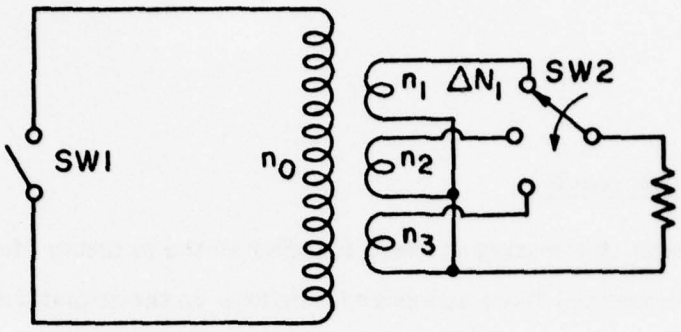

(a) MULTI-WINDING SECONDARY ENERGY EXTRACTION SYSTEM

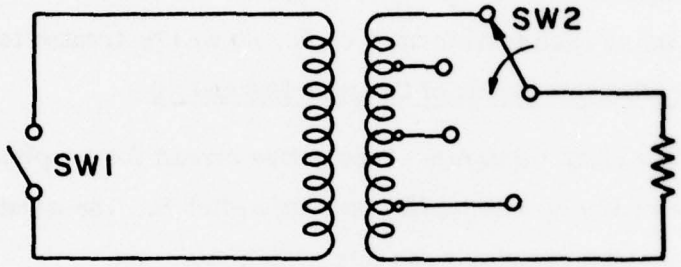

(b) SECONDARY MULTI-TAP ENERGY EXTRACTION SYSTEM

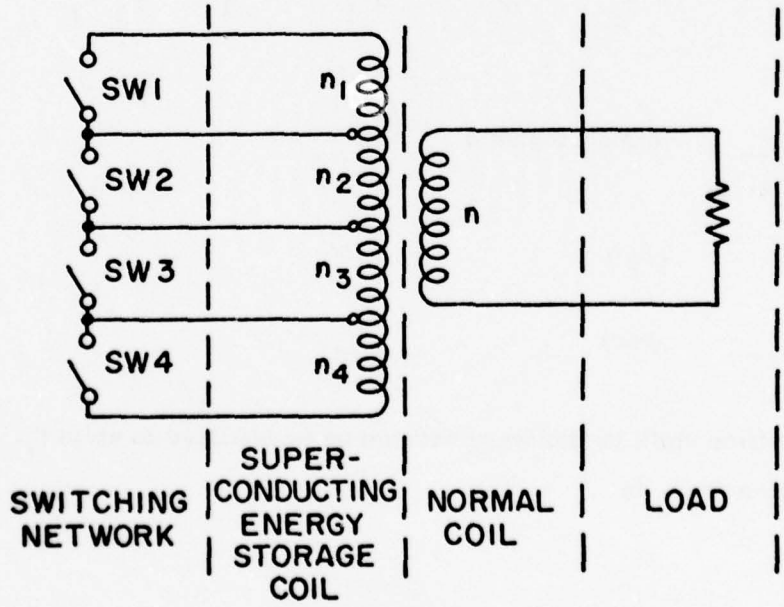

(c) MULTI-WINDING PRIMARY ENERGY EXTRACTION SYSTEM

Figure C.5 Various Arrangements of Multi-Winding Pulse Power Systems.

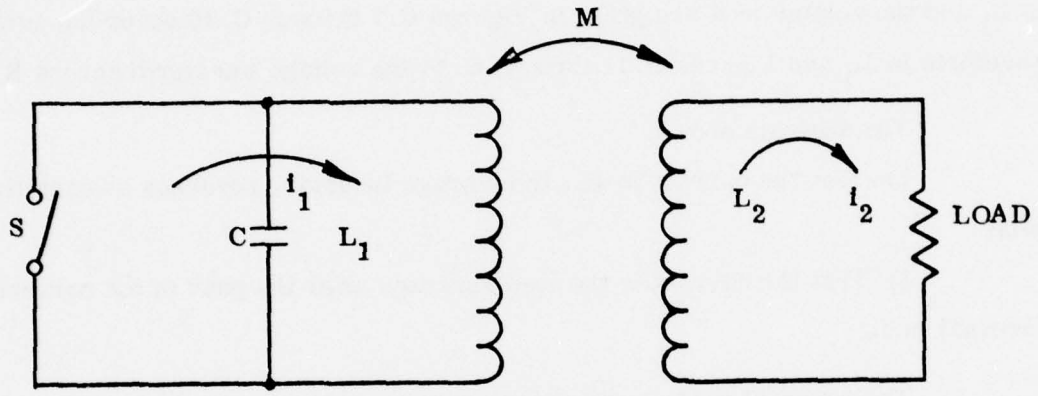

Figure C.6 Active Circuit for Transfer of Energy From Inductor L_1 to the Load Through Mutually Coupled Winding L_2.

$$\frac{d^3 i_2}{dt^3} + \frac{1}{1-k^2}\left\{\frac{1}{\tau_2}\cdot\frac{d^2 i_2}{dt^2} + \frac{di_2}{dt} + \frac{1}{\tau_2}\, i_2\right\} = 0$$

This circuit can be analyzed for a matrix of the two remaining constants (k and τ_2). This analysis has been completed for a matrix of k = 0.5, 0.6, 0.7, and 0.8 and τ_2 = 0.25, 0.5, 1, 2, and 4. The resulting waveforms for the current in L_1 and the voltage in R are given in Figures C.7 through C.10 cover the current waveform in L_1 and Figures C.11 through C.14 the voltage waveform across R.

The analysis shows:

1) That the current in L_1, the storage inductor, reverses on each output pulse.

2) That the current in the load reverses after the peak of the current reversal in L.

The reversal in the current in the storage inductor L_1 during each transfer cycle makes this system a poor candidate for a superconducting storage system, because it will maximize the hysteresis loss and the maximum rate of change in current in the storage coil. An additional drawback is that the switching capacitor must store all the energy returned in the storage inductor in addition to a fraction of the transferred energy. Superior circuits for transferring part of the storage inductor energy to the coil could be developed.

This circuit is considered to be unsatisfactory for this reason.

(2) Transfer Characteristics of the Figure C.5(c) Circuit

This circuit also has severe drawbacks. In practice, the mutual coupling between the individual primaries and the secondaries will be imperfect, and the coupling between the primaries will be imperfect. Thus, the circuit condition will lie somewhere between that shown in Figure C.5(c), with all windings perfectly coupled, and Figure C.15 where the primary windings are assumed to be completely decoupled and the coupling between the individual primaries and their individual

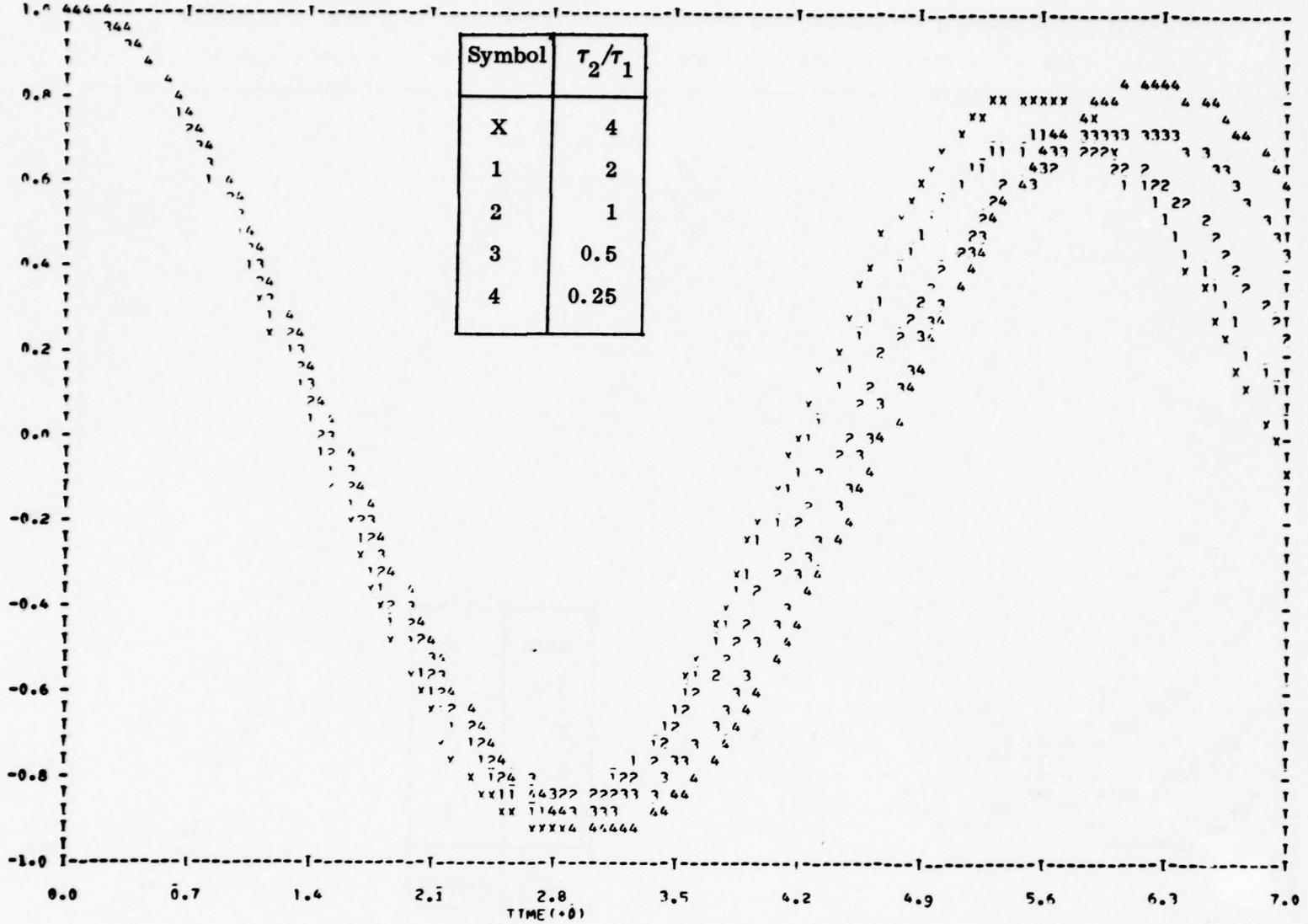

Figure C.7 Waveform of Current in Transformer Coupled Storage Inductor with a Coupling Coefficient k = 0.5

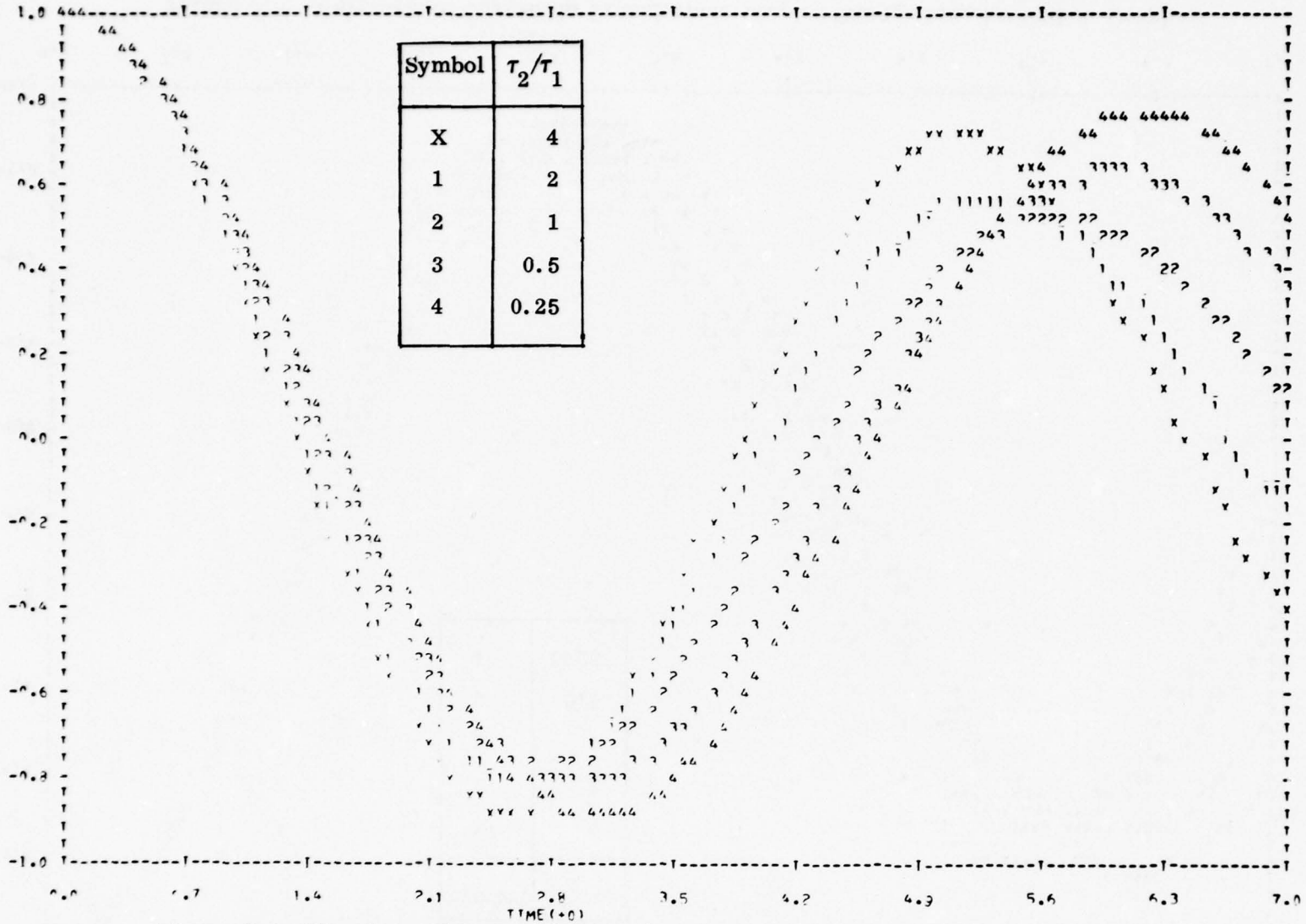

Figure C.8 Waveform of Current in Transformer Coupled Storage Inductor with a Coupling Coefficient k = 0.6

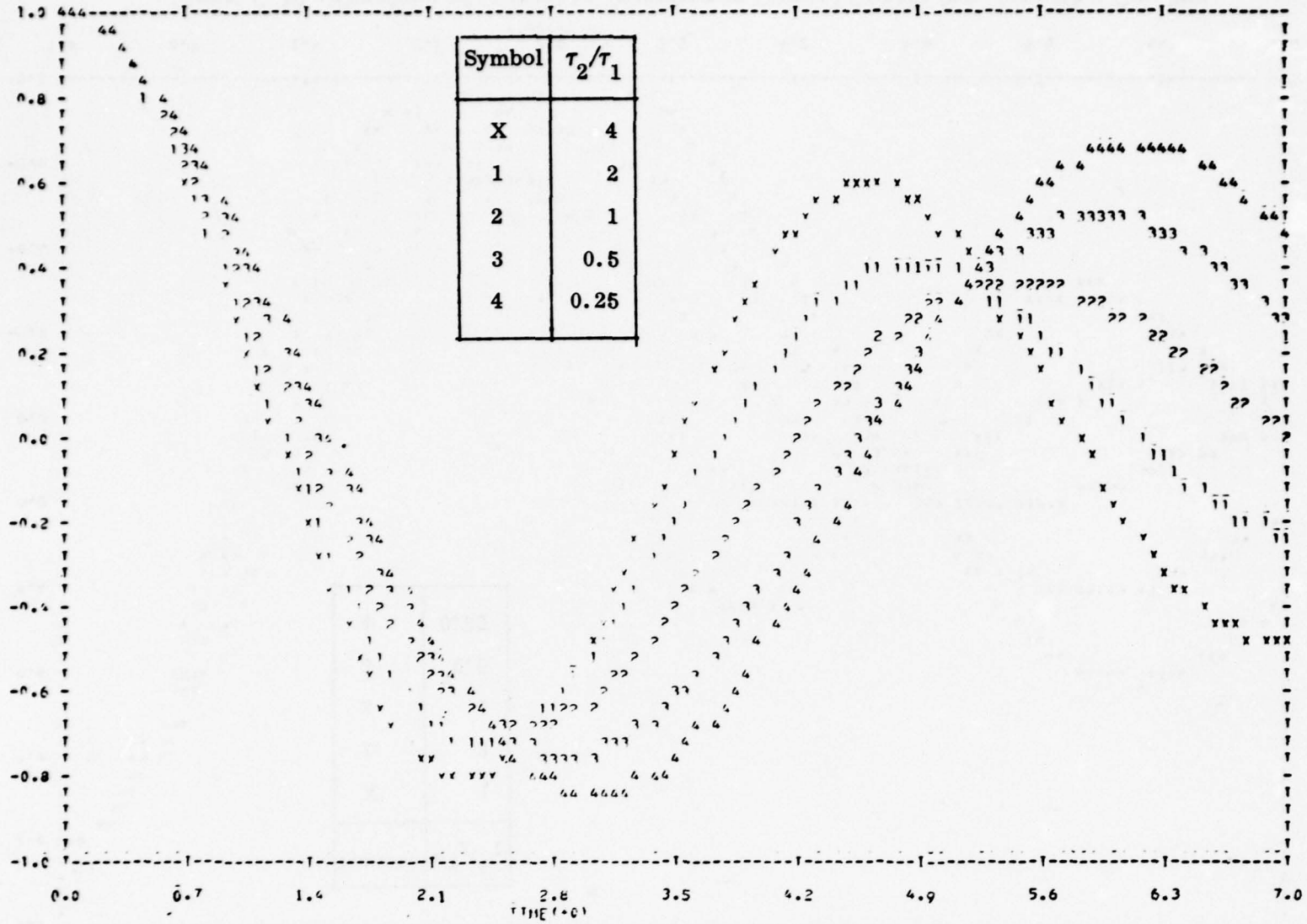

Figure C.9 Waveform of Current in Transformer Coupled Storage Inductor with a Coupling Coefficient $k = 0.7$

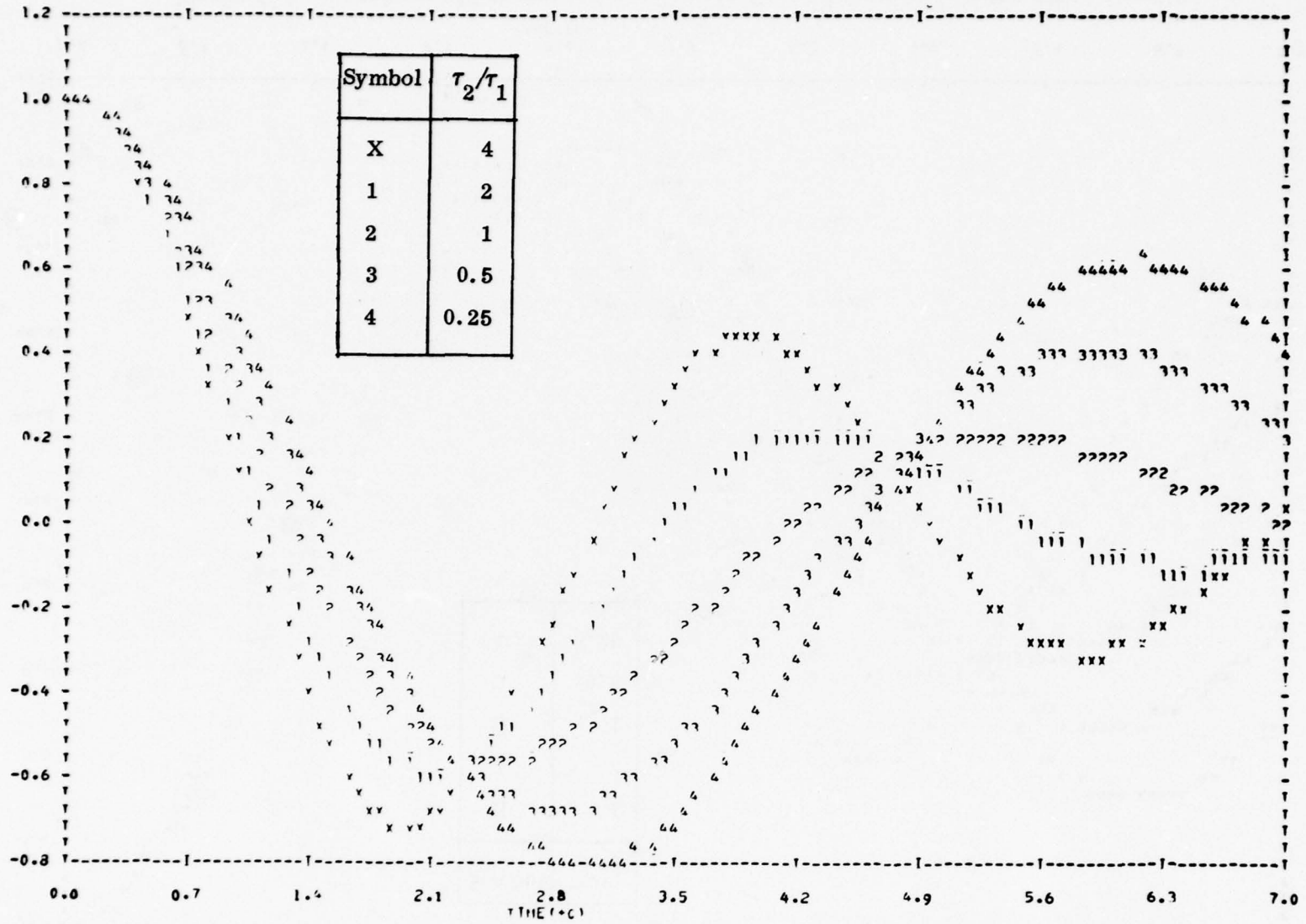

Figure C.10 Waveform of Current in Transformer Coupled Storage Inductor with a Coupling Coefficient k = 0.8

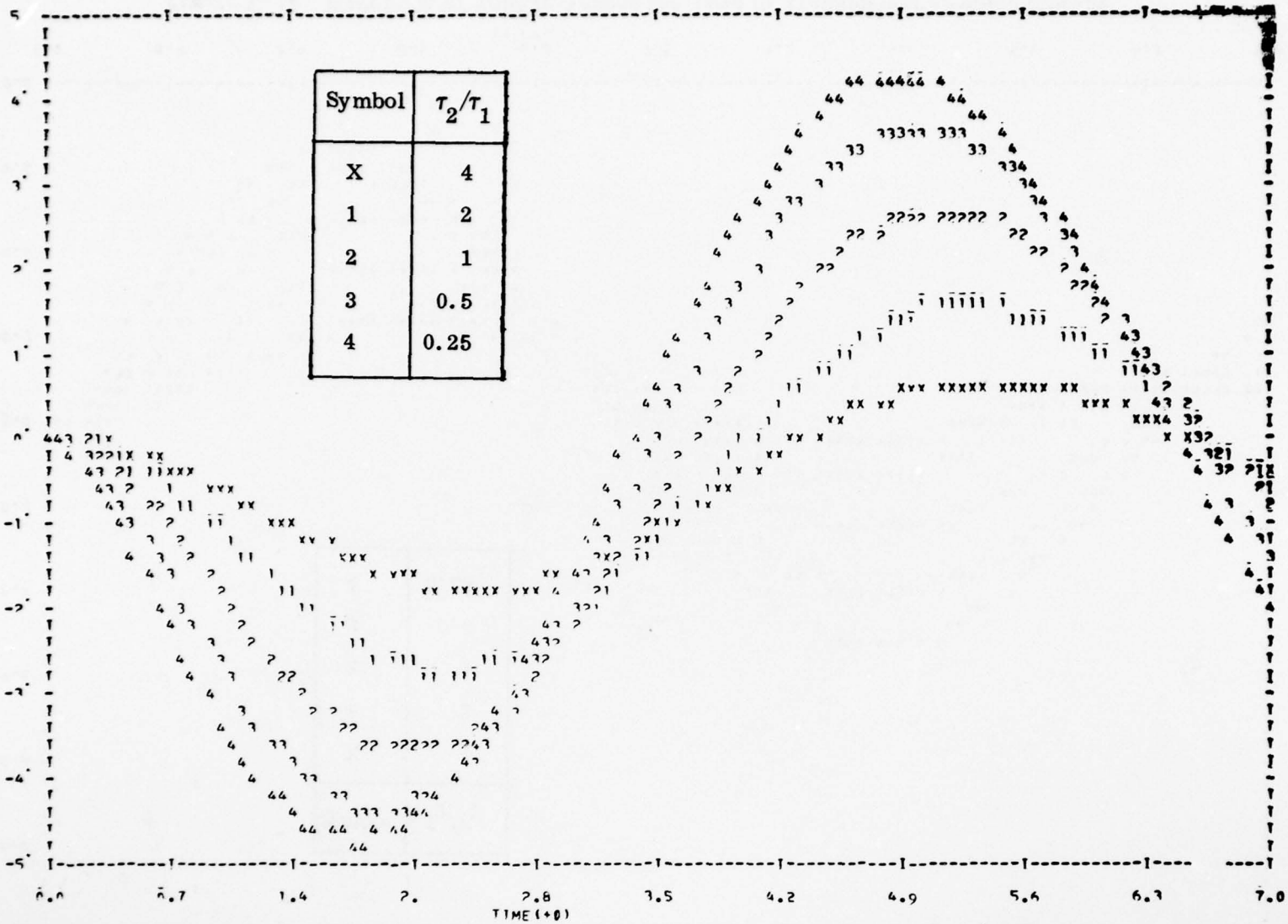

Figure C.11 Waveform of Voltage Across the Load in Transformer Coupled Storage Inductor with a Coupling Coefficient k = 0.5

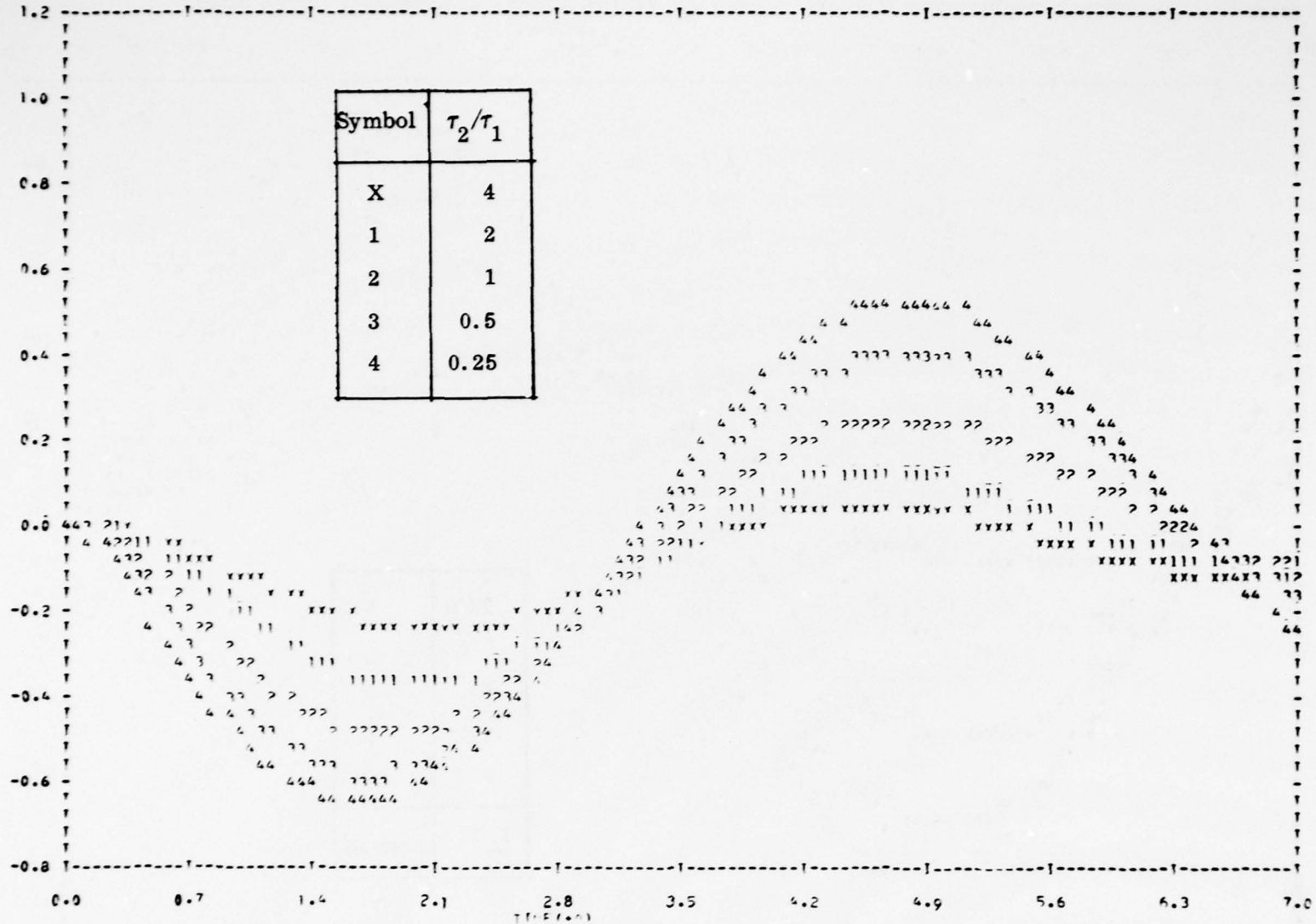

Figure C.12 Waveform of Voltage Across the Load in Transformer Coupled Storage Inductor with a Coupling Coefficient k = 0.6

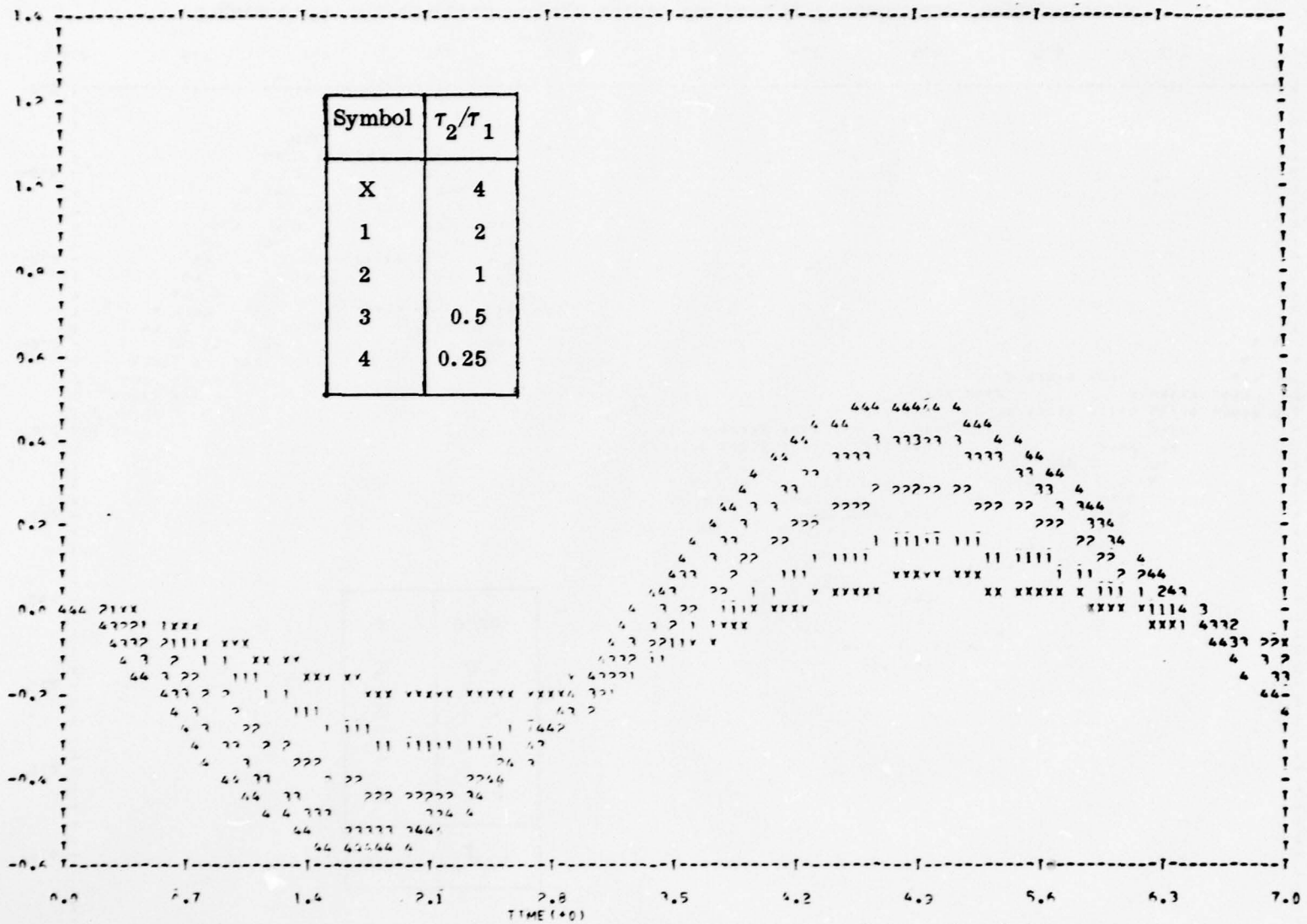

Figure C.13 Waveform of Voltage Across the Load in Transformer Coupled Storage Inductor with a Coupling Coefficient k = 0.7

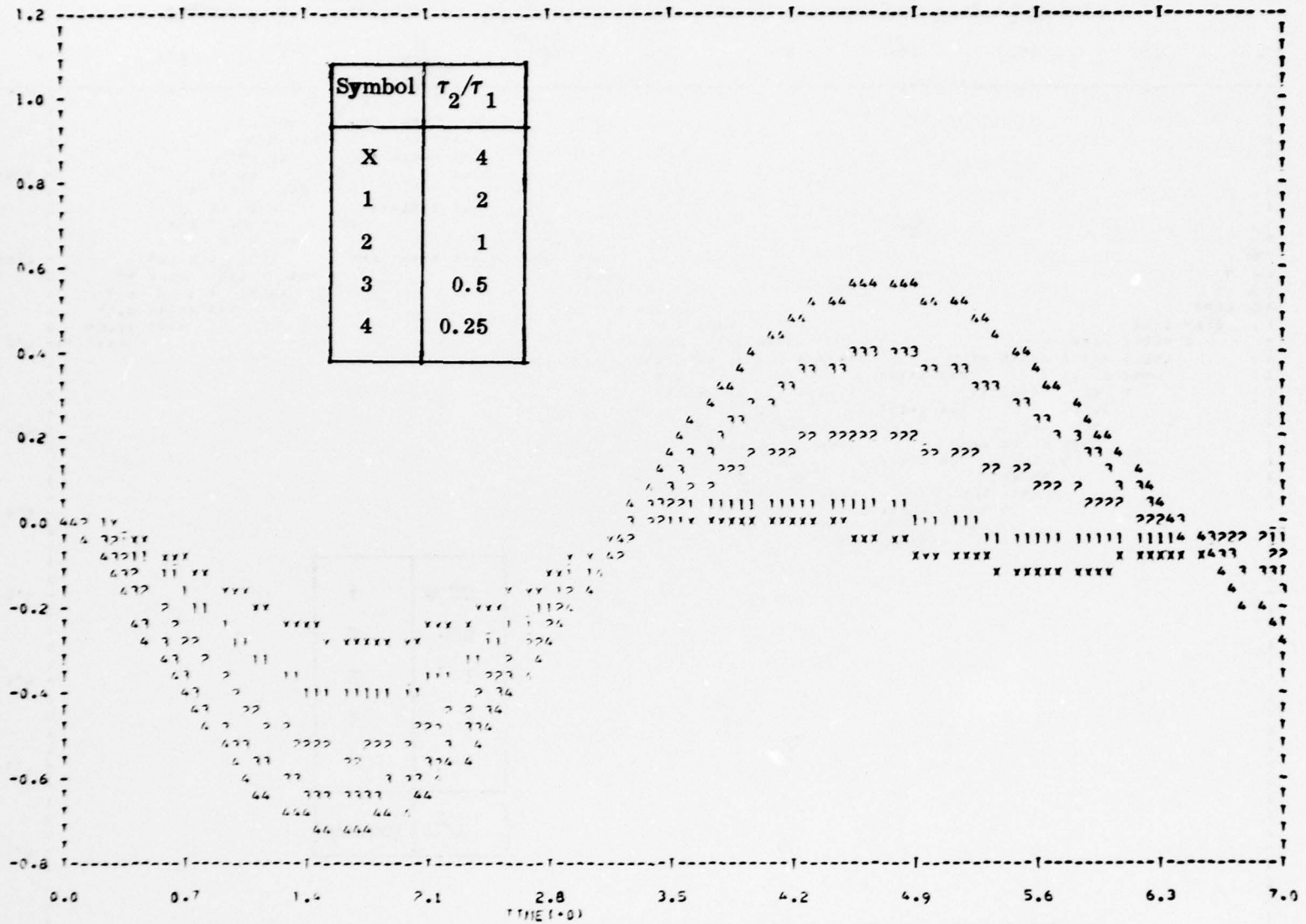

Figure C.14 Waveform of Voltage Across the Load in Transformer Coupled Storage Inductor with a Coupling Coefficient $k = 0.8$

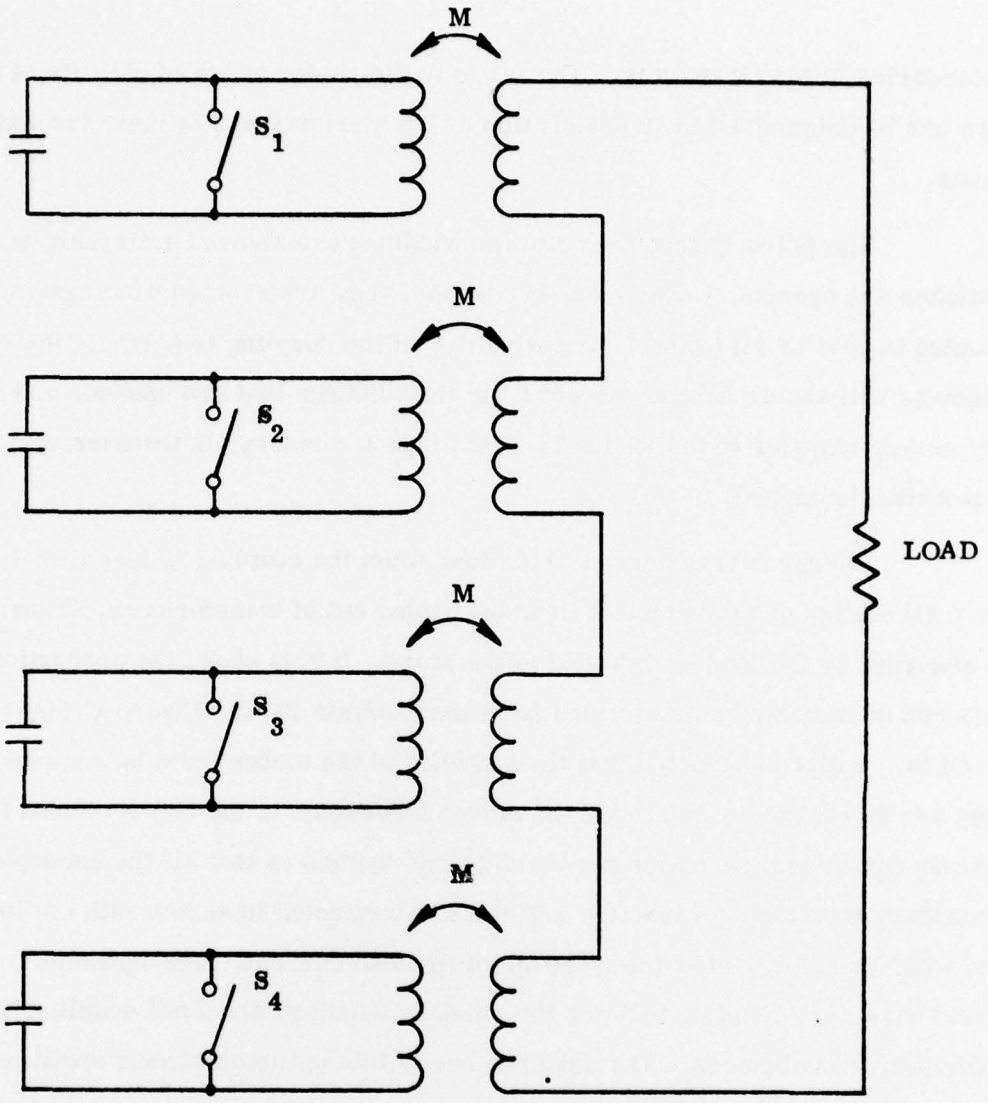

Figure C.15 Extreme Condition of Figure C.1 Circuit With No Mutual Coupling Between Primary Windings.

secondaries is less than unity. The range in the performance of circuits of this type can be determined by consideration of the performance of these two extreme cases.

The primary inductive storage windings are shorted until their associated switches are opened. Under these conditions, they are shorted windings, mutually coupled to part or all of the output winding. If the coupling is perfect, these shorted windings will absorb all the current from the windings that are opened, and prevent any energy transfer to the load. The total inductive energy is transferred when the last switch is opened.

Energy is transferred to the load when the coupling is less than 100%, and the total energy of each element in an uncoupled set of transformers, Figure C.15, is absorbed by the load or retained in the store. In this case, the proportion of retained energy can be determined from the analysis for the Figure C.5(a) and (b) circuits. It should be noted that the switches of the stores must be reclosed after they are discharged to minimize the series inductance in the output circuit for subsequent pulses. A major drawback to this system is that all the uncoupled secondary inductance of inactive inductors is connected in series with the load, and will, therefore, slow the risetime of the load current. The optimum circuit would have zero coupling between the primary windings and 100% coupling of the individual transformers. The performance of this optimum circuit would be similar to the multi-inductor systems of Approach 4. However, the system will have one opening switch for each output pulse. This and the use of secondary windings will make the system heavier than the Approach 4 systems.

c. Conclusion

The above discussion indicates that no benefits are gained by coupling the storage inductor to the load through a secondary winding, and that the transfer performance is degraded when such a scheme is used.

3. APPROACH 6

Approach 6 involves the transfer of energy from the superconducting storage coil at a slow rate to a normal coil. This normal coil will then deliver the pulse to the load at the required time of 20 - 40 μs. The room-temperature (normal) coil forms part of the discharge PFN. Therefore, after the energy has been transferred, Approach 6 reduces to Approach 1.

Attractiveness of this approach lies in the fact that, by having a slow discharge from the superconducting coil, the rate of change of flux is reduced and so is the rate of change of current. Therefore, AC losses in the superconductor as well as the coil voltage will be smaller which will reduce the demand on the opening switch.

Figure C.16 is a circuit diagram for the energy transfer between the two coils L_s is the main energy storage coil (superconducting) and L_t is the room-temperature transfer coil. C is the transfer capacitor. As shown in the figure, I_s and I_t are the two loop currents after switch S_1 is opened and S_2 is closed.

The two mesh equations for the circuit can be written as follows:

$$L_s \frac{dI_s}{dt} + \frac{1}{C} \int_o^t (I_s - I_t)\, dt = 0 \qquad (C.1)$$

$$-\frac{1}{C} \int_o^t (I_s - I_t)\, dt + L_t \frac{dI_t}{dt} = 0 \qquad (C.2)$$

Taking the Laplace transforms of the above equations,

$$L_s \left\{ S I_s(S) - I_o \right\} + \frac{1}{CS} \left\{ I_s(S) - I_t(S) \right\} = 0 \qquad (C.3)$$

$$-\frac{1}{CS} \left(I_s(S) - I_t(S) \right) + L_t S I_t(S) = 0 \qquad (C.4)$$

Note: The initial conditions are shown in Figure C.16.

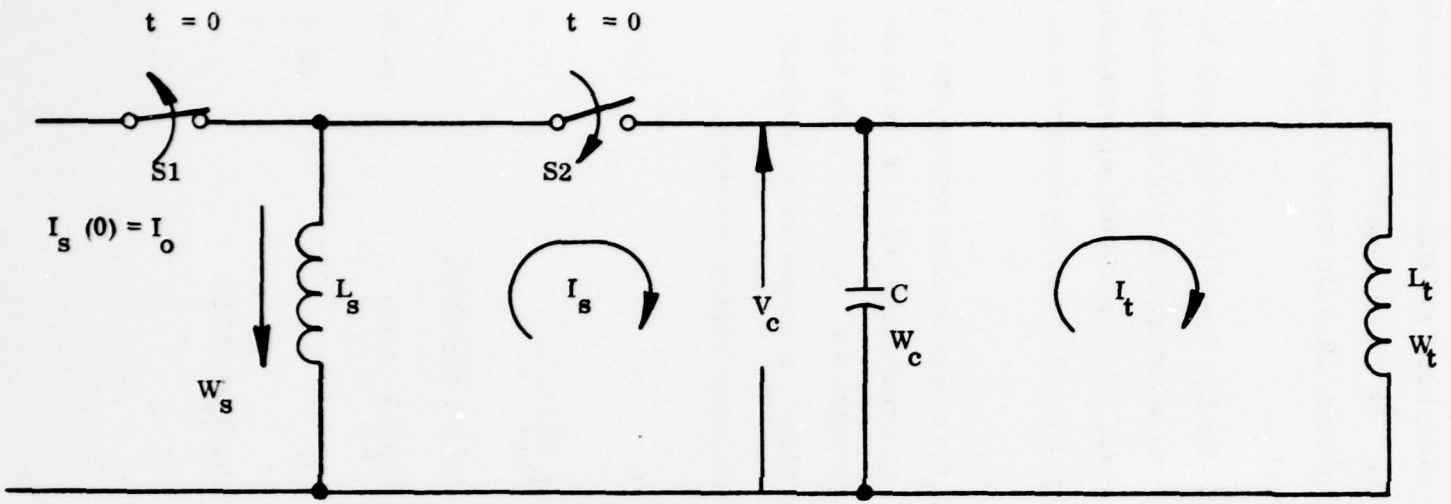

$$W_s = \frac{1}{2} L_s I_s^2$$

$$W_t = \frac{1}{2} L_t I_t^2$$

$$W_c = \frac{1}{2} C V_c^2$$

Figure C.16 Schematic of System For Case of Energy Transfer Between Two Coils.

Rewriting the above equations we obtain,

$$L_s S I_s(S) - L_s I_o + \frac{I_s(S) - I_t(S)}{SC} = 0 \qquad \text{(C.5)}$$

and

$$L_t S I_t(S) - \frac{I_s(S) - I_t(S)}{SC} = 0 \qquad \text{(C.6)}$$

Adding (C.5) and (C.6), we get

$$L_s S I_s(S) - L_s I_o + L_t S I_t(S) = 0$$

or

$$L_t S I_t(S) = L_s I_o - L_s S I_s(S) = L_s (I_o - S I_s(S))$$

$$\therefore I_t(S) = \frac{L_s (I_o - S I_s(S))}{L_t S} \qquad \text{(C.7)}$$

Substituting (C.7) in (C.6) we get,

$$I_s(S) = \frac{I_o (S^2 + 1/L_t C)}{S\left(S^2 + \frac{L_t + L_s}{L_t L_s C}\right)} \qquad \text{(C.8)}$$

Substituting for $I_o(S) =$ in (C.7) we get,

$$I_t(S) = \frac{L_s}{L_t S}\left(1 - \frac{S^2 + 1/L_t C}{S^2 + \frac{L_t + L_s}{L_t L_s C}}\right) I_o$$

or

$$I_t(S) = \frac{L_s\left(\frac{L_t + L_s}{L_t L_s C} - \frac{1}{L_t C}\right) I_o}{SL_t\left(S^2 + \frac{L_t + L_s}{L_t L_s C}\right)}$$

Simplifying further,

$$I_t(S) = \frac{I_o}{L_t C} \quad \frac{1}{S\left(S^2 + \frac{L_t + L_s}{L_t L_s}\frac{1}{C}\right)} \qquad \text{(C.9)}$$

Taking the inverse transform of (C.8) and (C.9) we get,

$$I_s = I_o \frac{L_s}{L_t + L_s} + I_o \frac{L_t}{L_t + L_s} \cos\omega t \quad \text{where } \omega = \sqrt{\frac{L_s + L_t}{L_s L_t} \cdot \frac{1}{C}}$$

$$I_t = I_s \frac{L_s}{L_t + L_s} [1 - \cos\omega t]$$

The waveforms of $I_s(t)$ and $I_t(t)$ are shown in Figure C.17. Initial energy stored in L_s is

$$W_o = \frac{1}{2} L_s I_o^2$$

Energy stored in <u>transfer coil</u> when its current reaches maximum at $\omega t = \pi$

$$W_t = \frac{1}{2} L_t \frac{4 I_o^2 L_s^2}{(L_t + L_s)^2} = \frac{2 L_t L_s^2}{(L_t + L_s)^2} I_o^2 = 2 \cdot L_t \left(\frac{L_s}{L_t + L_s}\right)^2 I_o^2$$

Energy retained by s.c. coil at $\omega t = \pi$ (i.e. when transfer coil stores its maximum energy) is

$$W_s = \frac{1}{2} L_s \left(\frac{L_s - L_t}{L_s + L_t}\right)^2 I_o^2$$

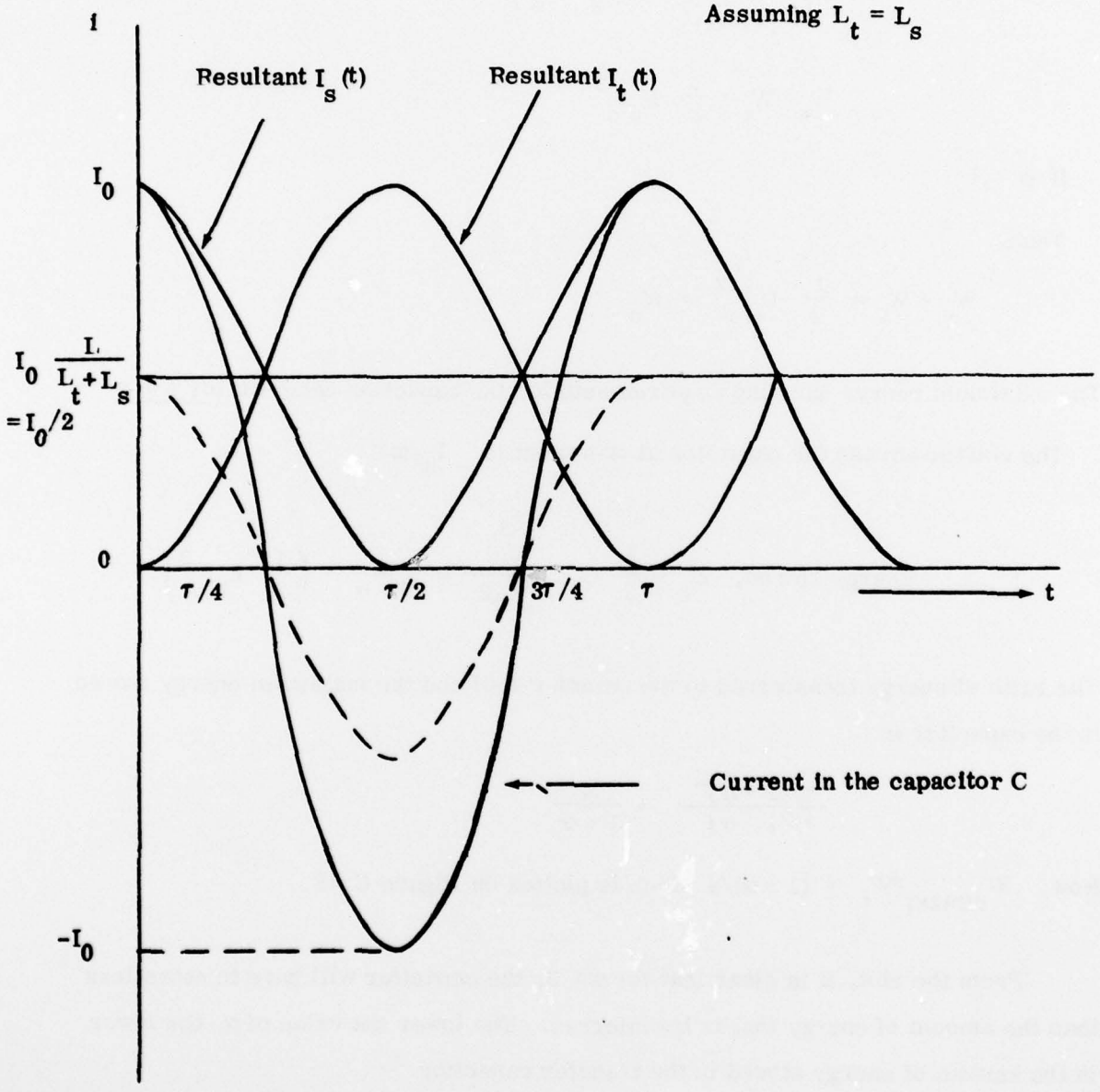

Figure C.17 Current Wave-Forms During Energy Transfer Process.

Taking $\frac{L_t}{L_s} = \alpha$

$$W_s\big|_{\omega t = \pi} = \frac{1}{2} L_s \left(\frac{1-\alpha}{1+\alpha}\right)^2 I_o^2 = \frac{1}{\alpha}\left(\frac{1-\alpha}{1+\alpha}\right)^2 \frac{L_t}{2} I_o^2$$

$$W_t = \frac{4}{(1+\alpha)^2} \cdot \left(\frac{L_t}{2} I_o^2\right)$$

$$W_s + W_t = \frac{1}{2} L_s I_o^2$$

If $\alpha = 1$

Then,

$$W_s + W_t = \frac{1}{2} L_s I_o^2 = W_o$$

The maximum energy handling requirements for the capacitor occur at $\underline{\omega t = \pi/2}$

The voltage across the capacitor at this point is $I_o/\omega C$

$$\therefore \text{ Energy stored, } W_c = \frac{1}{2} C \cdot \frac{I_o^2}{\omega^2 C^2} = \frac{1}{1+\alpha} \cdot \left(\frac{1}{2} L_t I_o^2\right)$$

The ratio of energy transferred to the transfer-coil and the maximum energy stored in the capacitor is

$$\frac{4/(1+\alpha)^2}{1/(1+\alpha)} = \frac{4}{1+\alpha}$$

Now, $W_{c(max)}/W_t = (1+\alpha)/4$ which is plotted on Figure C.18.

From the plot, it is clear that for $\alpha \leq 3$, the capacitor will have to store less than the amount of energy that is transferred. The lower the value of α, the lower is the amount of energy stored in the transfer capacitor.

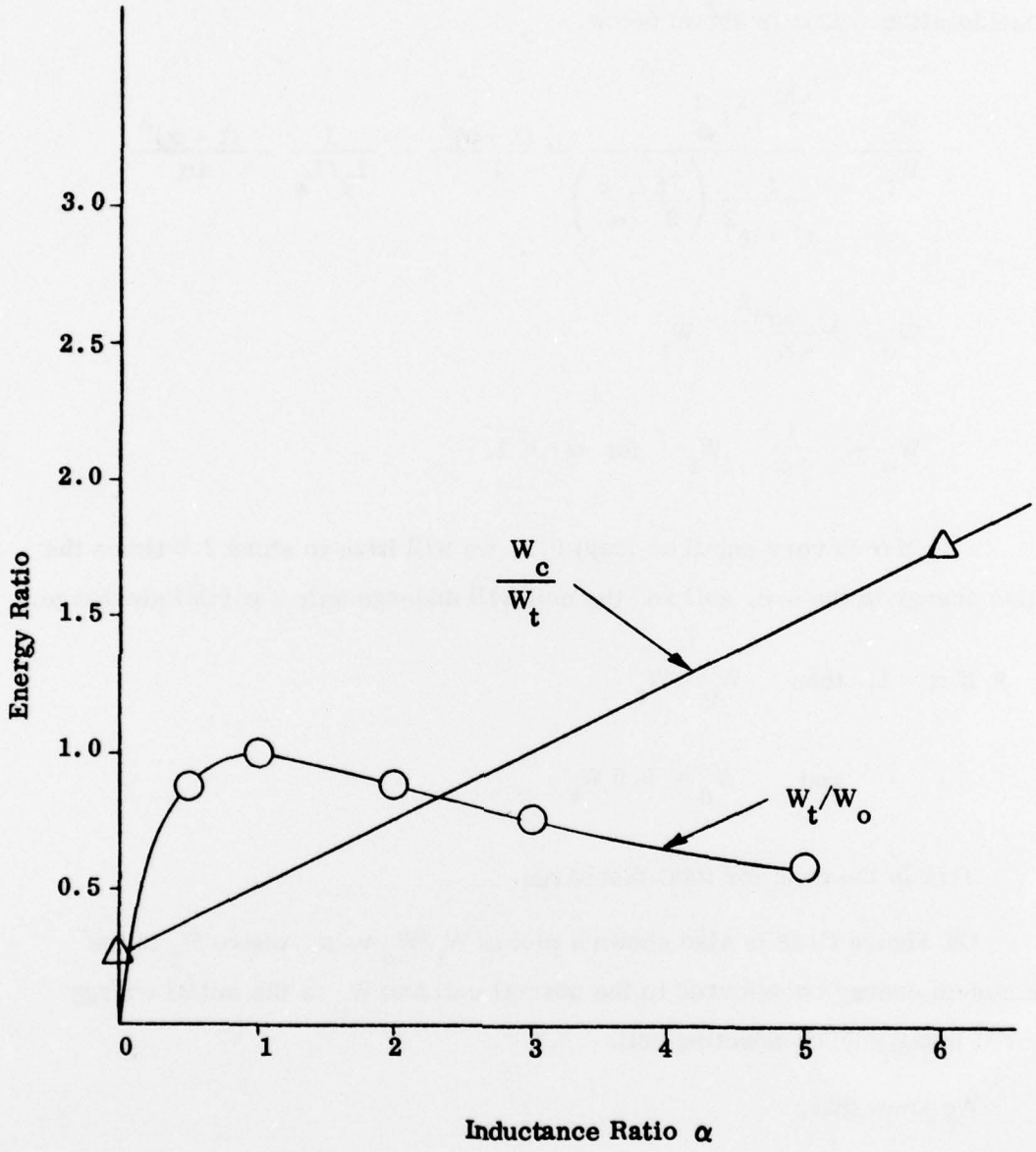

Figure C.18 Ratios of energy stored as a function of α.

The effect of low α on the ratio of W_o/W_t at $\omega t = \frac{\pi}{2}$ is also worthy of consideration. This is shown below.

$$\frac{W_o}{W_t} = \frac{\frac{1}{2} L_s I_o^2}{\frac{4}{(1+\alpha)^2}\left(\frac{L_t}{2} I_o^2\right)} = \frac{(1+\alpha)^2}{4} \cdot \frac{1}{L_t/L_s} = \frac{(1+\alpha)^2}{4\alpha}$$

$$W_o = \frac{(1+\alpha)^2}{4\alpha} W_t$$

$$W_o \simeq \frac{1}{4\alpha} W_t \quad \text{for } \alpha << 1$$

$\therefore$ If α is very small as (say) 0.1, we will have to store 2.5 times the pulse energy in the s.c. coil and the coil will undergo only a partial discharge.

If $\alpha = 1$, then $W_o = W_t$

and $W_c = 0.5\, W_t$

This is the case for total discharge.

On Figure C.18 is also shown a plot of W_t/W_o vs α, where W_t is the maximum energy transferred to the normal coil and W_o is the initial energy stored in the superconducting coil.

We know that,

$$\frac{W_t}{W_o} = \frac{4\alpha}{(1+\alpha)^2}$$

As stated earlier, for full discharge of the superconducting coil and theoretically total transfer of energy between the two coils, α has to be unity, as is evident from the plot. This, however, implies that the transfer capacitor will have to store 50% of the pulse energy. If we settle for a less efficient transfer of energy (say) 80% or below, then of course, the capacitor will have to store about 30 - 35% of the pulse energy. The coil under these circumstances will operate under Approach 2 (partial discharge) conditions. That means while we are trying to make the size of the capacitor smaller, we are paying for a larger coil and bigger cooling system. On this score, this method does not have any added attractions over Approach 2 where the demands on the superconductor is reduced substantially and its degradation is rather unlikely, precisely what we are trying to achieve here.

Looking from another point of view, that of the transfer-time, it seems that we have the same problem of having to increase the capacitance in order to achieve long discharge period of the superconducting coil.

From Figure C.17, it is seen that energy transfer is complete at time $\tau/2$, where τ is given by

$$\tau = 2\pi \sqrt{\frac{L_t L_s C}{L_t + L_s}}$$

$\therefore$ Transfer time,

$$\tau_t = \pi \sqrt{\frac{L_t L_s C}{L_t + L_s}}$$

or $$\tau_t = \pi \sqrt{\frac{\alpha}{1+\alpha}} \cdot \sqrt{L_s C}$$

From Figure C.19, where $f(\alpha) = \sqrt{\frac{\alpha}{1+\alpha}}$ is plotted against α, it is seen that $f(\alpha)$ is larger for large volumes of α. But as seen earlier, large values of α is detrimental to the efficiency of energy transfer. Therefore, in order to increase the transfer-time, the transfer capacitance has to be increased.

$$f(\alpha) = \sqrt{\frac{\alpha}{1+\alpha}}$$

$f(\alpha)$ is the normalized transfer-time

$$\frac{\tau_t}{\pi\sqrt{L_s C}}$$

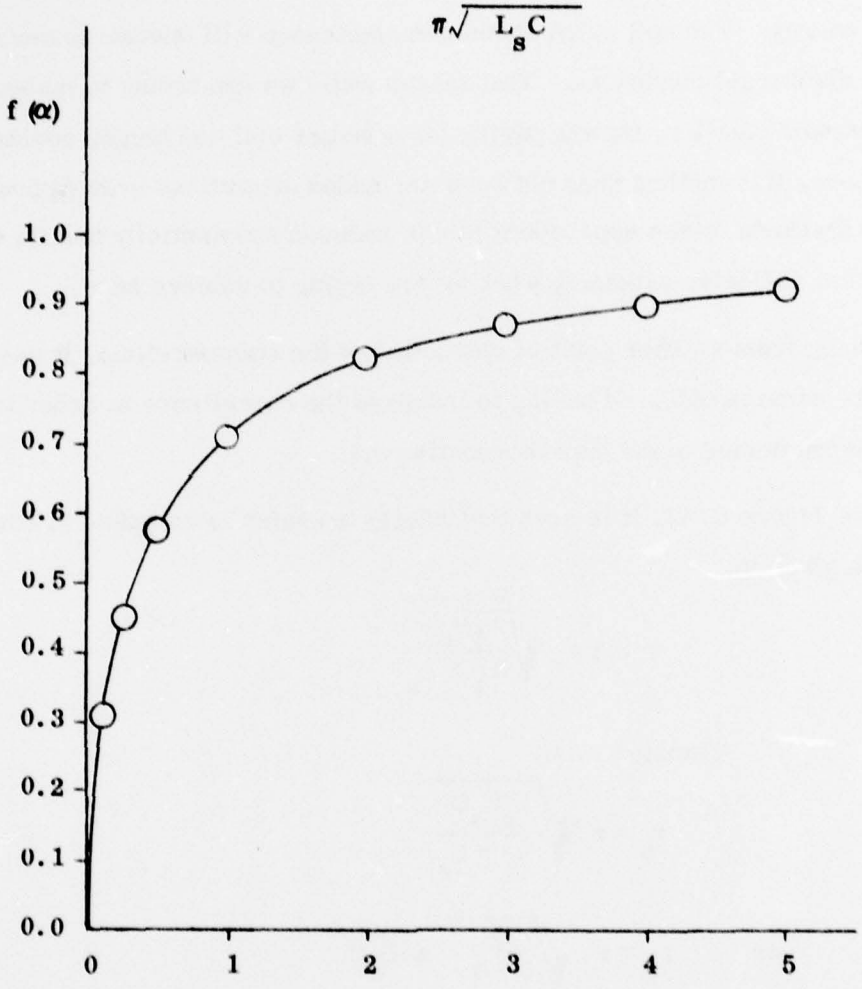

Figure C.19 Normalized transfer-time as a function of α.

Yet another point, which may be the last but not the least, is the Joule losses in the normal coil. Since the allowable current density in the normal coil is about two orders of magnitude lower than the superconducting coil, its weight will also be substantial.

An approximate calculation, based on our PFN inductor design equations, shows that a normal coil operating at 500 pps and storing a single 20 kJ pulse, will weigh about 145 lbs. The adiabatic temperature-rise will be about 300°C and it will have an average dissipation of 283 KW. It is needless to say that cooling required for this system will be extremely large.

From the discussion above, it is concluded that Approach 6 will not be very attractive when compared to Approach 2. The latter is expected to weigh much less than the present one and will have less complexities in switching.

☆U.S.Government Printing Office: 1978 — 757-080/358